3 June 2005

Science

Vol. 308 No. 5727
Pages 1361-1500 $10

125 YEARS OF GLOBAL Science

AAAS

WHEN ACCURACY IS THE NAME OF THE GAME.

Achieve up to six times higher reverse transcription accuracy with AccuScript™ RT from Stratagene

Reverse transcriptases (RT) exhibit significantly higher error rates than other known DNA polymerases, introducing errors at frequencies of one per 1,500 to 30,000 nucleotides during cDNA synthesis[1]. Our new AccuScript™ RT delivers 3- to 6-fold fewer reverse transcription errors than other reverse transcriptases, creating more accurate copies of RNA.

- **Greatly reduce sequence errors during first-strand cDNA synthesis**
- **Produce high yields of full-length cDNA**
- **Excellent RT-PCR sensitivity with low RNA amounts**

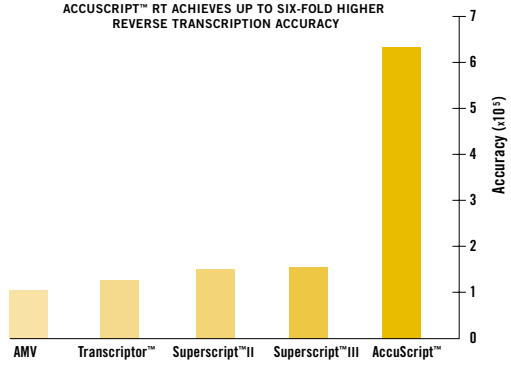

Need More Information? Give Us A Call:

Stratagene USA and Canada
Order: (800) 424-5444 x3
Technical Services: (800) 894-1304

Stratagene Europe
Order: 00800-7000-7000
Technical Services: 00800-7400-7400

Stratagene Japan K.K.
Order: 03-5159-2060
Technical Services: 03-5159-2070

www.stratagene.com

Ask us about these great products:

AccuScript™ Reverse Transcriptase System	50 rxns	600089
	200 rxns	600090
AccuScript™ First Strand cDNA Synthesis System		200820
AccuScript™ High Fidelity RT-PCR Kit with *PfuUltra*™ DNA Polymerase*		600180

STRATAGENE®

1. Roberts, J.D., Bebenek, K., Kunkel T.A. The Accuracy of Reverse Transcriptase from HIV-1. Science 1988 (242) 1171-1173.

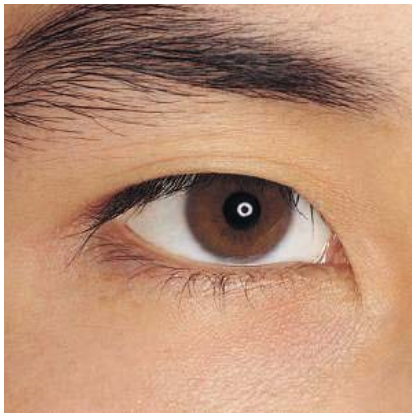


Successful research is important to all of us.

Use Clonetics® Melanocyte Cell Systems.

Clonetics® Melanocyte Cell Systems contain normal human epidermal neonatal melanocytes *(shown on left)* and optimized media for their growth. Each system can quickly generate melanocyte cultures for the study of pigmentation (melanogenesis), cellular differentiation, viral-induced transformation, antigen expression and cell adhesion. Clonetics Melanocyte Cell Systems are convenient and easy to use, allowing the researcher to focus on results.

Normal Human Epidermal Melanocyte Cell System NEW

- Cells are >90% functional based on verification of melanocyte conversion of L-dopa into dopa-melanin.
- New optimized media kit for melanocyte proliferation is superior to existing commercial media products.
- Guaranteed purity of >85% using immunofluorescent labeling of Mel-5.
- Cells, medium and reagents are quality tested together and guaranteed to give optimum performance as a complete "cell system".

Cambrex, the source for Clonetics® and Poietics™ Cell Systems, BioWhittaker™ Classical Media, SeaPlaque® and NuSieve® Agarose, and PAGEr® *Precast Gels.*

For more information contact us at:
www.cambrex.com/prod.NHEM
U.S. **800-638-8174** | Europe **32 (0) 87 32 16 11**

Cambrex Bio Science Walkersville, Inc.
8830 Biggs Ford Road | Walkersville, MD 21793

CAMBREX
Innovation. Experience. Performance.

GE Healthcare

Ni Sepharose™

4x greater binding capacity in histidine-tagged protein purification

Ni Sepharose™ products from GE Healthcare give you the highest binding capacity available for histidine-tagged protein purification. With up to four times the binding capacity, it's no longer pure imagination to dramatically increase your yield, while saving time and costs. Maximum target protein activity is assured, thanks to tolerance of a wide range of additives and negligible nickel ion leakage. The flexibility to use a variety of protocols ensures the highest possible purity. Ni Sepharose 6 FF is excellent for manual procedures such as gravity/batch and easy scale-up, while the HP version is designed for high-performance in automated purification systems – both are available in different formats, including prepacked columns. Outstanding performance has never been easier to achieve.

www.amershambiosciences.com/his

imagination at work

GE10-05

Science

COVER A male ivory-billed woodpecker (*Campephilus principalis*), sketched from life in the Singer Tract of northeastern Louisiana in 1935. Long suspected to be extinct in North America after the tract was logged in the early 1940s, this species has been rediscovered in the "Big Woods" region of Arkansas, about 300 km north of the tract. See page 1460. [Watercolor by George Miksch Sutton, courtesy of Cornell Laboratory of Ornithology]

Volume 308
3 June 2005
Number 5727

DEPARTMENTS

1371 *SCIENCE* ONLINE
1373 THIS WEEK IN *SCIENCE*
1377 EDITORIAL *by Donald Kennedy*
The Ivory-Bill Returns
related Browsings page 1415; Perspective page 1422; Report page 1460
1379 EDITORS' CHOICE
1384 CONTACT *SCIENCE*
1387 NETWATCH
1484 NEW PRODUCTS
1485 *SCIENCE* CAREERS

NEWS OF THE WEEK

1388 EMBRYONIC STEM CELLS
Spotlight Shifts to Senate After Historic House Vote
Moderate Republican Led the Winning Coalition
1391 TOXICOLOGY
Endocrine Disrupters Trigger Fertility Problems in Multiple Generations
related Report page 1466
1391 SCIENCESCOPE
1392 GENETICS
Spliced Gene Determines Objects of Flies' Desire
1393 BIOCHEMISTRY
Protein That Mimics DNA Helps Tuberculosis Bacteria Resist Antibiotics
related Report page 1480
1394 PUBLIC HEALTH
Europe's New Disease Investigator Faces an Uphill Start
1394 EVOLUTION POLITICS
Is Holland Becoming the Kansas of Europe?
1395 U.S. FUSION RESEARCH
With Domestic Program at Issue, House Votes to Hold Up Funding for ITER
1395 SCIENTIFIC PUBLICATION
HHS Asks *PNAS* to Pull Bioterrorism Paper
1397 U.S. IMMIGRATION POLICY
Law Leads to Degrees But Not Jobs in Texas
1397 ACADEMIC POLITICS
Boycott of Israeli Universities Overturned

NEWS FOCUS

1398 INTERVIEW
Elias Zerhouni: Taking Stock
1401 MEETING
The Biology of Genomes
Reading Ancient DNA the Community Way
related Science Express Report by J. P. Noonan et al.
Extinct Genome Under Construction

1398

1415

1416

1402 ORNITHOLOGY
Citizen Scientists Supplement Work of Cornell Researchers
1404 PONCE DE LEÓN AND ZOLLIKOFER PROFILE
Building Virtual Hominids: Musical Duo Reconstructs Ancient Fossils
1406 RANDOM SAMPLES

LETTERS

1409 **Regional Focus on GM Crop Regulation** *H. Okusu and K. N. Watanabe.* **Accommodation or Prediction?** *K. Stanger-Hall; D. Allchin; A. Aviv; S. G. Brush; J. Aach and G. M. Church.* ***Response*** *P. Lipton.* **Plutonium-238 and Cassini** *A. D. Rossin.* **A Historical Note on Superconductors** *P. W. Anderson*
1413 Corrections and Clarifications

BOOKS *ET AL.*

1414 HISTORY OF MEDICINE
Ancient Medicine
V. Nutton, reviewed by G. Lloyd
1415 FILM: ARCHAEOLOGY
Mummy The Inside Story
J. H. Taylor, reviewed by E. M. Sternberg
1415 Browsings
related Editorial page 1377; Perspective page 1422; Report page 1460

ESSAY

1416 GLOBAL VOICES OF SCIENCE
Science in the Arab World: Vision of Glories Beyond
W. Maziak

PERSPECTIVES

1419 MATERIALS SCIENCE
Electronics Without Lead
Y. Li, K. Moon, C. P. Wong
1420 CELL BIOLOGY
Prion Toxicity: All Sail and No Anchor
A. Aguzzi
related Research Article page 1435
1421 CHEMISTRY
Making Fuels from Biomass
J. R. Rostrup-Nielsen
related Report page 1446
1422 ECOLOGY
Rediscovery of the Ivory-billed Woodpecker
D. S. Wilcove
related Editorial page 1377; Browsings page 1415; Report page 1460

REVIEW

1424 BIOCHEMISTRY
Allosteric Mechanisms of Signal Transduction
J.-P. Changeux and S. J. Edelstein

Contents continued

Systems Biology — RNAi and Gene Expression Analysis

GeneGlobe — the world's largest database of matching siRNAs and RT-PCR assays

New

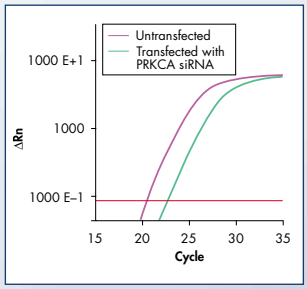

Reliable quantification after knockdown.

Visit www.qiagen.com/GeneGlobe .

New genomewide solutions from QIAGEN provide potent, specific siRNAs and matching, ready-to-use, validated primer sets for SYBR® Green based real-time RT-PCR assays.

- **One database** — easy online access to RNAi and gene expression solutions at the GeneGlobe™ Web portal
- **Two matching solutions** — siRNAs and matching real-time RT-PCR assays you can rely on
- **Three complete genomes** — siRNAs and RT-PCR assays are available for the entire human, mouse, and rat genomes

For matched siRNAs and real-time RT-PCR assays, go to www.qiagen.com/GeneGlobe !

QIAGEN

Science

SCIENCE EXPRESS www.sciencexpress.org

CLIMATE CHANGE: Penetration of Human-Induced Warming into the World's Oceans

T. P. Barnett et al.

Two separate climate models accurately reproduce the observed warming pattern in each ocean basin over the past 40 years only when they include anthropogenic CO_2 emissions. *related Research Article page 1431*

ASTROPHYSICS: The First Chemical Enrichment in the Universe and the Formation of Hyper Metal-Poor Stars

N. Iwamoto, H. Umeda, N. Tominaga, K. Nomoto, K. Maeda

A computer model of star evolution shows that stars containing very little metal are not a primitive class, but instead formed from the debris of older supernovae.

IMMUNOLOGY: Professional Antigen-Presentation Function by Human γδ T Cells

M. Brandes, K. Willimann, B. Moser

When triggered by nonpeptide compounds in invading microbes, special immune cells present foreign antigen on their surfaces to stimulate the immune response.

PALEONTOLOGY: Genomic Sequencing of Pleistocene Cave Bears

J. P. Noonan et al.

Reliable DNA sequences were obtained from 40,000-year-old cave bear fossils by screening for contaminants using existing sequences and by comparisons with modern dog and bear genomes. *related News story page 1401*

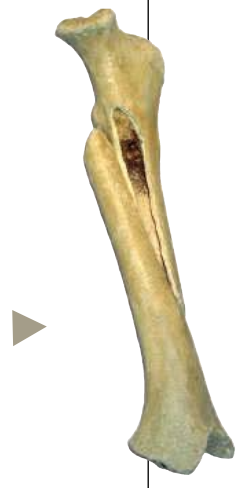

TECHNICAL COMMENT ABSTRACTS

1413 **PALEONTOLOGY**

Comment on "Abrupt and Gradual Extinction Among Late Permian Land Vertebrates in the Karoo Basin, South Africa"

C. R. Marshall

full text at www.sciencemag.org/cgi/content/full/308/5727/1413b

Response to Comment on "Abrupt and Gradual Extinction Among Late Permian Land Vertebrates in the Karoo Basin, South Africa"

P. D. Ward, R. Buick, D. H. Erwin

full text at www.sciencemag.org/cgi/content/full/308/5727/1413c

BREVIA

1429 **ATMOSPHERIC SCIENCE:** Disappearing Arctic Lakes

L. C. Smith, Y. Sheng, G. M. MacDonald, L. D. Hinzman

Satellite observations show that more than 1000 of the 10,000 lakes in Siberia have drained over the past 30 years as permafrost beneath them thawed.

1430 **PSYCHOLOGY:** Feeling the Beat: Movement Influences Infant Rhythm Perception

J. Phillips-Silver and L. J. Trainor

Infants bounced in a waltz (three-beat) or a march (two-beat) rhythm prefer the corresponding pattern in an otherwise ambiguous series of sounds.

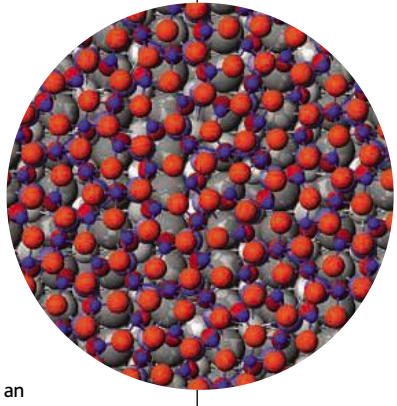

1440

RESEARCH ARTICLES

1431 **CLIMATE CHANGE:** Earth's Energy Imbalance: Confirmation and Implications

J. Hansen et al.

Earth is now absorbing nearly 1 W/m^2 more energy from the Sun than it is emitting to space, portending further warming even if greenhouse gas levels were immediately stabilized. *related* Science *Express Report by Barnett* et al.

1435 **MEDICINE:** Anchorless Prion Protein Results in Infectious Amyloid Disease Without Clinical Scrapie

B. Chesebro et al.

In mice in which the normal prion protein has been artificially severed from its membrane anchor, misfolded prion proteins produce amyloid plaques and brain damage, but not the clinical symptoms of scrapie. *related Perspective page 1420*

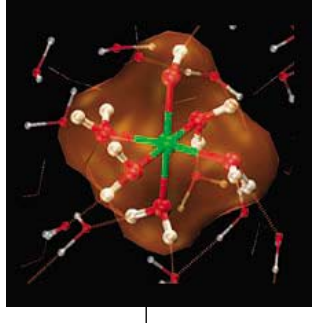

1450

REPORTS

1440 **MATERIALS SCIENCE:** Structure of the Ultrathin Aluminum Oxide Film on NiAl(110)

G. Kresse, M. Schmid, E. Napetschnig, M. Shishkin, L. Köhler, P. Varga

In aluminum oxide films widely used as substrates for catalysts, aluminum is pyramidally and tetrahedrally coordinated as $Al_{10}O_{13}$, not as Al_2O_3 as in the bulk crystal.

1442 **MATERIALS SCIENCE:** Directed Assembly of Block Copolymer Blends into Nonregular Device-Oriented Structures

M. P. Stoykovich, M. Müller, S. O. Kim, H. H. Solak, E. W. Edwards, J. J. de Pablo, P. F. Nealey

Mixing a simpler polymer with polymer blends that usually self-assemble into a regular grid yields a wide range of organized patterns, including angles and curves.

Contents continued

Synergy

exceptional products, outstanding service

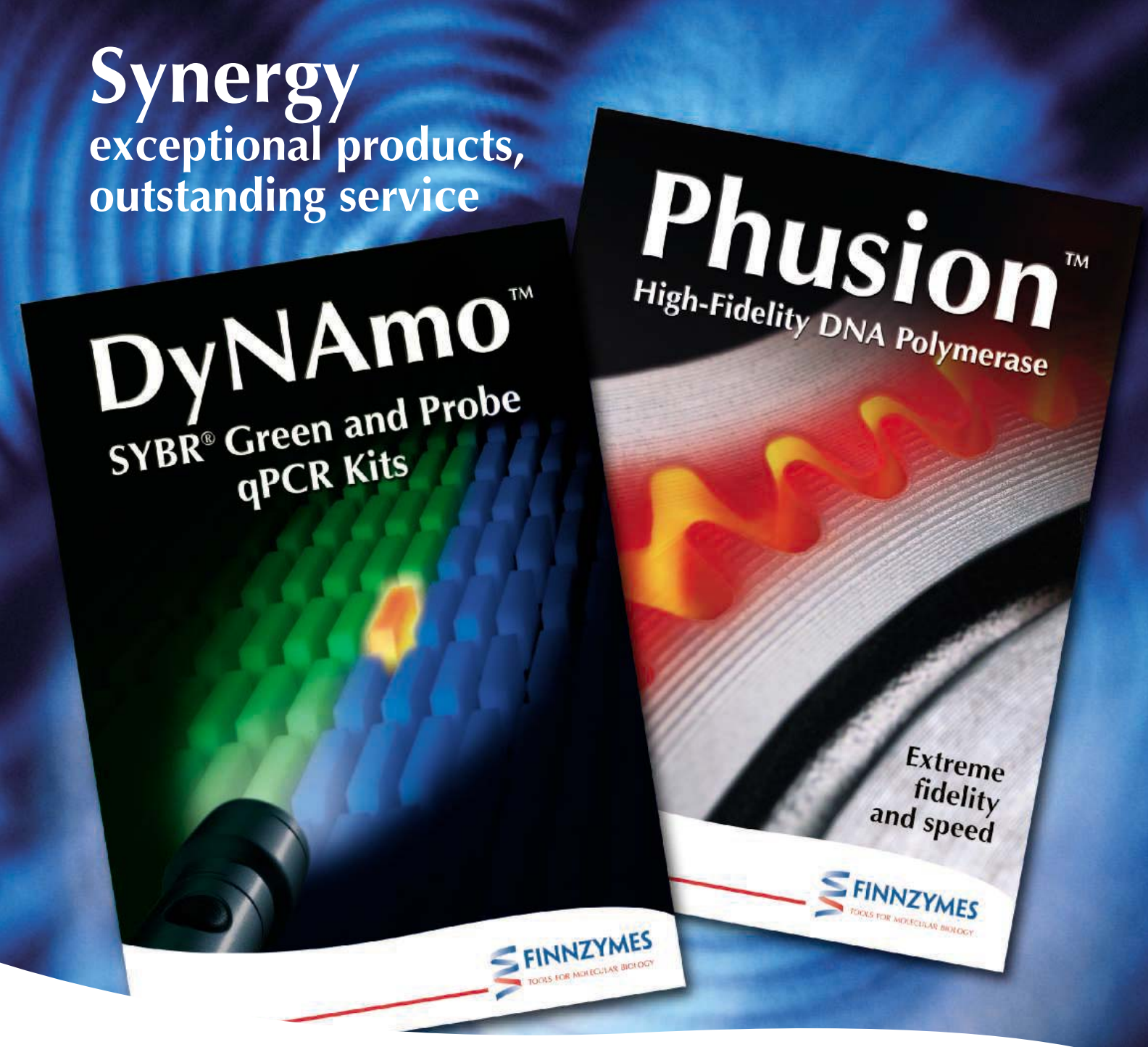

Finnzymes and New England Biolabs

Working Together to Advance PCR and qPCR Technology

New England Biolabs (NEB) is now the exclusive distributor of Finnzymes' PCR-licensed products: Phusion™ High-Fidelity DNA Polymerase, DyNAmo™ SYBR® Green qPCR Kits, and DyNAzyme™ DNA Polymerases in the United States and Canada. Together, the expertise of Finnzymes and NEB delivers an unsurpassed product offering for researchers utilizing modern molecular biology techniques. Finnzymes and NEB, state-of-the-art products, exceptional quality and outstanding service. That's synergy. For more information, visit **www.finnzymes.com** or **www.neb.com**

NEW ENGLAND BioLabs® Inc.
the leader in enzyme technology

FINNZYMES
TOOLS FOR MOLECULAR BIOLOGY

REPORTS CONTINUED

1446 **CHEMISTRY:** Production of Liquid Alkanes by Aqueous-Phase Processing of Biomass-Derived Carbohydrates
G. W. Huber, J. N. Chheda, C. J. Barrett, J. A. Dumesic
A reaction using sequential base and acid-metal catalysts converts biomass-derived sugars into sulfur-free alkanes that can be used as diesel fuel. *related Perspective page 1421*

1450 **CHEMISTRY:** Kinetic Evidence for Five-Coordination in $AlOH(aq)^{2+}$ Ion
T. W. Swaddle, J. Rosenqvist, P. Yu, E. Bylaska, B. L. Phillips, W. H. Casey
At moderate pH, dissolved aluminum ions bind five water molecules, yielding a coordinate species not found for other metals and forcing changes in reaction models for aluminum in the environment.

1453 **GEOPHYSICS:** An Observation of PKJKP: Inferences on Inner Core Shear Properties
A. Cao, B. Romanowicz, N. Takeuchi
The seismic shear wave that passes through Earth's inner core and provides direct evidence that it is indeed solid is detected after a long search.

1456 **PALEONTOLOGY:** Gender-Specific Reproductive Tissue in Ratites and *Tyrannosaurus rex*
M. H. Schweitzer, J. L. Wittmeyer, J. R. Horner
Specialized tissues, analogous to those providing calcium for eggs in female birds, line the marrow cavities in a *T. rex* bone, suggesting a way to sex dinosaur fossils.

1460 **ECOLOGY:** Ivory-billed Woodpecker (*Campephilus principalis*) Persists in Continental North America
J. W. Fitzpatrick et al.
Multiple observations over 1 year and a video show that the "extinct" ivory-billed woodpecker survives in the Mississippi River bottomlands. *related Editorial page 1377; Browsings page 1415; Perspective page 1422*

1463 **IMMUNOLOGY:** Accelerated Intestinal Epithelial Cell Turnover: A New Mechanism of Parasite Expulsion
L. J. Cliffe, N. E Humphreys, T. E. Lane, C. S. Potten, C. Booth, R. K. Grencis
Mice resist infection by an intestinal parasite by rapidly shedding gut epithelial cells, thus expelling the worm.

1466 **TOXICOLOGY:** Epigenetic Transgenerational Actions of Endocrine Disruptors and Male Fertility
M. D. Anway, A. S. Cupp, M. Uzumcu, M. K. Skinner
When pregnant rats are exposed to environmental toxins, four subsequent generations of offspring show impaired fertility and correlated changes in DNA methylation. *related News story page 1391*

1469 **CELL BIOLOGY:** Kinesin and Dynein Move a Peroxisome in Vivo: A Tug-of-War or Coordinated Movement?
C. Kural, H. Kim, S. Syed, G. Goshima, V. I. Gelfand, P. R. Selvin
High-resolution images of organelles moving along cytoskeletal tracks in living cells show that different motors drive the forward and backward motion, with only one type operating at a time.

1472 **CELL SIGNALING:** Mechanism of Divergent Growth Factor Effects in Mesenchymal Stem Cell Differentiation
I. Kratchmarova, B. Blagoev, M. Haack-Sorensen, M. Kassem, M. Mann
Improved proteomic analysis by mass spectrometry reveals the pathways activated by two similar growth factors, explaining why only one can trigger differentiation of bone cells.

1477 **STRUCTURAL BIOLOGY:** The Structure of Interleukin-2 Complexed with Its Alpha Receptor
M. Rickert, X. Wang, M. J. Boulanger, N. Goriatcheva, K. C. Garcia
The cytokine interleukin-2 first binds to a projection on one of three receptors on immune cells, then recruits the remaining two receptors to form the immune signaling complex.

1480 **BIOCHEMISTRY:** A Fluoroquinolone Resistance Protein from *Mycobacterium tuberculosis* That Mimics DNA
S. S. Hegde, M. W. Vetting, S. L. Roderick, L. A. Mitchenall, A. Maxwell, H. E. Takiff, J. S. Blanchard
Mycobacterium tuberculosis has an antibiotic resistance protein closely resembling DNA that can pair with a DNA-binding protein, protecting it from the antibacterial drug. *related News story page 1393*

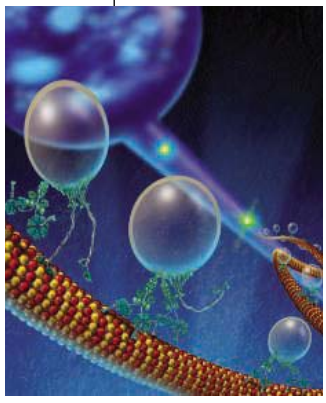

1469

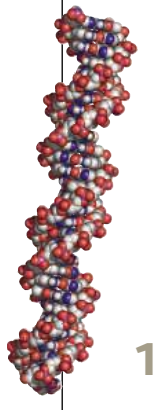

1480

AAAS
ADVANCING SCIENCE, SERVING SOCIETY

SCIENCE (ISSN 0036-8075) is published weekly on Friday, except the last week in December, by the American Association for the Advancement of Science, 1200 New York Avenue, NW, Washington, DC 20005. Periodicals Mail postage (publication No. 484460) paid at Washington, DC, and additional mailing offices.

Domestic individual membership and subscription (51 issues): $135 ($74 allocated to subscription). Domestic institutional subscription (51 issues): $550; Foreign postage extra: Mexico, Caribbean (surface mail) $55; other countries (air assist delivery) $85. First class, airmail, student, and emeritus rates on request. Canadian rates with GST available upon request, GST #1254 88122. Publications Mail Agreement Number 1069624. **Printed in the U.S.A.**

Change of address: allow 4 weeks, giving old and new addresses and 8-digit account number. **Postmaster:** Send change of address to *Science*, P.O. Box 1811, Danbury, CT 06813–1811. **Single copy sales:** $10.00 per issue prepaid includes surface postage; bulk rates on request. **Authorization to photocopy** material for internal or personal use under circumstances not falling within the fair use provisions of the Copyright Act is granted by AAAS to libraries and other users registered with the Copyright Clearance Center (CCC) Transactional Reporting Service, provided that $15.00 per article is paid directly to CCC, 222 Rosewood Drive, Danvers, MA 01923. The identification code for *Science* is 0036-8075/83 $15.00. *Science* is indexed in the *Reader's Guide to Periodical Literature* and in several specialized indexes.

Contents continued ▶

WHEN IT COMES TO INPUT/OUTPUT FLEXIBILITY, NOTHING WILL GET YOU TO AN IMAGE FASTER.

SCIENCE UTILITY VEHICLE.

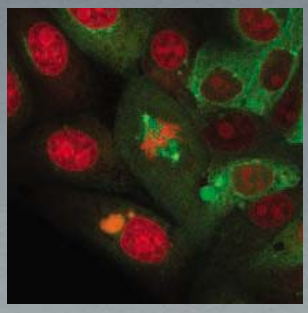

IX81 MOTORIZED INVERTED MICROSCOPE.

Olympus' most advanced motorized inverted microscope will position your research lab at the very vanguard of multi-wavelength advanced fluorescence, DIC and deconvolution techniques.

It is totally motorized from the built-in Z-Drive, 6-position nosepiece, 6-position condenser, 6-position fluorescence filter turret, and transmitted and epi shutters.

Nine access ports allow you to keep dedicated cameras and lasers in place and still have plenty of ports available for new devices.

The IX81 demonstrates Olympus' leadership in Total Internal Reflection Fluorescence Microscopy (TIRFM) with exceptional ease of operation and features such as the fully integrated TIRFM illuminator, a 1.45 NA TIRFM objective and the exclusive 1.65 NA objective.

The Olympus IX81 provides extraordinary system flexibility that will satisfy the most demanding research applications.

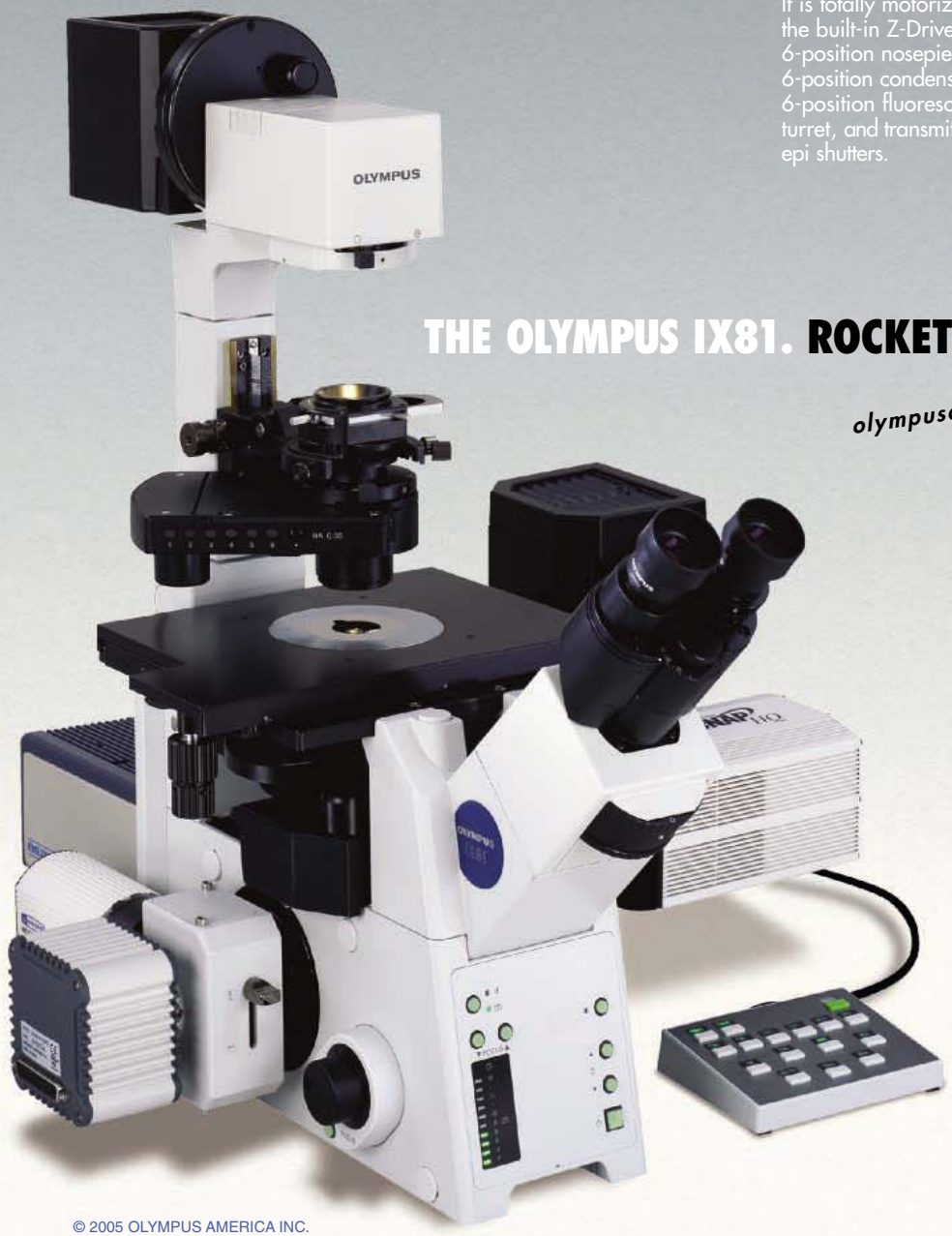

THE OLYMPUS IX81. ROCKET SCIENCE™.

olympusamerica.com/microscopes 800-455-8236

OLYMPUS®

Your Vision, Our Future

Science
www.scienceonline.org

sciencenow www.sciencenow.org Daily News Coverage

Found: The Stinkin' Rose's Tasty Thorn
A chemical in raw, but not baked, garlic trips sensitive pain nerve cells.

A New Suspect Behind Atherosclerosis
Blood vessel metabolism may play a role in hardening of arteries.

Americas Peopled by One Tribe?
A few trailblazers may have been the first migrants.

Funding for your research.

science's next wave www.nextwave.org Career Resources for Young Scientists

GrantsNet: June 2005 Funding News *Next Wave Staff*
Get the latest index of research funding, scholarships, fellowships, and internships.

US: NYU Changes Course on FICA—And So Do We *J. Austin*
NYU decided not to withhold social security tax from the paychecks of NIH postdoctoral fellows.

Canada: Spreading Your Postdoc Wings in Industry *A. Fazekas*
A molecular biology postdoc working at a Montreal biotech firm talks about her industry fellowship.

UK: Starting a Start-Up in the UK *R. Phillips*
What route is taken by those who wish to commercialize their research?

MiSciNet: The Road to a Neurobiology Ph.D. *C. Parks*
A doctoral student in neurobiology at UCLA talks about his motivation for studying science.

Postdoc Network: Postdocs at the Tipping Point *A. Reed and K. Micoli*
Executives discuss the future of postdocs and the National Postdoc Association.

science's sage ke www.sageke.org Science of Aging Knowledge Environment

Perspective: Misdirection on the Road to Shangri-La *S. J. Olshansky, B. A. Carnes, R. Hershow, D. Passaro, J. Layden, J. Brody, L. Hayflick, R. N. Butler, D. B. Allison, D. S. Ludwig*
The authors respond to a recent Perspective on a potential decrease in life expectancy.

News Focus: Ties That Bind the Brain *R. J. Davenport*
Parkin and glutathione deficits slay dopamine-producing neurons in flies.

News Focus: New Trick for an Old Enzyme *M. Leslie*
Famous as a chromosome capper, telomerase might also orchestrate general DNA repair.

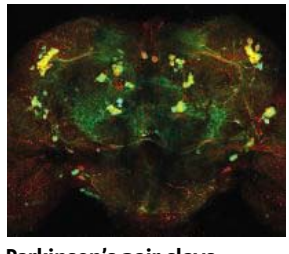

Parkinson's pair slays fly neurons.

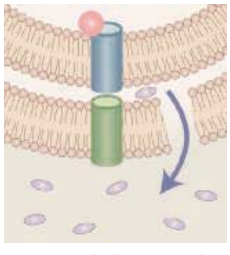

CypD and the mitochondrial permeability transition.

science's stke www.stke.org Signal Transduction Knowledge Environment

Perspective: Cyclophilin D—Knocking on Death's Door *M. D. Schneider*
Loss of cyclophilin D protects against cardiac ischemia-reperfusion injury.

Forum: Principles of Cell Signaling and Biological Consequences
Students participate in this discussion of signaling crosstalk.

Separate individual or institutional subscriptions to these products may be required for full-text access.

Spend less time looking for antibodies and more time doing research...

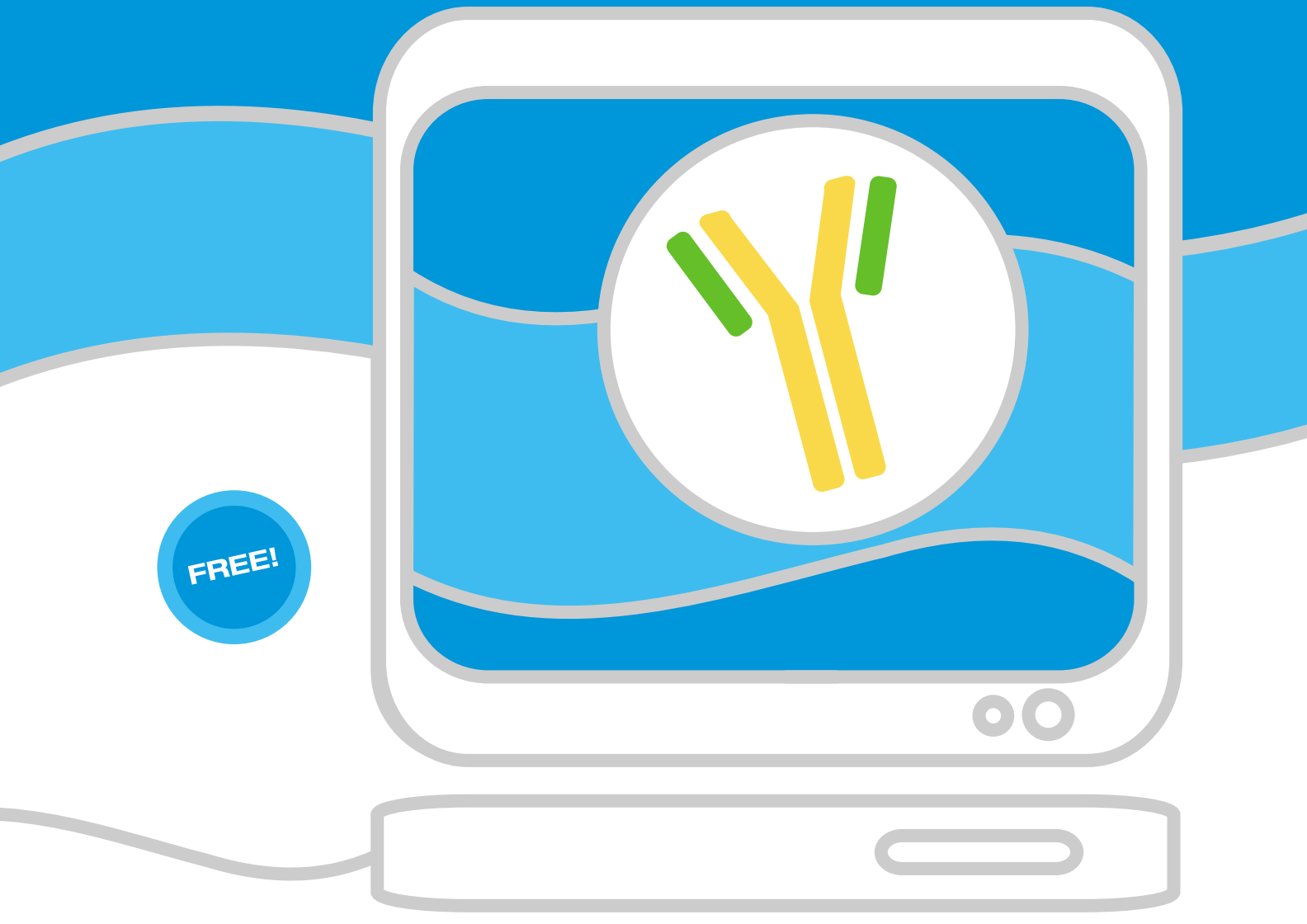

Find Antibodies Online

Search over 130,000 antibodies from over 100 companies by antigen, species reactivity, and application... free and online.

- Over 130,000 Antibodies
- Over 100 Antibody Companies
- No Registration Required
- Full Product Specifications
- Over 225,000 Research Products and Instruments
- Direct Access to Product Pages on Company Websites

biocompare®

The Buyer's Guide for Life Scientists™

www.biocompare.com

edited by Stella Hurtley and Phil Szuromi

A Lag in Global Warming

Earth's climate is thermally stable only when the amount of radiation it absorbs from the Sun is balanced by the amount emitted back into space. **Hansen *et al.*** (p. 1431, published online 28 April 2005) report results from a climate model and validate them with measurements of recent changes in the heat content of the ocean, which show that Earth now is absorbing 0.85 ± 0.15 watts per square meter more energy from the Sun than it is emitting to space. Their findings confirm that there is a lag in response of the climate system relative to the radiative forcing that drives it, and they predict that climate will continue to warm by more than half a degree Celsius even without further increases in atmospheric greenhouse gas concentrations because of the thermal inertia of the climate system.

Converting Biomass to Biodiesel

The conversion of the oxygenated hydrocarbons in biomass to saturated alkanes could provide a route to cleaner fuels from renewable sources. Recently, such conversions were demonstrated that produced volatile alkanes, such as hexane, from simple sugars. **Huber *et al.*** (p. 1446; see the Perspective by **Rostrup-Nielsen**) have now converted biomass-derived oxygenated hydrocarbons to liquid alkanes ranging from *n*-C_7 to C_{15}, which are in the range needed for diesel fuel and have the advantage of being sulfur-free. In this process, glucose or xylose is dehydrated over acid catalysts to aldehydes. These products, which may also be first cross-coupled to other aldehydes, are then hydrogenated and subjected to aldol condensations over solid base catalysts. Subsequent dehydration and hydrogenation reactions over bifunctional catalysts that contain acid and metal sites lead to the formation of alkanes.

Playing the Angles

Block copolymers are extremely useful for making simple patterns such as stripes or checkerboards because the pattern and length scale can be readily controlled by altering the lengths of the two covalently linked polymers. However, every change in the pattern dimensions requires a new polymer, and there are limits to the extent to which basic patterns can be altered. **Stoykovich *et al.*** (p. 1442) show that by adding homopolymers of the two block components to the mix, they can create nonregular patterns, including angled features with good resolution.

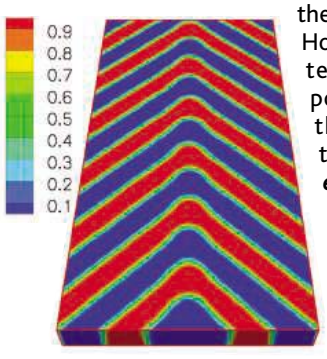

Aluminum Takes Five

Aqueous metal salts play a significant role in the chemical processes of organisms that live in or drink the water. Aluminum in particular is studied because of its abundance and toxicity. Trivalent aluminum binds six water molecules in strong acid and four in basic solution, but in the weakly acidic conditions, the most common in nature, the Al(III) ion has eluded definitive characterization. Among the many likely interconverting species, a short-lived five-coordinate structure has been proposed and would help to explain the occurrence of that geometry in solid minerals. However, there is little precedent for pentacoordination among other aqueous metal ions. **Swaddle *et al.*** (p. 1450, published online 28 April 2005) have now found support for five-coordinate Al(III) in water by measuring the pressure-dependent exchange rates of free and bound water ligands at Al(III) between pH 4 and 7 and comparing their results with theoretical simulations.

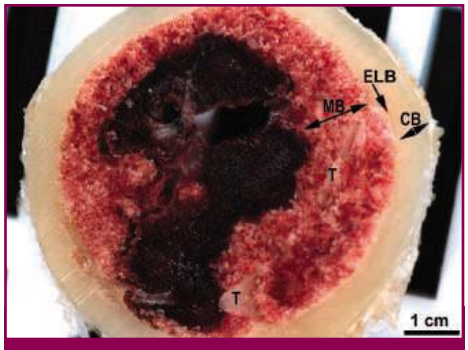

Is It a Bird, Is It a Dinosaur?

Female birds deposit a particular type of bone in their limbs, known as medullary bone, when laying eggs. This bone tissue provides a ready source of calcium for eggs. **Schweitzer *et al.*** (p. 1456) have identified bone tissues from the hind limbs of a *Tyrannosaurus rex* that closely resemble this medullary bone deposited by female birds. These data support the relation between tyrannosaurs and birds and provide a means of gender differentiation in dinosaurs.

Caught on Video

The ivory-billed woodpecker was once found in mature forests across the southeastern United States, but there had been no conclusive evidence for its survival in continental North America in more than 50 years. **Fitzpatrick *et al.*** (p. 1460, published online 28 April 2005; cover, see the Perspective by Wilcove) have conducted an intensive search of the Big Woods in eastern Arkansas and report the presence of at least one male bird. Repeated visual encounters and analysis of a video clip confirm the individual as an ivory-billed woodpecker. Extensive searches failed to locate additional birds elsewhere in the 220,000 hectares of bottomland forest, which indicates that the population density is extremely low.

Epithelial Escalator

The accelerated epithelial cell turnover observed in the cecum of mice infected with the nematode *Trichuris muris* may act as a mechanism of host defense against this enteric parasite and perhaps other enteric pathogens. Using mice resistant and susceptible to *T. muris* infection, **Cliffe *et al.*** (p. 1463) showed that crypt epithelial proliferation was increased in susceptible mice. Epithelial cell turnover, as measured by the movement of cells up the crypt, was faster in the resistant mice. Thus, crypt hyperplasia in susceptible mice reflects increased epithelial proliferation, without a matching increase in epithelial turnover.

The Epigenetic Sins of the Father

Chemotherapy, irradiation, and environmental toxins can cause DNA damage that, unless repaired, can be transmitted to the

CONTINUED ON PAGE 1375

CREDITS (TOP TO BOTTOM): SCHWEITZER *ET AL.*; STOYKOVICH *ET AL.*

Roche Applied Science

Only Two Steps To Success!

FuGENE 6 Transfection Reagent makes a big splash by:

> ***Works well, fast procedures, and doesn't kill cells***
>
> ***It's great for CHOs and cells are much healthier***
>
> ***Provides higher efficiency in High Five insect cells† than the recommended transfection reagent***
>
> ***Cos-1 cells >80% transfection efficiency***
>
> **Actual Customer Comments**

- **Saving time**
  Transfect with FuGENE 6 Reagent in just two easy steps by eliminating media changes.
- **Getting results quicker**
  Avoid having to test different reagents when transfecting new cell types. FuGENE 6 is proven to transfect more than 700 cell types. Visit our transfection database at ***www.roche-applied-science.com/fugene***.
- **Leading to results you can trust**
  Obtain more meaningful physiological results, because of the reagent's exceptionally low cytotoxicity.
- **Extending your resources**
  Increase productivity and lower costs by using less reagent per transfection.

Superior transient or stable transfection is closer and cheaper than you think. No wonder FuGENE 6 Reagent is cited in more than 3400 papers!

For more information, visit www.roche-applied-science.com/fugene

NEW! Available Now—

X-tremeGENE siRNA Transfection Reagent

For more information, visit *www.roche-applied-science.com/transfection* or contact your local representative.

Roche Diagnostics

Roche Diagnostics GmbH
Roche Applied Science
68298 Mannheim
Germany

next generation. Although effects have been seen in the first generation (F_1) after exposure, it is uncertain whether subsequent generations are affected. **Anway *et al.*** (p. 1466; see the news story by **Kaiser**) now show that when rats are exposed to endocrine disruptors at a critical stage of embryonic development, downstream generations (from F_1 to F_4) display decreased fertility. The transgenerational male fertility defect correlates with changes in DNA methylation, as opposed to DNA base mutation. Thus, endocrine disruptors have a transgenerational effect on male fertility, and the mechanism may involve epigenetic alteration.

Anchors and Amyloid Effects

It is not known whether amyloid deposited in the brain during protein misfolding diseases such as prion diseases and Alzheimer's disease is directly responsible for the neurotoxicity associated with these neurodegenerative syndromes. **Chesebro *et al.*** (p. 1435; see the Perspective by **Aguzzi**) describe scrapie infection experiments using transgenic mice expressing glycosylphosphatidylinositol (GPI)-negative prion protein (PrP), which is secreted from the cells where it is produced. Although the scrapie agent infected these mice and disease-associated protease-resistant prion protein (PrP-res) was produced, no clinical disease was detected during an observation period of more than 600 days. Lack of clinical disease correlated with PrP-res deposited in brain as amyloid plaques rather than as the diffuse PrP-res usually seen in mouse scrapie and human sporadic Creutzfeldt-Jakob disease, and the neuropathology at the ultrastructural level was similar to that of Alzheimer's disease. These marked differences in brain pathogenic effects of amyloid versus nonamyloid PrP-res suggest that amyloid PrP-res is actually less toxic than nonamyloid PrP-res. Furthermore, the PrP GPI anchor influences the pathogenic effects of scrapie infection and amyloid generation in vivo during prion disease.

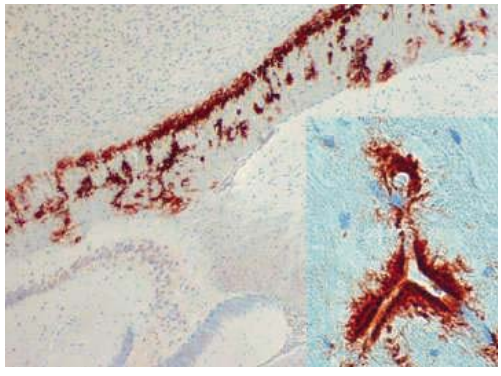

CREDIT: CHESEBRO *ET AL.*

Signaling Bone Formation

Improvements in mass spectrometry now allow global quantitation of phosphorylated proteins from cultured cells and comparison of signaling networks. **Kratchmarova *et al.*** (p. 1472) immunoprecipitated tyrosine-phosphorylated proteins (and associated proteins) and determined the relative abundance of peptides in the mixture to characterize the spectrum of signals initiated by two related receptor tyrosine kinases—the epidermal growth factor (EGF) receptor and the platelet-derived growth factor (PDGF) receptor. Human mesenchymal stem cells were induced to differentiate into bone-forming cells by EGF, but not by PDGF, and comparison of the two signaling networks revealed that the PDGF activated the phosphatidylinositol 3-kinase (PI3K) pathway whereas EGF did not. When the PI3K pathway was inhibited, PDGF could promote bone differentiation as effectively as EGF.

Insights into Tuberculosis Drug Resistance

Fluoroquinolone antibiotics are increasingly being used in the treatment of tuberculosis. They act by inhibiting DNA gyrase through binding to the enzyme-DNA complex in *Mycobacterium tuberculosis*. Genetic selection in *M. smegmatis* identified a protein, MFpA, that confers resistance to fluoroquinolones. **Hegde *et al.*** (p. 1480; see the news story by **Ferber**) have determined the structure of MfpA from *M. tuberculosis* to 2.0 angstrom resolution. It adopts a fold, the right-handed quadrilateral β-helix, that mimics double-helical DNA in size, shape, and charge distribution so that the protein competes with DNA for binding to DNA gyrase.

BIBLIOGRAPHY CENTRAL

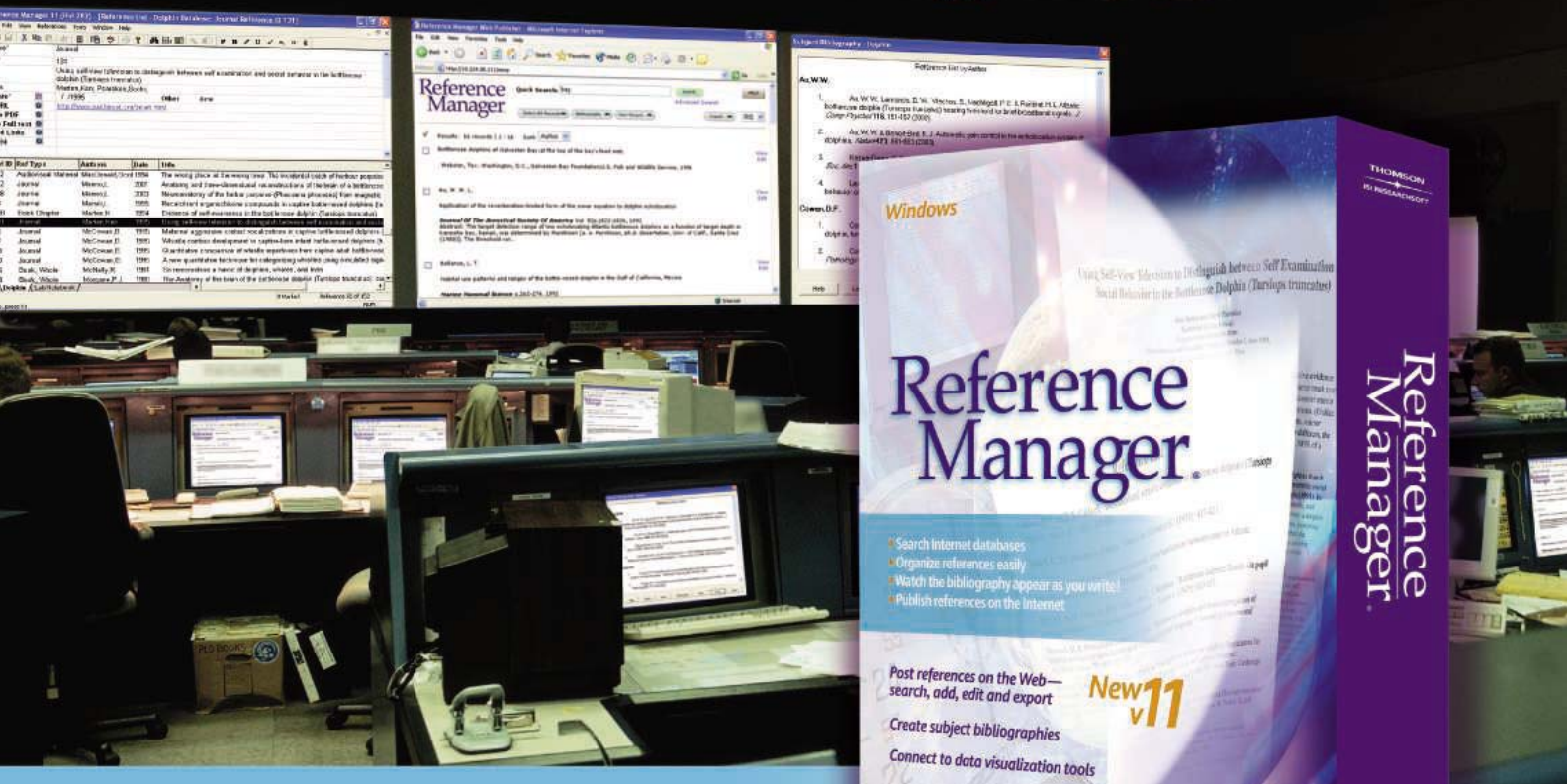

Your High-Tech Command and Control Center for References.

Introducing Reference Manager 11—a powerful upgrade to the bibliographic software that streamlines research, writing and publishing.

Reference Manager has served corporate, government and academic researchers worldwide for over 20 years. And now version 11 delivers new ways to share and view your reference collections: Post your databases to the Web. Collaborate with colleagues over a network. Link to full text pdf files.

These are just some of the powerful features that await you. Reference Manager is your command and control center for all things reference related.

What's new in v11:

- Publish Reference Manager databases to the Web or intranet
- Create subject bibliographies instantly
- Access new and updated content files at www.refman.com
- Share traveling libraries with colleagues
- Connect to data visualization tools

Put innovation into action. Order or upgrade today.
Available for Windows in a single-user and network edition.
Phone: 800-722-1227 • 760-438-5526 • info@isiresearchsoft.com

Download a Free Demo Today
www.refman.com

THOMSON
ISI RESEARCHSOFT™

The Ivory-Bill Returns

The announcement on *Science Online* (28 April 2005) of the persistence of the ivory-billed woodpecker has received more press attention than any bird news in my lifetime, and perhaps in all of history. In the hope that all the fuss has not exhausted our appetite for rejoicing over this development, we publish herewith the paper in print, along with an appropriate cover, and the following appreciation from your editor, a birder since boyhood.

Why is there so much excitement about this discovery—enough to generate over 300,000 Google searches, an editorial in the *New York Times*, and an Internet traffic jam on the many sites that serve America's six million birders? It should bring a thrill to everyone who cares about nature and about the diversity of life on Earth. My use of the word "return" in the title reflects much of the mainstream commentary about the finding, but it's not an apt description. It only seems as though the ivory-bill has arisen from the ashes. In fact, it never went away, so it can hardly be said to have returned.

Some will say, "It's only one bird." Well, maybe and maybe not. At least we now know that a mated pair of ivory-bills existed in these Arkansas forests and laid the egg that hatched this bird at least 40 years after the last confirmed record of the species from North America. We must now recognize that previous claimed sightings, some of them by experienced observers, should probably not have been disregarded. We should encourage future naturalists and other watchers in likely habitats to report their observations carefully so that they can be evaluated. Most important, this surprising news underscores the need to conserve ecologically suitable habitats for vanishing species, even when hope seems to have been lost.

I must add a note about the personal excitement and pleasure this discovery has brought me. The sense of excitement began about 2 months ago when I received a somewhat cryptic e-mail from John Fitzpatrick, the head of Cornell's Laboratory of Ornithology (located in a nice piece of deciduous forest called Sapsucker Woods). Fitzpatrick's message inquired as to whether *Science* would be interested in reviewing a report confirming the persistence of a bird (I believe he said "iconic" bird) long thought to have been extinct. That was not a difficult code to break, and I got back to him in a New York second!

The pleasure came because the involvement of the Cornell laboratory closed a circle for me. As a boy in the 1930s, I was a faithful follower of *National Geographic* accounts of Cornell expeditions to Louisiana to record and photograph these magnificent birds. I even wrote a fan letter to the expedition's leader, the pioneer Cornell ornithologist Arthur Allen. My mother supervised my 7-year-old grammar and penmanship but failed to edit the sign-off that kids use for relatives. I signed it "Love, Donny." I was happily surprised when Professor Allen responded to my questions with an official-looking letter on Cornell stationery. To my mother's amused delight, he signed it "Love, Arthur." How pleased this generous man would have been by his successors' find.

Cornell and the Nature Conservancy, a partner in the venture, deserve all the credit they have been given. But it is only fair to single out Gene Sparling of Hot Springs, Arkansas, who first found the bird, made the identification, and then guided two members of the Cornell team into the right area. No one who heard the interview of these three on National Public Radio can be unaware of the thrill this amateur naturalist had from his discovery or of the excitement it brought to his two colleagues. It is fortunate for science that it attracts people who may lack special training or higher degrees but have found the knowledge and confidence to know that they can do real science. Generations of British parson naturalists have given us centuries of first-flowering dates for British plants, and a national brigade of observers who assist Cornell with the Partners in Flight program have expanded our knowledge of bird distribution and migration. For Gene Sparling, the Cornell team, and the partner organizations who have helped preserve the Arkansas habitat, an appropriate salutation would be the ancient Hebrew blessing: "Baruch Mechayei haMetim": "Blessed is the one who gives life to the dead."

Donald Kennedy
Editor-in-Chief

10.1126/science.1115204

ILLUSTRATION: LARRY CHANDLER

HUMAN FRONTIER SCIENCE PROGRAM

12 Quai Saint-Jean, 67080 Strasbourg Cedex, FRANCE
Phone: +33 (0)3 88 21 51 27/34 Fax: +33 (0)3 88 32 88 97
E-mail: fellow@hfsp.org Web site: http://www.hfsp.org

OPPORTUNITIES FOR POSTDOCTORAL TRAINING ABROAD

The Human Frontier Science Program (HFSP) **promotes basic research in the life sciences.** Special emphasis is given to **novel and interdisciplinary research** aimed at **elucidating the complex mechanisms of living organisms.** The HFSP fellowship program provides support for training of postdoctoral researchers across national boundaries. To answer fundamental questions in the life sciences investigators should be able to span more than one scientific discipline. Applicants are therefore **encouraged to explore new areas of experimental research.**

Researchers from one of the supporting member countries can apply to work in any other country, while other nationals can apply for training only in a supporting country. Current supporting members are: Australia*, Canada, the European Union, France, Germany, Italy, Japan, the Republic of Korea*, Switzerland, the United Kingdom, and the United States of America (* new supporting members starting in award year 2006).

Important deadlines:
Compulsory pre-registration for password: **25 August 2005**
Submission of applications: **1 September 2005**

Long-Term Fellowships

Long-Term Fellowships are intended for postdoctoral fellows with a Ph.D. degree in the life sciences. Applicants are expected to **broaden their horizon and to move into a new research field** that is **different from their doctoral studies or previous postdoctoral training.**

Cross-Disciplinary Fellowships

Cross-Disciplinary Fellowships are intended for postdoctoral fellows with a Ph.D. degree in the physical sciences, chemistry, mathematics, engineering or computer sciences who **wish to receive training in the life sciences.** Applicants are expected **to move into a new research field through a significant change in discipline.**

Both programs provide up to 3 years of support for fellows to train in an outstanding laboratory of their choice in another country. Fellows can utilize their final year of postdoctoral support in the home country. Only the fellows who choose to return to their home country can defer their final year for up to two years while they are funded through other sources. The final year can then be used for an additional year of research training in the home country. Former HFSP fellows returning to their home country will be eligible to apply for a Career Development Award designed to establish themselves as independent young investigators.

The online system to submit applications will become available in summer 2005 on the HFSP web site.

Short-Term Fellowships

Short-Term Fellowships are intended for researchers early in their careers and provide up to 3 months of support to **learn techniques in a new area of research or establish new collaborations in another country**. Applications are accepted throughout the year.

Guidelines for all fellowships are available on the HFSPO web site (**www.hfsp.org**).

EDITORS' CHOICE

edited by Gilbert Chin

CLIMATE SCIENCE

Urban Air Quality

The oxidation of volatile organic compounds (VOCs) is an important step in the formation of photochemical smog in urban areas, but the rate at which VOCs are oxidized has been difficult to quantify. A reliable way to measure this rate would lead to improved prediction of smoke/fog events.

Volkamer *et al.* used differential optical absorption spectroscopy (DOAS) to make direct measurements of atmospheric glyoxal concentrations over Mexico City in the spring of 2003. They show that VOC oxidation, of which glyoxal is a product, begins about an hour after sunrise and continues throughout the day. These observations allow a lower limit to be placed on the rate of VOC oxidation and reveal that VOC chemistry is active throughout sunlit hours. On the basis of these results, satellite measurements of glyoxal appear to be feasible, which would support the identification of photochemical hot spots in the atmosphere. — HJS

Smog above Mexico City.

Geophys. Res. Lett. **32**, 10.1029/2005GL022616 (2005).

BIOMEDICINE

Weeding Out Osteoclasts

More than half of individuals age 50 and older are at risk for osteoporosis, a disorder characterized by low bone mass. One of the principal cell types regulating skeletal growth and integrity is the osteoclast, which functions to resorb bone. Several drugs currently in clinical use for osteoporosis, such as the bisphosphonates, act by inhibiting osteoclast activity.

A surprising new molecular player in bone growth and remodeling is identified by Idris *et al.*, who find that mutant mice deficient in cannabinoid type 1 (CB_1) receptors have increased bone mass that appears to be caused by aberrant apoptosis (cell death) of osteoclasts. Moreover, mutant female mice were protected against bone loss induced by ovary removal, which is a model of postmenopausal bone loss in women, and this protective effect could be reproduced pharmacologically in wild-type mice by the administration of cannabinoid antagonists. Thus, osteoporosis joins a growing list of human disorders, including obesity and nicotine dependence, that may be treatable by drugs targeting the cannabinoid receptors, a class of proteins originally discovered as the binding sites for the major psychoactive ingredient of marijuana. — PAK

Nat. Med. 10.1038/nm1255 (2005).

CHEMISTRY

Recovered on Tape

A central challenge in homogeneous catalysis is achieving facile separation and recovery of the catalyst once the reaction is over. An increasingly common solution is to append fluorocarbon chains to the catalyst. Because fluorocarbons are poorly miscible with most organic solvents, this modification makes it possible to remove the catalyst by extraction into a fluorous solvent or, in some cases, simply by cooling the reaction mixture to induce precipitation. However, both of these methods can be inefficient at low catalyst loadings.

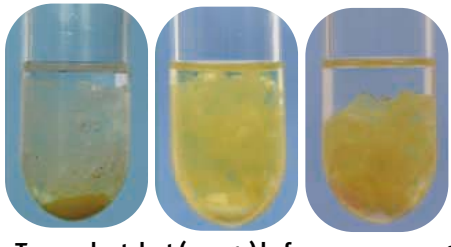

Tape and catalyst (orange) before reaction (left), at 55°C (center), and after cooling (right).

Dinh and Gladysz show that a rhodium catalyst for hydrosilylation of ketones can be recovered efficiently and easily using Teflon tape. The catalyst, bearing three fluoroalkylphosphine ligands, was dissolved with the reagents in dibutyl ether at 55°C, with a strip of tape added to the flask. Upon cooling, the orange catalyst stuck to the tape (and not to the stir bar!) and could be recycled two more times by heating in a fresh reaction mixture. — JSY

Angew. Chem. Int. Ed. 10.1002/anie.200500237 (2005).

CELL BIOLOGY

Complex Cellularization

Early insect development involves multiple nuclear divisions within a single cytoplasm to form syncytial embryos. The syncytium is divided into separate cells (each with a single nucleus) in a process termed cellularization, which involves the generation of membrane furrows between adjacent nuclei and produces a polarized cortical cell layer. The formation of the cleavage furrow requires concerted delivery (from the Golgi complex) of membrane components to the growing furrow. This delivery increases the cell surface area by 20-fold and is directed by the microtubule network. Papoulas *et al.* followed the apically directed movement of Golgi complexes toward the sites of furrow formation, which depended on the activity of the microtubule-based molecular motor dynein. The Golgi membranes themselves interacted with dynein and other motility factors via a peripheral Golgi membrane protein of the golgin family, Lava lamp. These interactions were disrupted and cellularization blocked when domains from the Lava lamp protein that bound to dynein or the motility factors were injected into living embryos. — SMH

Nat. Cell Biol. 10.1038/ncb1264 (2005).

PSYCHOLOGY

Is That Your Final Answer?

Taking a multiple-choice test or patronizing a crowded supermarket, we may find ourselves in a predicament, after having made a selection, in deciding whether to stick with it or to switch. The widespread belief is that it's better to stay put

CONTINUED ON PAGE 1381

CREDITS: (TOP) RAINER VOLKAMER; (BOTTOM) DINH AND GLADYSZ, *ANGEW. CHEM. INT. ED.* 10.1002/ANIE.200500237 (2005)

The Way Ahead™

in model organisms

Infinitely more array choices.

GeneChip® Model Organism Arrays

More choices, more discoveries, highest quality. Available arrays include: Arabidopsis ATH1, barley, bovine, *C. elegans,* canine, citrus, chicken, Drosophila, *E. coli,* maize, Medicago, *P. aeruginosa,* Plasmodium/Anopheles, porcine, poplar, *R. macaque,* rice, soybean, sugar cane, tomato, *V. vinifera,* wheat, Xenopus, yeast, and zebrafish. The full list of arrays can be found at www.affymetrix.com/products/arrays/index.affx **And if you don't see the one you are looking for, we can make a custom array for you—with the same quality that's made Affymetrix the gold standard in microarrays.**

www.affymetrix.com • 1-888-DNA-CHIP (362-2447)
Europe: +44 (0) 1628 552550 • Japan: +81-(0)3-5730-8200

AFFYMETRIX®

rather than moving to another, apparently faster-moving, checkout line. Similarly, on a test, college students believe that the first choice is more likely to be correct.

Using more than 2000 exams from 2 years of an undergraduate psychology course, Kruger *et al.* show that switching (detected as erasures) from an incorrect to a correct answer occurred twice as often as the converse, which is consistent with decades of empirical studies. Why then do we prefer to stay with our first choices? A series of follow-up experiments revealed that students became more frustrated after learning that they'd switched to a wrong answer as opposed to alighting on it at the start and that, as a consequence, the former instances were more memorable than the latter even though the outcomes (an incorrect choice) were precisely the same. In other words, the negative emotion engendered by having given up on the right choice weights the encoding/retrieval of memories so as to convince us of what the authors term the first instinct fallacy. — GJC

J. Pers. Soc. Psychol. **88**, 725 (2005).

CHEMISTRY

Cleaning Up CO

For use in fuel cells, hydrogen (H_2) can be produced by reacting alcohols or hydrocarbons with steam or oxygen, yielding byproducts that include CO and CO_2. Although CO can be removed or converted through the water-gas–shift reaction to CO_2 and additional H_2, even small amounts of residual CO inhibit reactions at the Pt anode of polymer electrolyte fuel cells (PEFCs). Onboard H_2 production would likely need to remove CO in the presence of its oxidation product, CO_2, and to do so without oxidizing the H_2 to water. Landon *et al.* report the selective oxidation of CO to CO_2 in the presence of H_2, water vapor, and CO_2 at 80°C, which is below the operating temperature of PEFCs, with a single-stage reactor. They report that a gold catalyst on an Fe_2O_3 support, prepared in a two-step heating process up to 550°C, created a catalyst with high CO oxidation activity but no H_2 oxidation activity under typical PEFC conditions. — PDS

Chem. Commun. 10.1039/b505295p (2005).

HIGHLIGHTED IN *SCIENCE*'S SIGNAL TRANSDUCTION KNOWLEDGE ENVIRONMENT

Science's stke www.stke.org

Geometry of Calcium Signaling

Changes in intracellular calcium concentration ($[Ca^{2+}]_i$) that occur after Ca^{2+} influx through *N*-methyl-D-aspartate–type glutamate receptors (NMDARs) play a key role in long-term plastic changes in postsynaptic function that are thought to underlie learning and memory. For most excitatory synapses in the central nervous system, the postsynaptic partners are dendritic spines: small protrusions on the dendritic shaft that have the effect of localizing changes in $[Ca^{2+}]_i$ to individual synapses (as opposed to the entire dendrite).

Noguchi *et al.* used two-photon photolysis of caged glutamate and two-photon Ca^{2+} imaging to release transmitter onto single spines of rat hippocampal neurons and to assess quantitatively the influence of spine structure on $[Ca^{2+}]_i$. NMDAR-dependent current increased with spine head volume. On the other hand, NMDAR-mediated increases in the $[Ca^{2+}]_i$ at the spine head were larger in small mushroom-shaped spines, whereas increases in dendritic shaft $[Ca^{2+}]_i$ at the base of the spine were greater for large stubby spines. These differences were dictated by the geometry of the spine neck. The stubby spine morphology favored a rapid diffusion (an energetically downhill process) of Ca^{2+} from the spine head through the neck into the dendritic shaft, whereas in small spines, the lower conductance of the thin necks means that clearance of calcium from the head relies in part on the energetically uphill and slower process of calcium extrusion. The authors conclude that these differences in Ca^{2+} handling enable the preferential induction of long-term potentiation, which depends on changes in $[Ca^{2+}]_i$ in smaller spines. — EMA

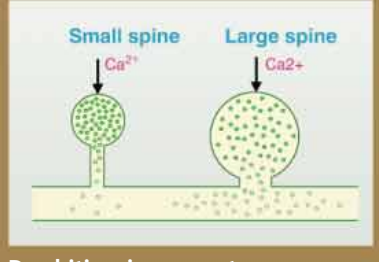

Dendritic spine geometry.

Neuron **46**, 609 (2005).

CREDITS: NOGUCHI *ET AL.*, *NEURON* **46**, 609 (2005)

GE Healthcare

What do you call making protein purification easy right from the start?

Pure imagination brought to life.

GE Healthcare is the one name behind all the leading tools in biomolecular research. Our focus is on providing protein purification systems, columns and media that make drug discovery simpler and faster from the outset to help you compete more effectively. Innovations like HiTrap™ and HisTrap™ columns, which offer outstanding convenience and reproducibility. Or the ÄKTAdesign™ platform, combined with the seamless control of UNICORN™ software, which gives you speed, ease and confidence whatever your application or scale.

At GE Healthcare we never stand still. We're constantly working to improve our offering – finding new ways of bringing pure imagination to life, to give you even better performance in tomorrow's race.

Visit www.amershambiosciences.com/pureimagination

imagination at work

GE08-05

www.sciencemag.org

Science

1200 New York Avenue, NW
Washington, DC 20005
Editorial: 202-326-6550, FAX 202-289-7562
News: 202-326-6500, FAX 202-371-9227

Bateman House, 82-88 Hills Road
Cambridge, UK CB2 1LQ
+44 (0) 1223 326500, FAX +44 (0) 1223 326501

Subscription Services For change of address, missing issues, new orders and renewals, and payment questions: 800-731-4939 or 202-326-6417, FAX 202-842-1065. Mailing addresses: AAAS, P.O. Box 1811, Danbury, CT 06813 or AAAS Member Services, 1200 New York Avenue, NW, Washington, DC 20005

Institutional Site Licences please call 202-326-6755 for any questions or information

Reprints Ordering/Billing/Status 800-635-7171; Corrections 202-326-6501

Permissions 202-326-7074, FAX 202-682-0816

Member Benefits Bookstore: AAAS/BarnesandNoble.com bookstore www.aaas.org/bn; Car purchase discount: Subaru VIP Program 202-326-6417; Credit Card: MBNA 800-847-7378; Car Rentals: Hertz 800-654-2200 CDP#343457, Dollar 800-800-4000 #AA1115; AAAS Travels: Betchart Expeditions 800-252-4910; Life Insurance: Seabury & Smith 800-424-9883; Other Benefits: AAAS Member Services 202-326-6417 or www.aaasmember.org.

science_editors@aaas.org (for general editorial queries)
science_letters@aaas.org (for queries about letters)
science_reviews@aaas.org (for returning manuscript reviews)
science_bookrevs@aaas.org (for book review queries)

Published by the American Association for the Advancement of Science (AAAS), *Science* serves its readers as a forum for the presentation and discussion of important issues related to the advancement of science, including the presentation of minority or conflicting points of view, rather than by publishing only material on which a consensus has been reached. Accordingly, all articles published in *Science*—including editorials, news and comment, and book reviews—are signed and reflect the individual views of the authors and not official points of view adopted by the AAAS or the institutions with which the authors are affiliated.

AAAS was founded in 1848 and incorporated in 1874. Its mission is to advance science and innovation throughout the world for the benefit of all people. The goals of the association are to: foster communication among scientists, engineers and the public; enhance international cooperation in science and its applications; promote the responsible conduct and use of science and technology; foster education in science and technology for everyone; enhance the science and technology workforce and infrastructure; increase public understanding and appreciation of science and technology; and strengthen support for the science and technology enterprise.

Information for Contributors

See pages 135 and 136 of the 7 January 2005 issue or access www.sciencemag.org/feature/contribinfo/home.shtml

EDITOR-IN-CHIEF **Donald Kennedy**
EXECUTIVE EDITOR **Monica M. Bradford**
DEPUTY EDITORS **R. Brooks Hanson, Katrina L. Kelner**
NEWS EDITOR **Colin Norman**

Editorial SUPERVISORY SENIOR EDITORS Barbara Jasny, Phillip D. Szuromi; SENIOR EDITORS Gilbert J. Chin, Lisa D. Chong, Pamela J. Hines, Paula A. Kiberstis (Boston), Beverly A. Purnell, L. Bryan Ray, Guy Riddihough (Manila), H. Jesse Smith, Valda Vinson, David Voss; ASSOCIATE EDITORS Marc S. Lavine, Jake S. Yeston; ONLINE EDITOR Stewart Wills; CONTRIBUTING EDITOR Ivan Amato; ASSOCIATE ONLINE EDITOR Tara S. Marathe; BOOK REVIEW EDITOR Sherman J. Suter; ASSOCIATE LETTERS EDITOR Etta Kavanagh; INFORMATION SPECIALIST Janet Kegg; EDITORIAL MANAGER Cara Tate; SENIOR COPY EDITORS Jeffrey E. Cook, Harry Jach, Barbara P. Ordway; COPY EDITORS Cynthia Howe, Alexis Wynne Mogul, Sabrah M. n'haRaven, Jennifer Sills, Trista Wagoner; EDITORIAL COORDINATORS Carolyn Kyle, Beverly Shields; PUBLICATION ASSISTANTS Chris Filiatreau, Joi S. Granger, Jeffrey Hearn, Lisa Johnson, Scott Miller, Jerry Richardson, Brian White, Anita Wynn; EDITORIAL ASSISTANTS Ramatoulaye Diop, E. Annie Hall, Patricia M. Moore, Brendan Nardozzi, Michael Rodewald; EXECUTIVE ASSISTANT Sylvia S. Kihara; ADMINISTRATIVE SUPPORT Patricia F. Fisher

News SENIOR CORRESPONDENT Jean Marx; DEPUTY NEWS EDITORS Robert Coontz, Jeffrey Mervis, Leslie Roberts, John Travis; CONTRIBUTING EDITORS Elizabeth Culotta, Polly Shulman; NEWS WRITERS Yudhijit Bhattacharjee, Jennifer Couzin, David Grimm, Constance Holden, Jocelyn Kaiser, Richard A. Kerr, Eli Kintisch, Andrew Lawler (New England), Greg Miller, Elizabeth Pennisi, Charles Seife, Robert F. Service (Pacific NW), Erik Stokstad; Amitabh Avasthi (intern); CONTRIBUTING CORRESPONDENTS Marcia Barinaga (Berkeley, CA), Barry A. Cipra, Adrian Cho, Jon Cohen (San Diego, CA), Daniel Ferber, Ann Gibbons, Robert Irion, Mitch Leslie (NetWatch), Charles C. Mann, Evelyn Strauss, Gary Taubes, Ingrid Wickelgren; COPY EDITORS Linda B. Felaco, Rachel Curran, Sean Richardson; ADMINISTRATIVE SUPPORT Scherraine Mack, Fannie Groom BUREAUS: Berkeley, CA: 510-652-0302, FAX 510-652-1867, New England: 207-549-7755, San Diego, CA: 760-942-3252, FAX 760-942-4979, Pacific Northwest: 503-963-1940

Production DIRECTOR James Landry; SENIOR MANAGER Wendy K. Shank; ASSISTANT MANAGER Rebecca Doshi; SENIOR SPECIALISTS Vicki J. Jorgensen, Jessica K. Moshell; SPECIALISTS Jay R. Covert, Stacey Ferebee; **Preflight** DIRECTOR David M. Tompkins; MANAGER Marcus Spiegler; SPECIALIST Jessie Mudjitaba;

Art DIRECTOR Joshua Moglia; ASSOCIATE ART DIRECTOR Kelly Buckheit; ILLUSTRATOR Katharine Sutliff; SENIOR ART ASSOCIATES Holly Bishop, Laura Creveling, Preston Huey, Julie White; ASSOCIATE Nayomi Kevitiyagala; PHOTO RESEARCHER Leslie Blizard

***Science* International**

Europe (science@science-int.co.uk) EDITORIAL: INTERNATIONAL MANAGING EDITOR Andrew M. Sugden; SENIOR EDITOR/PERSPECTIVES Julia Fahrenkamp-Uppenbrink; SENIOR EDITORS Caroline Ash (Geneva: +41 (0) 222 346 3106), Stella M. Hurtley, Ian S. Osborne, Peter Stern; ASSOCIATE EDITOR Stephen J. Simpson; EDITORIAL SUPPORT Emma Westgate; Deborah Dennison ADMINISTRATIVE SUPPORT Janet Clements, Phil Marlow, Jill White; NEWS: INTERNATIONAL NEWS EDITOR Eliot Marshall DEPUTY NEWS EDITOR Daniel Clery; CORRESPONDENT Gretchen Vogel (Berlin: +49 (0) 30 2809 3902, FAX +49 (0) 30 2809 8365); CONTRIBUTING CORRESPONDENTS Michael Balter (Paris), Martin Enserink (Amsterdam and Paris); INTERN Mason Inman

Asia Japan Office: Asca Corporation, Eiko Ishioka, Fusako Tamura, 1-8-13, Hirano-cho, Chuo-ku, Osaka-shi, Osaka, 541-0046 Japan; +81 (0) 6 6202 6272, FAX +81 (0) 6 6202 6271; asca@os.gulf.or.jp JAPAN NEWS BUREAU: Dennis Normile (contributing correspondent, +81 (0) 3 3391 0630, FAX 81 (0) 3 5936 3531; dnormile@gol.com); CHINA REPRESENTATIVE Hao Xin, + 86 (0) 10 6307 4439 or 6307 3676, FAX +86 (0) 10 6307 4358; haoxin@earthlink.net; SOUTH ASIA Pallava Bagla (contributing correspondent +91 (0) 11 2271 2896; pbagla@vsnl.com); CENTRAL ASIA Richard Stone (+7 3272 6413 35, rstone@aaas.org)

EXECUTIVE PUBLISHER **Alan I. Leshner**
PUBLISHER **Beth Rosner**

Fulfillment & Membership Services (membership@aaas.org) DIRECTOR Marlene Zendell; MANAGER Waylon Butler; SYSTEMS SPECIALIST Andrew Vargo SENIOR SPECIALIST Pat Butler; SPECIALISTS Laurie Baker, Tamara Alfson, Karena Smith

Business Operations and Administration DIRECTOR Deborah Rivera-Wienhold; BUSINESS MANAGER Randy Yi; SENIOR BUSINESS ANALYST Lisa Donovan; BUSINESS ANALYST Jessica Tierney; FINANCIAL ANALYST Farida Yeasmin; RIGHTS AND PERMISSIONS: ADMINISTRATOR Emilie David; ASSOCIATE Elizabeth Sandler; MARKETING: DIRECTOR John Meyers; MEMBERSHIP MARKETING MANAGER Darryl Walter; MARKETING ASSOCIATE Julianne Wielga; RECRUITMENT MARKETING MANAGER Allison Pritchard; ASSOCIATES Mary Ellen Crowley, Amanda Donathen, Catherine Featherston; DIRECTOR OF INTERNATIONAL MARKETING AND RECRUITMENT ADVERTISING Deborah Harris; INTERNATIONAL MARKETING MANAGER Wendy Sturley; MARKETING/MEMBER SERVICES EXECUTIVE: Linda Rusk; JAPAN SALES AND MARKETING MANAGER Jason Hannaford; SITE LICENSE SALES: DIRECTOR Tom Ryan; SALES AND CUSTOMER SERVICE Mehan Dossani, Catherine Holland, Adam Banner, Yaniv Snir; ELECTRONIC MEDIA: INTERNET PRODUCTION MANAGER Lizabeth Harman; ASSISTANT PRODUCTION MANAGER Wendy Stengel; SENIOR PRODUCTION ASSOCIATES Sheila Mackall, Amanda K. Skelton, Lisa Stanford; PRODUCTION ASSOCIATE Nichele Johnston; LEAD APPLICATIONS DEVELOPER Carl Saffell

Product Advertising (science_advertising@aaas.org); MIDWEST Rick Bongiovanni: 330-405-7080, FAX 330-405-7081 • WEST COAST/W. CANADA B. Neil Boylan (Associate Director): 650-964-2266, FAX 650-964-2267 • EAST COAST/E. CANADA Christopher Breslin: 443-512-0330, FAX 443-512-0331 • UK/SCANDINAVIA/FRANCE/ITALY/BELGIUM/NETHERLANDS Andrew Davies (Associate Director): +44 (0)1782 750111, FAX +44 (0) 1782 751999 • GERMANY/SWITZERLAND/AUSTRIA Tracey Peers (Associate Director): +44 (0) 1782 752530, FAX +44 (0) 1782 752531 JAPAN Mashy Yoshikawa: +81 (0) 33235 5961, FAX +81 (0) 33235 5852 ISRAEL Jessica Nachlas +9723 5449123 • TRAFFIC MANAGER Carol Maddox; SALES COORDINATOR Deiandra Simms

Classified Advertising (advertise@sciencecareers.org); U.S.: SALES DIRECTOR Gabrielle Boguslawski: 718-491-1607, FAX 202-289-6742; INTERNET SALES MANAGER Beth Dwyer: 202-326-6534; INSIDE SALES MANAGER Daryl Anderson: 202-326-6543; WEST COAST/MIDWEST Kristine von Zedlitz: 415-956-2531; EAST COAST Jill Downing: 631-580-2445; LINE AD SALES Emnet Tesfaye: 202-326-6740; SENIOR SALES COORDINATOR Erika Bryant; SALES COORDINATORS Rohan Edmonson, Christopher Normile, Joyce Scott, Shirley Young; INTERNATIONAL: SALES MANAGER Tracy Holmes: +44 (0) 1223 326525, FAX +44 (0) 1223 326532; SALES Christina Harrison, Suitlana Barnes; SALES ASSISTANT Helen Moroney; JAPAN: Jason Hannaford: +81 (0) 52 789 1860, FAX +81 (0) 52 789 1861; PRODUCTION: MANAGER Jennifer Rankin; ASSISTANT MANAGER Deborah Tompkins; ASSOCIATE Amy Hardcastle; SENIOR TRAFFICKING ASSOCIATE Christine Hall; SENIOR PUBLICATIONS ASSISTANT Robert Buck; PUBLICATIONS ASSISTANT Natasha Pinol

AAAS Board of Directors RETIRING PRESIDENT, CHAIR Shirley Ann Jackson; PRESIDENT Gilbert S. Omenn; PRESIDENT-ELECT John P. Holdren; TREASURER David E. Shaw; CHIEF EXECUTIVE OFFICER Alan I. Leshner; BOARD Rosina M. Bierbaum; John E. Burris; John E. Dowling; Lynn W. Enquist; Susan M. Fitzpatrick; Richard A. Meserve; Norine E. Noonan; Peter J. Stang; Kathryn D. Sullivan

AAAS
ADVANCING SCIENCE, SERVING SOCIETY

New!
Applied Biosystems 9800 Fast PCR System.

PCR in just 25 minutes.

The 9800 Fast PCR System is the first fully integrated solution delivering fast PCR performance in a standard 96-well format. The system reduces PCR reaction time from two hours to 25 minutes or less—advancing you quickly to the next step of your research. With the fast-optimized system including the 9800 thermal cycler, GeneAmp® reagents, integrated consumables, and world-class technical support, you can count on fast, reliable results. Put your trust in the 9800 Fast PCR System for faster PCR performance—visit http://info.appliedbiosystems.com/**9800**

iScience. Applied Biosystems provides the innovative products, services, and knowledge resources that are enabling new, integrated approaches to scientific discovery.

Applied Biosystems

Research Corporation proudly announces the

2005 Cottrell Scholar Awards

The Cottrell Scholar Award, $100,000 in discretionary funds, is designed to identify early-career faculty who show promise to be future leaders in research, and who are committed to making significant contributions to teaching, especially at the undergraduate level.

"It may well be that not all research faculty can do this simultaneously and early in their careers, but the very best can." - Dr. Jack Pladziewicz, Program Officer, Research Corporation

If you'd like additional information, please visit our website, www.rescorp.org

Research Corporation

a foundation for the advancement of science

Paramjit S. Arora
New York University
Control of protein-protein interactions with artificial alpha helices and innovations in the teaching and implementation of organic chemistry

Pierre Bergeron
University of Montreal
White dwarf stars as cosmochronometers and distance indicators

Helen E. Blackwell
University of Wisconsin, Madison
Regulation of bacterial communication pathways with synthetic ligands

Keith Fagnou
University of Ottawa
Preventing catalyst decomposition and achieving reactivity in the direct arylation and animation of C-H bonds

Boyd M. Goodson
Southern Illinois University at Carbondale
Enhancing NMR signals from biomolecular, organic and polymer thin films using optical nuclear polarization

Chuan He
University of Chicago
A chemical crosslinking method to study DNA repair/modification proteins

Eric W. Hudson
Massachusetts Institute of Technology
Searching for hidden order in exotic superconductors by scanning tunneling microscopy

Zhiqiang Mao
Tulane University
Studies of metamagnetic quantum critical phenomena in ruthenates

Teri W. Odom
Northwestern University
Nanoscaffolds for the growth and manipulation of chemical and biological structures at the single component-level

Chad M. Rienstra
University of Illinois at Urbana-Champaign
Science beyond the limits of diffraction and disciplinary borders: 3D magic-angle spinning NMR and the liberal arts

Gary Shiu
University of Wisconsin, Madison
Connecting string theory to experiment

Thomas Vojta
University of Missouri-Rolla
Disordered electronic quantum phase transitions and an interactive approach to teaching computational physics

Hongcai Zhou
Miami University
Hydrogen storage in novel C-N based porous materials

NetWatch

edited by Mitch Leslie

RESOURCES

Digging Up Weeds

It may look pretty, but the invasive purple loosestrife (*Lythrum salicaria*; right) is the scourge of American wetlands. The immigrant from Europe and Asia is crowding out native species of grasses and sedges and threatening some endangered plants and animals. Although it focuses on one part of the United States, the Southwest Exotic Plant Information Clearinghouse is a good general source of facts about nonnative plants such as purple loosestrife that are growing amok. Sponsored by federal agencies and Northern Arizona University, the database collects backgrounders on more than 300 invasive species, from the common dandelion to the ultracompetitive medusahead grass. Another feature lets users map reports of the species in the Southwest.

www.usgs.nau.edu/SWEPIC/index.html

FUN

In Tune With Physics

To explain relativity, Einstein lectured and wrote books and papers, but he never cut an album. He might have missed an opportunity. Setting physics ideas to music can amplify students' learning and enjoyment, according to Walter Smith, a physics professor at Haverford College in Pennsylvania. Smith's Web site caches lyrics sheets for hundreds of physics tunes, including many compositions he co-wrote. There are also sound files for more than 80 songs and some chord charts so you can play along. Einstein might not have donned lederhosen and yodeled about the speed of light, but other famous physicists have channeled their musical muse. Take the Englishman J. J. Thomson, who discovered the electron in 1897 and penned "Ions Mine" to the tune of "Oh My Darling Clementine":

In the dusty lab'ratory,
'Mid the coils and wax and twine,
There the atoms in their glory,
Ionize and recombine.

www.haverford.edu/physics-astro/songs

RESOURCES

Equation Central

Need the solution for the generalized Abel integral equation of the second kind? Stumped by the FitzHugh-Nagumo equation, which can describe heat transfer and the voltage across a cell membrane? Check out EqWorld, edited by Andrei Polyanin of the Russian Academy of Sciences in Moscow. For hundreds of equations, EqWorld gathers solutions that had been squirreled away in handbooks, journals, and other sources. The site includes ordinary and partial differential equations, integrals, and other types.

eqworld.ipmnet.ru/index.htm

DATABASE

Scanning Species

Many taxonomists want to expedite the often laborious task of identifying specimens by using a unique DNA sequence, or bar code, to recognize each species (*Science*, 18 February, p. 1037). At the Web headquarters of the Barcode of Life Initiative, hosted by the University of Guelph in Canada, visitors can read up on the concept, which proponents are hoping will accelerate the cataloging of Earth's disappearing life forms. The site already holds codes for more than 13,000 animal species. The codes, based on different sequences of the cytochrome *c* oxidase I gene in mitochondria, encompass 260 species of North American birds and a selection of insects, such as the *Halysidota tesselaris* moth (right). Users can compare a bar code from their specimen to the entries in the database. The site will soon add about one-fifth of North American butterflies and moths, says curator Paul Hebert.

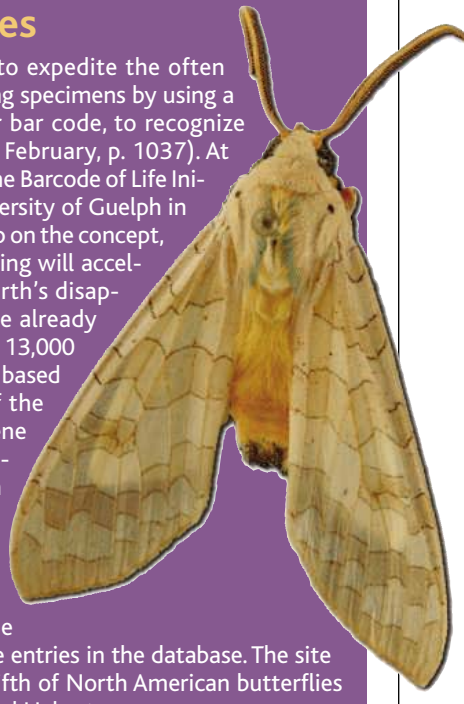

www.barcodinglife.org

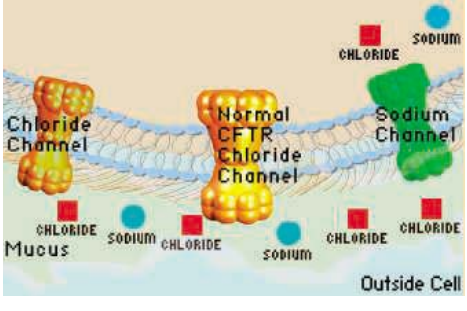

EDUCATION

Genetics Made Clear

From stem cells to gene chips, from prions to cloning, genetics and biotechnology can look forbiddingly complex to high school and lower-division college students. Beginners can ease into these subjects at the Genetic Science Learning Center, a graphics-rich tutorial from the University of Utah in Salt Lake City. Primers step through topics from DNA structure to the different types of stem cells; compared to embryonic stem cells, those from adults so far can't seem to form the same range of tissues. Animations illustrate techniques such as microarray analysis and investigate questions such as how cystic fibrosis upsets the ion balance in lung cells (left).

gslc.genetics.utah.edu

Send site suggestions to netwatch@aaas.org. Archive: www.sciencemag.org/netwatch

CREDITS (TOP TO BOTTOM): ROBERT H. MOHLENBROCK/USDA-NRCS; BIODIVERSITY INSTITUTE/UNIVERSITY OF GUELPH; GENETIC SCIENCE LEARNING CENTER/UNIVERSITY OF UTAH

This Week

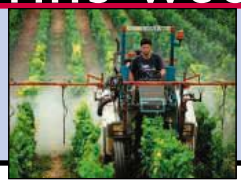

PAGE 1391
Multigenerational endocrine disruption?

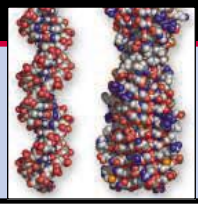

1393
The roots of TB resistance

EMBRYONIC STEM CELLS

Spotlight Shifts to Senate After Historic House Vote

Bone cell researcher Steven Teitelbaum had a brush with history last week as the U.S. House of Representatives weighed in on one of the most dramatic scientific debates in years.

Teitelbaum was on the sidelines, clarifying issues for undecided legislators during the 4-hour debate right up until the 238-to-194 vote in favor of using federal funds to conduct research on newly derived lines of human embryonic stem (ES) cells. "It was a great day," says the former president of the Federation of American Societies for Experimental Biology in Bethesda, Maryland. "This is what our country is all about; it was bipartisan," he told *Science*. The vote, he says, was not a political contest but rather "a contest between us as a society and disease."

Little in biomedical history can match the hot and heavy politicking that has surrounded the stem cell debate, which has evoked people's deepest concerns about suffering and disease, children, and the meaning of human life. President George W. Bush, who declared on 9 August 2001 that only ES cell lines developed before that date could be used in federally funded research, vowed before the vote to use his first veto if the measure passed, saying he opposed "the use of federal money, taxpayers' money, to promote science which destroys life."

Despite that threat, 50 Republicans defied their party leader and voted to allow federally funded scientists to do research with human ES cells derived after 9 August 2001. The primary sponsors, representatives Michael Castle (R–DE) (see next page) and Diana DeGette (D–CO), say they'll keep pushing to turn the bill (H.R. 810) into law. And supporters in the Senate claim to have enough votes to override a presidential veto. But first they'll need the consent of Senate Majority Leader Bill Frist (R–TN) to schedule a vote on the measure.

Stepping up for stem cells. Reps. Castle, DeGette (*at podium*), and Langevin (*seated*) hold a pep rally with patients the day of the House vote.

The day of the 24 May House vote began with crowded press conferences by both supporters and opponents of H.R. 810. The Castle team featured Teitelbaum, from Washington University in St. Louis, and John Gearhart, a stem cell researcher at Johns Hopkins University in Baltimore, Maryland. The opponents countered with 21 "snowflake" babies—the products of embryos "adopted" from fertility clinics—to suggest that even 5-day-old blastocysts are individuals.

Pat White, director of federal relations for the Association of American Universities in Washington, D.C., says pro–stem cell lobbyists conducted a slick "whip" operation before the vote. Patient lobbyists, scientists, and university federal relations people were all over the House on the big day. "We wanted to be in position to have scientists answer any question that came up by any member during the day or during the debate," says White.

Gearhart says a number of members asked him if the frozen embryos mentioned in the bill had ever been inside a womb. Teitelbaum says he thinks his conversation with Representative Jo Ann Emerson (R–MO) may have contributed to her 11th-hour decision to support the bill. Their knowledge served as a counterweight to comments from opponents such as Representative Dave Weldon (R–FL), a physician who erroneously told his supporters before the vote that adult stem cells "have been shown to be pluripotent" and, thus, just as useful as ES cells.

The recent success by Korean scientists has moved up the likely timetable for when nuclear transfer—otherwise known as research cloning—will become a feasible research tool (*Science*, 20 May, p. 1096). Polls show steady increases in public support for human ES cell research. A broad range of patients, politicians, and scientists, including several leaders at the National Institutes of Health, have expressed increasing dissatisfaction with the president's policy as the limitations of existing cell lines—22 of which are available—have become clear.

By omitting any mention of nuclear transfer, the Castle bill managed to attract 201 co-signers, including several opponents of abortion. The measure is aimed solely at allowing federally funded researchers to have access to stem cell lines derived after the presidential cutoff date—provided they come, with proper donor permission, from fertilized eggs that would otherwise be discarded from fertility clinics. The bill would not allow federally funded researchers to actually generate new ES cell lines or to use lines from any embryos created solely for research.

Those restrictions didn't mollify opponents. "Yes, sir. You, too, were an embryo once!" Representative Mike Ferguson (R–NJ) cried rhetorically to the bill's supporters. House Majority Leader Tom DeLay (R–TX), who has been lying low recently amid accusations of ethics improprieties, delivered a fire-breathing speech saying that "we cannot use U.S. taxpayer dollars to destroy" embryos. ▶

Bench strength. Scientists Steven Teitelbaum and John Gearhart answered questions before and during the debate.

CREDITS: MARTY KATZ, 2005

1398
Q&A with Elias Zerhouni

1402
Key roles for citizen-scientists

1404
Hominid reconstructors

Moderate Republican Led the Winning Coalition

Representative Mike Castle (R–DE) has received the lion's share of the credit for getting an up-or-down vote on his bill to expand the pool of human embryonic stem cells available to federally funded researchers. A seven-term member, he's the chair of the House subcommittee on education reform and president of the Republican Main Street Partnership, a centrist group that has championed tort reform and R&D tax credits. Stem cell researcher Steven Teitelbaum of Washington University in St. Louis, Missouri, calls him "one great guy. ... He's a real person: totally unpretentious and smart as a whip."

A former governor of Delaware, the 65-year-old Castle says he got on the stem cell bandwagon half a dozen years ago because of the large number of constituents worried about health issues. He told *Science* he started reading about stem cells and "realized this was probably the greatest hope extant out there" for many of them. He says he had no illusions about the chances of success in an increasingly polarized and conservative House of Representatives. "I knew we would gear up to run hard" with it.

Man of the hour. Representative Mike Castle rallied moderate Republicans behind the bill.

Republican Party leaders were in no hurry to hold a vote on H.R. 810. And proponents didn't want to rock the boat during an election year. But this spring Castle and Representative Diana DeGette (D–CO) decided to make their move. In March, Castle says he sent Speaker Dennis Hastert (R–IL) a message offering a deal, saying that "we were not interested in voting for the budget until such time as we had a date for a [stem cell] vote." After meeting with Castle's delegation, Hastert decided to schedule an up-or-down vote with no strings attached. Castle says he thinks Hastert wanted to remove the specter of the issue cropping up throughout the year in conjunction with other House bills.

Now that his hard work is starting to pay off, Castle says he plans to stick with the issue for as long as it takes. If the Senate passes the bill and the President vetoes it, "you're looking at a wasteland of 3 1/2 years," he says. "I'm not interested in that. ... [Instead] we'll do something."

Castle knows that somewhere down the road looms the question of human cloning. The previous House twice voted to outlaw all forms of cloning, including research cloning (otherwise known as nuclear transfer), which scientists say is necessary to realize the promise of the research. Castle agrees, predicting that nuclear transfer "will at some point probably be essential."

But that battle lies sometime in the future, he says: "I don't think we have to cross that bridge at this moment. ... The moderate cause is advanced one issue at a time." **–C.H.**

Immediately after the vote, the White House repeated the president's intention to veto the bill and broadcast his support for H.R. 2520, which encourages the collection of umbilical cord blood stem cells. That measure passed the House earlier in the day with only one dissenting vote.

The next day, Castle and DeGette ceremoniously handed a copy of their bill, topped with a red bow, to senators Arlen Specter (R–PA) and Tom Harkin (D–IA), sponsors of an identical measure (S. 471). "I've never been enthusiastic about a press conference," says Castle, but this one was an exception.

Opposing views. Representative Mike Pence (R–IN), with "snowflake" babies, speaks against the bill. At left is Rep. Dave Weldon (R–FL).

Although the Senate has generally been more supportive than the House toward ES cell research, getting a public vote may be tougher. Specter's and Harkin's bill has been awaiting action since February, and on the day of the House vote they wrote to Frist urging him to schedule a vote on it. Frist's resistance, say insiders, is fueled not just by his opposition to human ES cell research but also by his presidential ambitions for 2008.

Specter said that an alternative strategy to winning a direct vote would be attaching it to a spending bill. He predicted that the measure would pass by more than the 2:1 margin needed to override a presidential veto (and, along the way, stave off a filibuster). Last year 58 of the body's 100 senators sent a letter to the White House asking for a less restricted stem cell policy, he said, and "20 more are in the wings."

Overriding a veto would be a tall order in the House, however. House Rules Committee chair David Dreier (R–CA), who supported H.R. 810, last week suggested that some kind of compromise might be reached to avoid a presidential veto. But Castle says that "it would be very hard to tighten our bill" by narrowing its scope any further.

White says that the groundwork for last week's victory was laid shortly after Bush announced his policy in 2001 and that supporters now feel the momentum has shifted in their favor. And although Gearhart cautions that the House vote "is very much of a baby step," he is hopeful that an even more decisive Senate vote will make it clear that Bush is out of step with the wishes of the American people.

–CONSTANCE HOLDEN

CREDITS: MARTY KATZ, 2005

NEW ENGLAND BIOLABS

Antarctic Phosphatase

RECOMBINANT AND 100% HEAT LABILE — A BETTER ENZYME THAN SAP AT A BETTER PRICE

For many years, BAP, CIP and SAP were the only options for dephosphorylation protocols. Now, New England Biolabs introduces Antarctic Phosphatase – a superior reagent that saves time because you can ligate without purifying vector DNA, and since it's recombinant, you are guaranteed the quality and value you've grown to expect from New England Biolabs.

To Order:

M0289S ..... 1,000 units ..... $58 ($US)
M0289L ..... 5,000 units ..... $232 ($US)

Advantages:

- 100% heat inactivated in 5 minutes
- ligate without purifying vector DNA
- recombinant enzyme for unsurpassed purity and consistency; no nuclease contamination
- active on DNA, RNA, protein, dNTPs and pyrophosphate
- active on all DNA ends: blunt, 5´ and 3´ overhangs

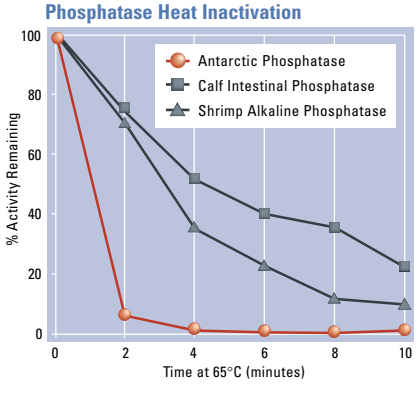

10 units of each phosphatase were incubated under recommended reaction conditions (including DNA) for 30 minutes and then heated at 65°C. Remaining phosphatase activity was measured by p-nitrophenyl-phosphate (pNPP) assay.

PRODUCTS YOU TRUST. TECHNICAL INFORMATION YOU NEED. www.neb.com

- **New England Biolabs Inc.** 32 Tozer Road, Beverly, MA 01915 USA 1-800-NEB-LABS Tel. (978) 927-5054 Fax (978) 921-1350 info@neb.com
- **Canada** Tel. (800) 387-1095 info@ca.neb.com
- **Germany** Tel. 0800/246 5227 info@de.neb.com
- **UK** Tel. (0800) 318486 info@uk.neb.com
- **China** Tel. 010-82378266 beijing@neb-china.com

NEW ENGLAND BioLabs® Inc.
the leader in enzyme technology

DISTRIBUTORS: Argentina (11) 4372 9045; Australia (07) 5594-0299; Belgium (0800)1 9815; Brazil (11) 3622 2320; Czech Rep. 0800 124683; Denmark (39) 56 20 00; Finland (09) 584-121; France (01) 34 60 24 24; Greece (010) 5226547; Hong Kong 2649-9988; India (044) 220 0066; Israel (3) 9021330; Italy (02) 381951; Japan (03) 5820-9408; Korea (02) 556-0311; Malaysia 603-80703101; Mexico 52 5525 5725; Netherlands (033) 495 00 94; Norway 23 17 60 00; Singapore 2731066; Spain 902.20.30.70; Sweden (08) 30 60 10; Switzerland (061) 486 80 80; Taiwan (02) 28802913

DEVELOPMENTAL BIOLOGY

Endocrine Disrupters Trigger Fertility Problems in Multiple Generations

A fungicide and a pesticide, both already known to be toxic to animals, have revealed a potentially even darker side: On page 1466, researchers report that the two chemicals cause fertility defects in male rats that are passed down to nearly every male in subsequent generations. No other known toxin has been shown to do that, according to the study's authors and other scientists. The startling results seem to support the controversial idea that such hormonelike chemicals, known as endocrine disrupters, could be causing population-wide reproductive problems, such as lowered sperm counts in men. But many scientists caution against drawing conclusions until other labs have confirmed the unexpected findings.

"These are remarkable observations. If they're solid and reproducible, they are going to have a large impact on how we look at these kinds of chemicals," says Earl Gray, a toxicologist with the Environmental Protection Agency (EPA). Biologists are stumped by the apparent mechanism of the chemicals; they may alter how genes are expressed in subsequent generations, but without mutating DNA. "It's provocative. But I don't think we have a clue as to what's really happening," says geneticist Robert Braun of the University of Washington, Seattle.

Unfertile ground. The fungicide vinclozolin, which is sprayed on vineyards like these, can cause fertility problems in male offspring of exposed rats.

CREDIT: NIK WHEELER/CORBIS

The work was led by reproductive biologist Michael Skinner of Washington State University, whose lab has been studying vinclozolin, a fungicide used in the wine industry. Vinclozolin blocks cell receptors that are normally activated by the hormone androgen. It is just one of a suite of widely used chemicals, from flame-retardants to ingredients in plastics, that can cause reproductive abnormalities in lab animals. Over the past 15 years, many scientists have come to think that these endocrine disrupters are potentially causing harmful effects, such as cancer and reproductive abnormalities, in humans, too.

It was already known that when pregnant rats are treated with relatively high doses of vinclozolin every day, their male offspring are sterile, Gray notes. But Skinner and his team found that when they injected vinclozolin into the abdomens of pregnant rats during a specific window of pregnancy—8 to 15 days into gestation—they got a different result. Although the offspring's testes appeared normal and the rodents could reproduce, their sperm count dropped 20% compared to control mice, their sperm motility was 25% to 35% lower, and the cells within the testes underwent higher rates of apoptosis—a form of cell death.

The researchers then bred these males with females born to other pregnant rats similarly treated with vinclozolin. To their surprise, more than 90% of males born from these matings had very similar reproductive abnormalities, as did similar numbers in the next two generations. To determine if the male rats inherited the defect from their fathers, they bred a second-generation vinclozolin male—its grandmother had been injected with the fungicide—with a normal female. Their male offspring again had nearly identical sperm and testes defects, whereas a vinclozolin-mother female offspring crossed with a normal male did not. The researchers got similar results when they treated rats with methoxychlor, a pesticide used as a substitute for DDT and whose metabolites include an antiandrogenic compound.

That only male offspring were affected suggested that the two compounds had caused mutations in the male cell's germ line, the cells that give rise to sperm, says Skinner. Radiation can increase the risk of cancer in multiple generations by mutating germ line cells, but it triggers such mutations in a small number of germ line cells, so that only a tiny percentage of offspring are ▶

ScienceScope

Northrop Withdraws as Los Alamos Race Opens

In an unexpected twist, there's now one less competitor for the 7-year contract to run Los Alamos National Laboratory in New Mexico. Northrop Grumman surprised insiders by dropping out of the race last week, despite public assurances that it was serious about a bid (*Science*, 27 May, p. 1244). Northrop's decision came a day before the University of California's Board of Regents voted 11–1 to vie for the management contract, which UC has held since 1943. Congress forced the competition for the $2.2 billion laboratory after persistent management and safety scandals. Although Lockheed Martin and a combined UC-Bechtel team lead the pack, the National Nuclear Security Administration has not said whether other teams are in the hunt.

–ELI KINTISCH

DOE Pushes for Solar Power

Officials at the Department of Energy (DOE) are testing the waters for what some are calling a "Manhattan Project" for solar energy. Despite decades of progress in solar cells and rising gas prices, electricity produced by the devices still costs up to 10 times as much as that produced by fossil fuels. DOE currently spends $10 million to $15 million a year on basic solar energy research, such as efforts to discover novel semiconductors that harvest sunlight more efficiently. If DOE officials get the go-ahead from congressional appropriators, that figure could rise as high as $50 million a year, according to Mary Gress, who manages DOE's photochemistry and radiation research. Officials will preview an upcoming report on solar research next week at a DOE advisory committee meeting.

–ROBERT F. SERVICE

A Lease on Life for SREL?

If the House of Representatives has its way, the Savannah River Ecology Laboratory (SREL) will have a bit more time to fight a White House plan to shutter it. Under that proposal, the $8-million-a-year lab would close on 30 September. Although the measure failed to provide new funds for the lab for 2006, language attached to a House spending bill passed last week would allow the Department of Energy lab to operate until next June using any "available funds." The Senate must now decide whether to appropriate new money for the 54-year-old lab.

–ELI KINTISCH

affected. Moreover, the effect gets smaller with each generation. In contrast, the vinclozolin-induced fertility changes occurred in almost every male rat descended from a treated mother. To Skinner and his colleagues, that suggested an epigenetic mechanism might explain their data.

Although they don't mutate the DNA sequence of an animal, epigenetic changes can be inherited and affect how genes are expressed. One common epigenetic change is the attachment of methyl groups to DNA, which can shut a gene off or turn it on. Indeed, Skinner's group showed that methylation patterns in the testes of affected rats differed from those in control rats. However, they didn't rule out mutation of the animal's DNA sequence, notes epigeneticist Emma Whitelaw of the University of Sydney, Australia. The changes in methylation might simply correlate with the declining fertility, she says: "I'm not sure it's an epigenetic mark."

"We're mostly describing a new phenomenon," acknowledges Skinner. But he is worried nonetheless. "The hazards of environmental toxins are much more pronounced than we realized," he asserts.

Still, according to EPA, the doses used in the experiment were much higher than the exposure levels allowed for people, and Gray says this single study won't change regulations for vinclozolin and similar antiandrogens. For now, "it's going to be very important for other people to look at this," he says. Adds Braun, "It baffles me."

–JOCELYN KAISER

GENETICS

Spliced Gene Determines Objects of Flies' Desire

The male fruit fly is a winged Casanova. He pursues lady flies with a repertoire of song, dance, and well-placed licks that many find impossible to resist. Now, by creating genetically engineered female flies that mimic the male courtship display, researchers have taken important steps toward understanding the biological basis of this complex, instinctive behavior.

In a pair of papers in the 3 June issue of *Cell*, Barry Dickson and colleagues at the Institute of Molecular Biotechnology in Vienna, Austria, report that a gene called *fruitless* (*fru*) sets up the fly brain to produce male courtship behavior in *Drosophila melanogaster*. Female flies altered to use the *fru* gene to make proteins normally made only by males woo other females much as males do. Additional experiments by Dickson's team identify a circuit of neurons in the fly brain that appears to mediate such courtship behavior and sexual orientation.

"I think it's quite remarkable," says Catherine Dulac, a neuroscientist at Harvard University. The work convincingly demonstrates that a single gene can regulate a complex sequence of behaviors, she notes. The team's "very elegant experiments" represent "a start toward understanding how an innate behavior is laid down in a nervous system," says Edward Kravitz, a Harvard neuroethologist.

In the 1960s, scientists discovered that male flies with a mutated *fru* gene become sexually indiscriminate—courting males as well as females. Then, in the mid-1990s, two teams reported that the *fru* gene operates differently in males and females; the cells of each sex read the gene in distinct ways, splicing together different mRNA transcripts. In males, these transcripts produce up to three distinct proteins, whereas the female mRNAs seem to lead to none. The DNA sequence of *fru* suggests that it encodes proteins that regulate the expression of other genes—but no one knows what those genes might be.

Scientists have hypothesized that male *fru* proteins are necessary and sufficient for male courting behavior, but Dickson's paper is the first to show that directly, says Daisuke Yamamoto of Tohoku University in Sendai, Japan, who led one of the teams that discovered the splicing difference.

The key was making very minor modifications to the region of *fru* that is spliced differently in males and females, forcing female flies, for example, to splice the gene as males normally do. Although the sexual anatomy of these females appeared to be entirely normal, their behavior was dramatically altered. They courted other female flies, using all steps of the male courtship ritual, short of attempting copulation. Yet, male flies altered to splice *fru* as females do barely courted at all. Dickson hypothesizes that "behavioral switch genes" like *fru* provide a way to hard-wire adaptive behaviors into the brain so that an animal can perform them instinctively. Still, he and others caution against extrapolating the results to sexual behavior in humans. "Clearly, we are vastly more complicated creatures than flies, and our common experience tells us that our sexual interests are not irreversibly set by our genes," Dickson says.

To investigate how *fru* programs the courtship routine into the fly brain, Dickson's team engineered additional fly strains. In one, a genetic marker identified all of the neurons in male flies that normally express the male-specific mRNAs of *fru*. Many of the labeled neurons appeared to form a circuit. Key elements of this circuit are olfactory neurons that may be specialized for pheromone detection. Inactivating these cells abolished courtship behavior in male flies, Dickson's team found. Somewhat puzzlingly, the researchers also found a similar circuit of neurons in female flies. This suggests to Dickson that courtship behavior depends not on anatomical differences between the male and female brain but rather on how this circuit functions.

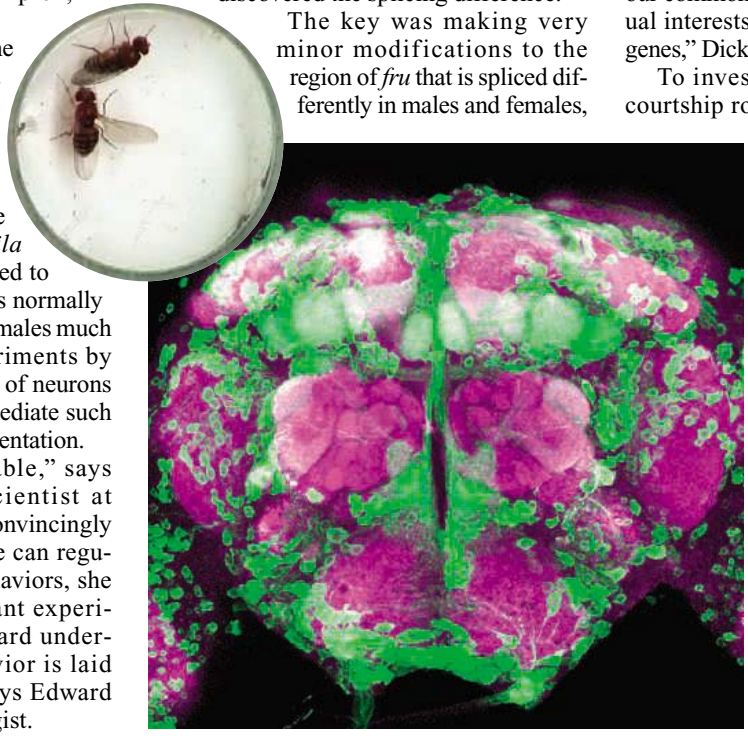

Going courtin'. Spliced the right way, *fru* establishes a "courtship" circuit of neurons (green) in the male fly brain and makes females court other females (*inset*).

Kravitz suspects that *fru* may also be involved in other instinctive behaviors that differ between the sexes—a possibility he will be investigating with a visiting postdoc from the Dickson lab. "We're pretty sure these same genes are involved in whether flies fight like males or females," he says. If so, *fru* may turn out to make male fruit flies fighters as well as lovers.

–GREG MILLER

CREDITS (TOP TO BOTTOM): E. DEMIR AND B. J. DICKSON, *CELL* **121**, 5 (2005); PETRA STOCKINGER

BIOCHEMISTRY

Protein That Mimics DNA Helps Tuberculosis Bacteria Resist Antibiotics

If imitation is the sincerest form of flattery, nature just paid DNA a big compliment. A novel protein that helps the tuberculosis bacterium resist antibiotics shares an uncanny resemblance to DNA, researchers report on page 1480. This resistance protein represents an entirely new way for bacteria to ward off antibiotics; it is also the first of a class of proteins that may play a key role in regulating bacterial growth. "It's a fascinating way to become resistant," says biochemist Gerry Wright of McMaster University in Hamilton, Canada. "This is really quite new and cool."

Biochemist John Blanchard of Albert Einstein College of Medicine in New York City and his colleagues happened on the protein while probing for new mechanisms of tuberculosis antibiotic resistance. Working on *Mycobacterium smegmatis*, a cousin of *M. tuberculosis*, coauthor Howard Takiff, now at the Venezuelan Institute of Scientific Investigations in Caracas, isolated a gene that helped the bacterium to withstand fluoroquinolone antibiotics. Dubbed *mfpA*, the gene, also found in the tuberculosis bacterium, encoded an unusual protein composed almost entirely of end-to-end repeats of five amino acid segments ending in leucine or phenylalanine.

Blanchard's postdocs Subray Hegde and Matthew Vetting then spent more than 2 years trying to purify and crystallize enough MfpA protein to determine its atomic structure. The researchers ultimately found that the five amino acid repeats in the sequence coil around in a rod-shaped, right-handed helix just about the width of DNA. One side of the protein has a strong negative charge, also like DNA. "It's so rare when you look at a structure, and the function of the protein just jumps out at you," Blanchard says.

From the protein's structure, the team could deduce how it confers fluoroquinolone resistance. It's long been known that cells compact long lengths of DNA by twisting the entire double helix, much as a phone cord folds up on itself when it's twisted too tight. The enzyme that performs that reaction in bacteria, gyrase, grabs hold of two segments of DNA, cuts one, passes the other through, and then reseals the cut segment. Fluoroquinolones bind to that gyrase-DNA complex, tricking the bacterial enzyme into chopping but not resealing the DNA, which kills the microbe.

Computer modeling showed that the MfpA protein could lie across the saddle-shaped active site of gyrase, just as DNA is thought to do. In test-tube experiments, the researchers showed that MfpA blocks gyrase's ability to twist and untwist DNA. By binding to gyrase in DNA's place, MfpA apparently deprives fluoroquinolones of their target; the drugs bind to gyrase-DNA complexes rather than to just the enzyme. MfpA's inhibition of gyrase function probably slows the bacteria down, but it's better than being killed by fluoroquinolones, Blanchard says.

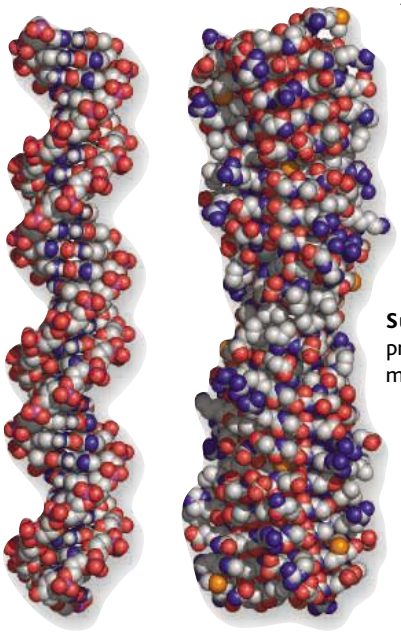

Surprise twin. A bacterial protein (*right*) has a structure much like that of DNA (*left*).

This is the first antibiotic-resistance protein that protects the target of the antibiotic by binding to it rather than, say, by degrading the drug, says Wright. Still, MfpA's public health impact is unclear. Fluoroquinolone-resistant tuberculosis strains isolated from people don't seem to depend on MfpA; they have mutations in gyrase itself.

It may be possible to turn the tables on bacteria by engineering MfpA to kill germs rather than protect them, researchers note. MfpA inhibits gyrase, which a bacterium needs in the long run to replicate its DNA and proliferate. "If I'm a clever chemist and I could build a small molecule that looks like that, then I have a new class of antibiotics," Wright says.

Fluoroquinolones are a relatively recent invention, so what is *mfpA* doing in bacteria in the first place? Related genes have been found in numerous bacteria, fruit flies, mice, and humans. Blanchard speculates that DNA-mimicking proteins could provide a general mechanism to regulate proteins that bind DNA. "The biology is extraordinarily rich and completely unknown," he says. "Who knows where it's going."

–DAN FERBER

CREDIT: COURTESY OF MATTHEW VETTING

ScienceScope

Non on E.U. Constitution

PARIS—France's rejection of the European Constitution last Sunday will have little immediate impact on European science policy, experts say. The proposed constitution, which was expected to face another defeat in the Netherlands this week, contained few new science provisions. And the ambitious, 7-year Framework Programme, proposed in April (*Science*, 15 April, p. 342), is based on the existing E.U. treaty, points out Peter Tindemans, a spokesperson for EuroScience. But in the long run, says former French science minister Claude Allègre, the vote will hamper attempts to create a more open, competitive research landscape. He adds that a cabinet reshuffle announced in the wake of the defeat seems set to further delay the long-awaited science reform bill in France.

–MARTIN ENSERINK

Italians Face Vote on Embryo Research

Dozens of Italian scientists are staging a 7-day hunger strike in an effort to persuade fellow citizens to vote in an upcoming referendum on fertility treatments and embryo research. On 12 and 13 June, Italians will have a chance to strike down four provisions in Italy's current law, including a ban on research on embryos created by in vitro fertilization that prevents scientists from deriving new human embryonic stem (hES) cell lines. Press coverage has been "very, very biased" and has left the impression that adult stem cell research makes work with hES cells unnecessary, says medical historian Gilberto Corbellini of the University of Rome, who helped launch the hunger strike campaign. If public participation doesn't top 50%, the referendum will be invalid, and opponents, including Catholic Church leaders, who say the research is immoral, are encouraging people not to vote.

–GRETCHEN VOGEL

Shakeup at SLAC

Administrators at the Stanford Linear Accelerator Center (SLAC) have reorganized the laboratory, a first step in a planned shift in focus away from high-energy physics (*Science*, 1 April, p. 38). Among other changes, Keith Hodgson, former director of SLAC's synchrotron laboratory, has been named the head of a new Photon Science division, which will concentrate on the basic energy sciences end of SLAC's portfolio. Physicist Persis Drell will head the new Particle and Particle Astrophysics Division, which will focus on high-energy physics at SLAC.

–CHARLES SEIFE

PUBLIC HEALTH

Europe's New Disease Investigator Faces an Uphill Start

PARIS—Europe finally has a watchdog for infectious diseases, but it is only beginning to sniff out its territory. Public health experts applaud the inauguration of the new European Centre for Disease Prevention and Control (ECDC) in Stockholm last week. Many say, however, that the new E.U. agency, led by Hungarian health administrator Zsuzsanna Jakab, will have to overcome formidable obstacles to become a significant player in Europe's fractured public health structure.

Working from a temporary site—the agency will move to the Karolinska Institute's campus later—Jakab has been hiring researchers and technical staff since March. Their key task: to develop a Europe-wide system of disease surveillance, risk assessment, and early warning. They will also advise countries on public health issues.

There's broad agreement that coordination is needed. Currently, information about the spread of diseases flows through a myriad of networks at institutes across the continent, but no central agency collects and analyzes the data. ECDC "is a sign that we understand the importance of surveillance," says Tamsin Rose, secretary-general of the European Public Health Association in Brussels.

Public health is traditionally an area of authority that countries are loath to relinquish. ECDC will have to build scientific credibility—"it can't be seen as an annex of bureaucrats in Brussels," says Marc Sprenger, who chairs the ECDC management board—even though doing so will be a challenge with a staff of about 100 and a $29 million budget by 2007. (By comparison, the $7 billion U.S. Centers for Disease Control and Prevention employs over 9000.) The agency will not have its own labs; instead, it will gather data by coordinating work across Europe, Jakab says: "We won't go around taking blood or urine samples."

It will be vital to get good, specialized labs as partners, says virologist Albert Osterhaus of Erasmus Medical Center in Rotterdam, the Netherlands. But ECDC will have to avoid duplicating structures such as the global influenza network to coordinated by the World Health Organization. "Nobody is interested in yet more meetings," says Osterhaus.

Because ECDC will have no labs, it may have difficulty recruiting top-notch scientists, notes Ragnar Norrby, director of the Swedish Institute for Infectious Disease Control, who helped lure the new center to Stockholm. Norrby has proposed that some ECDC staff use facilities at his own institute or at Karolinska. Jakab says she's interested in the idea. But interest in ECDC jobs has been healthy so far, Sprenger says.

Jakab has a symbolic role, too: She is the first national from one of the 10 states that joined the E.U. in 2004 to head an agency. Norrby says she is efficient and diplomatic—traits that should help her put ECDC on the map quickly. And she will need to do just that: The agency faces a review in 2007 that will determine whether it is succeeding and will continue to grow.

–MARTIN ENSERINK

EVOLUTION POLITICS

Is Holland Becoming the Kansas of Europe?

AMSTERDAM—Well, not quite Kansas—after all, this is the country that legalized euthanasia and invented gay marriage. But when science and education minister Maria van der Hoeven recently announced plans to stimulate an academic debate about "intelligent design" (ID)—the movement that believes only the existence of a creator can explain the astonishing complexity of the living world—she triggered an uproar not unlike that raging in the sunflower state.

Prominent biologists have denounced Van der Hoeven, a member of the Christian-Democratic Party and a Catholic, for blurring the line between church and state. Last week, she faced a barrage of hostile questions in the House of Representatives of the Dutch Parliament, where she was compared to the Kansas school board members who want to introduce ID in the classroom. "Does she want to go back to the Dark Ages?" the usually sober daily *NRC Handelsblad* lamented in an editorial. The minister has called the issue a "storm in a teacup" and claims she has been misunderstood.

Van der Hoeven's plan came to light in March, after she had what she called a "fascinating conversation" with Cees Dekker, a renowned nanophysicist at Delft University of Technology who believes that the idea of design in nature is "almost inescapable." ID could be a tool to promote dialogue between the religions, Van der Hoeven wrote in her Web log that week: "What unites Muslims, Jews, and Christians is the notion that there is a creator. … If we succeed in connecting scientists from different religions, it might even be applied in schools and lessons. A few of my civil servants will talk further with Dekker about how to shape this debate."

Showing her hand. Dutch science minister Van der Hoeven wants a debate about ID.

Except for a plan to hold a hearing about evolution and religion at her department in the fall, Van der Hoeven has issued few details about what she has in mind; instead, she has mostly been defending herself. In Parliament last week, the minister said she isn't a supporter of ID and isn't planning to impose or ban anything. But she insisted that she has the right and the duty to stimulate debates. (Van der Hoeven declined to be interviewed.)

That doesn't convince the scientists who have scolded her. "It's not a minister's job to get involved in biology," says biochemist Piet Borst, a former director of the Netherlands Cancer Institute. Vigilance is important, he adds: "Even in Holland, there are plenty of people ready to castrate Darwin." Borst has declined an invitation to the hearing, as has geneticist Ronald Plasterk, who heads the Hubrecht Laboratory in Utrecht. "I think Kansas has made us all a bit more sensitive," says Plasterk.

Dekker says he's puzzled by the outcry but chalks it up to a "Pavlov reaction" to ID. "Many scientists associate it with conservative Christians, Kansas, and George Bush—so it has to be bad," he says. He hopes the debate will get more serious after the impending publication of a collection of 22 essays about ID and related themes, most of them by Dutch scientists, which he has co-edited. Van der Hoeven has agreed to receive the first copy of the book at a ceremony in The Hague next week.

Meanwhile, Van der Hoeven's initiative is welcomed in the real Kansas. Says managing director John Calvert of the Intelligent Design Network in Shawnee Mission: "I think it's a dynamite idea."

–MARTIN ENSERINK

CREDIT: MINISTRY OF EDUCATION, CULTURE, AND SCIENCES

U.S. FUSION RESEARCH

With Domestic Program at Issue, House Votes to Hold Up Funding for ITER

The Department of Energy (DOE) has jousted with Congress for years over how to fund the U.S. share of the International Thermonuclear Experimental Reactor (ITER). Now some key members of Congress want to take the project hostage until the White House lays out a funding plan that covers both ITER and domestic fusion research.

Although the 2006 budget proposed by the White House would increase fusion research spending by 17%, to $291 million, it gouges U.S. projects while pledging $50 million for the nascent ITER. Last week, the House of Representatives restored the domestic money as part of a $3.7 billion budget for DOE's Office of Science. But it held up the 2006 ITER funds until March 2007, 5 months after the start of the fiscal year, and threatened to cut the funds in future spending bills. An amendment went a step further, preventing the United States from agreeing to join the $5 billion plasma reactor effort until that date.

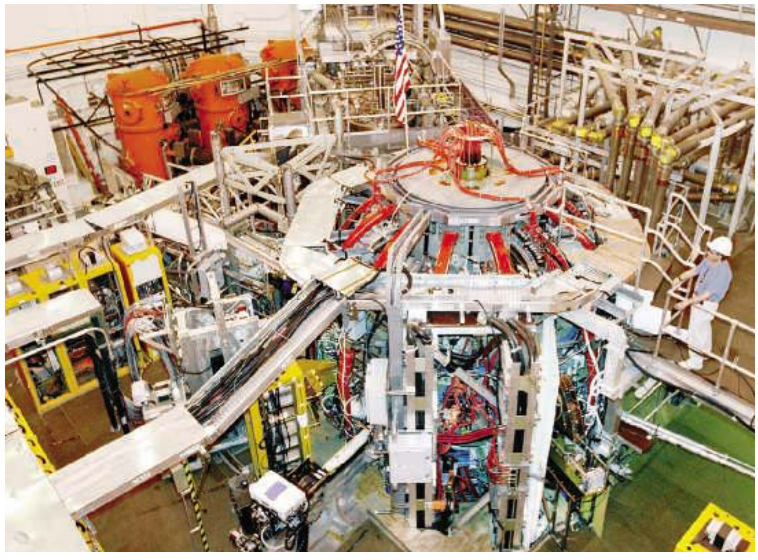

Defused. DOE's proposed 2006 budget for fusion contains no money to run the National Spherical Torus Experiment at Princeton.

House Science Committee Chair Sherwood Boehlert (R–NY), who introduced the delaying amendment, said its purpose is to force DOE to reveal "how we're going to pay for ITER before we sign on the dotted line." Other lawmakers, aware that yearly U.S. commitments to ITER are due to peak at $208 million by 2009, hope that the move pushes the White House into providing new funds for the entire field. Funding for domestic fusion research has been on the decline since 1995.

Run times at fusion facilities in Boston, San Diego, California, and Princeton, New Jersey—all of which, like ITER, use the well-developed, doughnutlike "tokamak" shape to hold plasma—would be cut by two-thirds under the president's budget. The cuts would also starve research into promising but less developed plasma-containment methods, say legislators.

DOE officials declined comment on the congressional move, although in March, Ray Orbach, head of the Office of Science, testified that he's trying to "reorient the domestic program toward ITER." Boehlert, for his part, said last week that the Administration tradeoff strategy "makes sense."

Cadarache, France, appears to have won the race to host the six-partner ITER project (*Science*, 13 May, p. 934), and it seems unlikely that the latest congressional move will affect final negotiations between the European Union and Japan over the location. Scientists at JET, the fusion reactor near Oxford, U.K., believe the U.S. dithering is "no big deal," according to a lab spokesperson, because the United States is slated to fund only 10% of the project's cost. Richard Hazeltine, chair of DOE's advisory board on fusion, says he feels Congress was justified in taking such harsh steps, although he is "uncomfortable" with the tactics.

The House action revives the possibility that the United States could repeat its 1997 decision to leave ITER, a project it helped launch 2 decades ago and then rejoined in 2003. "It will be important for us to be part of it," says Stephen Dean of Fusion Power Associates in Gaithersburg, Maryland, but not at the expense of domestic work. And will U.S. scientists utilize ITER if their government fails to help build it? "[S]omehow or another, we'll participate," Dean predicts.

The debate now moves to the Senate, which last year agreed in conference to reverse proposed cuts for domestic fusion work.

–ELI KINTISCH

SCIENTIFIC PUBLICATION

HHS Asks *PNAS* to Pull Bioterrorism Paper

In an unprecedented move, officials at the Department of Health and Human Services (HHS) asked the *Proceedings of the National Academy of Sciences* (*PNAS*) to pull a bioterrorism-related paper that the journal planned to publish online on 30 May. The journal took the paper off its publication schedule and was reviewing it internally when this issue of *Science* went to press.

The paper, by mathematician Lawrence Wein of Stanford University and graduate student Yifan Lu, models how bioterrorists could wreak havoc by slipping a small amount of botulinum toxin into the U.S. milk supply, and it spells out interventions that the government and the dairy industry could take to prevent this nightmare scenario.

Stewart Simonson, HHS's assistant secretary for public health emergency preparedness, acknowledges that the idea of using botulinum as a bioweapon has already been widely discussed. "It's not the concept itself; you can't control everything," says Simonson. "It is the granularity of the detail." Wein, concerned about harming the chances that *PNAS* will eventually publish his paper, declined to discuss publicly HHS's request or the journal's interaction with him. On 30 May, however, *The New York Times* published an opinion piece by Wein—which the newspaper had accepted before *PNAS* decided to hold the report—that described the study in some detail.

PNAS highlighted the paper in its weekly tip sheet sent to journalists on 25 May and also made an embargoed draft available. Simonson—whose office had received an earlier draft from Wein months before—says the *PNAS* paper first came to his attention the following evening. The next morning, he sent a letter to Bruce Alberts, president of the National Academy of Sciences, the journal's publisher, asking *PNAS* not to publish the paper. Later that day, *PNAS* sent an e-mail to reporters that publication of the paper had been delayed, simply noting that a new publication date will be announced. "We made a request," says Simonson. "There wasn't anything coercive."

Simonson recognizes that the flap will probably draw more attention to the paper than it otherwise might have received. "We thought about that," he says, "but it's a balance, and it struck us as the right thing to do."

–JON COHEN

CREDIT: PRINCETON PLASMA PHYSICS LABORATORY

eppendorf PhysioCare Concept criteria 5 and 6

- 50% less force
- Colorcoding system
- Comfortable fit
- Ergonomics approved by TÜV

Fantastic fit.

Intuitive operation – Minimal user exertion

PhysioCare Concept pipettes.
Our new pipettes requires up to 50 % less force to operate than similar pipettes on the market.
With our new color coding system you achieve quick and easy identification. The easy to grip handle and well placed operating buttons ensure comfortable fit.

TÜV Rheinland approved our manual pipettes as: ergonomic, user-friendly and user tested.

PhysioCare concept

Check out how good your pipette really is!
PhysioCare Concept™ website
www.physiocare-concept.info

eppendorf

In touch with life

Your local distributor: www.eppendorf.com/worldwide · Application Hotline: +49 180-3 66 67 89
Eppendorf AG · Germany · +49 40 538 01-0 • Eppendorf North America, Inc. 800-645-3050

U.S. IMMIGRATION POLICY

Law Leads to Degrees But Not Jobs in Texas

Iride Gramajo's dream of becoming a mathematics professor has always been a long shot. Growing up on a coffee plantation in Guatemala, she didn't have access to a good school. And even after she slipped into Texas illegally with her family in 1995, a college education was unthinkable on her mother's salary as a nanny. But a 2001 state law allowing illegal immigrants to pay in-state tuition rates made it possible for her to attend the University of Houston. And this spring she earned her B.S. degree and was accepted into Houston's doctoral program in mathematics.

So far, so good. But despite their talents, undocumented residents like Gramajo and her classmates stand no chance of being hired by a reputable U.S. institution or company. In fact, it will take an act of Congress for Gramajo to work in her chosen profession. And that's exactly what a bipartisan group of senators hopes will happen this year.

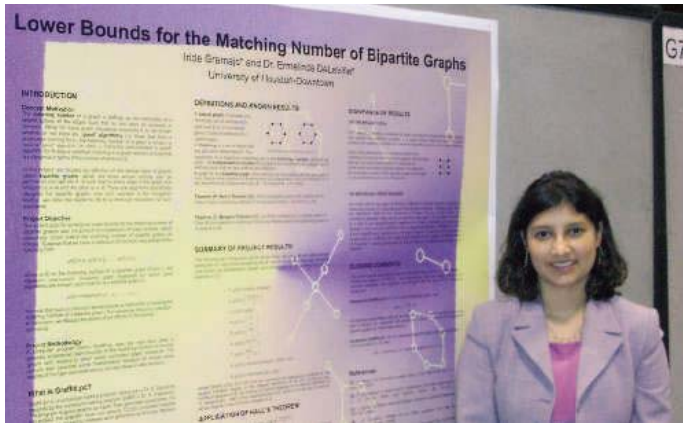

Long road. Iride Gramajo is counting on the DREAM Act to help her become a mathematics professor.

Gramajo is one of an estimated 90 undocumented students graduating this year from public 4-year colleges and universities in Texas, with another 1200 in the state's community colleges. And their numbers will only increase: Since 2001, eight other states have passed their own in-state tuition laws making higher education more affordable to immigrants lacking proper documentation.

But granting them legal residency, which would allow them to work lawfully in the United States, is a federal matter. That's why senators Orrin Hatch (R–UT) and Richard Durbin (D–IL) are hoping that their Development, Relief, and Education for Alien Minors (DREAM) Act will become part of a comprehensive immigration reform bill that Congress is expected to take up later this year. "These students should not be penalized for having an immigration status for which they are not responsible," says Adam Elggren, a Hatch aide. Instead, says Elggren, "we should be welcoming them to become productive members of our society."

The DREAM Act would put undocumented college students on the path to citizenship by qualifying them for a green card, which would enable them to join the nation's workforce in science, engineering, and other occupations. "It seems like a huge waste to tell them in the end that they cannot contribute to the economy," says an aide to Texas representative Rick Noriega (D–Houston), who helped write the state law.

But others say that giving them amnesty would snatch employment opportunities away from U.S. citizens and serve as an incentive for illegal immigration. "It would be a statement to the world that we have no intention of enforcing immigration laws," says U.S. Senator Jeffrey Sessions (R–AL). A better alternative, says Jack Martin of the Federation for American Immigration Reform (FAIR) in Washington, D.C., would be for undocumented students to "return to their native countries and apply their education there."

That logic is bewildering to Carlos Hernandez, a petroleum engineer graduating from the University of Texas (UT), Austin, who says he played no role in his family's decision to move to the United States from Mexico when he was 9. When he was in high school his father, a construction worker, and his mother, a waitress, took him to a career fair in Houston where UT officials told him about the university's perfect record of placing petroleum engineering grads. "If I got permission to work in the United States, it would not be a reward for illegal immigration but for the 4 years of effort I put in to become an engineer," says Hernandez. Although he's applied to work at Mexican companies, he'll most likely end up pursuing graduate studies at UT.

Gramajo says she is optimistic that the DREAM Act will pass before she receives her doctorate. "My mentors have told me that there's a high demand for math professors in the U.S., so much so that universities have to hire faculty from Europe and Asia," she says. "That gives me hope of being able to work here."

–YUDHIJIT BHATTACHARJEE

CREDIT: I. LAFLAQUIS

ACADEMIC POLITICS

Boycott of Israeli Universities Overturned

CAMBRIDGE, U.K.—Buffeted by international criticism, the U.K. Association of University Teachers (AUT) has revoked a decision to boycott two Israeli universities. The boycott was approved at AUT's annual meeting in April and called on members to shun Bar Ilan University in Ramat-Gan because of its ties with a school in a contested settlement, and the University of Haifa for alleged harassment of a lecturer who oversaw a study critical of the Israeli military (*Science*, 29 April, p. 613). Haifa University denied the allegation and threatened to sue AUT for defamation.

Scholarly institutions quickly issued statements denouncing AUT on grounds that such boycotts violate academic freedom and are counterproductive. Among those who asked AUT to reconsider were the U.S. National Academy of Sciences, the New York Academy of Sciences, AAAS (which publishes *Science*), and the U.K.'s Royal Society.

AUT members also protested. A group of 25 petitioned for a special meeting to reconsider the boycott, which they claimed had not been fully debated. Roughly 250 attended a meeting on 27 May at which two-thirds voted to overturn the resolution. They also asked AUT to review its international policies, including a call to the European Union to withhold funding from Israeli organizations "until Israel opens meaningful negotiations with the Palestinians."

"We are relieved that this counterproductive [boycott] policy has been overwhelmingly rejected," says sociologist David Hirsh of Goldsmiths College in London, co-founder of Emerge, a campaign set up to oppose the boycott.

Some who urged sanctions on Israel say the vote hasn't changed their plans, however: "The boycott remains," says one of the leaders, neurobiologist Steven Rose of the Open University in Milton Keynes, U.K., who will continue to honor it. But AUT is taking a different tack. The group's general secretary, Sally Hunt, said in a statement, "It is now time … to commit to supporting trade unionists in Israel and Palestine working for peace."

–MASON INMAN

The director of the National Institutes of Health looks back at 3 years on the job and how much more needs to be done

Elias Zerhouni: Taking Stock

When radiologist Elias Zerhouni took the helm of the National Institutes of Health (NIH) 3 years ago, he thought that steering the now-$28.4-billion institute to slower budget growth after a 5-year doubling would be his biggest challenge. The former research dean at Johns Hopkins University in Baltimore, Maryland, seemed like the right fit for an agency in need of tighter fiscal management. And his first major initiative—a $2 billion research "Roadmap" that brought together NIH's 27 institutes and centers—won kudos from Congress and the biomedical community.

Within months, however, political interference from the Bush Administration and congressional objections to grants involving sexual research signaled that the honeymoon was over. And since December 2003, NIH has been rocked by a scandal over drug company consulting payments to its scientists (*Science*, 19 December 2003, p. 2046). A 1995 relaxation of limits on consulting put in place by Zerhouni's predecessor, Harold Varmus, led to problems with some intramural researchers who either didn't report outside income or received approved payments that raised ethical questions. Yet his solution—a ban on most paid consulting and strict limits on stock ownership—has been equally controversial (*Science*, 11 February, p. 824). Even his boss, Department of Health and Human Services Secretary Michael Leavitt, has suggested that it be revised.

Last week, in a visit to the Washington, D.C., offices of *Science*, Zerhouni reflected on how he's dealt with these and other controversies. He also used the opportunity to explain his surprising decision last month to cancel a Roadmap competition for translational centers, designed to move new treatments into the clinic, after deciding that initiative wasn't sufficiently "transforming," and to describe fundamental changes he wants to encourage in academic medical centers.

–JOCELYN KAISER

Here are excerpts from the 25 May interview:

What led to the new rules on conflict of interest?

All universities have established these central conflict-of-interest committees where peer faculty look at the issues. … If you have any contractual relationship with an outside entity, the contract itself needs to be reviewed by a central committee. NIH had no process for that. … Every institute [had] 17 different ways of managing ethics. All the ethics [was] done between the ethics officer and the scientist. … Not only that, but we had no data on exactly how much money was being collected, by whom, and in what form.

Was the decision to relax the rules in 1995 a mistake?

Maybe [it was] justified in the general sense of saying we need to recruit and retain [good scientists]. But I think people should have realized this was a vulnerable way to do business. To not have any sense of who was doing what in a world that has changed a lot in terms of outside activities. … The way it was managed—don't ask, don't tell, let it be, no peer review, no disclosure of the amounts, there was nothing.

What adjustments are you now making to the interim ethics rule?

I think a [stock] divestiture for everybody is a good prophylactic rule for a regulatory agency like the FDA. … [But] I don't think it's as good a rule for an agency that doesn't have many employees who have a direct and predictable effect on [regulations]. … The other thing that I find problematic is [that] everything's banned unless you get an exception, including [activities with] the trade associations and professional associations. I find that to be restrictive of the normal academic exchange that needs to occur.

Do people need to take a look at the rules in academia?

I don't think we can equate our rules. … It's apples and oranges, because you have that fundamental public service conflict-of-interest definition that does not apply to an extramural person who receives a grant that covers only 20% of your funding and that you have to compete for every 5 years. …

Preserving science is, I think, a discussion that we need to have. Is it okay to be on the payroll of the marketing department [of a drug company] and to make thousands of dollars going to medical meetings and saying, 'I'm a scientist, I'm very trusted, I'll tell you what, this drug is better than this drug'? The trading of scientific credibility units for dollars for a marketing or promotional goal is something that we need to talk about. … We are seeing a very worrisome trend in the trust factor of science, especially when it comes to human subjects science.

The president says he will veto a law that would expand the stem cell lines. Have you briefed the president since 2001 on this issue?

Yes. What I've told in public is what I tell him in private. So the White House is completely aware of all of the aspects of the scientific evolution of the field. … But it's a morally and ethically based decision, it's not a scientifically based decision.

Are the restrictions now limiting scientists?

If you say, "Can you do all of the science that scientists would like to do with 22 cell lines?," the answer is no. What is it that you couldn't do? Well, you could certainly not look at genetically deficient lines that have a genetic defect of one kind or another …

CREDIT: MARTY KATZ

[or in some cases] different stages of maturation of the cell line.

Are you concerned that the U.S. will fall behind other countries?
On both sides of this debate, I see a lot of hyperbole. I think that if you look at our investment, we invest $520 million [per year] at NIH in all [adult and embryonic stem cell research]. … Nobody comes close to that. … Most of the papers published are U.S. papers. … I really believe that with the combination of federal, and private, and state funding, I can't see the U.S. falling behind.

How well have you explained to the public what it got from doubling NIH's budget?
I think we've made enormous progress. You go to Congress, I travel around the country—the Roadmap, I'm amazed, actually, about how people get it. … This year, we're one of two agencies that did not get a cut [in the president's budget]. And as meager as the [0.7%] increase is, it came in the context of a 2% decrease in domestic spending.

Are you concerned about falling grant success rates?
We look at two things. We look at success rate per application and success rate per investigator. And the success rate per investigator is higher than the success rate per application. [But the trend] is not good. Whenever you go at a flat [budget] level, you're not going to keep that. The optimal support for principal investigators is really what's of great interest to me. And that's why I want to make a special effort for young investigators, to preserve their potential.

What have you been telling the community about translational and clinical research?
This topic has been talked about for the last 20 years. … If you look at the past 10 years, we've spent almost $6 billion on translational training, if you combine GCRCs [General Clinical Research Centers], the K12 [training grants], and all of the awards, and they haven't transformed anything. …

We want to challenge the community to put together real academic homes for translational science and for clinical science. Where, A, you can have a joint appointment, [and] B, you can really train in what you need to train in translational science. … And it needs degree-granting programs, it needs graduate programs, it needs postdocs. …

"We are seeing a very worrisome trend in the trust factor of science, especially when it comes to human subjects science."

If the institution is interested and they want to get a fusion reaction, we will supplement that. … Let's stimulate institutions to come forward with innovative ways of truly supporting what I think is just as much of a discipline that requires rigor, that requires a faculty that's dedicated to it, and is not just a service to companies. Because it is the hardest field of science to go into. It's much easier to go into basic science or clinical science. It's so hard because you don't really publish 10 papers a year, what you do is often a failure, as you can see from pharmaceutical research.

But this is not something you can do in 1 year. This is going to take 10 years, 15 years. If you look at transformations like this in academic life, if you look at molecular biology departments, the first started [around] 1955, and it took about 25 years for the transformation to occur.

The National Cancer Institute has set a goal of eliminating suffering and death from cancer by 2015. Is that realistic?
All goals are goals: something you strive for. And I think [NCI] firmly believes that this is a way to energize their field, to really go toward a—not eliminating cancer, but making cancer a chronic disease. That's what [NCI Director] Dr. von Eschenbach will tell you. That's really what the idea of doing that is, to sort of project the need for a measurable endpoint.

NIH hasn't been very visible in the debate over intelligent design.
Why would it? Why do you think NIH should be visible in that debate? … Nobody has asked NIH what our position is, [although] I think we've made it very clear.

Are you concerned that if the intelligent design movement really takes off in schools and colleges across the country, it will be harder to get the biologists the country needs?
I am very concerned about it. And I don't think it's a good direction. I think we should continue to teach science based on facts and experiments and provable hypotheses.

Have you encouraged the president to speak about the issue?
I think he has enough problems of his own. I don't think that it's come up. I'm not the creationism adviser.

What do you want your legacy at NIH to be?
I tell you, the last thing I expected was to clean up an ethics mess. I don't want to be associated with that for posterity. …

I had the guts to challenge the organization, to challenge institutes, to change the governance. It is an internal revolution, to truly lower the barriers to adaptation and make the agency more nimble. I've been able to recruit top-notch directors. I have two vacancies right now. I've been able to preserve NIH in a rocky time. Remember, we were challenged by Congress on the sex grants. I responded very forcefully to them. I think defending science is going to be important as we go into these cultural, political times.



CREDITS: MARTY KATZ

WIN A $250 GIFT CHEQUE!

Download the conference brochure by August 1 at www.drugdisc.com/us and you will automatically entered in the American Express Gift Cheque drawing.

Optimizing the Discovery & Development Interface to *Improve Productivity*

Enhance Safety & Efficacy

Develop New Business

Explore New Markets

10th Anniversary DRUG DISCOVERY TECHNOLOGY® & Development

Keynote Sessions

Lester M. Crawford, D.V.M., Ph.D.
Acting Commissioner, FDA

John L. LaMattina, Ph.D.
President, Pfizer Global R&D

Keynote Panel Discussion

Exploring the Industry and Regulatory Interface in Drug Development

Moderator:

Robert R. Ruffolo, Jr., Ph.D.
President, R&D, Wyeth

The Boston Convention & Exhibition Center, Boston, MA

Conference: **August 8-11, 2005**

Exhibition: **August 9-11, 2005**

Visit www.drugdisc.com/us

- ✔ Review the 150+ conference session options
- ✔ Create a customized schedule
- ✔ Participate in an industry survey & "quiz"
- ✔ Download the brochure & enter the drawing

Presidential Sponsors:

Executive Sponsor:

Supporting Publications:

Association Sponsor:

Massachusetts Biotechnology Council

Organized by:

Reading Ancient DNA the Community Way

COLD SPRING HARBOR, NEW YORK—At the Biology of Genomes meeting here, 11 to 15 May, genomicists reported on past as well as future genomes.

There's a reason *Jurassic Park* is in the fiction aisle. Extracting and sequencing ancient DNA has proved difficult and controversial, in a large part because it is likely to be contaminated with DNA from a host of organisms that have come in contact with the fossilized source over the millennia—not to mention DNA from the humans trying to extract it.

But at the Cold Spring Harbor meeting, James Noonan and Edward Rubin of Lawrence Berkeley National Laboratory in Berkeley, California, presented a new way to distinguish ancient DNA from that of more recent hangers-on. And they reported that they successfully used the method to sequence nuclear genes of cave bears from the Pleistocene epoch. (Their work is also published online by *Science* this week; see www.sciencemag.org/cgi/content/abstract/1113485). Next, they hope to use this so-called paleometagenomics technique to decipher Neandertal DNA.

As DNA in fossils ages, it falls apart; water and other chemicals degrade the molecules. That makes it an extreme challenge to interpret any changes seen in a fossil's DNA. "One of the key issues is disentangling the evolutionary changes from DNA degradation," says Stephen Brown, a mouse geneticist at the Medical Research Council in Harwell, U.K.

Microbes colonizing bone and the surrounding soil also leave behind their genes, which greatly complicates isolating the DNA belonging to a skeleton. "It's really been a hurdle" to get clean, decipherable samples, says Rubin.

His and Noonan's brute-force solution: Take whatever DNA the fossil contains, sequence it all, and then use comparative genomics to pull out the DNA of interest. "In some ways, we are looking for a needle in a haystack," Rubin explains. "But in this case, we have a magnet." That magnet is already-sequenced DNA from related, living organisms.

For their first foray into paleometagenomics, he and Noonan, a postdoctoral fellow, worked with Svante Pääbo and Michael Hofreiter of the Max Planck Institute for Evolutionary Anthropology in Jena, Germany. They studied bones from two extinct 40,000-year-old cave bears. Weighing a ton, these ancient bears (*Ursus spelaeus*) made grizzlies seem puny. But they were gentle giants, and before the last ice age, they lumbered throughout Europe, feasting primarily on berries, honey, and grass and passing time in caves, where their fossilized bones remain today.

The researchers chose *U. spelaeus* because its fossils are plentiful and because the bear bones are about as old as Neandertal material, thus providing DNA as degraded as one would see when looking at bones of the hominid. Bears offered another advantage, compared to fossil humans: Any DNA contamination from the researchers themselves would be quite apparent.

Once Noonan sequenced all the DNA samples from the bear fossils, he looked for any sequences that resembled canine DNA; dog genomes are about 93% the same as a bear's. Noonan found that about 6% of the total fossil DNA resembled the dog's. That small fraction was expected, says Rubin, given that microorganisms had thousands of years to settle in and around the bear bones. Indeed, "we found a lot of [DNA] matches to dirt [microbes]," Rubin reported.

Even though they had only fragments of *U. spelaeus* DNA sequences, he and Noonan matched many of them up with a modern bear's genetic sequence and came up with 27,000 bases of real bear material. The DNA of the fossil and extant animals was 98% the same.

Rubin and Noonan were also able to match the fossil DNA up against dog genes. And when they used the fossil DNA to build a bear family tree, the cave bear fit in right with black bears, grizzly bears, and polar bears. "The study serves as a proof of principle for the Neandertal Metagenome Project," says Rubin.

Piecing together Neandertal DNA could shed light on how closely related they were to humans or whether breeding between them and modern humans occurred, says Peter Little, a geneticist at the University of New South Wales in Sydney, Australia. Still, he has reservations about the new approach, noting that Neandertals are likely to be only as different genetically from modern humans as individuals are from each other. Making sure identified base differences are real, and not the result of degradation, will be key, Wales notes: "But if they can do it, it's going to be great."

CREDIT: KENNIS & KENNIS

Gentle giant. Ancient-DNA sequencing strategy has passed its first test on lost cave bears.

Extinct Genome Under Construction

The chromosomes of animals from the distant past may be long gone, but that hasn't stopped bioinformaticists from trying to reconstruct what that old DNA looked like. At the meeting, collaborators from two laboratories—those of David Haussler of the University of California, Santa Cruz, and Webb Miller, a computer scientist at Pennsylvania State University, University Park—described how they analyzed DNA sequence data from living placental mammals, including humans, dogs, mice, and rats, to trace the ancient evolution of individual bases in those animals. Miller's lab already has a rough idea of what one chromosome looked liked in the

animals' common ancestor, which lived an estimated 100 million years ago, and the two groups hope to know the sequence of its entire genome by the end of the year.

Once they have determined the sequence of the "mother" of all placental mammal genomes, researchers should be able to make evolutionary sense of the genetic differences between species, especially as the data stream in from the more than a dozen vertebrate genomes now slated for partial sequencing. "Reconstructing mammalian sequence to the base [level]—this is amazing," says Francis Collins, director of the National Human Genome Research Institute (NHGRI) in Bethesda, Maryland.

Haussler and Miller focused on placental mammals because the various subgroups alive today arose at basically the same time, from a shrewlike ancestor. The rapid subsequent evolution of these groups makes it easier to verify base changes through time. In contrast, determining the ancestral genome of all mammals would be much more difficult, if not impossible, because marsupials and monotremes branched off at very different times, making DNA comparisons less reliable.

The approach Haussler, Miller, and their colleagues took resembles that of molecular evolutionists, who for decades have used DNA differences to build evolutionary trees. Typically, those researchers focus on one gene, such as that for a ribosomal RNA. They count the number and type of base changes in that gene: The more changes between two species, the more distant the kinship. Those DNA bases shared by all the species under consideration likely represent ancestral ones.

With new computer programs and sophisticated simulations of genome evolution, Haussler's and Miller's groups have taken this approach considerably further by looking across the whole genome and not just at one gene. The computers search among the DNA of many species for common sequences in large stretches of chromosomes and then check individual bases for changes in each species. The group validated the accuracy of the reconstructed genome by crosschecking the simulations with phylogenetic trees derived from modern DNA.

Last year, Haussler's postdoctoral fellow Mathieu Blanchette, now at McGill University in Montreal, Canada, did a test run analyzing a 1-million-base piece of chromosome 7, the region that contains the cystic fibrosis gene, from 19 placental mammals. The simulations indicated the ancestral sequence of that region is about 98% right.

Miller's graduate student Jian Ma has now taken on the task of reconstructing a much bigger chunk of DNA, the ancestral chromosome 15. Although it remains fairly intact in some living mammals, in others it has become quite chopped up and redistributed. In both mice and rats, this ancient DNA is now scattered among five chromosomes, she reported. In humans, however, most of the sequence of the reconstructed ancestral chromosome 15 now appears to make up one arm of human chromosome 13. In dogs, it's divided up between chromosomes 22 and 25.

Mother mammal. *Eomaia scansoria* gave rise to placental mammals.

These whole-chromosome studies include just nine placental species, leading Blanchette to estimate that the ancestral chromosome 15 is only about 90% accurate. But that percentage will improve, says Ma: "The more species we have, the more accuracy we can get."

Robert Waterston, a geneticist at the University of Washington, Seattle, believes the goal of rebuilding the entire genome within a year is achievable. "[They] will be able to reconstruct most of it," he predicts. Researchers will then be able to work from these reconstructed chromosomes to determine how long a particular base has been part of the human genome and how it has changed, says Haussler. Geneticists will also learn more about how chromosomes evolve, says Waterston: "It provides a chance to think about genome evolution systematically and to look at all that's happened." —ELIZABETH PENNISI

Ornithology

Citizen Scientists Supplement Work of Cornell Researchers

A half-century of interaction with bird watchers has evolved into a robust and growing collaboration between volunteers and a leading ornithology lab

BOYCE, VIRGINIA—On a sunny April morning, Kaycee Lichter has driven 32 kilometers to the Virginia State Arboretum here in the Shenandoah Valley to meet her friend Greg Baruffi. Walking to the edge of a meadow, the two open a box containing a bluebird nest and place an electronic device no larger than a coat button under the five eggs inside. The button will record the fluctuating temperature inside the nest as the female bluebird departs and returns periodically in search of food. In 3 days, Lichter and Baruffi will download the data to a computer and reset the button.

Lichter, 46, is a medical transcriptionist at a nearby mental health clinic and Baruffi, 50, is a carpenter. They are not scientists, but their work is crucial to a study by researchers at the Cornell Lab of Ornithology in Ithaca, New York, of whether birds lay fewer eggs in cooler climates because of the energy costs of incubation. The results could provide insights into how environmental factors affect the number of hatchlings in a brood.

Over the past decade, Cornell has harnessed the enthusiasm of such volunteers—or citizen scientists, as they are known—to explore questions such as the dynamics of infectious disease in bird populations and the impact of acid rain on their reproductive success. Those efforts have resulted in a long list of peer-reviewed publications, demonstrating the value of citizen science as a research tool. "Having an army of assistants on the ground allows you to ask questions that require simultaneous observation across

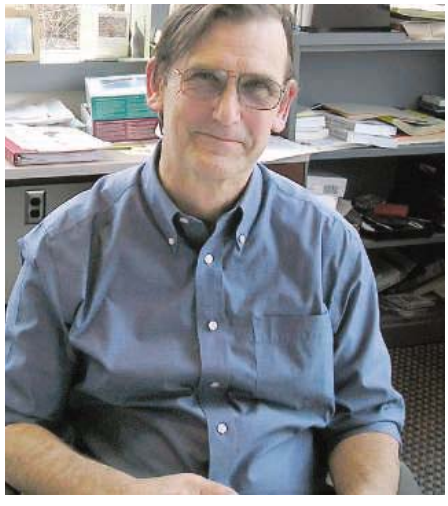

Group think. Cornell's Andre Dhondt says a volunteer network allows him to ask large-scale ecological questions.

CREDITS (TOP TO BOTTOM): MARK A. KLINGLER/CMNH; Y. BHATTACHARJEE/*SCIENCE*

large spatial and temporal scales," says Andre Dhondt, an ecologist at Cornell. "It opens up a world of scientific possibilities."

Nobody has pursued those possibilities as seriously and successfully as Dhondt and his colleagues at Cornell. "There are 15 million citizens in the U.S. alone who spend untold amounts of time and money on bird watching. The Lab of Ornithology has capitalized on this public interest to produce some very good science," says Peter Marra, an ecologist at the Smithsonian Environmental Research Center in Edgewater, Maryland. Cornell has even created an endowed professorship dedicated to citizen science—the first position of its kind in the country—that it hopes to fill this year.

Helping hands

Cornell's tradition of engaging citizens in bird studies dates to the 1950s, when lab founder Arthur Allen conducted informal Monday evening seminars to raise public awareness about ornithology. At those sessions, Allen would read out a list of birds and ask for a show of hands indicating how many people in the audience had sighted each species. He logged the results of the weekly poll in a register, providing a rough picture of the relative abundance of different birds over time.

Decades later, lab researchers thumbing through those registers wondered if they could get volunteers to be more scientific. That idea led to Project Tanager, a large-scale experiment begun in 1994 to study the impact of forest fragmentation on tanager populations and their nesting success. Over 3 years, nearly 1500 volunteers around the country took a census of four tanager species—often by playing taped calls supplied by the lab—and recorded signs of predation in their nests. Researchers found that tanagers in fragmented habitats were more likely to thrive in regions that had a high percentage of forest cover.

Volunteers also played a key role in helping scientists understand an epidemic of conjunctivitis among house finches in the mid-1990s. Following up on sightings in Maryland of finches with red, crusty eyes, Dhondt printed and distributed 60,000 computer-scannable forms to 9000 volunteers to record daily sightings of both healthy and sick birds. Within months, researchers had documented the spread of the disease across the Northeast and Midwest.

"The speed at which we were able to track the epidemic was simply amazing; we couldn't have dreamed of doing it without a volunteer network," says Dhondt. Over the next 5 years, more data revealed patterns showing seasonal and geographical variations in the spread of the disease. In 2000, Dhondt and his colleagues used those data to win a $2.4 million grant from the National Institutes of Health and the National Science Foundation (NSF) under a joint program on the ecology of infectious diseases. The team developed predictive models of the spread of aerially transmitted bacterial diseases.

The grant marked a coming of age for Cornell's citizen science efforts, which had previously been supported through NSF's informal science education program. Dhondt says NSF reviewers had rejected earlier proposals because of doubts that volunteer-generated data could be trusted. But the publications from the house finch survey "countered that skepticism effectively," says NSF program director Samuel Scheiner.

Cornell researchers have also studied the reliability of citizen scientists. During the pilot phase of Project Tanager, for example, ornithologist Ken Rosenberg and his colleagues compared observations made by volunteers to data collected by researchers themselves. At 17 of the 19 sites where this comparison was made, the data were identical. "Volunteers are extra-careful because they aren't professionally trained," says Rosenberg. "They doubt themselves."

By using statistical tools to look at broad patterns, the Cornell researchers are able to detect and discard individual data points that appear suspect. And although there are differences between volunteers in their ability to see and hear birds, "the variation tends to be random," says ecologist Wesley Hochachka. "The larger the data set, the greater the chances of detecting a signal."

Even so, Cornell researchers face constant reminders that volunteers are not trained scientists. Dhondt remembers a lament from one despondent volunteer in Quebec, who wrote him that "I've been reporting for 48 months, and I've yet to see a sick house finch." Dhondt used his reply as an instructional tool. "Your data are so valuable," Dhondt wrote back. "As soon as you have seen your feeder and recorded your observation, you've made your contribution. Not seeing birds is biologically important information."

Fieldworkers. Citizen scientists Kaycee Lichter and Greg Baruffi of Virginia devote up to 15 hours a week to Cornell-based projects.

The lab thinks citizen scientists are capable of even more sophisticated observations. For example, Stefan Hames is using volunteers to investigate the mechanism by which acid rain affects wood thrush populations. The protocol asks them to soak a square piece of cardboard in unchlorinated water and place it on a patch of earth covered with twigs and fallen leaves. The next day they record the number of snails and other invertebrates found under the cardboard. Eating these calcium-rich animals helps the birds lay eggs with secure shells. Knowing that acid rain takes a toll on these invertebrates, Hames and his colleagues hope to find out whether the scarcity of calcium-rich prey explains the decline of wood thrushes at sites with high levels of acid rain.

The lab also hopes to expand its network of volunteers. "Right now, the northeastern seaboard is well covered," says lab director John Fitzpatrick. "We'd like more observers on the ground in states like Arizona and Nevada. Eventually, we'd like to test hypotheses and conduct experiments on a continental scale."

–YUDHIJIT BHATTACHARJEE

CREDIT: Y. BHATTACHARJEE/*SCIENCE*

Building Virtual Hominids: Musical Duo Reconstructs Ancient Fossils

Researchers team up professionally and personally to perfect the art of putting distorted fossils back together in the computer

ZURICH, SWITZERLAND—By the time anthropologist Marcia Ponce de León and neurobiologist Christoph Zollikofer received permission to analyze the famous Le Moustier Neandertal skull, it was in bad shape. Uncovered in France's Dordogne region in 1908 by an amateur archaeologist, the specimen is still the most complete adolescent Neandertal skeleton known. But during the first 2 decades after the find, researchers made numerous crude attempts to reconstruct the fragmented skull, using glue and varnish to put it together and take it apart again at least five times and damaging and losing some pieces in the process. During World War II, the cranium, housed in a Berlin museum, was thought to have been destroyed in a bombing raid, but it eventually turned up again. In recent decades, curators at Berlin's Museum for Pre- and Early History have wisely refused requests by scientists to have yet another go at it.

In 1995, however, the museum allowed Ponce de León and Zollikofer to take the skull to their shared office at the University of Zurich and dismantle and reassemble it once again. But they didn't use glue or varnish. Instead the pair scanned the fragile cranium, now a patchwork of several dozen fragments, using high-resolution computed tomography (CT). Then they used a specialized computer graphics program they had developed, along with their own formidable knowledge of human anatomy, to electronically isolate each fragment and recreate missing ones. They were able to put the entire long-abused cranium back together inside the computer, unveiling a complete skull that could be analyzed and compared to other specimens.

This study was one of the first in a series of high-profile projects carried out by Zollikofer and Ponce de León, the acknowledged leaders in computer-aided fossil reconstructions. The pair, who share personal and professional lives, are in ever-increasing demand by researchers the world over who seek to extract the maximum information from rare and often fragmentary and distorted hominid fossils. "They have raised the art of reconstructing fossil material to the level of a science," says Harvard University anthropologist Daniel Lieberman.

Most recently, they reconstructed the skull of *Sahelanthropus tchadensis*, claimed to be the oldest member of the human lineage, in collaboration with discoverer Michel Brunet of the University of Poitiers, France, Lieberman, and others. The team uncovered new evidence that *Sahelanthropus* was not a gorilla ancestor, as some had argued, and that it was bipedal, a basic requirement for hominid status (*Science*, 8 April, p. 179). "For virtual reconstruction, they are the best in the world," says Brunet, who packed up his priceless skull and took it to Zurich for scanning because Ponce de León and Zollikofer do not work on casts.

Virtual realists. Christoph Zollikofer and Marcia Ponce de León.

"Their work shows up with increasing frequency and has had a growing impact," says Harvard paleoanthropologist David Pilbeam. "More and more researchers want them to 'dedistort' their finds." The pair has become a regular fixture at top anthropology meetings, where the tall, soft-spoken Zollikofer and the petite, intense Ponce de León are invariably seated together.

Making music

The paths that led Ponce de León and Zollikofer to the small office and laboratory they now share in the University of Zurich's Anthropological Institute followed very different trajectories. Ponce de León, 48, was born in La Paz, Bolivia, where she studied civil engineering and was also a serious piano student. In the mid-1980s she moved to Zurich, entered the university there, and switched to biology. In 2000, she received a Ph.D. in anthropology, focusing on Neandertal development.

Zollikofer, 47, was born and raised in Zurich. Although he showed an early interest in the sciences, his greatest passion was music, and he long planned a career playing cello. He took up biology at the University of Zurich but then studied cello at a Zurich musical conservatory for 3 years before returning to the university for his Ph.D. studies on the locomotion of desert ants. The ants "run incredibly fast, about 1 meter per second," says Zollikofer. "And when they really get going, they raise up on their hind legs. That's how I got interested in bipedality," he says with a smile.

Even after receiving his doctorate in neurobiology in 1988, Zollikofer continued to vacillate between science and music, teaching at the university while playing professionally in a local orchestra. "That's when Marcia came on the scene," he says. The two met when Ponce de León took an undergraduate neurobiology course he was teaching. Yet both agree that at first it was a shared love of music, not science, that brought them together. "We would play together and go to concerts," Ponce de León says. Adds Zollikofer admiringly: "She knew all of the cello suites of [Johann Sebastian] Bach."

The turning point in both their careers came in 1990 when Ponce de León urged Zollikofer to attend a university seminar she was taking from computer graphics pioneer Peter Stucki. The pair realized that computer graphics could help solve the problems that plague interpretation of hominid fossils. "The fossils are usually incomplete and deformed and often encrusted with sediments," explains Zollikofer. Ponce de León, who spent countless frustrating hours trying to measure casts of *Homo erectus* for her master's degree, adds that conventional methods of analyzing skulls and other fossils rely on taking measurements of the distances between two fixed points. "You can't get information about the three-dimensional shape of a fossil this way," she says.

CREDIT: COURTESY OF M. PONCE DE LEÓN AND C. ZOLLIKOFER

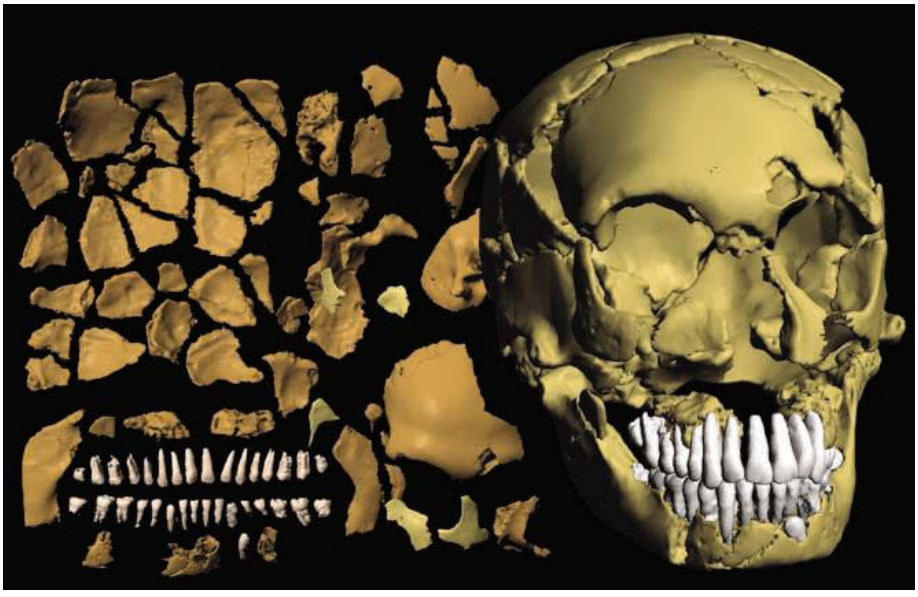

Sum of its parts. The Le Moustier Neandertal before and after its computerized reconstruction.

The pair landed two grants from the Swiss National Science Foundation to develop a prototype of the computer program they use today, which they named FoRM-IT (Fossil Reconstruction and Morphometry Interactive Toolkit). But the grants paid them both only part-time salaries. To raise funds, they began building three-dimensional plastic models for local doctors preparing to do surgery on patients with facial deformities. The models, based on CT scans, use a computer-guided laser beam to polymerize liquid resin into an exact model of a skull. "We raised more than $100,000 making those models," says Ponce de León. The model-building, which they call "real virtuality," later came in handy as a way of doing reality checks on their computerized reconstructions and is now an integral part of their reconstruction process.

Paleoanthropologist Robert Martin, director of the Anthropological Institute at the time and now provost of the Field Museum in Chicago, Illinois, says it is no surprise that Ponce de León and Zollikofer were able to turn their nascent ideas into virtual reality. "I was struck by Marcia's originality and her striking ease with quantitative concepts," says Martin. "And Christoph was outstandingly brilliant."

No more calipers

The pair made their first big splash with FoRM-IT in 1995, when they published a short paper in *Nature* detailing their reconstruction of the skull of a 3- or 4-year-old Neandertal child found in Gibraltar. From five existing fragments, Ponce de León and Zollikofer recreated the entire skull and also solved a long-standing debate about whether the fragments represented one child or two. Earlier researchers had noted that the apparent state of eruption of the teeth suggested an older child, whereas the development of the skull's inner ear region seemed younger. But the reconstruction showed that the pieces of the skull made a precise fit, meaning that it belonged to only one individual—and that the teeth of Neandertal children erupted earlier than those of modern humans.

This conclusion led the two onto a whole new research track: the study of Neandertal growth and development. They analyzed the Le Moustier skull and then compared virtual reconstructions of Neandertal skulls ranging from babies to adults to those of modern humans of similar ages. In each reconstruction, they used anatomical points of reference called landmarks to measure the shapes of three-dimensional objects rather than two-dimensional measurements. Human origins experts say that although a number of researchers now use landmark analysis, the combination of landmark analysis with virtual reconstruction has put Ponce de León and Zollikofer on the cutting edge of physical anthropology. "Just 8 or 10 years ago we were still using calipers" to measure the distances between points on skulls, says paleoanthropologist Chris Stringer of the Natural History Museum in London. "We were getting only a very poor measure of the three-dimensional shapes." Stringer adds that unlike virtual reconstructions, which can be scaled up or down and compared directly on a computer screen, these older techniques made it very difficult to compare "a very big skull with a very small skull"—comparisons essential to tracking development as well as to understanding the relationships among different-sized species.

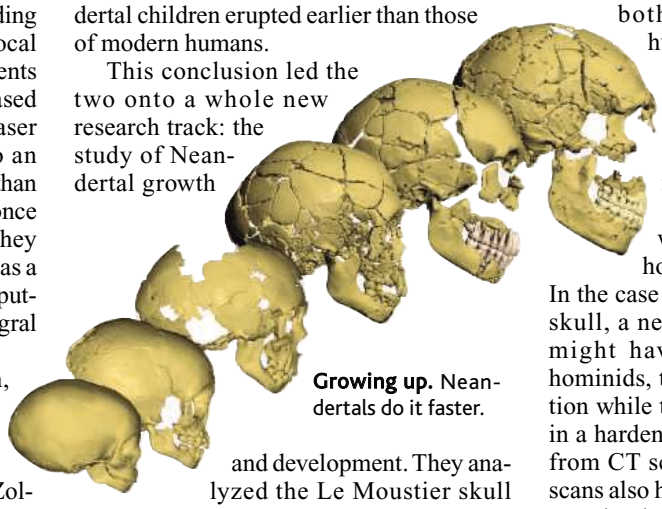

Growing up. Neandertals do it faster.

Ponce de León and Zollikofer developed new mathematical techniques to make it easier to use landmark analysis to follow the growth of different parts of the skull at the same time. Recently, after studying specimens of all ages, they concluded that the notable differences in skull and jaw shape between Neandertals and modern humans arise very early during development, possibly even before birth—thus making it more likely that they represent different species. "Their work demonstrates more clearly than anyone else's that the ontogeny of Neandertals and modern humans is different from as early an age as we can document," says Lieberman. Stringer agrees: "They have made a wonderful contribution; … we now have a much clearer view of the developmental and evolutionary processes that produce both Neandertals and modern humans."

In addition to the Neandertal work, Zollikofer and Ponce de León have also been called in to reconstruct a series of 1.8-million-year-old hominid skulls found at Dmanisi, Georgia, which represent the first known hominid migration out of Africa. In the case of the most recently discovered skull, a nearly toothless individual who might have been cared for by other hominids, the pair began their reconstruction while the cranium was still embedded in a hardened block of sediments, working from CT scans of the entire block. These scans also helped the Dmanisi team to excavate the skull without damaging it. "Both of them are unassuming, collegial, and unfailingly helpful," says Dmanisi team leader and Georgian National Museum general director David Lordkipanidze. "You rarely meet people so dedicated to our profession."

Although they are often called in to solve such technical problems, Ponce de León says that gaining new insights into ancient hominids is what matters most to them. "A lot of researchers think that we are technical or methods people," she says. "But this is not true. We only developed these methods so that we could carry out the research we want to do."

–MICHAEL BALTER

CREDITS: M. PONCE DE LEÓN AND C. ZOLLIKOFER

Random Samples

Edited by Constance Holden

Arms and the Man

Swinging swords around for hours on end left its mark on the bones of Medieval soldiers. In fact, their right arms resemble those of baseball pitchers, according to researchers at the University of Bradford in the U.K.

Forceful, repetitive movements make bones bend and thicken in response to the stress. So anthropologists Jill Rhodes and Christopher Knusel reasoned that Medieval swordplay should have produced skeletal distortions. They looked at the excavated skeletons of 10 men who had died of sword wounds between the 10th and 16th centuries. The right arms showed changes in shape and thickness similar to those found in professional baseball pitchers, Knusel says. "Swinging a sword is very, very similar [to pitching]. It's an overhead type of motion," he says. The changes weren't seen in nine uninjured male skeletons in the same York cemetery, they reported in last month's *American Journal of Physical Anthropology*.

The authors also reported on 13 skeletons buried in a mass grave after the Battle of Towton in 1461. These men showed different changes: Their left arms were bent and thickened. Knusel says the skeletons may be the bones of archers who held their powerful longbows with their left arms.

Kelly DeVries, a specialist in Medieval military history at Loyola College in Baltimore, Maryland, says this technique should be useful in the emerging study of battlefield archaeology. It could help sort out the archers from the swordsmen, or the knights from the casual soldiers, he says.

Color: In the Eye of the Beholder?

Humans everywhere appear to recognize the same six basic colors—black, white, red, yellow, green, and blue—regardless of their language, according to new research.

Some scientists think color perceptions are shaped by language because cultures divvy them up in different ways: In some New Guinea tongues, for example, there are just two color groups (light and dark), whereas other languages have more than a dozen. Some languages don't distinguish between blue and green.

Linguist Paul Kay of the International Computer Science Institute in Berkeley, California, and colleagues tested people's color sense by asking 2700 speakers of 110 different languages to name and sort 330 differently colored chips, grouping them according to color terms they knew and then picking the best examples of each category. The subjects tended to gravitate to the six colors regardless of the categories used in their languages, suggesting that people classify color according to universal visual principles, the researchers reported online last week in the *Proceedings of the National Academy of Sciences*.

But Debi Roberson, a psychologist at the University of Essex in the United Kingdom, says that doesn't end the debate. There were many exceptions, she says, and there wouldn't be if colors were truly universal.

A Puzzling Protist

The biggest example yet of a single-celled foraminiferan has been found in 100-million-year-old marine rocks

near the coast of northern California. Foraminiferans are members of the protist family: hard-shelled relatives of the amoeba. Most are microscopic or nearly so. But some taxa, which exist today in deep-sea environments, can grow to a relatively colossal size.

This latest find beats them all. The fossil shell is 143 millimeters long, and the live protist may have been as large as 175 mm. Micropaleontologist William Miller of Humboldt State University in Arcata, California, says it's still a puzzle how and why this species (*Bathysiphon aaltoi*) got so big. It grows by building a hard tubular shell from particles such as sand and sponge spines lying around on the seabed. In the current issue of the journal *Neues Jarhbuch für Geologie und Paläontologie Monatshefte*, Miller, whose team found the specimen last year, suggests that it must have had unique adaptations not shared with other protists, such as multiple nuclei to cope with the business of sporting such a large shell.

CREDITS (TOP TO BOTTOM): CAROLINE D. NEEDHAM; WILLIAM MILLER

Where the Winds Are

Two Stanford University researchers have put together a global "wind map" that pinpoints areas around the globe that are well suited for wind power. After analyzing wind speed measurements in some 8000 locations, hydrologists Cristina Archer and Mark Jacobson conclude that wind could generate power equivalent to 35 times current global electricity use.

Good locations are far more common than previously thought, says Archer. "If you randomly pick 10 locations in the world, one or two of them will be suitable for wind power generation," she claims. Two such areas are the south and southeast coasts of the United States. Northern Europe also has a lot of prime wind spots. Unfortunately, the authors relate, the developing world has few such spots. Exceptions are some sites in Vietnam, the Caribbean islands, and the southern tips of Chile and South Africa.

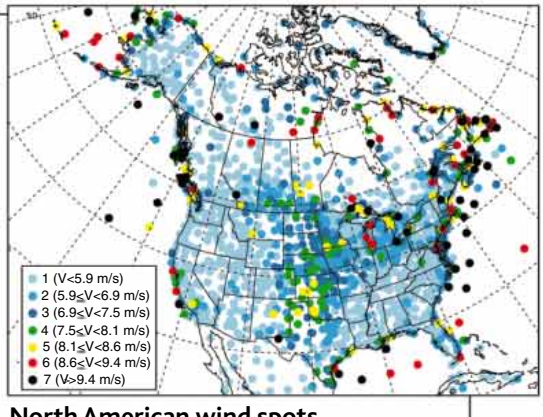

North American wind spots.

Edited by Yudhijit Bhattacharjee

JOBS

Googling the universe. The challenge of scanning the heavens with a powerful telescope has lured a top computer expert from Google. Wayne Rosing, vice president of engineering at the Internet search engine, has left the company after 4 years to work as an unpaid adviser on the proposed Large Synoptic Survey Telescope (LSST) project at the University of California, Davis.

The telescope will use its 8.4-meter mirror to sweep the entire visible sky every three nights searching for signs of hidden dark matter and transient objects such as asteroids and gamma ray bursts. Managing its 30 terabytes of data each night poses a "wonderful engineering problem" similar to what his team faced at Google, says Rosing. He will help devise data-analysis strategies for LSST's scientists and engineers.

"The sheer boldness and scale of this project is just extraordinary," says Rosing, 58, who was captivated by the telescope's potential after meeting its director, J. Anthony Tyson. In years past, Rosing designed and constructed a robotic camera for an ongoing sky survey based in Chile and founded the Las Cumbres Observatory near Santa Barbara, California, for astronomy education and outreach.

Who's left? The start of a second presidential term is traditionally a time for job reshuffling. But the past 6 months have seen an unusually high turnover rate at the White House Office of Science and Technology Policy (OSTP), with five senior managers moving to greener pastures.

The two most recent departures, announced last week, involve new postings for long-time government hands. Neuroscientist Kathie Olsen (right), associate director for science since 2001, has been nominated to be deputy director of the National Science Foundation (NSF). She would replace engineer Joseph Bordogna, who came to NSF in 1991. And astronomer William Jeffrey (above), who has handled national and homeland security issues for the past 3 years, has been tapped to head the National Institute of Standards and Technology. NIST has had an acting director since Arden Bement moved to NSF in February 2004.

Olsen's shop has recently lost two veteran civil servants. Rachel Levinson left this spring to set up a Washington, D.C., office for Arizona State University's new Biodesign Institute. And Cliff Gabriel decamped in January for the Environmental Protection Agency. Likewise, Brett Alexander, who handled space issues, left in January to handle government relations for the start-up Transformational Space Corp. in Reston, Virginia.

AWARDS

Congratulatory call. Former Motorola chief Robert Galvin, who turned the company into a technology powerhouse and fueled the growth of the cell phone industry, last week received the Vannevar Bush Award for lifetime contribution to the nation in science and technology. Founded in 1980, the award is given every year by the National Science Board (NSB).

Galvin began working for Motorola in 1940 and became its chief executive officer in 1959. Under his stewardship, the company developed semiconductor technology for applications in computer-controlled two-way radio communications for public safety, national defense, and space exploration. Galvin also served on many panels advising the government on science and technology policy, including the Special Commission on the Future of the National Science Foundation in the early 1990s.

NSB also honored the winners of its public service awards last week: science journalist Ira Flatow and the Computing Research Association's Committee on the Status of Women in Computing Research.

Got any tips for this page? E-mail people@aaas.org

IN THE COURTS

Painful memory. Stephen Jay Gould's widow has sued three Boston doctors for not noticing a 1-centimeter tumor in his lung that ultimately led to the death of the noted evolutionary biologist 3 years ago.

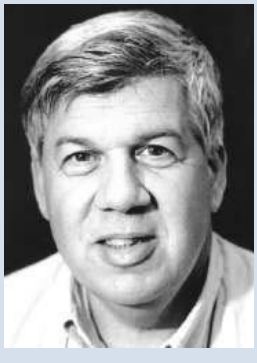

In the suit, filed 20 May in Middlesex Superior Court in Massachusetts, artist Rhonda Roland Shearer says oncologist Robert Mayer of the Dana-Farber Cancer Institute in Boston, Massachusetts, gave Gould a "clean bill of health" 15 months before his death even though the tumor was visible in an x-ray taken at the time. The radiological report, prepared by two radiologists who worked at Brigham and Women's Hospital, said the lungs were clear. Although the suit doesn't quote a settlement figure, Shearer estimates the loss from Gould's death to be several million dollars. "He had uncommon talents and uncommon income," says her lawyer, Alex MacDonald. Shearer plans to use a portion of any damages collected to create a free Web site of her husband's writings and notes, "as Steve would have done."

A Dana-Farber spokesperson says the suit is "without merit."

CREDITS (TOP TO BOTTOM): OSTP; GOOGLE; OSTP; MOTOROLA ARCHIVES

Science
AAAS

AFFYMETRIX®

AAAS Newcomb Cleveland Prize

Supported by

AFFYMETRIX

CALL FOR NOMINATIONS

This $25,000 prize is awarded to the author or authors of an outstanding paper published in the Research Articles or Reports sections of *Science*.

Readers are invited to nominate papers published during the period 1 June 2004 – 31 May 2005. An eligible paper is one from the relevant sections that includes original research data, theory, or synthesis or one that presents a fundamental contribution to basic knowledge or a technical achievement of far-reaching consequence. Reference to pertinent earlier work by the author may be included to give perspective.

DEADLINE: 30 JUNE 2005

Phone ..... (202) 326-6507

E-mail ..... skihara@aaas.org

Additional information about the prize and the nomination procedure can be found at:
www.aaas.org/about/awards/

Regional Focus on GM Crop Regulation

THE RECENT MEDIA COVERAGE OF THE DEVELopments in Brazil, China, and Mexico (*1*–*3*) demonstrates their emergence as the future developing country forerunners for commercial genetically modified (GM) crops in both the scientific and regulatory arena.

The release of GM crops in these countries might result in the unintentional entry of GM seeds into neighboring countries that have not yet harnessed the technology and implemented sufficient regulatory systems. Unregulated "genetic contamination" of areas intended for growing GM-free or organic products, perhaps for export, could be potentially devastating for some neighboring economies and could set a negative example in the international efforts for the safe use of GM crops."

Should Brazil, China, or Mexico decide to allow the commercial release of GM crops,

GM Bt cotton crop in China.

CREDIT: ZHANG ZUI/CHINA FEATURES

countries in the region must ensure that a border control system is included in their biosafety framework. Sharing information on the risk assessment and risk management strategies could also help. A regional perspective in national decision-making is necessary to maintain the benefits for small-scale farmers while pursuing export-oriented agricultural priorities. Current efforts such as the United Nations Environmental Programme–Global Environment Facility biosafety projects (*4*) might provide a forum for such discussions, although it must be owned and driven by the countries themselves for its success in the long run.

HARUKO OKUSU[1] AND KAZUO N. WATANABE[2]
[1]Sheffield Institute of Biotechnological Law and Ethics (SIBLE), University of Sheffield, Sheffield S10 1FL, UK. [2]Gene Research Center, Graduate School for Life and Environmental Science, University of Tsukuba, 1-1-1 Tennoudai, Tsukuba, Ibaraki, 305-8572, Japan. E-mail: nabechan@gene.tsukuba.ac.jp

References
1. "A boost for genetically modified crops," *Economist*, 20 Nov. 2004, p. 65.
2. J. Huang *et al.*, *Science* **308**, 688 (2005).
3. C. Peregrina, J. Crúz, "Mexico approves planting and sale of GM crops," SciDev.net (online), 22 Feb. 2005 (available at www.scidev.net/content/news/eng/mexico-approves-planting-and-sale-of-gm-crops.cfm
4. See www.unep.ch/biosafety.

Accommodation or Prediction?

IN HIS COMPARISON BETWEEN ACCOMMOdating (a posteriori) and predictive (a priori) hypotheses, P. Lipton asks which is better suited for scientific investigation ("Testing hypotheses: prediction and prejudice," 14 Jan., p. 219). This question is misleading because it ignores the process of scientific inquiry, which starts with observations about the natural world. These observations are interpreted using the tools, worldviews, and values of the scientific community [Kuhn's (*1*) paradigms] that are available to the observer, and an accommodating hypothesis is formed. This hypothesis is the prerequisite for the continuation of the scientific process.

The real focus of Lipton's article is whether this next step should be additional observations leading to more accommodation, or whether a prediction should precede additional observations. He concludes that predictive hypotheses should be preferred. He acknowledges that well-supported hypotheses often have both accommodations and successful predictions to their credit, but he ignores the historical component. Lipton assumes that both options are equally available to the observer. In reality, the availability of this choice will depend on the field of science, and its state in history. An astronomer in 1531, upon seeing the comet that would be later known as Halley's Comet, would have been unable to predict its return in 1607, because most of the hypotheses on the motion of comets were not published until the early 1600s (*2*). By the time of Halley's prediction (1705), many observations of comet movements and accommodating hypotheses of their pathways were available. W. D. Hamilton accommodated the influence of Darwin (focus on the individual), R. D. Fisher (genetic theory of natural selection), and his personal knowledge of insects in the concept of inclusive fitness (Hamilton's rule). This concept is very powerful in generating predictive hypotheses in the field of evolutionary biology and has paved the way to an entirely new field, sociobiology (*3*). Before Fisher or Darwin, or without sufficient background knowledge in natural history, this would not have been possible. If predictions are formulated without sufficient background knowledge, they are unlikely to be successful. If accommodation is the only method employed, it is likely not very convincing. It is only when sufficient information is available that successful predictive hypotheses can be formulated, and this is where Lipton's discussion is relevant. The incorporation of predictive hypotheses at this point does more than just reduce "fudging"—it adds a new framework to an otherwise accommodation-based process of inquiry, which should strengthen our confidence in the outcome. Together, accommodation and prediction will lead to scientific progress where either one in isolation would be incapable of doing so.

KATHRIN STANGER-HALL
Department of Integrative Biology, University of Texas at Austin, 1 University Station, CO930, Austin, TX 78712, USA.

References
1. T. S. Kuhn, *The Structure of Scientific Revolutions* (Univ. of Chicago Press, Chicago, ed. 2, 1970).
2. M. C. Festou, H. Rickman, *Astron. Astrophys. Rev. Part I* **4**, 363 (1993); or www.eso.org/outreach/info-events/hale-bopp/comet-history-1.html
3. See entry on W. D. Hamilton at http://en.wikipedia.org/wiki/The_Genetical_Theory_of_Natural_Selection.

IN HIS REVIEW "TESTING HYPOTHESES: PREDICtion and prejudice" (14 Jan., p. 219), P. Lipton echoes widespread impressions that predictions, because they cannot be "fudged," are epistemically superior to ad hoc accommodations. His analysis lacks appropriate controls and reference classes. Predictors can fudge too, through excess predictions. They may also hedge by using alternative versions of a hypothesis. Many other predictions are loosely consistent with, but not rigorously determined by, their hypotheses. Failed efforts in such cases are typically disregarded. Thus, Mendeleev's predictions of eka-aluminum (gallium) and eka-boron (scandium) are widely celebrated, whereas his failed predictions of eka-niobium and eka-caesium are largely forgotten (*1*). Meselson and Stahl's dramatic results on DNA replication kindly hide the predictive uncertainty that preceded their study (*2*). By discounting error, predictors indirectly "accommodate" available evidence. Like astrologers' or psychics' missed guesses, failures belong in a complete epistemic analysis of predictions. Conversely, accommodations are not so easily fudged—if they are to meet the standards of systematicity and coherence ("simplicity"). Accommodators thus encounter risk and may discard hypotheses well before any announcement. Their failures matter too. Darwin's evolutionary synthesis and Einstein's special relativity were extraordinary accommodations (*3*). They justly earned merit by the conventional

standards of evidence and theoretical virtues of scope and accuracy. By not controlling for relevant error, Lipton gives predictors the appearance of risk and rigor and accommodators only the ability to fudge.

DOUGLAS ALLCHIN

Minnesota Center for the Philosophy of Science, University of Minnesota, Minneapolis, MN 55455, USA.

References

1. W. H. Brock, *The Norton History of Chemistry* (Norton, New York, 1993).
2. F. L. Holmes, *Meselson, Stahl and the Replication of DNA* (Yale Univ. Press, New Haven, CT, 2001).
3. M. Janssen, *Perspect. Sci.* **10**, 457 (2002).

P. LIPTON SHOULD BE COMMENDED FOR HIS lucid and persuasive argument in support of testing hypotheses by predictions rather than by accommodations ("Testing hypotheses: prediction and prejudice," Reviews, 14 Jan., p. 219). I wish Lipton had addressed another central theme in the search for truth in biomedical science, namely, testing hypotheses through experimentation (intervention) versus observations.

For ethical and other reasons, clinical research leaves little room for hypothesis testing through human experiments. As such, it often yields data that demonstrate association rather than causality. The so-called "descriptive" nature of many clinical investigations is frequently contrasted with the precise, cause-and-effect methodology of bench research. The not-so-subtle message here is that while basic biological research is real science, most clinical research is not.

Snap judgments that employ the "descriptive/mechanistic" yardstick tell us little about quality or relevance. Far too much effort and expense have been wasted on exploring "mechanistic" trivialities. The true standard that gauges the merit of any biomedical enterprise is the dividend of biological insight into how we came to be and who we are.

Darwin's *The Origin of Species* and *The Descent of Man* are quintessentially "descriptive," and for that matter accommodative, yet the ramifications of these works have transformed biology. The original investigations that found associations of cardiovascular disease with hypertension and elevated LDL cholesterol have ushered in large-scale preventive and therapeutic interventions, changing forever the way we practice medicine and saving millions of lives in industrialized societies. Very few "mechanistic" studies in yeast, worms, mice, and, for that matter, humans can claim the same impact on humanity as these originally "descriptive" achievements.

ABRAHAM AVIV

University of Medicine and Dentistry of New Jersey, Hypertension Research Center, Room F-464, MSB, 185 South Orange Avenue, Newark, NJ 07103–2714, USA.

P. LIPTON ("TESTING HYPOTHESES: PREDIC-tion and prejudice," Reviews, 14 Jan., p. 219) argues that a prediction published before it is verified by observation provides more support than an "accommodation" published afterward (the "advantage thesis"). Lipton gives no evidence that scientists, past or present, actually accept this thesis. He asserts that the successful prediction of the 1758 appearance of Halley's Comet was "far more impressive" evidence for the hypothesis that it was the same comet as those seen in 1531, 1607, and 1682 than the fact that those previous appearances could be accommodated by postulating a comet that returns every 75 or 76 years. But the only evidence he cites to support this assertion (*1*) does not mention Halley's Comet at all.

Lipton cites five authors who found it irrelevant whether observations supporting a hypothesis were made before or after the prediction was published: They still furnish the same amount of support for the hypothesis. As one of those authors, I would like to clarify my position. In the specific case of Einstein's general theory of relativity, theoretical physicists in the 1920s did not give greater weight to the observed bending of starlight by the sun just because it was a prediction published before the observation was reported; they gave equal (or sometimes greater) weight to the fact that the theory explained the advance of Mercury's perihelion, an observation made decades earlier but not satisfactorily explained (*2*).

Although Lipton's "advantage thesis" was refuted in this case, it could be true in others. I looked at the reception of several well-known theories and found that in most cases, confirmation after publication of a prediction did not count more than supporting evidence known earlier (*3*–*9*). In only two cases, Mendeleev's periodic law (*10*) and Morgan's chromosome theory (*11*), did scientists explicitly mention predictiveness as a reason for acceptance, but even in those cases it was not the most important reason. So there is little reason so far to accept the advantage thesis as a general statement about science.

STEPHEN G. BRUSH

Institute for Physical Science and Technology, University of Maryland, College Park, MD 20742, USA.

References and Notes

1. M. Grosser, in *Dictionary of Scientific Biography*, C. C. Gillispie, Ed. (Scribner's, New York, 1970), vol. 1, pp. 53–54. This is an article about John Couch Adams.
2. S. G. Brush, *Science* **246**, 1124 (1989).
3. S. G. Brush, *Eos* **71**, 19 (1990).
4. S. G. Brush, *Perspect. Sci.* **1**, 565 (1993).
5. S. G. Brush, *Riv. Storia Sci.* [serie II] **1** (no. 2), 47 (1993).
6. S. G. Brush, in *PSA 1994, Proceedings of the 1994 Biennial Meeting of the Philosophy of Science Association*, vol. 2, D. Hull *et al.*, Eds. (Philosophy of Science Association, East Lansing, MI, 1995), p. 133.
7. S. G. Brush, *J. Conflict Resolution* **4**, 523 (1996).
8. S. G. Brush, *Stud. Hist. Philos. Sci.* **30**, 263 (1999).
9. S. G. Brush, *Phys. Perspect.* **1**, 184 (1999).
10. S. G. Brush, *Isis* **87**, 595 (1996).
11. S. G. Brush, *J. Hist. Biol.* **35**, 471 (2002).
12. I thank D. Allchin for calling my attention to Lipton's article.

IN HIS REVIEW "TESTING HYPOTHESES: PRE-diction and prejudice" (14 Jan., p. 219), P. Lipton argues that we sometimes have more reason to accept a confirmed prediction than a corresponding accommodation of a hypothesis because accommodations have more opportunity to be affected by fudging than predictions. This emphasis on fudging overlooks the powerful ability of statistics to evaluate the degree of validity of confirmed predictions and accommodations. We illustrate this with the example of Halley's prediction of the comet of 1758 mentioned by Lipton. Halley found a sequence of 3 of 24 comet appearances observed over 362 years that were separated by ~76-year intervals and had similar orbital characteristics, and on this basis predicted an appearance in 1758 that was subsequently confirmed (*1*). Using randomly simulated comet appearances, we estimate a P value of ~0.03 for confirmed prediction (P_{pred}) of a fourth appearance beyond a 362-year period that continues a sequence of three found within it, and P values for corresponding accommodations (P_{acc}) for finding four appearances in sequence anywhere within a period of $362 + x$ years, finding P_{acc} ranging between ~0.09 ($x = 10$) and ~0.11 ($x = 60$) (*2*). As here $P_{pred} < P_{acc}$, there is indeed more reason for confidence in prediction than accommodation, but this may not always obtain. For example, if instead of predicting a fourth appearance from three observations, we consider prediction of a fifth based on four, P_{pred} should stay nearly the same because it depends mainly on the random success of a single prediction with unchanged probability, while P_{acc} should drop because it depends on finding random sequences of five versus four; here $P_{pred} = \sim 0.02$ and $P_{acc} = \sim 0.08$ ($x = 60$). With increasingly well-fit data and no change in free parameters, accommodation should eventually impart greater confidence than prediction.

Because, as Lipton notes, fudging may be "neither fully conscious nor readily visible," it is difficult to evaluate its impact. Science has thus developed objective data collection and analysis procedures to supress it, allowing the validity of confirmations to be assessed statistically. When these procedures are employed and statistics are comparable, there is no reason to stress predictions over accommodations.

JOHN AACH AND GEORGE M. CHURCH

Department of Genetics and Lipper Center for Computational Genetics, Harvard Medical School, NRB 238, 77 Avenue Louis Pasteur, Boston, MA 02115, USA. Email: aach@genetics.med.harvard.edu

References

1. P. Lancaster-Brown, *Halley and His Comet* (Blandford Press, Dorset, UK, 1985). See Table 1, p. 179 for Halley's list of 24 comets and orbital data.
2. See supplementary information at http://arep.med.harvard.edu/Halley.

Response

I AM GRATEFUL FOR THE MANY THOUGHTFUL responses to my discussion of prediction and accommodation. Two recurring and well-taken points are that predictions are sometimes unavailable (Stanger-Hall) and that a theory may be strongly supported without them (Allchin, Aviv). The aim of my discussion was to suggest that predictions sometimes have an edge over accommodations because they do not encourage theory-fudging, not to deny that accommodations ever provide powerful support.

Other Letters suggest liabilities of prediction that may remove any net advantage over accommodation (Aach and Church, Allchin). Even if prediction is not susceptible to theory-fudging, because the investigator does not know the right answer in advance, it is susceptible to "data-fudging," where the empirical results are either massaged or selectively ignored. Data-fudging occurs, but it does not cancel out the asymmetry between accommodation and prediction. For one thing, it applies to accommodation as well as to prediction; for another, data fudging may often be easier to detect and control than theory-fudging. I also accept Allchin's more specific point that predictions may in practice serve to select from different versions of a hypothesis, but I do not see that this necessarily introduces additional fudging. Of course, if the investigator reacts to a failed prediction by mangling the hypothesis to get a fit, that is indeed fudging, but I would also count it as an accommodation, not a prediction.

Another recurrent reaction to my argument is that the difference between prediction and accommodation may be simply irrelevant. Thus, Brush, a distinguished historian of science, suggests that scientists have in fact typically not given greater weight to predictions. On the historical question, there is a variety of views and cases to be distinguished. Brush has studied a number of instances where he has found no contrast, although he has also found two cases where scientists did claim to put particular weight on predictiveness. And in the case of Halley that I cited in my essay, the entry in the *Dictionary of Scientific Biography* states that "although [Halley's cometary views] aroused the interest of astronomers, it was not until the 1682 comet reappeared as predicted in 1758 that the whole intellectual world of western Europe took notice… This successful prediction acted as a strong independent confirmation of Newtonian gravitation…" (*1*). Moreover, the claim Brush makes of the similar weight given to perihelion shift (known beforehand) and starlight bending (predicted) in the confirmation of the general relativity may not bear directly on my argument, for I do not claim that each of a theory's predictions is worth more than any of its accommodations. Moreover, it is not clear that the data concerning the shift in the perihelion of Mercury count as an accommodation in the sense relevant to my argument, since Einstein claimed not to have used those data to form his theory. Thus, he and Infeld wrote, "The deviation of the motion of the planet Mercury from the ellipse was known before the general relativity theory was formulated, and no explanation could be found. On the other hand, general relativity developed without any attention to this special problem" (*2*). It is interesting both that the theory was developed independently and that Einstein and Infeld thought this a point worth emphasizing.

Of course, it is possible that even if scientists in fact place weight on the distinction between accommodation and prediction that they ought not do so, or vice versa, and my Review focused on the normative question. Aach and Church suggest that the case for taking account of whether data were accom-

modated or predicted will evaporate where sophisticated statistical techniques are available to evaluate the data. Those techniques are important, but I doubt that, even when they are applicable, they obviate any appeal to the contrast between accommodation and prediction. One reason for this is that fudging, as many of my commentators have observed, may take so many different forms.

PETER LIPTON

Department of History and Philosophy of Science, University of Cambridge, Free School Lane, Cambridge CB2 3RH, UK.

References

1. C. Ronan, in *Dictionary of Scientific Bibliography*, C. C. Gillispie, Ed. (Scribner's, New York, 1972), vol. VI, p. 69. The reference given in my Essay was in error.
2. A. Einstein, L. Infeld, *The Evolution of Physics* (Simon & Schuster, New York, 1960), p. 239.

Plutonium-238 and Cassini

SCIENCE IS TO BE COMMENDED FOR THE Cassini series of articles (25 Feb., pp. 1222–1276). Plutonium-238–powered isotopic generators supplied the electricity that allowed Cassini's data gathering and transmission. Without Pu-238 sources, there would have been no Cassini. Yet, Cassini was almost scrubbed because activists tried hard to block the Pu-238 generators. Worst-case scenarios of Cassini disasters were ubiquitous in Washington, DC. The Office of Management and Budget became a last-resort safety review board that had to be convinced before the White House would allow the Department of Energy to proceed with Cassini. The plutonium-powered sources worked, and now we have marvelous data from Saturn via Cassini.

A. DAVID ROSSIN*

University Park, FL, USA.

*Assistant Secretary for Nuclear Energy, U.S. Department of Energy 1986–87, Director of the Nuclear Safety Analysis Center at EPRI 1981–86, and President of the American Nuclear Society 1992–93

A Historical Note on Superconductors

I ENJOYED READING M. RICE'S PERSPECTIVE "Superfluid helium-3 has a metallic partner" (12 Nov. 2004, p. 1142) about the elegant work of K. D. Nelson *et al.* ("Odd-parity superconductivity in Sr_2RuO_4," Reports, 12 Nov. 2004, p. 1151), in which they confirmed the nature of superconductivity in strontium ruthenate to be odd parity $l = 1$, as had been supposed but not proven for a number of years. In Rice's second paragraph, I found a historical remark that does not describe the actual course of events. Rice writes, "Not long after this [the BCS] theory was developed, Kohn and Luttinger speculated that superconductors in which the pairs have finite angular momentum… could also occur." It is true that it was "not long after BCS" that such ideas appeared, but it was some 5 to 6 years before the Kohn-Luttinger paper (*1*) in 1965.

The first papers on higher angular momentum states appeared within a few months of each other in 1960, by Pitaevskii (*2*), Brueckner *et al.* (*3*), and Emery and Sessler (*4*), all independently and approximately in that order. These focused on ^{3}He to some extent, but a more comprehensive and general study of this kind of state was made shortly after by Anderson and Morel (*5*, *6*). The classic papers of Balian and Werthamer (*7*) and of Leggett (*8*) had also appeared by 1965.

PHILIP W. ANDERSON

Department of Physics, Princeton University, Princeton, NJ 08544, USA.

References

1. W. Kohn, J. M. Luttinger, *Phys. Rev. Lett.* **15**, 524 (1965).

2. L. P. Pitaevskii, *Sov. Phys. JETP* **10**, 1267 (1960).
3. K. A. Brueckner, T. Soda, P. W. Anderson, P. Morel, *Phys. Rev.* **118**, 1442 (1960).
4. V. J. Emery, A. M. Sessler, *Phys. Rev.* **119**, 43 (1960).
5. P. W. Anderson, P. Morel, *Physica* **26**, 671 (1960).
6. P. W. Anderson, P. Morel, *Phys. Rev.* **123**, 1911 (1961).
7. R. Balian, N. R. Werthamer, *Phys. Rev.* **131**, 1553 (1961).
8. A. J. Leggett, *Phys. Rev. Lett.* **14**, 536 (1965).

CORRECTIONS AND CLARIFICATIONS

ScienceScope: "Pig flu scare—case closed?" (15 Apr., p. 339). Henry Niman, who has backed claims that Korean pigs harbor the WSN/33 virus, is not based in Philadelphia, but in Pittsburgh.

Special Section: Cassini at Saturn: Reports: "Ultraviolet imaging spectroscopy shows an active saturnian system" by L. W. Esposito *et al.* (25 Feb., p. 1251). On page 1252, in the third column, in the paragraph after reactions 4 and 5, line 10, the citation of reference 8 is incorrect. The citation should be to the following paper, which is not in the reference list: M. T. Leu, M. A. Biondi, R. Johnsen, *Phys. Rev. A* **7**, 292 (1973).

Reports: "Control of excitatory and inhibitory synapse formation by neuroligins" by B. Chih *et al.* (25 Feb., p. 1324). While this manuscript was under review, a related paper was published in *Cell* reporting a role for neuroligins and neurexins in GABA synapse assembly: E. R. Graf, X. Z. Zhang, S. X. Jin, M. W. Linhoff, A. M. Craig, "Neurexins induce differentiation of GABA and glutamate postsynaptic specializations via neuroligins," *Cell* **119**, 1013 (2004).

Reviews: "Editing at the crossroad of innate and adaptive immunity" by P. Turelli and D. Trono (18 Feb., p. 1061). Didier Trono's e-mail address was listed incorrectly; it is Didier.Trono@epfl.ch.

Reports: "Two abundant bioaccumulated halogenated compounds are natural products" by E. L. Teuten *et al.* (11 Feb., p. 917). There was a small error in reference 32. Line 12 should read "(with funding provided by The Camille and Henry Dreyfus Foundation, Inc...."

TECHNICAL COMMENT ABSTRACTS

COMMENT ON "Abrupt and Gradual Extinction Among Late Permian Land Vertebrates in the Karoo Basin, South Africa"

Charles R. Marshall

Reanalysis of the high-precision field data of Ward *et al.* (Reports, 4 February 2005, p. 709) fails to significantly support a gradual extinction prior to the Permian-Triassic boundary and more strongly suggests that the Triassic taxa originated in the Triassic than in the Permian. Thus, the data are consistent with a simple catastrophic extinction and concomitant recovery.

Full text at
www.sciencemag.org/cgi/content/full/308/5727/1413b

RESPONSE TO COMMENT ON "Abrupt and Gradual Extinction Among Late Permian Land Vertebrates in the Karoo Basin, South Africa"

Peter D. Ward, Roger Buick, Douglas H. Erwin

Our data from the land vertebrate record of the Permian-Triassic transition of the Karoo Basin of South Africa support both gradual and sudden extinction mechanisms. In our response, we show why Marshall's support of a single catastrophic event is untenable.

Full text at
www.sciencemag.org/cgi/content/full/308/5727/1413c

Letters to the Editor

Letters (~300 words) discuss material published in *Science* in the previous 6 months or issues of general interest. They can be submitted through the Web (www.submit2science.org) or by regular mail (1200 New York Ave., NW, Washington, DC 20005, USA). Letters are not acknowledged upon receipt, nor are authors generally consulted before publication. Whether published in full or in part, letters are subject to editing for clarity and space.

HISTORY OF MEDICINE

Diverse Roots Even Only in the West

Geoffrey Lloyd

Ancient Medicine
by Vivian Nutton
Routledge, London. 2004. 500 pp. $115, £65. ISBN 0-415-08611-6. Sciences of Antiquity.

The study of Greco-Roman medicine has, in recent years, been radically transformed. There was a time when histories concentrated almost exclusively on great men (Hippocrates, Galen) or great discoveries (that of the valves of the heart or of the nervous system). Now historians recognize the importance of recovering the full variety of medical theories and practices across the Greco-Roman world. We consider not just the naturalistic traditions but also the work of many other groups: the herbalists and drug sellers, the practitioners of temple medicine (preeminently in the shrines of Asclepius), and (not least) the contributions of women healers, previously all too often dismissed as mere midwives. In addition, one can no longer treat Greco-Roman medicine in isolation from that of the rest of the Mediterranean world. One must locate it in relation to the beliefs and practices of ancient Near Eastern societies—especially Egypt and Babylonia—even though precise answers to questions of indebtedness (for instance, in the matters of drug therapies or beliefs such as the "wandering womb") are still difficult to give. At the other end of antiquity, the Arab contributions both to preserving Greek medical texts and to interpreting them are of great importance. Lastly, there are issues concerning the social contexts of medical practice and theory. These include questions of how doctors made a living, what legal constraints they worked under, and the ways in which ideas about health and well-being, disease and illness, throw light on values, ideologies, and even the concepts of good and evil themselves.

Vivian Nutton is among the leading practitioners of this new-style medical history. Nutton, a professor at the Wellcome Trust Centre for the History of Medicine at University College London, is an expert not only on Greco-Roman antiquity but also on later European developments. In *Ancient Medicine*, he offers a comprehensive, immensely learned, methodologically sophisticated but still eminently readable survey of Greco-Roman medicine from pre-Homeric times to the seventh century CE. He examines the entire range of sources: literary, epigraphical, papyrological, archaeological, and paleopathological. Time and again Nutton is able to cite such sources as striking funerary inscriptions or honorary decrees to illuminate what contemporaries thought of doctors famous to them but otherwise essentially unknown to us. The statue set up in the little city of Tlos at the end of the first century BCE to commemorate the work of Antiochis, for example, is just one piece of evidence that women practitioners were not limited to anonymous obstetricians but also included respected and wealthy members of the literate elite.

An older view of medicine's roots. In this 13th-century Italian fresco (from the Cathedral of Santa Maria, Anagni, Lazio), Galen receives knowledge about medicine from Hippocrates.

The Hippocratic corpus and Galen naturally receive full coverage, but so too do less thoroughly studied authors such as Scribonius Largus, Rufus of Ephesus, Aretaeus of Cappadocia, Caelius Aurelianus, and Paul of Aegina along with the fragmentary remains of scores of more shadowy figures (especially those from early Hellenistic times). Nutton thus gives the reader a far fuller picture than is usual of the 1500 years or so under consideration. He organizes his main narrative in 20 uncluttered chapters but backs his arguments with massive learning (the bibliography runs to 45 pages) and ample footnotes (100 pages). At the same time, the author repeatedly warns of evidence gaps and of problems that have yet to be—and in some cases may never be—resolved. Nevertheless, he gives us an eminently judicious appraisal of the state of the debate on problems as diverse as the relations between Aristotle and Diocles, the practice of human vivisection in Alexandria, the rise of Methodism, and the relations between pagan and Christian miraculous healing.

Let me select for comment just two facets of the picture that emerges from the book. The first is the rivalry that existed not merely between elite physicians and practitioners of "alternative" medicine but also within the elite themselves. With few exceptions, most of our major extant texts should be seen as engaging explicitly or implicitly in ongoing debates with opponents. These debates extended beyond particular issues having to do with the causes of diseases or the right modes of treatment to encompass methodology and the question of what constitutes medicine itself. Greek medicine shares with Greek philosophy not just an openness to alternative views but also a deep-seated adversarial spirit. My second and related point concerns the long shadow of Galen, both as historian and as medical practitioner—a shadow that prompts Nutton to describe the book as the first anti-Galenic history of medicine. Galen's brilliance as practitioner is undeniable, as is his excellence as an experimental anatomist. Yet we still have some way to go fully to liberate ourselves from the bias of his reporting on his predecessors: both the unfairness of his characterizations of those he despised and the effects of what Nutton calls his "suffocating friendship" for those he saw as allies. Meanwhile, we have to register how different the subsequent history of European medicine would have been if, rather than Galen, it had been the Methodists, or others not wedded to Galenic humoral theory, who had come to be seen to be the models to follow.

As a comparativist myself, I must conclude by protesting at the use of the term "ancient" in the book's title (as in others in this series) where that refers at most to the ancient Mediterranean world, and antiquity further east than Iran is ignored. Nonetheless, Nutton provides a good template for a companion volume covering ancient medicine in other parts of the world.

The reviewer is at the Needham Research Institute, 8 Sylvester Road, Cambridge, CB3 9AF, UK. E-mail: gel20@hermes.cam.ac.uk

10.1126/science.1113111

FILM: ARCHAEOLOGY

It's a Wrap

Esther M. Sternberg

This short movie includes flying coffins, a morphing skeleton, a mysterious death, magical amulets, and a mistake that was kept secret for close to 3000 years. We are guided by the sonorous intonations of Ian McKellan. But he is no longer Gandalf, and the scene is not Middle Earth. It is Egypt in the middle of the 22nd Dynasty, 2800 years ago. And the story is not fantasy but is factual. *Mummy: The Inside Story*, currently showing at the British Museum, is about a priest at the Temple of Karnak: how he lived, how he died, and what became of his body. The three-dimensional (3D) film takes the viewer through the mummy's coffin, the layers of linens in which he is wrapped, and the desiccated remains of his skin and soft tissues to his skeleton and resin-soaked internal organs—all without opening his gorgeously decorated wooden case.

Mummy
The Inside Story
At the British Museum, London, through 14 August 2005. www.thebritishmuseum.ac.uk/mummy

Mummy
The Inside Story
by John H. Taylor
British Museum Press, London, 2004. 48 pp. Paper, £5.99. ISBN 0-7141-1962-8. Abrams, New York. Paper, $14.95, C$22.50. ISBN 0-8109-9181-0.

How this is accomplished is as amazing as the film itself. The project, a collaboration between the British Museum and Silicon Graphics Incorporated, used computerized tomography (CT) scanning to produce 1500 cross-sectional images. These were combined in a single 3D volumetric data set that can be sliced at any angle. Real-time volume rendering allows viewers to delve behind any layer to see what is inside. Thus, the precious specimen can be examined in intricate detail without opening its case and unwrapping it—a practice, popular in the 19th century, that destroyed many mummies forever.

Data from the CT scans together with the known archaeology and history of the period are used to reconstruct the life of the mummy. The film starts with the hieroglyphs and symbols on the coffin. As each symbol flies off the case, it is translated into Roman alphabet to form the name that the body carried in life, Nesperennub. We learn that he was a priest at the Temple of Karnak, descended from a line of priests who led privileged lives while they served the great deity Amun-Ra and the moon god Khons. Footage of the modern site of the Temple at Karnak, including actors re-enacting the rituals of the ancient priests, makes this history come alive.

But it is modern imaging technology that truly makes the long-dead man's life and death seem real. The mummy emerges from the CT scanner to re-materialize in 3D, as if Dr. Who's time machine was run in reverse. His skull morphs into a life-like clay head, which is reconstructed using a forensic peg technique to determine soft-tissue depth. Then, to the gasps of the audience, he morphs again into a living person—an actor who looks just like the computer images predict. With this animated sleight of hand, we feel a link to the past and to this person. After all, he wasn't always a desiccated, shriveled skeleton but was once a living human, just like us.

As we pass through the linen wraps, we see amulets that were carefully placed within the folds to help the soul safely through the "other world." Reaching the inner layers, we learn more about how Nesperennub died and how he was embalmed. We even learn the identity of a mysterious object atop his skull, a source of speculation since the mummy's skull was x-rayed in the 1960s.

As marvelous as the film is, serious historians, archaeologists, and physicians may view it with some skepticism because it is so filled with special effects. It leaves the viewer hungry for answers to questions such as the exact methodology of the 3D reconstruction, the differential diagnosis of the skull lesion that appears to be the cause of death, and details as to how the mummy was actually scanned.

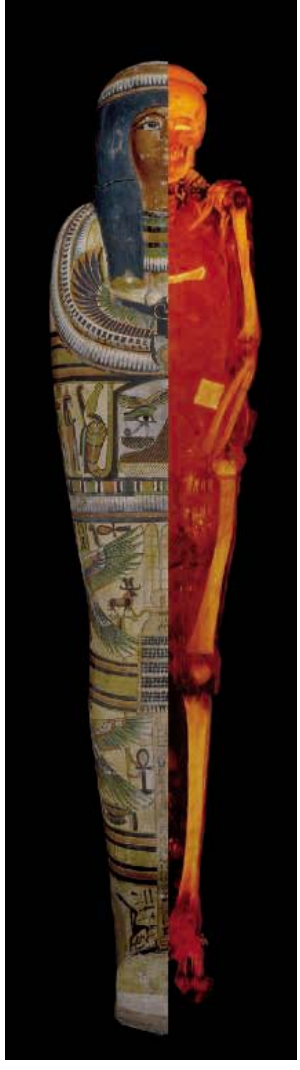

However, the children's squeals of delight as the mummy case and its hieroglyphs fly into the 3D, virtual reality space and the adults' "ah"s as the skull morphs into a living human amply compensate for the film's minimal presentation of technological production details. A small exhibition, which the audience enters after seeing the film, offers some additional information about ancient Egypt and the production process. The room contains the actual mummy, explanations of all the symbols on the brightly painted coffin, examples of amulets and eyes from the wrappings of other mummies, and more details about the CT-scanning procedure and the methodology used to create the 3D reconstructions. Those seeking still more information will enjoy the glossy catalog by John Taylor, an archaeologist at the British Museum. It offers a wealth of images and explanations of hieroglyphs and history, amulets and art, and even the forensic sleuthing that identified the object on the mummy's head.

When the film was over, I heard a small girl give her mother an excellent review of *Mummy*: "Now my favorite story will be the mystery of the mummy." The film and book should be made widely available as teaching tools. In addition to informing children about ancient Egypt, they show how exciting a marriage of interdisciplinary science, history, and the arts can be when applied to solve the mysteries of our past.

10.1126/science.1113656

The reviewer is the author of *The Balance Within: The Science of Connecting Health and Emotions*. Web site: www.esthersternberg.com

BROWSINGS

In Search of the Ivory-billed Woodpecker. *Jerome A. Jackson.* Smithsonian Books, Washington, DC, 2004. 304 pp. $24.95. ISBN 1-58834-132-1.
The Race to Save the Lord God Bird. *Phillip Hoose.* Farrar, Straus and Giroux, New York, 2004. 204 pp. $20, C$30. ISBN 0-374-36173-8.
The Grail Bird. Hot on the Trail of the Ivory-billed Woodpecker. *Tim Gallagher.* Houghton Mifflin, Boston, 2005. 288 pp. $25. ISBN 0-618-45693-7.

These three books provide background details for the ivory-billed woodpecker story covered elsewhere in this issue. Jackson discusses the natural history and cultural lore of the species and surveys the history of searches for the bird in the United States and Cuba. Hoose's profusely illustrated account considers the bird's decline in the context of conservation efforts, especially the unsuccessful attempts to preserve the Singer Tract in Louisiana. Gallagher's personal narrative—which includes evaluations of several disputed reports of the species from recent decades—follows the successful search in Arkansas through February 2005.

Science in the Arab World: Vision of Glories Beyond

Wasim Maziak

Of all its accomplishments, the West is perhaps most proud of its scientific revolution, which has been unfolding for the past half-millennium. Only students of history remain consistently mindful of the pivotal and catalytic role that the Arab world played in the early phases of this revolution. Now, all of us should have a vested interest in advancing science and technology in the Arab community. Science and technology provide the means to feed people, improve their health, and create wealth. They can help to reduce societal tensions and build international bridges for badly needed dialogue and mutual understanding. To usher science and technology more thoroughly into Arab culture and society, however, the West needs to acknowledge the Arab world's historical contributions, and the Arab world needs to stop dwelling on its golden past by also embracing lessons about science and technology that the West learned long ago.

This yearlong essay series celebrates 125 years of *Science* by inviting researchers from around the world to provide a regional view of the scientific enterprise. Series editor, Ivan Amato

In medieval Europe, where the Christian dogma that the world unfolded according to a divinely predetermined plan prevailed, there was little space for those willing and eager to understand nature in order to use it for their own benefit. Beginning in the 11th century, the ailing Arab provinces in Spain (Al-Andalus) were falling to European armies, and with them came priceless spoils that changed the world: the epic intellectual achievement of Arab-Islamic scholars since the 8th century. Flourishing libraries in cities like Toledo and Cordoba contained thousands of books on every field of knowledge. Unlike the Moguls, who in the 13th century destroyed Baghdad and its libraries, thereby abruptly ending the golden era of the Arab-Islamic civilization, the Europeans were quick to realize the value of these windfalls of knowledge.

During the Abbasid reign (750 to 1258), learning in Islam was encouraged in every field of knowledge, and scholars of every color and creed traveled to Damascus and Baghdad to study and work. In these tolerant times, Islam's leaders encouraged learning and the use of reason to understand nature. The early Abbasid Caliphs—most notably Al-Mansur, Harun Al-Rachid, and Al Ma'mun, who reigned from 754 to 833—embraced science as a state's defining policy, ushering in a golden era of Arab-Islamic civilization. An avid movement of translation and studying of ancient books and of advancing new knowledge ensued on an unprecedented scale. Arab and Muslim scholars scored achievements in every field of science: mathematics, astronomy, medicine, optics, and philosophy. Al Razi's (Rhazes) and Al-Khwarizmi's seminal work in the 9th and 10th centuries laid the foundation for modern clinical medicine and mathematics (the word "algorithm" derives from the name Al Khwarizmi). This thirst for knowledge was soon transferred to other parts of the Islamic empire, and Al-Andalus soon competed with Baghdad as the cultural hub for Arabs and Muslims.

Of equal importance to the influence of the Arab-Islamic scientific discoveries on the European Renaissance was the reintroduction of ancient Greece's natural philosophy to medieval Europe by way of translations by Islamic scholars. The historian James Burke identifies several knowledge shocks that ignited the Renaissance. One was delivered by Ibn-Sina (Avicenna, 980 to 1037), whose Kitab Al-Shifa ("The Book of Healing") introduced medieval Europe to the principles of logic and their use to gain knowledge, and placed science and religion on equal terms as sources of knowledge and understanding of the universe. Another major shock was delivered by Ibn-Rushd* (Averroes, 1126 to 1198), whose writings and commentaries reintroduced to medieval Europe the Aristotelian approach to studying nature by observation and reasoning.

From that point on, the scientific paradigm of knowledge production advanced relentlessly throughout Europe. At the same time, the Arab-Islamic civilization and its contributions to science and knowledge started its long decline with Ibn-Khaldun (1332 to 1395), who established in his

Wasim Maziak
Syria

Wasim Maziak is the director of the Syrian Center for Tobacco Studies in Aleppo, a pioneer collaborative research and research capacity–building center in the Arab world. He earned an MD in 1984 from the Aleppo School of Medicine, Syria, and in 1990 he received his Ph.D. in allergy immunology from Kiev Medical Institute, Ukraine. He built his research experience in epidemiology and clinical medicine at the Institute of Epidemiology and Social Medicine in Muenster, Germany, and the National Heart and Lung Institute in London, UK. Much of his research career has been devoted to the study of asthma as well as tobacco use and addiction, including the emerging public health threat of waterpipe smoking. Most recently he initiated the Research Assistance Matching (RAM) program aimed at helping researchers in developing countries get specialized assistance in their research projects. For this essay, he has synthesized his experience and observations as a working scientist in Syria to analyze the larger context of science in the Arab world.

All essays and interactive features appearing in this series can be found at www.sciencemag.org/sciext/globalvoices/

CREDIT: WASIM MAZIAK

Arab seed of science. Ibn-Rushd (Averroes, 1126 to 1198) helped to open new ways of thinking by attempting to overcome the contradictions between Aristotelian philosophy and revealed religion by distinguishing between two separate systems of truth—a scientific body of truths based on reason and a religious body of truths based on revelation.

"Muqaddamah" the basic tenets of modern sociology, being the last prominent Arab thinker of the era. Moreover, this descent was accompanied by a major shift in the dominant thought paradigms in Arab-Islamic contexts, from the rational and tolerant to a more conservative school of thinking that denounced philosophy and rationalism. This conservative, indoctrinated view of the world continues to be influential today with no real challenge to it other than that of the reformists of the 19th and early 20th centuries, such as Jamal Eddin Al-Afghani and Muhammed Abduh.† Both scholars explicitly opposed Western colonialism, but they embraced rationalism and sought to reconcile Islamic principles with those of modernism.

The Decline of Science in the Arab World

Currently, the scientific output of Arabs is disproportionate to their human and economic capacities. Taking biomedical research as an example, Arab countries currently produce less than 1% of citations in the world and contribute less than 0.5% of papers appearing in the 200 leading medical journals.‡ Annual spending on research and development in Arab countries is estimated at 0.15% of their gross domestic product (GDP), compared to a world average of 1.4%.§ Lack of funding, poor institutional support, and meager integration within the international scientific community are among the many reasons that analysts have cited to explain the current status of science in Arab states. More general factors, such as wars, conflicts, and international political and economic sanctions, also have been implicated.

These undoubtedly are important factors, but they do not include the more fundamental roots of science's current situation in the Arab world. For example, countries enjoying relatively long periods of stability and affluence (most of the Gulf States) do not fare better in terms of biomedical research, especially when the large number of foreign scientists working there is taken into consideration. On the other hand, countries like Lebanon and Jordan, which suffered from long internal strife and poverty, fare better than other Arab states when their scientific production is weighed against their GDP.‖ This suggests that less obvious factors are playing decisive roles in the valuation of science in Arab societies.

Even as most poor Arab states viewed science as a luxury that they could not afford, wealthy Arab states perpetrated an illusory adoption of science and technology. Rich Arabs believed that oil money plus Western technology was a simple formula for industrialization and modernization. Thus, acquiring the latest technological products or shares in hi-tech industries became synonymous with being partners in the technological revolution of the modern world. After all, most Arabs view science as a commodity that can be separated from the thought processes and sociocultural attributes of its producers. This perspective makes it hard to appreciate the differences in culture and values between technology-producing and technology-consuming societies.

At the same time, the "West" was doing its part to solidify this schism by treating Arabs as a mere market sector rife with insatiable consumers that it had to appease, but without any commitment to developing this sector's own science and technology capacities. This view resulted in a business-type alliance with contractual commerce, but no real dialogue beyond that. For a while, this state of affairs seemed to suit both sides, but the rapidly advancing information-communication technology disrupted the quietude. But who among us could have foreseen the profound impact of these technological developments on nearly all aspects of life of nearly every society a decade or two ago?

Perhaps more than anyone, those in traditional Islamic societies felt the shock: The proliferation and expansion of information technologies brought a ruthless invasion of Western culture into virtually every sphere of life. With satellite TV, the Internet, and electronic communication, Western lifestyles, fashion, behavior, and values infiltrated Arab homes with no real way to keep this influx in check. I suspect that this unsolicited invasion of Western culture and values has been felt more directly by Arabs today than by their grandfathers in the 19th and early 20th centuries, who faced European armies occupying their homelands.

Arabs were awakened to the fact that the arrival of innovations brings with it, directly or indirectly, the lifestyle and sociocultural values of their innovators. Wealth, it seems, is powerless against the culture of those who create and own the technology. For most Arab societies today, the tides of inputs coming from all directions—from their conflict-ridden present, from the unjust distribution of wealth, and from their tyrant-controlled regimes that tolerate no dissent—have been confusing, relentless, and exhausting. The resulting frustration has been channeled outward toward the West in the form of disdain and hostility, and inward in the form of an antagonistic view of the world.

In this conflicted sociological and emotional context, there has been little space in the Arab mind to distinguish between market dynamics, politics, and nations, to perceive the valuable discourse and diversity within Western societies, or to appreciate the moral values and work ethics of Western culture. Instead, the entirety of the West has been gradually demonized. And by linking modern Western culture to the period of the Crusades, many Arab opinion-makers forged a historical basis for this vilification as an uninterrupted continuation of the evils of the past (arguably many people in the West, especially after 9/11, have adopted a similar mind-set toward Arabs and Muslims). From a psychological standpoint, such an attitude is understandable. As a proud people, Arabs turned to their golden past for a refuge, and as a threatened culture, they turned to their native thought system (Islam) for answers. More than that, however, this reaction has proceeded to the point where the past has become

Renaissance maker. In this manuscript illumination, the Arab scientist and philosopher Ibn-Sina (Avicenna, 980 to 1037) converses with others in a pharmacy. His "Al Qanun of Medicine" served as the standard medical text in Europe for seven centuries, and he also laid some groundwork for the European Renaissance by advocating the use of reason and logic as the way to gain knowledge.

distilled and purified, and Islamic teachings have been selectively used to embrace and abet the emerging anti-Western sentiment.

With little reason for pride or celebration, Arabs leaned toward trivializing mortal earthly life, choosing instead to reassess the main purpose of existence as ensuring heavenly immortality. A logical extension of this existential reevaluation has been to view the West's interest in science as an improper indulgence in material trivialities. For decades, these changes were proliferating and festering under the surface, creating an atmosphere inimical to science and one effectively closed to the possibility of learning from the Western experience.

Science was caught in the crossfire. Subconsciously for many Arabs, modern science's ties to the West, to rationalism, and to natural materialism gave it the flavor of enmity. And because science cannot be practiced nowadays without close collaboration with Western academic institutions, research has become, in the minds of many Arabs, a suspicious activity and yet another potential gateway for Western incursion.

As a result, the pathway to the future shifted from one involving science to one based on the return to true Islam. Left unanswered in this choice was what a shunning of science would entail and how to face the challenges of the inevitable technology gap that would come with the choice. On the other side of the equation, the main competing view to the Islamic one in Arab countries today, the liberal-democratic paradigm, focuses mainly on political structure and is equally ambivalent about the centrality of science as a driving force for development. With the scientific community being all but mute, science in the Arab world has currently no one to speak on its behalf, and it occupies an insignificant niche. Moreover, its approach to understanding and investigating nature, as well as its own history, attracts virtually zero interest.

Reawakening of Arab Science

Science thrives on freedom of inquiry and unfettered flow of information. Most Arab societies are run by dictatorships that practice different levels of censorship on their citizens, leading to a weakening of democratic institutions. Such institutions are vital for the development of science by unlocking the diversity within the society, making it less prone to quietly adopt rigid dogmas and doctrines, advocating the importance of science and freedom of inquiry, and shielding scientists from social and political pressures against research dealing with sensitive social and cultural issues, such as the influence of polygamy on the physical and mental health of women.¶ If they were in place, functional democratic institutions also would make it more difficult for rulers to spend most of the national income on arms while other areas, including science, suffer greatly from the lack of funding.

Most higher scientific institutions in Arab countries are run by governments, which, in undemocratic systems, means that their goals actually are more political than scientific. This mode of governance reflects unfavorably on many aspects of academic life, rendering scientific merit and research of little importance for career advancement and precluding any genuine evaluation of the scientific performance of these institutions. Lack of high-quality research by faculty members, in turn, limits training opportunities for students and hinders the development of the very organizational structures that would support the growth of research capacity. This has turned most Arab universities merely into centers for knowledge dissemination, not for questioning, criticism, and an authentic search for new knowledge.

To allow research and science to take off once again in Arabic countries, universities and academic institutions need to be redefined as centers for both the dissemination and generation of knowledge, and research funding needs to be allotted according to proper evaluation mechanisms.

But what are the prospects for Arabs in today's science landscape? The same information revolution that has been perceived by so many Arabs as threatening also presents an unprecedented opportunity for every nation in the world to close the science and technology gap. Every society now has the means to build its own science and technology capacities and in ways that do not necessarily follow the path of the West's scientific revolution. Such a prospect should make it easier for Eastern cultures to build their science base, and indeed, many nations in Asia are doing just that without much concern about the loss of their cultural identity or moral values.

But for Arabs, there is a sizable price to pay for being able to instantly know the weather forecast in remote areas or to gather 100 opinions on any topic with little more than a few keystrokes. After all, this technology is forging its own global culture with mainly Western influences. To buy into it as a non-Westerner, therefore, is to personally accept a nonleading role in the cross-national cultural arena. This is not to say that there is a master Western mind at the controls in some global information-communication headquarters. The global arena is open to everybody, and the more a nation is advanced technologically and open to new ideas, the more it is likely to contribute to, and influence, this emerging global culture. The dilemma for Arabs today comes down to choosing between self-exile from the global community for the sake of preserving cultural identity, or contributing one's own identity to a global culture with no specific or chosen color, religion, or ideology. Were Arabs to take the leap into this new global context, it may not be a farfetched prediction that the center of influence of this culture might start to shift to the East within a few decades.

The same information revolution that has been perceived by so many Arabs as threatening also presents an unprecedented opportunity for every nation in the world to close the science and technology gap.

A moment of opportunity is at hand. The Arab world needs to reopen its collective mind to the West, by acknowledging the West's contribution of modern science to the world. At the same time, the West should recognize the Arabic contribution to the scientific revolution without downplaying the role that Islam has played. Real pride of the golden past of Arabs means extracting the right lessons from it: adoption of science by the state, encouragement of free scientific inquiry, promotion of science among the masses, and most importantly, embracing the scientific accomplishments of other cultures without fear or prejudice. Certainly, the highest standard of piety should become once again the individual's contribution to the welfare of his society, and the greatest sin, the acceptance of a continuing and avoidable backwardness and dependence.

References and Notes

*During the Renaissance, Ibn-Rushd was often referred to as the "The Commentator," in comparison to Aristotle "The Philosopher," signifying his status and contribution.

†On his return from a journey to Europe, Sheikh Muhammad Abduh, signifying the precedence of deeds over rituals in the Islamic context, said, "In Europe I found Islam but not Muslims. Here in the East, I find Muslims but not Islam."

‡A. A. Al-Khader, *Saudi Med. J.* **25**, 1323 (2004).

§E. Massod, *Nature* **416**, 120 (2002).

‖G. O. Tadmouri, N. Bissar-Tadmouri, *Lancet* **362**, 1766 (2003).

¶W. Maziak, T. Asfar, *Health Care Women Int.* **24**, 313 (2003).

The author is at the Syrian Center for Tobacco Studies, Post Office Box 16542, Aleppo, Syria. He is also affiliated with the Institute of Epidemiology and Social Medicine in Muenster, Germany. E-mail: maziak@net.sy

10.1126/science.1114330

MATERIALS SCIENCE

Electronics Without Lead

Yi Li, Kyoung-sik Moon, C. P. Wong

Tin-lead alloys are widely used as solder in the electronics industry (*1*, *2*). They serve as interconnects that provide the conductive path required to achieve connection from one circuit element to another (see the figure). In 2000, 10% of the lead consumed by U.S. industries was used to produce alloy solders for consumer electronics. Most of these products—such as cell phones and electronic toys—have a short service life, often ending up in a landfill within a few months or years. The disposed lead can leach into the drinking water, posing a severe health risk to humans. Attempts to recycle the lead in printed wiring boards of consumer electronic products have not been successful.

In response to concerns for the environment and human health, Japan required all new electronic products to be lead-free from January 2005; the European Union has introduced legislation to ban lead from electronic products by 1 July 2006. The U.S. government has not yet legislated against the use of lead in electronic products. In response to the new legislation, most major electronic manufacturers, including those in the United States, have stepped up their search for alternatives to lead-containing solders. To date, these efforts have focused on two alternatives: lead-free alloys and electrically conductive adhesives.

The most promising lead-free alloys contain tin as the primary element, because it melts at a relatively low temperature (232°C) and easily wets other metals. Depending on the application, different elements (such as silver, copper, bismuth, zinc, indium, and nickel) may be added (*3*–*5*). Among these alloys, tin/silver/copper alloys have been widely accepted as the most promising lead-free solders. A mixture of 95.4% tin, 3.1% silver, and 1.5% copper provides optimal strength, fatigue resistance, plasticity, and reliability.

However, the melting point of the latter alloy is 217°C; like most other lead-free alloys, this is more than 30°C higher than that of the tin-lead alloy with the lowest melting point (183°C). To obtain sufficient wetting by lead-free solders, the processing temperature during electronic assembly must therefore be raised by 30° to 40°C. This temperature increase reduces the integrity, reliability, and functionality of printed wiring boards, components, and other attachments (*6*). Preliminary research has shown that the use of metal nanoparticles may lower the melting temperature of lead-free solders (*7*–*9*). Even if the melting temperature can be lowered, several other important issues must be addressed, such as the implementation of a lead-free assembly process, the development of compatible lead-substrates, and the reliability of the lead-free solder joints.

Electrically conductive adhesives are the other promising alternative to tin-lead solder. They consist of a polymeric resin (for example, an epoxy, silicone, or polyimide) that provides mechanical properties such as adhesion, mechanical strength, and impact strength and a metal filler that conducts electricity. Electrically conductive adhesives offer numerous advantages over conventional solder technology. They are environmentally friendly, require fewer processing steps (reducing processing cost), and allow a lower processing temperature (enabling the use of heat-sensitive and low-cost components and substrates) and smaller distances between the electrical lines in circuits (enabling the manufacture of smaller devices) (*10*).

Currently, there are many conductive adhesives on the market that are primarily targeted to low-power devices such as driver chips for liquid crystal displays. However, no commercially available conductive adhesive can replace tin-lead metal solders in all applications. Especially for high-power devices such as microprocessors, these polymer-based materials have critical drawbacks, including conductivity fatigue in reliability tests, limited current-carrying capability, and poor impact strength (*2*, *5*, *10*).

Recently, some progress has been made in elucidating the mechanisms underlying the conductivity fatigue and the limited current-carrying capability of conductive adhesives. Because galvanic corrosion is the main cause of conductivity fatigue, oxygen scavengers, corrosion inhibitors, and sacrificial additives (alloys with lower corrosion potential) have been used to stabilize the contact resistance and improve the reliability of conductive adhesives (*2*, *11*). To enhance the current-carrying capability of conductive adhesives, self-assembled monolayers with high current density were incorporated into the interface between metal fillers and substrates; the electrical conductivity and current-carrying capability of the resulting adhesives can compete with those of traditional solder joints (*12*).

Another critical property for electronic components is the ability to withstand impacts generated by, for example, dropping, strong vibration, or mechanical shock. Most microelectronic commercial conductive adhesives have poor impact strength. Thus, components that are assembled with conductive adhesives tend to sep-

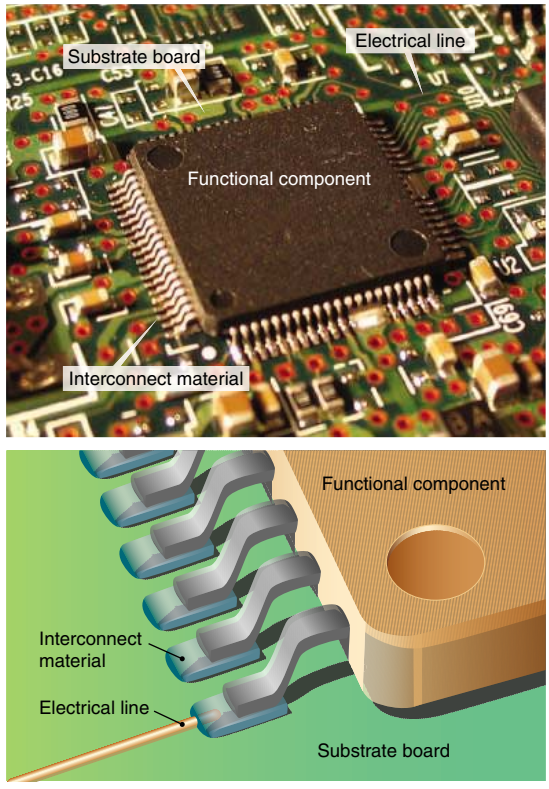

Lead on the board. (**Top**) Photo of a functional component that is assembled on the board substrate via interconnects. (**Bottom**) Side view of the bonding between the component and the substrate via the interconnect material.

CREDIT: (BOTTOM PANEL) PRESTON HUEY/*SCIENCE*

The authors are in the School of Materials Science and Engineering, Georgia Institute of Technology, Atlanta, GA 30332, USA. E-mail: cp.wong@mse.gatech.edu

arate from the substrate upon being subjected to a sudden shock (*13*, *14*). The impact strength of conductive adhesives may be increased by decreasing the filler loading, using resins that absorb the impact energy generated by shock, and encapsulation of the surface-mounted devices (*15*).

Many challenges to producing lead-free interconnects remain to be addressed by scientists and engineers, but both lead-free solders and conductive adhesives show much promise. To make the two lead-free alternatives viable, conductive adhesives that can carry high currents and lead-free solders that have low processing temperature, high reliability, and good thermal mechanical properties are needed.

References

1. J. Lau, C. P. Wong, N. C. Lee, S. W. R. Lee, Eds., *Electronics Manufacturing: With Lead-free, Halogen-Free, and Conductive-Adhesive Materials* (McGraw Hill, New York, 2002).
2. K. J. Puttlitz, Kathleen A. Stalter, Eds., *Handbook of Lead-Free Solder Technology for Microelectronic Assemblies* (Dekker, New York, 2004), chap. 1.
3. M. Abet, G. Selvaduray, *Mater. Sci. Eng.* **27**, 95 (2000).
4. A. Z. Miric, *Soldering and Surface Mount Technology* **10**, 19 (1998).
5. J. S. Hwang, Ed., *Environment-Friendly Electronics: Lead-Free Technology* (Electrochemical Publications, Port Erin, UK, 2001).
6. P. Zarrow, *Circuits Assem.* **10**, 18 (1999).
7. K. S. Moon *et al.*, *J. Electron. Mater.* **34**, 168 (2005).
8. Y. Matsuba, *Erekutoronikusu Jisso Gakkaishi* **6**, 130 (2003).
9. M. Y. Efremov *et al.*, *Phys. Rev. Lett.* **85**, 3560 (2000).
10. J. Liu, Ed., *Conductive Adhesives for Electronics Packaging* (Electrochemical Publications, Port Erin, UK, 1999).
11. Y. Li, C.P. Wong, in *Proceedings of the 4th International IEEE Conference on Polymers and Adhesives in Microelectronics and Photonics*, Portland, OR, 14 to 16 September 2004 (IEEE, Piscataway, NJ, 2004), pp. 1–7.
12. Y. Li, K. Moon, C. P. Wong, *J. Electron. Mater.* **34**, 266 (2005).
13. J. Liu, B, Weman, in *Proceedings of the 2nd International Symposium on Electronics Packaging Technology*, Shanghai, China, 9 to 12 December 1996 (Shanghai Univ. Press, Shanghai, China, 1996), pp. 313–319.
14. Q. K. Tong, S. A. Vona, R. Kuder, D. Shenfield, *Proceedings of the 3rd International Conference on Adhesive Joining and Coating Technology in Electronics Manufacturing*, Binghamton, NY, 28 to 30 September 1998 (IEEE, Piscataway, NJ, 1998), pp. 272–277.
15. D. Lu, C. P. Wong, in *Encyclopedia of Smart Materials*, M. Schwartz, Ed. (Wiley, New York, 2002), vol. 1, pp. 331–316.

10.1126/science.1110168

CELL BIOLOGY

Prion Toxicity: All Sail and No Anchor

Adriano Aguzzi

Within the past 2 years, our understanding of the infectious particles responsible for fatal neurological conditions such as mad cow disease, scrapie, and Creutzfeld-Jakob disease has seen considerable progress (*1*). There is now strong evidence that prions, the culprit infectious particles, can be synthesized in systems that are completely free of cellular material (*2*, *3*). This may essentially settle the score as to the purely proteinaceous nature of the infectious agent. As to the march of prions toward the brain, or "neuroinvasion," a wealth of players has been uncovered, as well as an intricate relationship between immunological and nervous compartments of the host organism (*4*, *5*). Still, the physiological function of PrP^C, the form of prion protein that cells normally harbor, remains essentially mysterious. Also, we do not understand how the infectious form of the prion protein, a structurally distorted form of its normal counterpart, achieves brain damage. A tantalizing inroad has now been made by Chesebro and colleagues as to the latter question on page 1435 of this issue (*6*).

The causative agent of transmissible spongiform encephalopathies (TSEs) such as scrapie is PrP^{Sc}, a misfolded, protease-resistant version of the normal PrP^C protein (encoded by the *Prnp* locus in mice). PrP^{Sc} forms orderly aggregates that often progress into large extracellular deposits commonly described as brain plaques. It is argued that PrP^{Sc} multiplies by recruiting and converting PrP^C into further PrP^{Sc}. But this hypothesis does not explain how infectious prions proceed to induce the spongy brain lesions of TSEs and, eventually, extensive neuronal death. Curiously, PrP^{Sc} itself is innocuous: When the brain of a mouse lacking normal prion protein is grafted with brain tissue replete with PrP^C and then subsequently exposed to infectious prions, sizable amounts of PrP^{Sc} are produced, yet the mouse fails to develop TSE (*7*). So why aren't PrP^C-deficient neurons affected by the infectious agent?

Chesebro *et al*. have investigated this question in a sophisticated model system. During its early biogenesis, PrP^C is directed to the lumen of the endoplasmic reticulum, thus entering the cellular secretory pathway. A glycosylphosphatidylinositol (GPI) lipid anchor is then added to its C terminus, tethering the protein to the outer side of the cell membrane. Chesebro *et al*. redacted a *Prnp* transgene to remove the signal peptide responsible for GPI anchoring. As a consequence, the resulting GPI-negative transgenic mice expressed a monomeric, soluble secreted form of PrP^C.

When infected with PrP^{Sc}, the GPI-negative transgenic mice never developed clinical prion disease. Quite surprisingly, though, their brains were packed with PrP^{Sc} plaques! Evidently, removal of the GPI anchor abolished susceptibility to clinical disease while preserving the competence of the soluble PrP^C molecule to support prion replication. This interpretation fits very nicely with the growing body of evidence that normal prion protein may function as a signaling molecule, just like many other GPI-linked proteins. Altered PrP^C signaling may therefore be unhealthy (see the figure). Indeed, cross-linking of PrP^C on the surface of hippocampal neu-

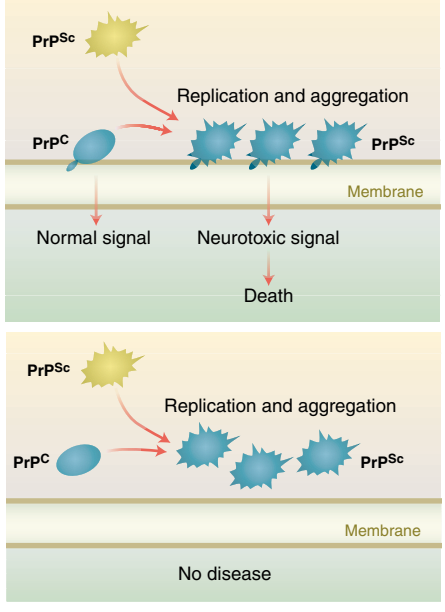

Membrane anchoring is a crucial prerequisite for prion toxicity. (**Top**) Under normal circumstances, the cellular prion protein PrP^C is anchored to the cell membrane with a glycolipid moiety. Upon prion infection, PrP^C is converted into aggregates of a β-sheet conformer called PrP^{Sc}. This may affect signaling events involving normal, membrane-bound PrP^C, leading to neurotoxicity. (**Bottom**) Chesebro *et al*. (*6*) have generated transgenic mice expressing an anchorless, secreted version of PrP^C. When infected with prions, these mice never develop disease, although the secreted PrP^C is efficaciously transformed into PrP^{Sc}.

The author is at the Institute of Neuropathology, University Hospital of Zürich, CH-8091 Zürich, Switzerland. E-mail: adriano@pathol.unizh.ch

rons with antibodies sends the cells into untimely demise (*8*). Hence, we are led to wonder whether the damage wrought on neurons by clustered PrP^C proteins relates to TSE neurodegeneration. If so, could the mechanism by which prion infections lead to brain damage be related to the normal function of PrP^C?

Mice lacking normal prion protein live a healthy and long life without pathological phenotypes, so loss of function of PrP^C is most certainly not a cause of brain damage in TSE. Could any gain of function of PrP^C trigger disease pathogenesis? Morphological findings would appear to depose against this hypothesis as well. Although the clustering of molecules at the cell surface is a common way to initiate signaling, injecting antibodies to PrP^C into a mouse brain does not elicit spongiosis. Conversely, ordered aggregation is a crucial event in the formation of PrP^{Sc} and may represent the true mechanism by which infectivity is generated (*9*).

Chesebro *et al.*'s findings yield powerful support for a link between the cell surface topology of PrP^{Sc} and prion disease pathogenesis. By disengaging PrP^C from the cell surface, the authors have effectively uncoupled clinical disease from prion replication, PrP^{Sc} formation, and its assembly into higher order aggregates and the hallmark brain plaques. It is almost unavoidable to conclude that prion replication avails itself of membrane-bound signal transducers to elicit brain damage.

Another twist to Chesebro *et al.*'s story relates to the structural requirements for prion replication. In contrast to GPI-negative mice, transgenic mice that express a soluble dimeric version of PrP^C do not accumulate PrP^{Sc} in their brains or spleens upon prion infection, nor do they develop or transmit TSE (*10*). Instead, the soluble dimeric form efficaciously competes with endogenous PrP^C and delays prion pathogenesis in normal mice. In combination with Chesebro *et al.*'s results, this indicates that detachment of PrP^C from the membrane does not necessarily abolish its prion replication competence. The soluble dimeric form may act as a dominant-negative form that sequesters PrP^{Sc}, rendering it unavailable and thereby inhibiting disease progression.

Brain extracts of prion-infected GPI-negative mice did not elicit plaque formation when injected into other GPI-negative mice. The importance of this failed attempt at transmission is unclear, but such a result may point to some kind of deficiency in the prion replication machinery of these transgenic mice.

For all the insight brought about by Chesebro *et al.*'s findings, a central question remains. Accruing evidence suggests that signaling at the membrane involving PrP^C underlies TSE pathogenesis. Infectious prions may damage the brain by distorting signaling events that PrP^C normally controls. If that is true, the best way to find out what exactly goes wrong in the brains of prion-infected individuals may be to sort out the normal function of PrP^C. Yet despite 13 years of availability of mice lacking normal prion protein, progress toward resolving the latter question has been painstakingly slow. Although Chesebro *et al.*'s work exemplifies the awesome power of mouse transgenetics, a next important step may consist of porting the prion signaling system to simpler, genetically tractable organisms such as worms, flies, or fish, whose use is already having a tremendous impact on the study of other neurodegenerative diseases.

References

1. A. Aguzzi, C. Haass, *Science* **302**, 814 (2003).
2. J. Castilla, P. Saa, C. Hetz, C. Soto, *Cell* **121**, 195 (2005).
3. G. Legname *et al.*, *Science* **305**, 673 (2004).
4. M. Prinz *et al.*, *Nature* **425**, 957 (2003).
5. M. Heikenwalder *et al.*, *Science* **307**, 1107 (2005); published online 20 January 2005 (10.1126/science.1106460).
6. B. Chesebro *et al.*, *Science* **308**, 1435 (2005).
7. S. Brandner *et al.*, *Nature* **379**, 339 (1996).
8. L. Solforosi *et al.*, *Science* **303**, 1514 (2004); published online 29 January 2004 (10.1126/science.1094273).
9. J. T. Jarrett, P. T. Lansbury Jr., *Cell* **73**, 1055 (1993).
10. P. Meier *et al.*, *Cell* **113**, 49 (2003).

10.1126/science.1114168

CHEMISTRY

Making Fuels from Biomass

Jens R. Rostrup-Nielsen

Recent high oil prices have put the spotlight on biofuels and other alternative energy sources. Energy safety and the environment are high on the political agenda. Biofuels cannot replace oil completely, because sufficient agricultural area is unavailable. However, the conversion of biomass from different sources (including waste) may, in conjunction with other energy sources, help to make our societies less dependent on oil.

The challenge for scientists is not only to find new ways to generate useful fuels, but also to guide politicians toward decisions with minimum costs. The conversion of biomass to fuels is one example, which is illustrated by the conversion of carbohydrates to hydrocarbons reported by Huber *et al.* on page 1446 of this issue (*1*).

The author is at Haldor Topsøe A/S, Nymøllevej 55, 2800 Lyngby, Denmark. E-mail: jrn@topsoe.dk

Carbohydrates—such as sugars, starch, hemicellulose, and cellulose—are found for example in grain, wood, and agricultural waste. Sugars and starch can be converted to ethanol by fermentation, whereas cellulose and hemicellulose require chemical and physical pretreatment followed by enzymatic breakdown of the molecules. Pure ethanol can be added to gasoline; however, this requires an energy-intensive distillation step. This and the energy used in fertilizers, transportation of biomass, etc., should be subtracted from the energy gained from the biofuel to assess the net energy output. One may question the net energy output when the biomass is provided as a primary product at the locations with intensive agriculture. It has been estimated that the ratio of energy output to energy input is no more than 1.1 for corn-based ethanol in the United States; the energy input is provided mainly from fossil fuels (*2*).

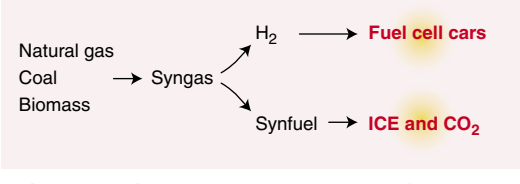

Fuels via synthesis gas. One can use synthesis gas to make hydrogen for fuel cell driven cars or convert it into synthetic diesel or gasoline (synfuel) to be used in conventional internal combustion engines (ICE). The conversion of fossil fuels to synfuels does not solve the CO_2 problem. This is achieved by using biomass or by coupling centralized production of hydrogen from fossil fuels with CO_2 sequestration.

The distillation problem can be reduced if ethanol is converted to hydrogen. Ethanol may thus serve as an energy carrier for a future hydrogen society. The technology for this conversion is available (*3*), but as demonstrated in an earlier paper by Huber *et al.* (*4*), hydrogen may also be formed directly from the carbohydrates by reaction with water (steam reforming) in the liquid phase, hence saving the energy and costs associated with distillation.

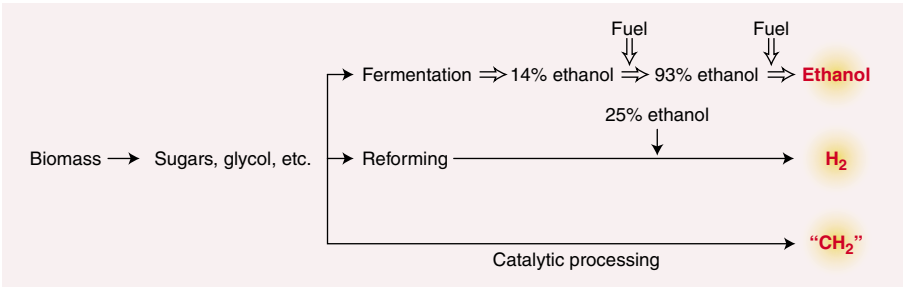

Process routes for conversion of carbohydrates to fuels. These routes include ethanol via fermentation and distillation (**top**), hydrogen via ethanol or directly by liquid-phase steam reforming (**middle**), and hydrocarbons ("CH_2") by the process described by Huber *et al.* (*1*) (**bottom**).

Now, Huber *et al.* (*1*) raise the question why one should not make hydrocarbon fuel directly, instead of aiming for hydrogen as a fuel, which would require an expensive new infrastructure. Modern diesel engines are almost as efficient as fuel cell–driven cars that use hydrogen fuel are likely to be. Why not then make "sustainable" synthetic liquid fuels (synfuels) instead of hydrogen (*5*)?

The same question may be asked for a hydrogen society built on fossil fuels and sequestration of carbon dioxide. Fossil fuels may be converted by gasification or steam-reforming to synthesis gas (a mixture of carbon monoxide and hydrogen) (see the first figure). Carbon monoxide may be further converted to hydrogen and carbon dioxide; the latter may be reinjected in oil fields or in cavities (sequestration). Alternatively, the synthesis gas can be reacted to synthetic liquid fuels in the form of synthetic diesel or gasoline (synfuels) (see the first figure).

Automotive fuels (that is, diesel and gasoline) have an atomic hydrogen-to-carbon ratio, H:C, of 2 ("CH_2"). Ethanol can be converted to hydrocarbon fuel by catalytic processing over zeolites, but the conversion of carbohydrates faces a fundamental problem: Although carbohydrates ($C_nH_{2n}O_n$) contain a lot of hydrogen, this hydrogen is bound to oxygen, meaning that the "effective" H:C ratio is 0.

The earlier liquid-phase reforming method of Huber *et al.* (*4*) solves this problem by extracting oxygen as carbon dioxide, and then making hydrogen. Now, Huber *et al.* (*1*) show that the use of well-known organic syntheses makes it possible to convert carbohydrates into hydrocarbons that are of interest for use as fuels. The process scheme eliminates the expensive distillation process, because separation of the hydrocarbon product from the aqueous phase is simple. Although the reaction paths should be optimized and the cost of the process must still be analyzed and compared with alternative routes (see the second figure), the work of Huber *et al.* (*1*) shows how explorative work can create new options for the supply of energy.

References

1. G. W. Huber, J. N. Chheda, C. J. Barrett, J. A. Dumesic, *Science* **308**, 1446 (2005).
2. P. B. Weisz, *Phys. Today* **57** (no. 7), 47 (2004).
3. G. A. Deluga, J. R. Salge, L. D. Schmidt, X. E. Verykios, *Science* **303**, 993 (2004).
4. G. W. Huber, J. W. Shabaker, J. A. Dumesic, *Science* **300**, 2075 (2003).
5. J. R. Rostrup-Nielsen, *Catal. Rev.* **46**, 247 (2004).

10.1126/science.1113354

ECOLOGY

Rediscovery of the Ivory-billed Woodpecker

David S. Wilcove

A book on North American wildlife, published in 2000, scoffed at the notion that the ivory-billed woodpecker (*Campephilus principalis*) might still be alive somewhere in the southern United States: "Although it remains the Holy Grail of American birdwatchers, with persistent rumors of its presence in remote forests, most ornithologists now concede that it vanished from the United States sometime in the past 40 years…Its presence today in the sterile, industrial forestlands of the South, however wonderful a thought, would be as out of place as a buckskin-clad settler with a musket in the streets of modern-day Atlanta" (*1*). As the author of that book, I now know that sometimes it's great to be wrong. As reported by Fitzpatrick *et al.* on page 1460 of this issue (*2*), the ivory-billed woodpecker has been rediscovered in eastern Arkansas, its presence confirmed by multiple sightings and a grainy but diagnostic videotape. The rediscovery stunned birdwatchers and generated headlines around the world. But those not under the spell of this charismatic species might well wonder what all the fuss is about. What is the ecological significance of the ivorybill's reappearance?

Enhanced online at www.sciencemag.org/cgi/content/full/308/5727/1422

The author is at the Woodrow Wilson School, Princeton University, Princeton, NJ 08544, USA. E-mail: dwilcove@princeton.edu

The outlook for the species is uncertain. Fitzpatrick *et al.* did not find any breeding pairs in 14 months of nearly continuous field work, and they concede that all of their observations may refer to a single individual. Ivorybills naturally occur at very low densities. J. Tanner, who undertook the only field studies of the species in the late 1930s (*3*) estimated the density of ivorybills to be no more than 1 pair per 16–44 km^2 of suitable habitat. This characteristic, combined with the degraded condition of the current habitat and the paucity of sightings, suggests that any breeding population must be extremely small, perhaps only a few pairs. Such a tiny population would be highly vulnerable to stochastic extinction processes. Other North American birds, however, have rebounded from remarkably low numbers. The whooping crane (*Grus americana*) population was down to 14 adult individuals in 1938 (*4*); today, it exceeds 200. No more than 7 Laysan ducks (*Anas laysanensis*) survived in 1912 (*5*); the current population is ~500. Also, given the ivorybill's apparent dependence on old forests (*3*) (see photo), the passage of time should result in more and better habitat for the woodpeckers, as second-growth forests age.

Events preceding and following the ivorybill's rediscovery illustrate the relative benefits of two different approaches to conservation. The Cache River National Wildlife Refuge, where Fitzpatrick *et al.* made their discovery, was established in 1986 with the transfer of 154 ha from The Nature Conservancy, a private nonprofit conservation organization, to the U.S. Fish and Wildlife Service. Subsequent land-acquisition efforts by The Nature Conservancy and

the federal government increased the refuge's size to ~22,300 ha (*6*). At the time the land was acquired, no one was anticipating the discovery of ivory-billed woodpeckers. Conservationists valued the area for its concentrations of wintering waterfowl and as an example of the swamp and bottomland hardwood forests that once dominated millions of hectares in the southeastern United States. The discovery of the ivorybill within the refuge's borders validates the wisdom of conserving representative examples of all types of ecosystems, regardless of whether they contain known populations of imperiled species. Such preservation can act as a "coarse filter" for protecting little-known or overlooked species (*7*).

Yet the documented presence of an ivorybill has resulted in an outpouring of support for conservation efforts in the region. On the day the bird's discovery was announced, for example, the U.S. Departments of Interior and Agriculture pledged $10 million for efforts to protect the ivorybill and its habitat. Unless these departments receive increased appropriations, that money will have to be taken from other worthy projects, presumably ones that lack a species as charismatic as the ivorybill, thereby demonstrating the value of a flagship species in generating support for conservation.

Still hanging on in the woods. The Singer Tract in Louisiana, where this 1935 photograph was taken, was logged during World War II, but bottomland forests are now regenerating across the ivorybill's ancestral range.

The resurrection of the ivorybill also raises an intriguing question: If a bird last sighted decades ago can return from the dead, might we be too hasty in writing the obituaries of other species? Indeed, the case of the ivorybill, while astounding, is not unprecedented. The black-hooded antwren (*Formicivora erythronotos*), for example, was rediscovered in southeastern Brazil in 1987 after more than 100 years without a sighting; the New Zealand storm-petrel (*Oceanites maorianus*), last recorded in the early to mid-19th century, was refound in January 2003.

Not surprisingly, environmental skeptics seize upon events such as these to question the prevailing opinion among ecologists that the world is facing an impending anthropogenic extinction crisis (*8*). Estimates of contemporary extinction rates are based largely on calculations relating the number of species to the amount of suitable habitat; as the amount of habitat decreases owing to human activities so, too, will the number of species. Considerable uncertainty surrounds the timing of this relationship. If small, isolated populations are indeed prone to extinction but disappear slowly, then rediscoveries of supposedly extinct species do not necessarily invalidate extinction predictions. Instead, such events offer a ray of hope for conservationists: If sufficient amounts of habitat can be restored (a big "if"), perhaps the loss of these species can be averted. Time is of the essence, however. A recent report from BirdLife International found that the status of most of the world's threatened birds continues to deteriorate (*9*).

Finally, the good news about the ivorybill should not obscure the bigger, uglier picture of avian extinction in the United States. No nation has lost more species of birds in the past 25 years than the United States, largely as a result of recent extinction events in Pacific islands (see the table). It would take multiple rediscoveries nearly as miraculous as that of the ivorybill to alter this shameful fact.

RECENTLY EXTINCT U.S. BIRDS

Species	Last sighting	Reference
Olomao (*Myadestes lanaiensis*)	1980	(*10*)
Mariana mallard (*Anas oustaleti*)*	1981	(*11*)
Guam flycatcher (*Myiagra freycineti*)	1983	(*4*)
Kamao (*Myadestes myadestinus*)	1985	(*10*)
Oahu alauahio (*Paroreomyza maculata*)	1985	(*10*)
Kauai oo (*Moho braccatus*)	1987	(*10*)
Dusky seaside sparrow (*Ammodramus* [*maritimus*] *nigrescens*)†	1987	(*12*)
Ou (*Psittirostra psittacea*)	1989	(*10*)
Poouli (*Melamprosops phaeosoma*)	2004	(*13*)

*Disputed species, not recognized by American Ornithologists' Union. †Considered a subspecies of *Ammodramus maritimus* by American Ornithologists' Union.

Birds native to the United States that have become extinct since 1980. One additional species, Hawaiian crow (*Corvus hawaiiensis*), is now extinct in the wild but survives in captivity.

CREDIT: COURTESY OF DAVID ALLEN AND THE CORNELL LABORATORY OF ORNITHOLOGY

References and Notes

1. D. S. Wilcove, *The Condor's Shadow: The Loss and Recovery of Wildlife in America* (Anchor Books, New York, 2000).
2. J. W. Fitzpatrick *et al.*, *Science* **308**, 1460 (2005); published online 28 April 2005 (10.1126/science.1114103).
3. J. T. Tanner, *The Ivory-Billed Woodpecker, Research Report no. 1* (National Audubon Society, New York, 1942).
4. BirdLife International, *Threatened Birds of the World* (Lynx Ediciones and BirdLife International, Barcelona and Cambridge, 2000).
5. A. J. Berger. *Hawaiian Birdlife* (Univ. of Hawaii Press, Honolulu, ed. 2, 1981).
6. "Restoring the Big Woods: A timeline of the Nature Conservancy's activities," www.nature.org/ivorybill/habitat/recovery.html (accessed 7 May 2005).
7. C. R. Groves, *Drafting a Conservation Blueprint: A Practitioner's Guide to Planning for Biodiversity* (Island Press, Washington, DC, 2003).
8. H. Fountain. "Extinct? Prove it." *New York Times*, Week in Review, 1 May 2005.
9. BirdLife International, *State of the World's Birds: Indicators for Our Changing World* (BirdLife International, Cambridge, 2004).
10. M. H. Reynolds, T. J. Snetsinger, in *Evolution, Ecology, Conservation, and Management of Hawaiian Birds: A Vanishing Avifauna*, J. M. Scott, C. Conant, C. Van Riper III, Eds., no. 22 of *Studies in Avian Biology* (Cooper Ornithological Society, Camarillo, CA, 2001), pp. 133–143.
11. "Gone but not forgotten: Mariana mallard"; www.fws.gov/pacific/pacificislands/wesa/mallardmariaindex.html (accessed 16 May 2005).
12. U.S. Fish and Wildlife Service, *Fed. Reg.* **55**, 51112 (1990).
13. American Bird Conservancy, "Hawaiian Bird Likely Extinct: Government Must Act Now to Prevent Dozens More Losses" (press release, 1 December 2004).

14. I thank E. Dinerstein, A. Dobson, N. Gregory, C. Kremen, J. Lepson, J. M. Scott, and W. Turner for their helpful comments.

10.1126/science.1114507

Allosteric Mechanisms of Signal Transduction

Jean-Pierre Changeux[1]* and Stuart J. Edelstein[1,2]

Forty years ago, a simple model of allosteric mechanisms (indirect interactions between distinct sites), used initially to explain feedback-inhibited enzymes, was presented by Monod, Wyman, and Changeux. We review the MWC theory and its applications for the understanding of signal transduction in biology, and also identify remaining issues that deserve theoretical and experimental substantiation.

The elaboration of the allosteric theory spanned the years 1961 to 1967 and developed in two principal steps. The first issue involved the mechanisms by which a regulatory ligand (such as an enzyme feedback inhibitor) controls the state of activity of a biologically active site, such as an enzyme catalytic site, despite being structurally different from the active-site substrate. Regulatory effectors and substrates were proposed to behave as two distinct categories of ligands, which bind to their target protein at topographically "distinct sites" (Fig. 1A) (*1*) that mutually influence each other through a reversible conformational change. The proposal relied on the induced-fit theory of Koshland (*2*), which initially was developed not to explain the regulation of enzyme activity by a metabolic signal but to account for the specificity of enzyme action. This concept of indirect or "allosteric" interactions between stereospecifically distinct sites (*3*) differed from the classical explanations of enzyme inhibition through steric hindrance at a common binding site. The second issue was raised by the analysis of the complex patterns of kinetics encountered with bacterial regulatory enzymes, particularly L-threonine deaminase and aspartate transcarbamylase. Both of these enzymes showed intertwined cooperative (homotropic) interactions between identical ligands (i.e., oxygen and hemoglobin), as well as signaling (heterotropic) interactions between different ligands (i.e., between a regulatory molecule and a substrate).

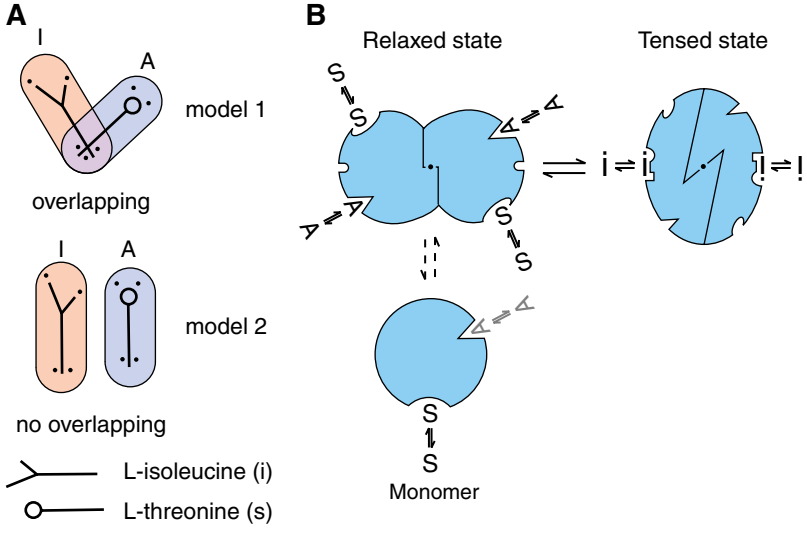

Fig. 1. Initial models of allosteric sites and allosteric transitions. (**A**) Nonoverlapping regulatory and catalytic sites for (s) substrate, L-threonine and (i) inhibitor, L-isoleucine (*1*). (**B**) Conformational transitions preserving the symmetry of the quaternary structure (*33*). Three classes of molecules are shown that bind to the enzyme (as indicated by solid double arrows): A (activator), I (inhibitor), and S (substrate). Transition between two states, R (relaxed) and T (tensed), is depicted horizontally, as well as a hypothetical monomeric state below, designated (with possible binding of A) as indicated by the gray double arrows.

To deal with these issues, Monod, Wyman, and Changeux (*4*) proposed two unifying concepts in their 1965 "MWC" model. The first proposes that regulatory proteins have a quaternary structure (the spatial arrangements and interactions of individual polypeptide chains that together make a complex protein) with identical subunits regularly organized into finite assemblies, or "oligomers," with symmetry properties (defined in terms of axes about which one polypeptide chain with its precise three-dimensional structure can be rotated to superimpose on another chain within the same quaternary structure) (Fig. 1B). The second postulates that, to account for the observed linkage between homotropic and heterotropic interactions, the signaling oligomers undergo reversible transitions between discrete conformations, which primarily affect the quaternary organization, preserve its symmetry, and are accessible in the absence of ligand (Fig. 1B). In other words, the cooperative structural changes intrinsic to the protein molecule determine the observed cooperative binding properties.

Such spontaneous "conformational switches," whose states are selectively stabilized by the ligands to which they preferentially bind, contrast with the sequential, induced-fit mechanism (*5*) initially suggested for hemoglobin. In an induced-fit mechanism, the very binding of the ligand to its site causes a subsequent change of conformation that would be "adapted" to the particular structure of the ligand. The initial versions of the MWC theory (*3*, *4*)—which relied on the then available structural data of Perutz for hemoglobin—dealt with regulatory enzymes, but a plausible application to hormone nuclear receptors and gene repressors was suggested. An extension of the theory to membrane receptors, in particular to neurotransmitters, was later proposed (*6*, *7*). This introduced the concepts of vectorial organization and rotational symmetry related to receptor integration into the biological membrane, along with the possible cooperative interactions in large-scale two-dimensional lattices. Detailed applications to hemoglobin were promptly pursued (*8*) and remain a subject of interest (*9*, *10*). The issue then became an experimental one: Which conformational mechanism faithfully represents the empirical observations collected with regulatory enzymes, hemoglobin, transcription factors, and

[1]Receptors and Cognition, Institut Pasteur, 75724 Paris Cedex 15, France. [2]Department of Biochemistry, University of Geneva, CH-1211 Geneva 4, Switzerland.

*To whom correspondence should be addressed. E-mail: changeux@pasteur.fr

membrane receptors and is the general mechanism of signal transduction?

Distinct Protein Domains for Signaling Ligands and the Issue of Symmetry

Crystallography and electron microscopy studies of signaling molecules—including, in addition to hemoglobin, regulatory enzymes (threonine deaminase, aspartate transcarbamylase, phosphorylase B, phosphofructokinase, L-lactate dehydrogenase), membrane receptors (acetylcholine receptor, glutamate receptor, bovine rhodopsin), and nuclear receptors (lactose repressor, estrogen, or retinoic acid receptors)—have abundantly shown that distant residues participate in the recognition of the regulatory ligand and in the biologically active site [see (*11*, *12*)]. The average distance is 30 to 40 Å. Moreover, distinct protein domains may form that show striking autonomy. In many signaling proteins, domains can be separated by biochemical or genetic methods. Such domains preserve ligand-binding capacity in solution, as found with aspartate transcarbamylase, nuclear receptors, tyrosine kinases, and the nicotinic receptors. In many of these systems, chimeric molecules joining domains with different specificities may even be functional—as shown, for instance, with the nicotinic receptor [e.g., (*13*)].

Crystallographic studies show that, in agreement with the MWC theory, most signaling proteins are made up of a finite number of identical subunits regularly organized around symmetry axes that allow their three-dimensional structure to be exactly described by defined rotations (*11*, *14*) (Fig. 2). Single rotational axes are observed in membrane receptors (Fig. 3) and nuclear receptors (*15*), and there is increasing evidence that dimerization is a requisite for function in G protein–coupled receptors (GPCRs) (*16*).

Exceptions to perfect symmetry do exist, in particular for membrane receptors in which one or several subunits can be substituted by homologous but distinct subunits coded by different genes, yielding a considerable diversification of oligomer composition [see (*12*)]. In some instances, the genesis of a functional receptor even requires association of different subunits with a defined stoichiometry, as in the case of γ-aminobutyric acid type B ($GABA_B$) receptors.

Ligand-Binding Sites at Subunit Interfaces

In the original MWC theory, two unsuspected features of oligomeric proteins were missed. First, the binding sites for regulatory ligands, substrates, or pharmacological agents are, in many cases, located at subunit interfaces, with different interfaces accommodating different categories of stereospecific ligands. Second, physiological ligands (as well as synthetic drugs) may bind within an axial cavity of the molecule, along a symmetry axis. Crystallographic structure determination of several regulatory enzymes—aspartate transcarbamylase, phosphorylase B, phosphofructokinase, and bacterial L-lactate de-

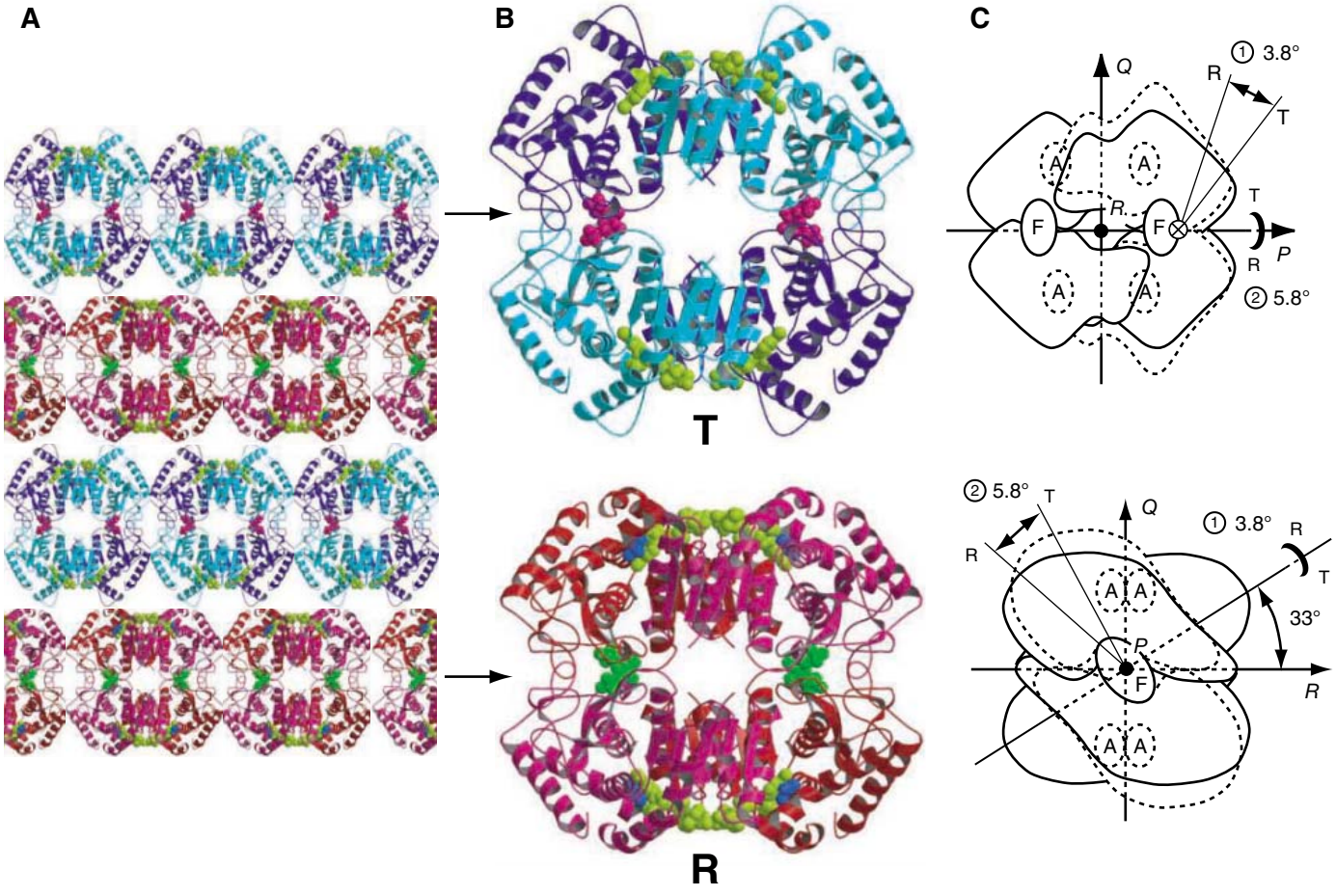

Fig. 2. Structural demonstration of the MWC model: The T and R states coexist in the crystals of bacterial L-lactate dehydrogenase (*14*). (**A**) Planar view of crystal. (**B**) T and R states enlarged showing bound ligands [coenzyme: NADH (reduced form of nicotinamide adenine dinucleotide), light green; regulatory signal: fructose 1,6-bisphosphate, fuchsia in T, green in R; substrate analog: oxalate, blue] at topographically distinct sites and conservation of symmetry of the quaternary structure with little change in tertiary organization of the subunits. (**C**) Two views showing the rotations corresponding to the T-R transition with respect to the three orthogonal axes denoted by *P*, *Q*, and *R* (viewed looking down the *R* axis in the upper schema and down the *P* axis in the lower schema). A and F refer to the analog, oxalate, and to fructose-1,6-bisphosphate, respectively.

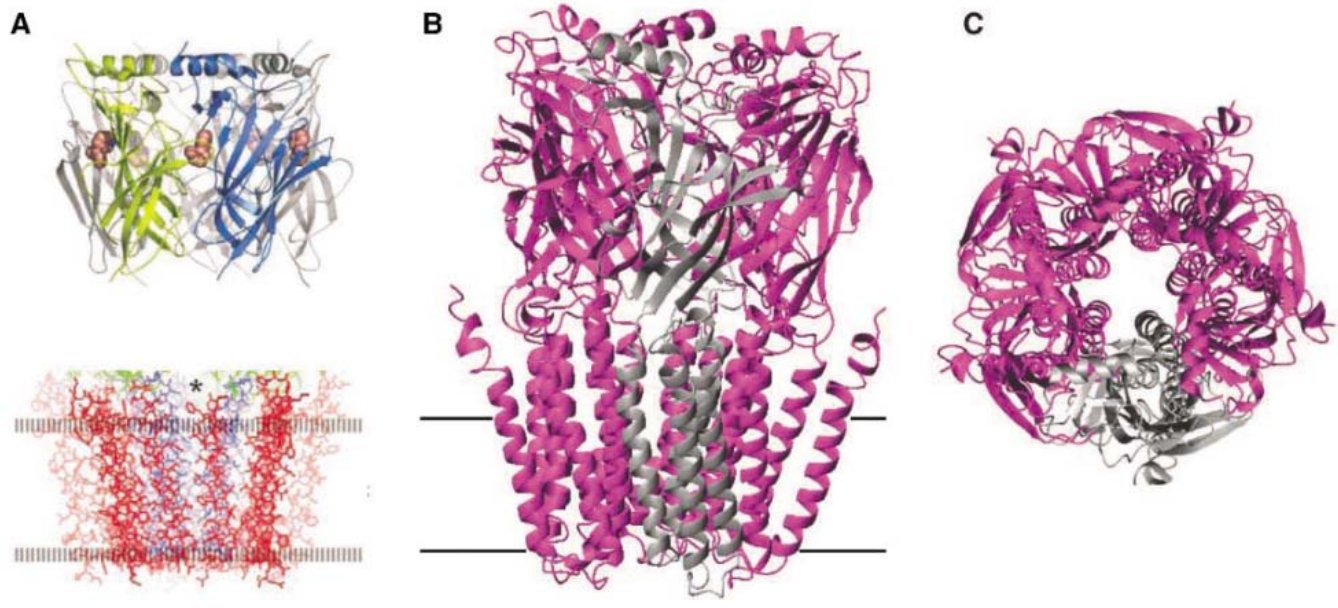

Fig. 3. The acetylcholine nicotinic receptor, a typical allosteric membrane protein. (**A**) Top: X-ray structure of the soluble molluscan acetylcholine binding protein (*34*). Bottom: High-resolution electron microscopy structure of the Torpedo nicotinic receptor transmembrane region (*35*). (**B** and **C**) A three-dimensional computer model of the pentameric α7 acetylcholine nicotinic receptor derived from the structural data in (A) (*36*), in side view (B) and top view (C). The vectorial organization of the oligomeric molecule shows the five-fold rotational axis of symmetry, the nicotine binding site at the boundaries between subunits, and the topographically distinct ion channel.

hydrogenase, among others (*11*, *14*)—revealed the location of the regulatory sites at protein interfaces distinct from the catalytic site. In membrane receptors, binding sites for signaling molecules also occur at subunit interfaces. In muscle nicotinic receptor, for instance, the acetylcholine binding sites are located at subunit boundaries and display structural differences and distinct ligand-binding properties, with no evidence for ligand binding at the three other possible interfaces. In $GABA_A$ receptors, synthetic pharmacological agents—the benzodiazepines—bind at such ''free'' interfaces (*12*), much like anti–sickle cell anemia drugs bind to hemoglobin (*11*). Yet in some GPCRs such as rhodopsin, the ligand-binding domain is located not at a subunit interface but rather within the transmembrane heptahelical domain. In others, such as the metabotropic receptors for glutamate and $GABA_B$ and the ionotropic receptor for glutamate, the neurotransmitter binding pocket lies between distinct ''lobes'' from the same subunit, but the ligand-binding cores assemble as dimers (*15*) within which pairs of sites strongly interact.

An original position for a site binding a signaling molecule, which was not mentioned in the MWC theory but appears perfectly consistent with it, is the axial cavity of the protein molecule. Initially demonstrated for 2,3-diphosphoglycerate with hemoglobin, it served as a structural model for the action of synthetic or natural channel blockers that target a large number of ion channels, including the nicotinic receptor and the Na^+ and K^+ channels. These blockers were instrumental in the first identification of a channel lumen at the intersection of the five subunits of the nicotinic receptor and the demonstration of its interactions with the acetylcholine binding site 20 to 40 Å away (*12*). The strategic location of binding sites for signaling molecules at protein subunit (or lobe) interfaces adequately fits with the concept of the MWC theory that the conformational transitions primarily concern a reorganization of their quaternary structure.

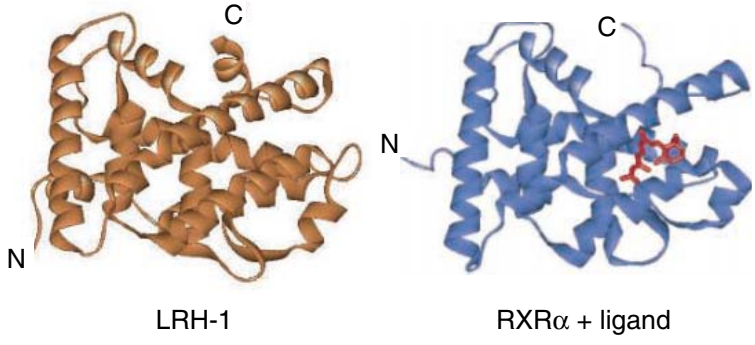

Fig. 4. Structure of the ligand-binding domain (LBD) of LRH-1, a constitutive orphan nuclear receptor (*20*) on the left (PDB 1PK5) and the standard RXRα LBD bound to 9-*cis*-retinoic acid (PDB 1FBY) on the right. The LRH-1 molecule is in an active conformation, as observed by the similarity with the structure of RXRα, but has no ligand in its binding pocket, in contrast to the presence of 9-*cis*-retinoic acid for RXRα.

The Allosteric Transition and "Constitutive" Receptors

A critical statement of the MWC theory was that, in essence, the conformational transition that links the multiple sites present on the allosteric oligomer and mediates signal transduction involves states that are populated in the absence of ligand and may spontaneously interconvert with each other. Moreover, it was postulated that these conformations are present in small numbers and differ in the strength of the interactions between subunits, but preserve the symmetry of the subunit assemblies. Crystallographic studies of hemoglobin, phosphofructokinase, bacterial L-lactate dehydrogenase, aspartate transcarbamylase, and other regulatory enzymes revealed that, as predicted, the transitions between a low-activity, low-affinity T state and a high-activity, high-affinity R state can be resolved at the subunit assembly level into rotations about symmetry axes (*11*). However, minor changes of the tertiary structure of individual subunits can be expected to take place. In other words, the quaternary organization am-

plifies the tertiary changes and gives rise to the cooperative interactions (*11*, *14*, *17*). In the case of membrane receptors, crystallographic analyses of the ligand-binding domain of ionotropic (*18*) and metabotropic (*19*) glutamate receptors have identified a resting conformation—in which the above-mentioned lobes are mostly "open" and which is stabilized by competitive antagonists—as well as a ''closed'' glutamate or agonist-bound conformation. The tertiary folding of the two lobes does not differ between the two situations (*18*, *19*). Similarly, the homo- or heterodimeric ligand-binding domains of several nuclear receptors display different conformations in the agonist-bound versus antagonist-bound states, with a few characteristic changes in helix structure within a largely common protein fold structure [see (*20*)]. Crystallographic studies elucidated the structural changes of multisubunit potassium channels between the closed and open states (*21*). In agreement with the MWC theory, a hydrophobic gate located in the axis of symmetry frees ion movement through the concerted symmetrical motions of the transmembrane helices.

A key statement of the MWC theory is that the conformational R-T equilibrium is an intrinsic property of the allosteric oligomers accessible in the absence of ligand, with the ligand stabilizing the conformation to which it binds with higher affinity. This concept was initially demonstrated by biochemical methods with regulatory enzymes such as aspartate transcarbamylase (*22*), but it took a long time to be accepted by the physiology and pharmacology communities. Two sets of evidence changed the frame of thought: First, a broad spectrum of receptors are found spontaneously (or constitutively) active in vivo in the absence of ligand, as observed initially for ionotropic receptors (*23*). Several synthetic pharmacological agents referred to as inverse agonists have been identified that stabilize—through binding to allosteric sites—the receptor in its inactive or resting conformation (*24*). Second, mutations have been identified in various receptor systems that cause a constitutive activation, or gain of function, in the absence of ligand. These include regulatory enzymes, ligand-gated ion channels such as the acetylcholine receptor (*12*), many GPCRs (*25*), and nuclear receptors (*20*). In several of these systems, these mutations alter the pharmacological response so that antagonists may become agonists. Such mutations occurring spontaneously in human populations can cause diseases such as congenital myasthenia, frontal lobe nocturnal epilepsy, familial male precocious puberty, and retinitis pigmentosa. Moreover, in the case of GPCRs and receptor tyrosine kinases, many of these mutations can be oncogenic.

Structural studies of a constitutively active orphan nuclear receptor (LRH-1) have brought a striking confirmation of the MWC theory (*20*). At 2.4 Å resolution, the receptor in the absence of hormone adopts an active conformation with a large but empty hydrophobic pocket (Fig. 4). Adding bulky side chains in this pocket results in full or greater activity, which indicates that although the receptor could accommodate potential ligands, they are not a prerequisite for constitutive activity.

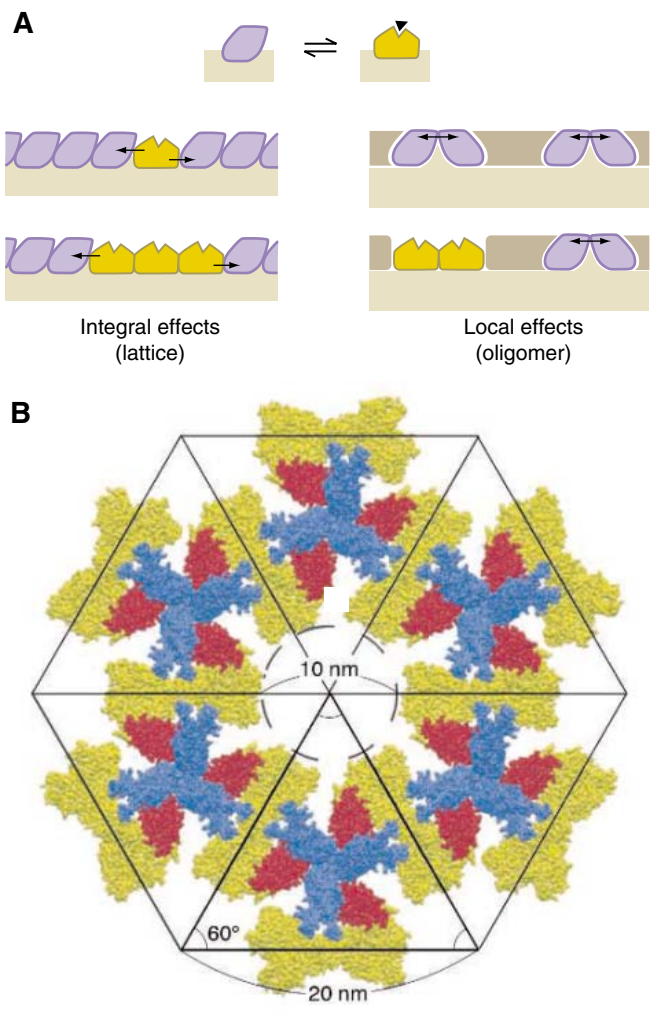

Fig. 5. Allosteric membrane lattice. (**A**) Extension of the allosteric theory to a membrane lattice (*6*). (**B**) The extended cooperative lattice of *E. coli* chemotactic receptors as visualized looking onto the plasma membrane; receptors are in blue, and the linking proteins CheW and CheA are in red and yellow, respectively (*37*).

Cascade of Multiple Transitions in Membrane Receptors and the Question of "Intermediate" States

The original MWC theory hypothesized that the allosteric oligomers exist under a minimum of two discrete (R, T) conformational states with conserved symmetry. Such minimal representation may suffice to account for the kinetics of regulatory enzymes (*11*, *14*) and the all-or-none gating of ion channels in the picosecond to millisecond time range (*12*). However, in most ligand-gated ion channels—and in some GPCRs—the observed kinetics recorded upon prolonged exposure to the signaling ligand involve multiple transitions occurring on a time scale that is much slower (10 ms to several minutes). A cascade of transitions involving high-affinity, slowly interconverting, inactive states must be postulated to account for the physiologically reversible process of desensitization (*12*).

High-resolution electron microscopy studies with the heteromeric muscle nicotinic receptor suggest that exposure to the neurotransmitter causes a nonsymmetrical quaternary reorganization of the molecule, with α subunits more tangentially inclined than other subunits with respect to the axis of symmetry of the molecule (*26*). Yet the structures of the active and desensitized states at atomic resolution remain to be determined. On the other hand, both active and desensitized states have been shown to occur in the absence of ligand. The slow conformational transitions to desensitized states have been proposed to play a critical role in the short-term regulation of synaptic efficacies (*12*).

A most appealing aspect of the MWC theory is its simplicity. Nonetheless, the postulated two-state ''concerted'' transition has been and still is a debated issue. The alternative sequential model postulates multiple conformations, each with different numbers of ligand molecules bound (*5*). From the theoretical side, more sophisticated models, which include combinations of subunit tertiary conformations, have been proposed (*10*, *12*, *27*). Experimentally, data from enzyme kinetics revealing "negative" cooperativity or from patch-clamp recordings (disclosing, for instance, subconductance states in

non-nicotinic channels) have been interpreted as evidence for intermediate states, but none of these observations are fully conclusive. In particular, for the latter examples, the strictly electrophysiological techniques used do not allow for distinctions between local fluctuations of amino acid side chains and changes in the quaternary organization (*12*).

Hemoglobin has been the paradigmatic system to investigate the mechanism of cooperative ligand binding and, in particular, to test the MWC theory (*8*, *9*). Single-crystal studies, together with a vast array of equilibrium, spectroscopic, and complex kinetic analyses (including time-resolved spectroscopy from the picosecond to the millisecond regime), have shown that the cooperative binding of oxygen is mediated by quaternary changes consistent with a two-state mechanism [(*9*, *10*), but see (*28*)]. However, synthetic allosteric inhibitors such as inositol hexaphosphate and bezafibrate also change O_2 affinity without a change of quaternary structure (*29*). Trapping of transient unstable conformations by encapsulation in silica gels revealed tertiary conformations of individual subunits that coexist within a given quaternary conformation (*10*). The data can be explained by a generalization of the MWC theory to tertiary states (*30*). Similar evidence for trapping of intermediate states within two principal quaternary states has been obtained for *Escherichia coli* aspartate transcarbamylase (*17*). X-ray crystallography of a mutant enzyme for which the allosteric equilibrium is shifted toward the T state showed that in the presence of substrate analogs that push the equilibrium toward the R state, intermediate T′ or R′ conformations could be captured with differential rotation and separation of the catalytic trimers. As in the case of hemoglobin, conditions can be found that trap intermediates within the two principal quaternary states. At this level of resolution, the MWC theory has reached its limits of applicability.

Supramolecular Allosteric Assemblies

Membrane receptors frequently cluster at specific sites in the cell, such as the postsynaptic membrane beneath a nerve ending. Such localized distribution results from their interaction with scaffolding molecules that can modulate their activity (*31*). An extended MWC theory addressed multimolecular planar arrays of identical subunits forming two-dimensional cooperative lattices (*7*). However, studies on diverse specialized membranes did not reveal the anticipated phase transitions. It seems that such scaffolds, if they allow allosteric interactions with individual receptor molecules, may prevent multimeric transitions that would interfere with the repetitive firing of the synapse in millisecond time scales. Bacterial chemotaxis receptors (*32*), however, do appear to form cooperative lattices (Fig. 5). A few molecules of attractant cause a large change in swimming bias, which is mediated by a conformational change that spreads in a large lattice of receptor trimers of dimers. Allosteric cross-talk between 10 to 100 ryanodine receptors has also been reported in heart muscle sarcoplasmic reticulum and may occur between the elementary subunits of flagella or actin filaments.

Conclusions: The Quest for Theory

After 40 years, the allosteric theory of signal transduction has been applied to signaling molecules as diverse as regulatory enzymes, nuclear receptors, and the various classes of membrane receptors. It has even been extended to ribo switches within which folded RNA domains serve as receptors for specific metabolites and to the allosteric cascade of spliceosome activation. As expected, each signaling system displays features of its own. But the concept of signal transmission mediated by discrete conformational transitions that exist before ligand binding would appear to be universal, as is the occurrence of mutations—often pathological—causing constitutive activation of the receptor in the absence of ligand. The simplicity of the theory facilitates its experimental test. However, both the theory and the available technology have reached their limits. This is an important area for future research. Another lies at a more macroscopic scale: It includes the deciphering of the networks of allosteric interactions taking place in supramolecular assemblies within the cell and between cells. The future study of allosteric proteins is more promising than ever, and we expect that theorizing will become more important as we refine our understanding of the mechanisms that allow elaborate physiological control of protein function.

References and Notes

1. J.-P. Changeux, *Cold Spring Harbor Symp. Quant. Biol.* **26**, 313 (1961).
2. D. E. Koshland Jr., *J. Cell. Comp. Physiol.* **54**, 245 (1959).
3. J. Monod, J.-P. Changeux, F. Jacob, *J. Mol. Biol.* **6**, 306 (1963).
4. J. Monod, J. Wyman, J.-P. Changeux, *J. Mol. Biol.* **12**, 88 (1965).
5. D. E. Koshland, G. Némethy, D. Filmer, *Biochemistry* **5**, 365 (1966).
6. J.-P. Changeux, in *Nobel Symposium: Symmetry and Functions in Biological Systems at the Molecular Level*, A. Engström, B. Stranberg, Eds. (Wiley, New York, 1969), pp. 235–256.
7. J.-P. Changeux, J.-P. Thiéry, T. Tung, C. Kittel, *Proc. Natl. Acad. Sci. U.S.A.* **57**, 335 (1967).
8. S. J. Edelstein, *Nature* **230**, 224 (1971).
9. R. G. Shulman, *IUBMB Life* **51**, 351 (2001).
10. C. Viappiani *et al.*, *Proc. Natl. Acad. Sci. U.S.A.* **101**, 14414 (2004).
11. M. F. Perutz, *Q. Rev. Biophys.* **22**, 139 (1989).
12. J.-P. Changeux, S. J. Edelstein, *Neuron* **21**, 959 (1998).
13. J. L. Eiselé *et al.*, *Nature* **366**, 479 (1993).
14. S. Iwata, K. Kamata, S. Yoshida, T. Minowa, T. Ohta, *Nat. Struct. Biol.* **1**, 176 (1994).
15. A. I. Sobolevsky, M. V. Yelshansky, L. P. Wollmuth, *Neuron* **41**, 367 (2004).
16. G. Milligan, *Mol. Pharmacol.* **66**, 1 (2004).
17. K. Stieglitz, B. Stec, D. P. Baker, E. R. Kantrowitz, *J. Mol. Biol.* **341**, 853 (2004).
18. E. Gouaux, *J. Physiol.* **554**, 249 (2004).
19. N. Kunishima *et al.*, *Nature* **407**, 971 (2000).
20. E. P. Sablin, I. N. Krylova, R. J. Fletterick, H. A. Ingraham, *Mol. Cell* **11**, 1575 (2003).
21. R. MacKinnon, *FEBS Lett.* **555**, 62 (2003).
22. J.-P. Changeux, M. M. Rubin, *Biochemistry* **7**, 553 (1968).
23. M. B. Jackson, *Biophys. J.* **49**, 663 (1986).
24. F. Gasparini, R. Kuhn, J. P. Pin, *Curr. Opin. Pharmacol.* **2**, 43 (2002).
25. R. J. Lefkowitz, S. Cotecchia, P. Samama, T. Costa, *Trends Pharmacol. Sci.* **14**, 303 (1993).
26. N. Unwin, *J. Mol. Biol.* **346**, 967 (2005).
27. M. Eigen, *Nobel Symp.* **5**, 333 (1967).
28. G. K. Ackers *et al.*, *Proteins Struct. Funct. Genet.* **4** (suppl.), 23 (2000).
29. T. Yonetani, S. I. Park, A. Tsuneshige, K. Imai, K. Kanaori, *J. Biol. Chem.* **277**, 34508 (2002).
30. E. R. Henry, S. Bettati, J. Hofrichter, W. A. Eaton, *Biophys. Chem.* **98**, 149 (2002).
31. D. Choquet, A. Triller, *Nat. Rev. Neurosci.* **4**, 251 (2003).
32. D. Bray, T. Duke, *Annu. Rev. Biophys. Biomol. Struct.* **33**, 53 (2004).
33. J.-P. Changeux, *Bull. Soc. Chim. Biol. (Paris)* **47**, 281 (1965).
34. P. H. Celie *et al.*, *Neuron* **41**, 907 (2004).
35. A. Miyazawa, Y. Fujiyoshi, N. Unwin, *Nature* **424**, 949 (2003).
36. A. Taly *et al.*, *Biophys. J.*, published online 1 April 2005 (10.1529/biophysj.104.050229).
37. T. S. Shimizu *et al.*, *Nat. Cell Biol.* **2**, 792 (2000).

38. Supported by the Collège de France, CNRS, the Pasteur Institute, the University of Geneva, the Association Française contre les Myopathies, and the European Community. We apologize for not citing many relevant references because of space limitations.

10.1126/science.1108595

Disappearing Arctic Lakes

L. C. Smith,[1]* Y. Sheng,[2] G. M. MacDonald,[1] L. D. Hinzman[3]

Arctic warming has accelerated since the 1980s, driving an array of complex physical and ecological changes in the region (*1*). Particularly puzzling has been evidence for perturbations to the terrestrial water cycle (*2*), which plays an integral role in nearly every aspect of the Arctic system. We compared satellite imagery acquired across ~515,000 km^2 of Siberia in the early 1970s with recent (1997 to 2004) satellite data to inventory and track ongoing changes in more than 10,000 large lakes after three decades of rising soil and air temperatures in the region (*1*, *3*, *4*). Our analysis reveals a widespread decline in lake abundance and area, despite slight precipitation increases (*4*). The spatial pattern of lake disappearance strongly suggests that thawing of permafrost is driving the observed losses.

Between 1973 and 1997–98, the total number of large lakes (those >40 ha) decreased from 10,882 to 9712, a decline of 1170 or ~11% (SOM text). Most did not disappear altogether, but instead shrank to sizes below 40 ha. Total regional lake surface area decreased by 93,000 ha, a ~6% decline. One hundred and twenty-five lakes vanished completely and are now revegetated, as indicated by sharp increases in near-infrared reflectance (Fig. 1, B and C). Subsequent monitoring of these former lakebeds (2000 to 2004) confirms that none have refilled since 1997–98. These lakes are therefore considered to be permanently drained.

The regional totals indicate a net decline in Siberian lake cover but mask an interesting spatial pattern. In continuous permafrost, total lake area increased by 13,300 ha (+12%), and lake numbers rose from 1148 in 1973 to 1197 by 1997–98 (+4%) (Fig. 1D). This trend of net lake growth in continuous permafrost stands in sharp contrast with more southerly zones of discontinuous, sporadic, and isolated permafrost, all of which experienced net declines in total lake number (–9%, –5%, and –6%, respectively) and in area (–13%, –12%, and –11%) (Fig. 1D). These declines have outpaced lake gains in the north, lending an overall loss to the region.

Numerous studies have described increased surface ponding in warming permafrost environments, driven primarily by slumping and collapsed terrain features (thermokarst) that subsequently fill with water (SOM text). Such observations are in apparent conflict with the phenomenon seen here and also near Council, Alaska, where thermokarst ponds in discontinuous permafrost are also shrinking (*5*). Geophysical surveys at the Alaskan site suggest that warming temperatures lead to thinning and eventual "breaching" of permafrost near lakes, greatly facilitating their drainage to the subsurface. The apparent discrepancy between these opposing sets of observations is in fact resolved if the process is understood as a continuum: Initial permafrost warming leads to development of thermokarst and lake expansion, followed by lake drainage as the permafrost degrades still further. This conceptual model is supported by the broad geographic pattern observed in Siberia (i.e., lake increases in continuous permafrost and losses where permafrost is thinner and less contiguous) and by the fact that permanently drained lakes are commonly found alongside undisturbed neighbors (suggesting a spatially patchy process, rather than a direct climatic mechanism such as increased evaporation). It also raises the possibility of a diffuse lake drainage "front" where warming permafrost first experiences widespread degradation. The fact that ~85% of the vanished lakes reported here occur within 200 km of the continuous permafrost boundary lends some support to this concept (Fig. 1A).

Clearly, other factors besides permafrost influence substrate permeability and lake drainage. In west Siberia, shallow water tables and extensive, low-permeability peatlands (*6*) ensure continued survival of many lakes, even where permafrost is absent. Overlay of our lake maps with a detailed peatland inventory (*7*) shows that, although lakes in continuous permafrost are found on all substrates, they exist only as perched systems on peatlands further south. In such regions, factors besides permafrost degradation will be important to lake persistence. However, aside from low-permeability environments and/or beneficent water balance adjustments (i.e., further increases in net precipitation), the ultimate effect of continued climate warming on high-latitude, permafrost-controlled lakes and wetlands may well be their widespread disappearance.

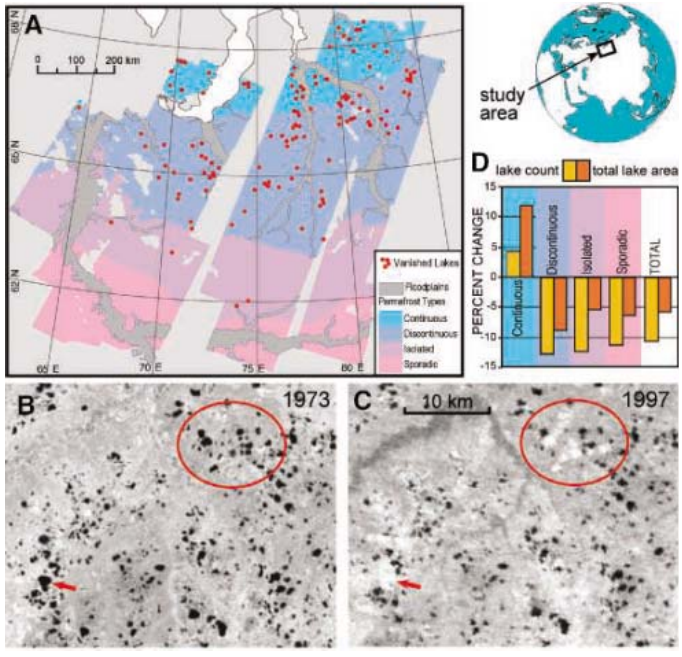

Fig. 1. (**A**) Locations of Siberian lake inventories, permafrost distribution, and vanished lakes. Total lake abundance and inundation area have declined since 1973 (**B**), including (**C**) permanent drainage and revegetation of former lakebeds (the arrow and oval show representative areas). (**D**) Net increases in lake abundance and area have occurred in continuous permafrost, suggesting an initial but transitory increase in surface ponding.

References and Notes

1. M. C. Serreze *et al.*, *Clim. Change* **46**, 159 (2000).
2. B. J. Peterson *et al.*, *Science* **298**, 2171 (2002).
3. A. V. Pavlov, N. G. Moskalenko, *Permafrost Periglac. Process.* **13**, 43 (2002).
4. K. E. Frey *et al.*, *Polar Res.* **22**, 287 (2003).
5. K. Yoshikawa, L. D. Hinzman, *Permafrost Periglac. Process.* **14**, 151 (2003).
6. L. C. Smith *et al.*, *Science* **303**, 353 (2004).
7. Y. Sheng *et al.*, *Global Biogeochem. Cycles* **18**, GB3004 (2004).

8. Supported by the NSF Office of Polar Programs, ARCSS Freshwater Initiative grant no. ARC-023091.

Supporting Online Material
www.sciencemag.org/cgi/content/full/308/5727/1429/DC1
Materials and Methods
SOM Text
References and Notes

1 December 2004; accepted 24 March 2005
10.1126/science.1108142

[1]Department of Geography, 1255 Bunche Hall, University of California–Los Angeles, Los Angeles, CA 90095, USA. [2]College of Environmental Science and Forestry, State University of New York, Syracuse, NY 13210, USA. [3]Water and Environmental Research Center, University of Alaska, Fairbanks, AK 99775, USA.

*To whom correspondence should be addressed. E-mail: lsmith@geog.ucla.edu

Feeling the Beat: Movement Influences Infant Rhythm Perception

Jessica Phillips-Silver and Laurel J. Trainor*

We hear the melody in music, but we feel the beat. People in all cultures move their bodies to the rhythms of music, whether drumming, singing, dancing, or rocking an infant (*1*). Body movement involves motor, proprioceptive (perception of body position), vestibular (perception of movement and balance), visual, and auditory systems (*2*), but few studies have examined auditory-vestibular interactions.

The ability to feel and interpret the strong and weak beats in a rhythm pattern allows people to move and dance in time to music. Typically, the strong beats of a rhythm pattern are played louder, longer, or both, and the metrical structure (what you move to) is derived from, and consistent with, these physical accents (*3*). However, in an ambiguous rhythm pattern with no physical accents, different movements might give rise to different metrical interpretations. In other words, how we move may influence what we hear.

We tested the hypothesis that movement influences the auditory encoding of rhythm patterns in human infants. In experiment 1, we trained 7-month-olds by having them listen to a 2-min repetition of an ambiguous (without accented beats) rhythm pattern (Fig. 1A, row 1, and sound file S1). Half of the infants were bounced on every second beat, and half on every third beat. After training, infants' listening preferences were tested for two auditory versions of the rhythm pattern, which included intensity accents on either every second beat (the duple form) or every third beat (the triple form) (Fig. 1A, rows 2 and 3, and sound files S1 and S3). Infants controlled how long they listened to each version of the rhythm pattern in a head-turn preference procedure (*4*). Infants chose to listen longer to the auditory test stimulus with accented beats that matched the beats on which they were bounced [$t(15) = 4.00$, P(two-tailed) = 0.001] (Fig. 1B). Thus, their bouncing determined whether infants later preferred the auditory rhythm pattern congruent with duple or triple form.

Experiment 2 was identical to experiment 1 except that infants were blindfolded during training. Infants still preferred to listen to the auditory stimulus that matched the metrical form of their movement training [$t(15) = 2.93$, $P = 0.01$] (Fig. 1C), indicating that visual information was not necessary for the effect.

Experiment 3 investigated whether personal motion experience was necessary. During training, infants watched without moving as the experimenter bounced either on every second or on every third beat of the ambiguous rhythm pattern. In this case, infants showed no preference for the two auditory versions [$t(15) = 0.51$, $P = 0.62$] (Fig. 1D), indicating that movement of the infant's own body was critical for the multisensory effect observed in experiments 1 and 2.

In order to confirm that the movement itself did not induce auditory accents due to changing room acoustics as the subjects moved, we trained a group of adult listeners with headphones. Those who bounced (mimicking a model) on every second beat during training identified the duple form as familiar at test, whereas those who bounced on every third beat identified the triple form. Finally, we tested infants' preferences without any movement training and found no preference for either auditory interpretation, again indicating that movement is crucial for the multisensory effect.

These studies illustrate the strong multisensory connection between body movement and auditory rhythm processing when inputs from both sources are experienced concurrently. Because infants did not engage in self-movement, the observed effect likely involves the vestibular and perhaps proprioceptive systems. The early development of the vestibular system (*5*), and infant delight at vestibular stimulation when bounced to a play song or rocked to a lullaby, suggest that we are observing a strong, early vestibular-auditory interaction that is critical for the development of human musical behavior. It has long been known that infants are attracted to music and responsive to its emotional content (*6*, *7*). Our findings provide evidence that the experience of body movement plays an important role in musical rhythm perception.

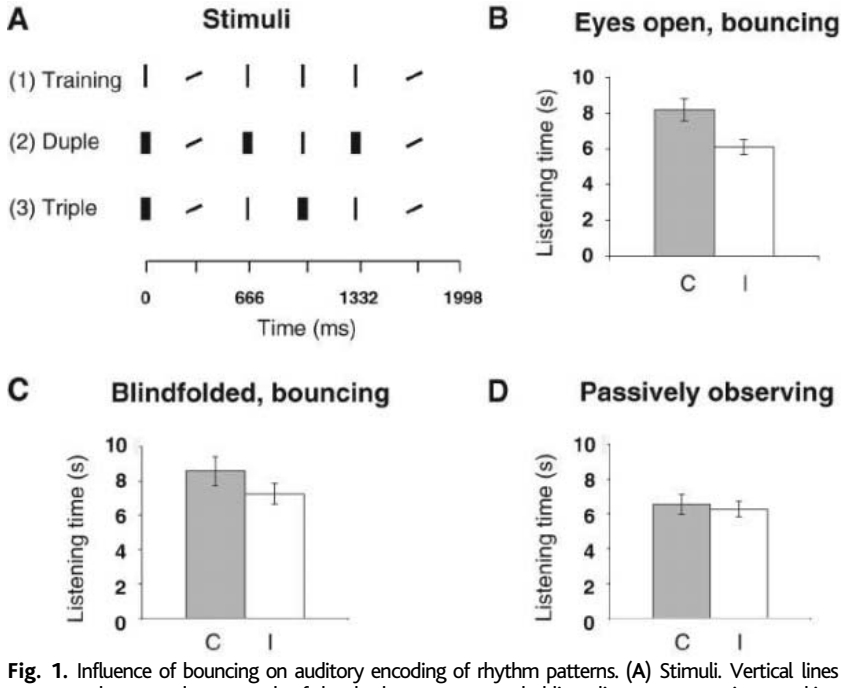

Fig. 1. Influence of bouncing on auditory encoding of rhythm patterns. (**A**) Stimuli. Vertical lines represent the snare drum sounds of the rhythm patterns, and oblique lines represent time-marking slapstick sounds (*4*). (**B** to **D**) Results. The *y* axis represents listening time preference; the *x* axis represents congruency between bouncing (duple or triple) during training and auditory accents (duple or triple) during testing. Error bars represent the standard error of the mean. C, congruent; I, incongruent.

References and Notes

1. N. L. Wallin, B. Merker, S. Brown, *The Origins of Music* (MIT Press, Cambridge, MA, 2000).
2. J. R. Lackner, *J. Vestib. Res.* **2**, 307 (1992).
3. F. Lehrdal, R. Jackendoff, *A Generative Theory of Tonal Music* (MIT Press, Cambridge, MA, 1983).
4. Materials and methods are available as supporting material on *Science* Online.
5. D. L. Clark, *Science* **196**, 1228 (1977).
6. L. J. Trainor, L. A. Schmidt, in *The Cognitive Neuroscience of Music*, I. Peretz, R. Zatorre, Eds. (Oxford Univ. Press, Oxford, 2003), pp. 310–324.
7. S. E. Trehub, *Nat. Neurosci.* **6**, 669 (2003).

8. We thank J. Tang for assistance and T. Lewis for comments. Supported by a grant to L.J.T. from the Natural Sciences and Engineering Research Council of Canada.

Supporting Online Material
www.sciencemag.org/cgi/content/full/308/5727/1430/DC1
Materials and Methods
References and Notes
Sound Files S1 to S3

10 February 2005; accepted 25 March 2005
10.1126/science.1110922

Department of Psychology, McMaster University, Hamilton, ON L8S 4K1, Canada.

*To whom correspondence should be addressed. E-mail: LJT@mcmaster.ca

Earth's Energy Imbalance: Confirmation and Implications

James Hansen,[1,2]* Larissa Nazarenko,[1,2] Reto Ruedy,[3] Makiko Sato,[1,2] Josh Willis,[4] Anthony Del Genio,[1,5] Dorothy Koch,[1,2] Andrew Lacis,[1,5] Ken Lo,[3] Surabi Menon,[6] Tica Novakov,[6] Judith Perlwitz,[1,2] Gary Russell,[1] Gavin A. Schmidt,[1,2] Nicholas Tausnev[3]

Our climate model, driven mainly by increasing human-made greenhouse gases and aerosols, among other forcings, calculates that Earth is now absorbing 0.85 ± 0.15 watts per square meter more energy from the Sun than it is emitting to space. This imbalance is confirmed by precise measurements of increasing ocean heat content over the past 10 years. Implications include (i) the expectation of additional global warming of about 0.6°C without further change of atmospheric composition; (ii) the confirmation of the climate system's lag in responding to forcings, implying the need for anticipatory actions to avoid any specified level of climate change; and (iii) the likelihood of acceleration of ice sheet disintegration and sea level rise.

Earth's climate system has considerable thermal inertia. This point is of critical importance to policy- and decision-makers who seek to mitigate the effects of undesirable anthropogenic climate change. The effect of the inertia is to delay Earth's response to climate forcings, i.e., changes of the planet's energy balance that tend to alter global temperature. This delay provides an opportunity to reduce the magnitude of anthropogenic climate change before it is fully realized, if appropriate action is taken. On the other hand, if we wait for more overwhelming empirical evidence of climate change, the inertia implies that still greater climate change will be in store, which may be difficult or impossible to avoid.

The primary symptom of Earth's thermal inertia, in the presence of an increasing climate forcing, is an imbalance between the energy absorbed and emitted by the planet. This imbalance provides an invaluable measure of the net climate forcing acting on Earth. Improved ocean temperature measurements in the past decade, along with high-precision satellite altimetry measurements of the ocean surface, permit an indirect but precise quantification of Earth's energy imbalance. We compare observed ocean heat storage with simulations of global climate change driven by estimated climate forcings, thus obtaining a check on the climate model's ability to simulate the planetary energy imbalance.

The lag in the climate response to a forcing is a sensitive function of equilibrium climate sensitivity, varying approximately as the square of the sensitivity (*1*), and it depends on the rate of heat exchange between the ocean's surface mixed layer and the deeper ocean (*2*–*4*). The lag could be as short as a decade, if climate sensitivity is as small as 0.25°C per W/m^2 of forcing, but it is a century or longer if climate sensitivity is 1°C per W/m^2 or larger (*1*, *3*). Evidence from Earth's history (*3*–*6*) and climate models (*7*) suggests that climate sensitivity is 0.75° ± 0.25°C per W/m^2, implying that 25 to 50 years are needed for Earth's surface temperature to reach 60% of its equilibrium response (*1*).

We investigate Earth's energy balance via computations with the current global climate model of the NASA Goddard Institute for Space Studies (GISS). The model and its simulated climatology have been documented (*8*), as has its response to a wide variety of climate forcing mechanisms (*9*). The climate model's equilibrium sensitivity to doubled CO_2 is 2.7°C (~2/3°C per W/m^2) (*10*).

Climate forcings. Figure 1A summarizes the forcings that drive the simulated 1880 to 2003 climate change. Among alternative definitions of climate forcing (*9*), we use the effective forcing, F_e. F_e differs from conventional climate forcing definitions (*11*) by accounting for the fact that some forcing mechanisms have a lesser or greater "efficacy" in altering global temperature than an equal forcing by CO_2 (*9*). F_e is an energy flux change arising in response to an imposed forcing agent. It is constant throughout the atmosphere, because it is evaluated after atmospheric temperature has been allowed to adjust to the presence of the forcing agent.

The largest forcing is due to well-mixed greenhouse gases (GHGs)—CO_2, CH_4, N_2O, CFCs (chlorofluorocarbons)—and other trace gases, totaling 2.75 W/m^2 in 2003 relative to the 1880 value (Table 1). Ozone (O_3) and stratospheric H_2O from oxidation of increasing CH_4 bring the total GHG forcing to 3.05 W/m^2 (*9*). Estimated uncertainty in the total GHG forcing is ~15% (*11*, *12*).

Atmospheric aerosols cause climate forcings by reflecting and absorbing radiation, as well as through indirect effects on cloud cover and cloud albedo (*11*). The aerosol scenario in our model uses estimated anthropogenic emissions from fuel use statistics and includes temporal changes in fossil-fuel use technologies (*13*). Our parameterization of aerosol indirect effects (*9*, *14*) is constrained by empirical evidence that the aerosol indirect forcing is ~ −1 W/m^2 (*9*). The effective aerosol forcing in 2003 relative to that in 1880, including positive forcing by absorbing black carbon aerosols, is –1.39 W/m^2, with a subjective estimated uncertainty of ~50%.

Stratospheric aerosols from volcanoes cause a sporadically large negative forcing, with an uncertainty that increases with age from 15% for the 1991 Mount Pinatubo eruption to 50% for the 1883 Krakatau eruption (*9*). Land use and snow albedo forcings are small on a global average and uncertain by about a factor of 2 (*9*). Solar irradiance is taken as increasing by 0.22 W/m^2 between 1880 and 2003, with an estimated uncertainty of a factor of 2 (*9*). All of these partly subjective uncertainties are intended as 2σ error bars. The net change of effective forcing between 1880 and 2003 is +1.8 W/m^2, with a formal uncertainty of ±0.85 W/m^2 due almost entirely to aerosols (Table 1).

Climate simulations. The global mean temperature simulated by the GISS model driven by this forcing agrees well with observations (Fig. 1B). An ensemble of five simulations was obtained by using initial conditions at intervals of 25 years of the climate model control run, thus revealing the model's inherent unforced variability. The spatial distribution of the simulated warming (fig. S1) is slightly excessive in the tropics, as much as a few tenths of a degree Celsius, and on average the simulated warming is a few tenths of a degree Celsius less than that observed in middle latitudes of the Northern Hemisphere, but there is substantial variation from one model run to another (fig. S1).

[1]NASA Goddard Institute for Space Studies, New York, NY 10025, USA. [2]Columbia Earth Institute, Columbia University, New York, NY 10025, USA. [3]SGT Incorporated, New York, NY 10025, USA. [4]Jet Propulsion Laboratory, Pasadena, CA 91109, USA. [5]Department of Earth and Environmental Sciences, Columbia University, New York, NY 10025, USA. [6]Lawrence Berkeley National Laboratory, Berkeley, CA 94720, USA.

*To whom correspondence should be addressed. E-mail: jhansen@giss.nasa.gov

Discrepancy in the spatial distribution of warming may be partly a result of the uncertain aerosol distribution, specifically the division of aerosols between fossil-fuel and biomass-burning aerosols (*9*). However, excessive tropical warming in our model is primarily in the Pacific Ocean, where our coarse-resolution ocean model is unable to simulate climate variations associated with El Niño–Southern Oscillation processes.

The planetary energy imbalance in our model (Fig. 1C) did not exceed a few tenths of 1 W/m^2 before the 1960s. Since then, except for a few years following each large volcanic eruption, the simulated planetary energy imbalance has grown steadily. According to the model, Earth is now absorbing 0.85 ± 0.15 W/m^2 more solar energy than it radiates to space as heat.

Ocean heat storage. Confirmation of the planetary energy imbalance can be obtained by measuring the heat content of the ocean, which must be the principal reservoir for excess energy (*3*, *15*). Levitus *et al*. (*15*) compiled ocean temperature data that yielded increased ocean heat content of about 10 W year/m^2, averaged over the Earth's surface, during 1955 to 1998 [1 W year/m^2 over the full Earth ~ 1.61 × 10^{22} J; see table S1 for conversion factors of land, air, water, and ice temperature changes and melting to global energy units]. Total ocean heat storage in that period is consistent with climate model simulations (*16*–*19*), but the models do not reproduce reported decadal fluctuations. The fluctuations may be a result of variability of ocean dynamics (*17*) or, at least in part, an artifact of incomplete sampling of a dynamically variable ocean (*18*, *19*).

Improved definition of Earth's energy balance is possible for the past decade. First, the predicted energy imbalance due to increasing GHGs has grown to 0.85 ± 0.15 W/m^2, and the past decade has been uninterrupted by any large volcanic eruption (Fig. 1). Second, more complete ocean temperature data are available, including more profiling floats and precise satellite altimetry that permits improved estimates in data-sparse regions (*20*).

Figure 2 shows that the modeled increase of heat content in the past decade in the upper 750 m of the ocean is 6.0 ± 0.6 (mean ± SD) W year/m^2, averaged over the surface of Earth, varying from 5.0 to 6.6 W year/m^2 among five simulations. The observed annual mean rate of ocean heat gain between 1993 and mid-2003 was 0.86 ± 0.12 W/m^2 per year for the 93.4% of the ocean that was analyzed (*20*). Assuming the same rate for the remaining 6.6% of the ocean yields a global mean heat storage rate of 0.7 × 0.86 = 0.60 ± 0.10 W/m^2 per year or 6 ± 1 W year/m^2 for 10 years, 0.7 being the ocean fraction of Earth's surface. This agrees well with the 5.5 W year/m^2 in the analysis of Levitus *et al*. (*21*) for the upper 700 m that was based only on in situ data.

Figure 3 compares the latitude-depth profile of the observed ocean heat content change with the five climate model runs and the mean of the five runs. There is a large variability among the model runs, revealing the chaotic ''ocean weather'' fluctuations that occur on such a time scale. This variability is even more apparent in maps of change in ocean heat content (fig. S2). Yet the model runs contain essential features of observations, with deep penetration of heat anomalies at middle to high latitudes and shallower anomalies in the tropics.

The modeled heat gain of ~0.6 W/m^2 per year for the upper 750 m of the ocean differs from the decadal mean planetary energy imbalance of ~0.75 W/m^2 primarily because of heat storage at greater depths in the ocean. On average for the five simulations, 85% of the ocean heat storage occurred above 750 m, with the range from 78 to 91%. The mean heat gain below 750 m was ~0.11 W/m^2. The remaining 0.04 W/m^2 warmed the atmosphere and land and melted sea ice and land ice (see supplementary information).

Earth's energy imbalance. We infer from the consistency of observed and modeled planetary energy gains that the forcing still driving climate change, i.e., the forcing not yet responded to, averaged ~0.75 W/m^2 in the past decade and was ~0.85 ± 0.15 W/m^2 in 2003 (Fig. 1C). This imbalance is consistent with the total forcing of ~1.8 W/m^2 relative to that in 1880 and climate sensitivity of ~2/3°C per W/m^2. The observed 1880 to 2003 global warming is 0.6° to 0.7°C (*11*, *22*), which is the full response to nearly 1 W/m^2 of forcing. Of the 1.8 W/m^2 forcing, 0.85 W/m^2 remains, i.e., additional global warming of 0.85 × 0.67 ~ 0.6°C is ''in the pipeline'' and will occur in the future even if atmospheric composition and other

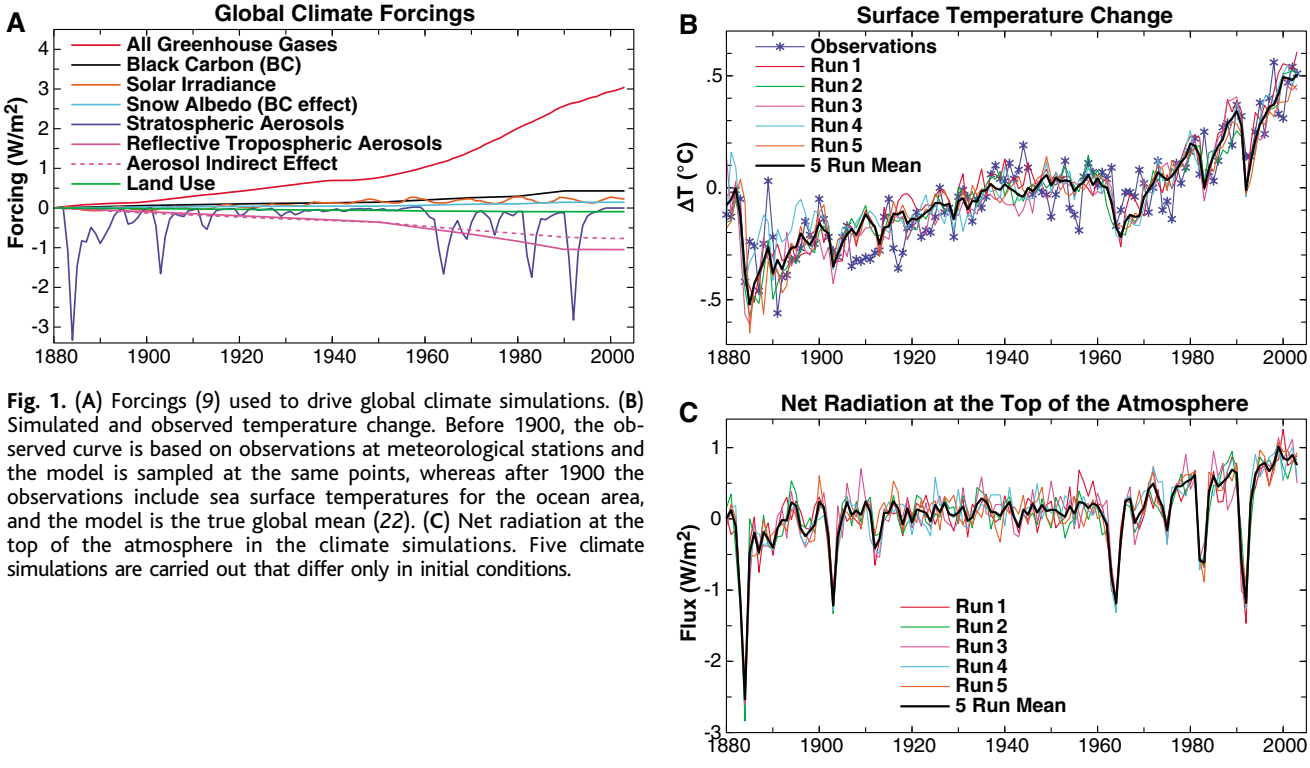

Fig. 1. (**A**) Forcings (*9*) used to drive global climate simulations. (**B**) Simulated and observed temperature change. Before 1900, the observed curve is based on observations at meteorological stations and the model is sampled at the same points, whereas after 1900 the observations include sea surface temperatures for the ocean area, and the model is the true global mean (*22*). (**C**) Net radiation at the top of the atmosphere in the climate simulations. Five climate simulations are carried out that differ only in initial conditions.

climate forcings remain fixed at today's values (*3*, *4*, *23*).

The present planetary energy imbalance is large by standards of Earth's history. For example, an imbalance of 1 W/m^2 maintained for the last 10,000 years of the Holocene is sufficient to melt ice equivalent to 1 km of sea level (if there were that much ice) or raise the temperature of the ocean above the thermocline by more than 100°C (table S1). Clearly, on long time scales, the planet has been in energy balance to within a small fraction of 1 W/m^2.

An alternative interpretation of the observed present high rate of ocean heat storage might be that it results, not from climate forcings, but from unforced atmosphere-ocean fluctuations. However, if a fluctuation had brought cool water to the ocean surface, as needed to decrease outgoing heat flux, the ocean surface would have cooled, whereas in fact it warmed (*22*). A positive climate forcing, anticipated independently, is the more viable interpretation.

The present 0.85 W/m^2 planetary energy imbalance, its consistency with estimated growth of climate forcings over the past century (Fig. 1A), and its consistency with the temporal development of global warming based on a realistic climate sensitivity for doubled CO_2 (Fig. 1B) offer strong support for the inference that the planet is out of energy balance because of positive climate forcings. If climate sensitivity, climate forcings, and ocean mixing are taken as arbitrary parameters (*24*), one may find other combinations that yield warming comparable to that of the past century. However, (i) climate sensitivity is constrained by empirical data; (ii) our simulated depth of penetration of ocean-warming anomalies is consistent with observations (fig. S2), thus supporting the modeled rate of ocean mixing; and (iii) despite ignorance about aerosol changes, there is sufficient knowledge to constrain estimates of climate forcings (*9*).

The planetary energy imbalance and implied warming "in the pipeline" complicate the task of avoiding any specified level of global warming. For example, it has been argued, on the basis of sea level during previous warm periods, that global warming of more than 1°C above the level of 2000 would constitute "dangerous anthropogenic interference" with climate (*25*, *26*). With 0.6°C global warming "in the pipeline" and moderate growth of non-CO_2 forcings, a 1°C limit on further warming limits peak CO_2 to about 440 parts per million (ppm) (*12*). Given the current CO_2 concentration of ~378 ppm, annual growth of ~1.9 ppm (*12*), and a still expanding worldwide fossil-fuel energy infrastructure, it may be impractical to avoid a CO_2 concentration of 440 ppm. A conceivable, though difficult, reduction of non-CO_2 forcings could increase the peak CO_2 limit for 1°C warming to a more feasible 520 ppm (*12*). This example illustrates that the 0.6°C unrealized warming associated with the planet's energy imbalance implies the need for near-term anticipatory actions, if a low limit on climate change is to be achieved.

Sea level. Sea level change includes steric (mainly thermal expansion) and eustatic (mainly changes of continental ice and other continental water storage) components. Observed temperature changes in the upper 700 to 750 m yield a steric sea level rise of 1.4 to 1.6 cm (*20*, *21*). The full ocean temperature changes in our five simulations yield a mean steric 10-year sea level increase of 1.6 cm. Our climate model does not include ice sheet dynamics, so we cannot calculate eustatic sea level change directly. Sea level measured by satellite altimeters since 1993 increased 2.8 ± 0.4 cm/decade (*27*), but as a measure of the volume change (steric + eustatic) of ocean water, this value must be increased by ~0.3 cm to account for the effect of global isostatic adjustment (*28*). We thus infer a eustatic contribution to sea level rise of ~1.5 cm in the past decade.

Both the rate of total sea level rise in the past decade and that of the eustatic component, which is a critical metric for ice melt, are accelerations over the rate of the preceding century. IPCC (*11*) estimated the rate of sea level rise of the past century to be 1.5 ± 0.5 cm/decade, with a central estimate of only 0.2 cm/decade for the eustatic component, albeit with a large uncertainty. Decadal var-

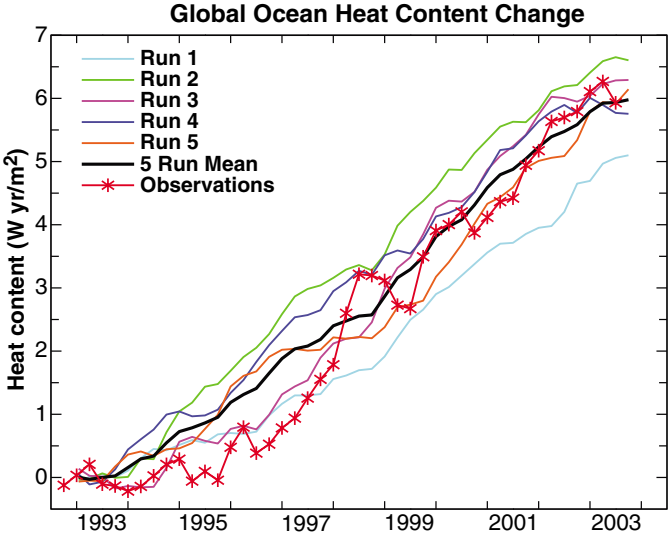

Fig. 2. Ocean heat content change between 1993 and 2003 in the top 750 m of world ocean. Observations are from (*20*). Five model runs are shown for the GISS coupled dynamical ocean-atmosphere model (*8*, *9*).

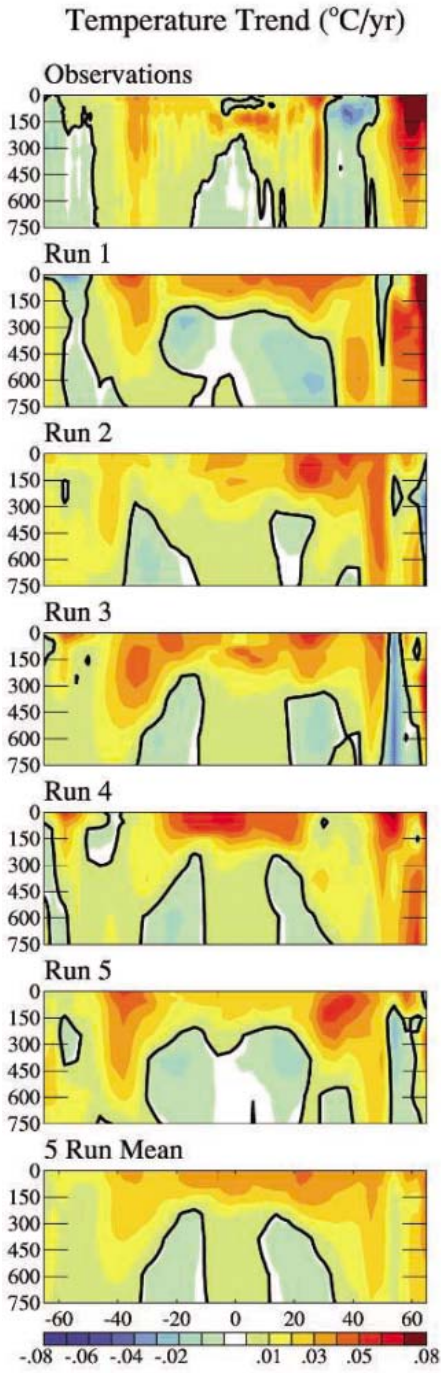

Fig. 3. Trend of zonally averaged temperature versus depth and latitude. Observations are from (*20*). The five model runs are as in Fig. 2.

iability limits the significance of sea level change in a single decade (*28*, *29*). However, we suggest that both the steric and eustatic increases are a product of the large, unusual, persistent planetary energy imbalance that overwhelms normal variability and as such may be a harbinger of accelerating sea level change (*26*).

The estimated ~1.5-cm eustatic sea level rise in the past decade, even if entirely due to ice melt, required only 2% of Earth's present energy imbalance (table S1). Much more rapid melt is possible if iceberg discharge is accelerating, as some recent observations suggest (*30*, *31*), and has occurred in past cases of sharp sea level rise that accompanied rapid global warming (*32*). Unlike ice sheet growth, which is limited by the snowfall rate in cold dry regions, ice sheet disintegration can be a wet process fed by multiple radiative and dynamical feedbacks (*26*). Thus, the portion of the planetary energy imbalance used for melting is likely to rise as the planet continues to warm, summer melt increases, and melt-water lubricates and softens the ice sheets. Other positive feedbacks include reduced ice sheet albedo, a lowering of the ice sheet surface, and effects of rising sea level on coastal ice shelves (*26*).

Table 1. Effective climate forcings (W/m²) used to drive the 1880 to 2003 simulated climate change in the GISS climate model (*9*).

Forcing agent*		Forcing (W/m²)
Greenhouse gases (GHGs)	–	–
Well-mixed GHGs	2.75	–
Ozone†‡	0.24	–
CH_4-derived stratospheric H_2O	0.06	–
Total: GHGs		3.05 ± 0.4
Solar irradiance		0.22 (×2)
Land use		−0.09 (×2)
Snow albedo		0.14 (×2)
Aerosols		
Volcanic aerosols	0.00	–
Black carbon‡	0.43	–
Reflective tropospheric aerosols	−1.05	–
Aerosol indirect effect	−0.77	–
Total: aerosols	–	−1.39 ± 0.7
Sum of individual forcings	–	1.93
All forcings at once	–	1.80 ± 0.85

*Effective forcings are derived from five-member ensembles of 120-year simulations for each individual forcing and for all forcings acting at once [see (*9*) and supporting online material]. The sum of individual forcings differs slightly from all forcings acting at once because of nonlinearities in combined forcings and unforced variability in climate simulations. †This is the ozone forcing in our principal IPCC simulations; it decreases from 0.24 to 0.22 W/m² when the stratospheric ozone change of Randel and Wu (S1) is used [see (*9*) and supporting online material]. ‡Ozone and black carbon forcings are less than they would be for conventional forcing definitions (*11*), because their "efficacy" is only ~75% (*9*).

Implications. The thermal inertia of the ocean, with resulting unrealized warming "in the pipeline," combines with ice sheet inertia and multiple positive feedbacks during ice sheet disintegration to create the possibility of a climate system in which large sea level change is practically impossible to avoid. If the ice sheet response time is millennia, the ocean thermal inertia and ice sheet dynamical inertia are relatively independent matters. However, based on the saw-toothed shape of glacial-interglacial global temperature and qualitative arguments about positive feedbacks, substantial ice sheet change could occur on the time scale of a century (*26*).

The destabilizing effect of comparable ocean and ice sheet response times is apparent. Assume that initial stages of ice sheet disintegration are detected. Before action to counter this trend could be effective, it would be necessary to eliminate the positive planetary energy imbalance, now ~0.85 W/m², which exists as a result of the ocean's thermal inertia. Given energy infrastructure inertia and trends in energy use, that task could require on the order of a century to complete. If the time for a substantial ice response is as short as a century, the positive ice-climate feedbacks imply the possibility of a system out of our control.

A caveat accompanying our analysis concerns the uncertainty in climate forcings. A good fit of observed and modeled temperatures (Fig. 1) also could be attained with smaller forcing and larger climate sensitivity, or with the converse. If climate sensitivity were higher (and forcings smaller), the rate of ocean heat storage and warming "in the pipeline" or "committed" would be greater, e.g., models with a sensitivity of 4.2° to 4.5°C for doubled CO_2 yield ~1°C "committed" global warming (*3*, *4*). Conversely, smaller sensitivity and larger forcing yield lesser committed warming and ocean heat storage. The agreement between modeled and observed heat storage (Fig. 2) favors an intermediate climate sensitivity, as in our model. This test provided by ocean heat storage will become more useful as the period with large energy imbalance continues.

Even if the net forcing is confirmed by continued measurement of ocean heat storage, there will remain much room for tradeoffs among different forcings. Aerosol direct and indirect forcings are the most uncertain. The net aerosol forcing that we estimate, −1.39 W/m², includes a large positive forcing by black carbon and a negative aerosol indirect forcing. Both of these aerosol forcings reduce sunlight reaching the surface and may be the prime cause of observed "global dimming" (*33*) and reduced pan evaporation (*34*).

Given the unusual magnitude of the current planetary energy imbalance and uncertainty about its implications, careful monitoring of key metrics is needed. Continuation of the ocean temperature and altimetry measurements is needed to confirm that the energy imbalance is not a fluctuation and to determine the net climate forcing acting on the planet. The latter is a measure of the changes that will be needed to stabilize climate. Understanding of the forcings that give rise to the imbalance requires more precise information on aerosols (*35*). The high rate of recent eustatic sea level rise that we infer suggests positive contributions from Greenland, alpine glaciers, and West Antarctica. Quantification of these sources is possible using precise satellite altimetry and gravity measurements as initiated by the IceSat (*36*) and GRACE satellites (*37*), which warrant follow-on missions.

References and Notes

1. J. Hansen *et al.*, *Science* **229**, 857 (1985).
2. M. I. Hoffert, A. J. Callegari, C. T. Hsieh, *J. Geophys. Res.* **85**, 6667 (1980).
3. J. Hansen *et al.*, *Am. Geophys. Union Geophys. Monogr. Ser.* **29**, 130 (1984).
4. T. M. L. Wigley, M. E. Schlesinger, *Nature* **315**, 649 (1985).
5. M. I. Hoffert, C. Covey, *Nature* **360**, 573 (1992).
6. J. Hansen, A. Lacis, R. Ruedy, M. Sato, H. Wilson, *Natl. Geogr. Res. Explor.* **9**, 143 (1993).
7. R. Kerr, *Science* **305**, 932 (2004).
8. G. A. Schmidt *et al.*, in preparation.
9. J. Hansen *et al.*, *J. Geophys. Res.*, in preparation.
10. The climate simulations for 1880 to 2003 used here will be included in the Intergovernmental Panel on Climate Change (IPCC) 2007 report and are available with other IPCC runs at http://www-pcmdi.llnl.gov/ipcc/about_ipcc.php or via www.giss.nasa.gov/data/imbalance.
11. Intergovernmental Panel on Climate Change (IPCC), *Climate Change 2001: The Scientific Basis*, J. T. Houghton *et al.*, Eds. (Cambridge Univ. Press, New York, 2001).
12. J. Hansen, M. Sato, *Proc. Natl. Acad. Sci. U.S.A.* **101**, 16,109 (2004).
13. T. Novakov *et al.*, *Geophys. Res. Lett.* **30**, 1324 (2003).
14. S. Menon, A. Del Genio, in preparation.
15. S. Levitus, J. I. Antonov, T. P. Boyer, C. Stephens, *Science* **287**, 2225 (2000).
16. S. Levitus *et al.*, *Science* **292**, 267 (2001).
17. T. P. Barnett, D. W. Pierce, R. Schnur, *Science* **292**, 270 (2001).
18. S. Sun, J. E. Hansen, *J. Clim.* **16**, 2807 (2003).
19. J. M. Gregory, H. T. Banks, P. A. Stott, J. A. Lowe, M. D. Palmer, *Geophys. Res. Lett.* **31**, L15312 (2004).
20. J. K. Willis, D. Roemmich, B. Cornuelle, *J. Geophys. Res.* **109**, C12036 (2004).
21. S. Levitus, J. I. Antonov, T. P. Boyer, *Geophys. Res. Lett.* **32**, L02604 (2004).
22. J. Hansen *et al.*, *J. Geophys. Res.* **106**, 23947 (2001).
23. R. T. Wetherald, R. J. Stouffer, K. W. Dixon, *Geophys. Res. Lett.* **28**, 1535 (2001).
24. R. S. Lindzen, *Geophys. Res. Lett.* **29**, 1254 (2002).
25. J. Hansen, *Sci. Am.* **290**, 68 (March 2004).
26. J. Hansen, *Clim. Change* **68**, 269 (2005).
27. E. W. Leuliette, R. S. Nerem, G. T. Mitchum, *Mar. Geodesy* **27**, 79 (2004).
28. B. C. Douglas, W. R. Peltier, *Phys. Today* **55**, 35 (2002).
29. W. Munk, *Proc. Natl. Acad. Sci. U.S.A.* **99**, 6550 (2002).
30. I. Joughin, W. Abdalati, M. Fahnestock, *Nature* **432**, 608 (2004).
31. R. Thomas *et al.*, *Science* **306**, 255 (2004).
32. G. Bond *et al.*, *Nature* **360**, 245 (1992).
33. B. Liepert, *Geophys. Res. Lett.* **29**, 1421 (2002).
34. M. L. Roderick, G. D. Farquhar, *Science* **298**, 1410 (2002).
35. M. I. Mishchenko *et al.*, *J. Quant. Spectrosc. Radiat. Transfer* **88**, 149 (2004).
36. H. J. Zwally *et al.*, *J. Geodyn.* **34**, 405 (2002).

37. B. D. Tapley, S. Bettadpur, J. C. Ries, P. F. Thompson, M. M. Watkins, *Science* **305**, 503 (2004).
38. We thank W. Abdalati, B. Chao, J. Dickey, W. Munk, and J. Zwally for helpful information; D. Cain for technical assistance; and J. Kaye, D. Anderson, P. DeCola, T. Lee, and E. Lindstrom (NASA Earth Science Research Division managers) and H. Harvey (Hewlett Foundation) for research support. These data were collected and made freely available by the International Argo Project and the national programs that contribute to it (www.argo.ucsd.edu, http://argo.jcommops.org). Argo is a pilot program of the Global Ocean Observing System.

Supporting Online Material
www.sciencemag.org/cgi/content/full/1110252/DC1
SOM Text
Figs. S1 and S2
Table S1
References

26 January 2005; accepted 19 April 2005
Published online 28 April 2005;
10.1126/science.1110252
Include this information when citing this paper.

Anchorless Prion Protein Results in Infectious Amyloid Disease Without Clinical Scrapie

Bruce Chesebro,[1]* Matthew Trifilo,[2] Richard Race,[1] Kimberly Meade-White,[1] Chao Teng,[2] Rachel LaCasse,[1] Lynne Raymond,[1] Cynthia Favara,[1] Gerald Baron,[1] Suzette Priola,[1] Byron Caughey,[1] Eliezer Masliah,[3] Michael Oldstone[2]

In prion and Alzheimer's diseases, the roles played by amyloid versus nonamyloid deposits in brain damage remain unresolved. In scrapie-infected transgenic mice expressing prion protein (PrP) lacking the glycosylphosphatidylinositol (GPI) membrane anchor, abnormal protease-resistant PrPres was deposited as amyloid plaques, rather than the usual nonamyloid form of PrPres. Although PrPres amyloid plaques induced brain damage reminiscent of Alzheimer's disease, clinical manifestations were minimal. In contrast, combined expression of anchorless and wild-type PrP produced accelerated clinical scrapie. Thus, the PrP GPI anchor may play a role in the pathogenesis of prion diseases.

Transmissible spongiform encephalopathies (TSEs) or prion diseases (*1*) include Creutzfeldt-Jakob disease (CJD) in humans, bovine spongiform encephalopathy or "mad cow dissease" in cattle, scrapie in sheep, and chronic wasting disease in deer and elk of North America. These diseases are similar to nontransmissible protein deposition diseases, such as the systemic amyloidoses and Alzheimer's disease, where a host-derived protein is misfolded and persists in an aggregated form that may damage nearby cells. Amyloid may be present in all these diseases; however, there are important differences among these disease families. In systemic amyloidoses, amyloid deposits in organs appear to be directly pathogenic (*2*), whereas in Alzheimer's disease, pre-amyloid forms (rather than amyloid itself) may be the major neuropathogenic moiety (*3*, *4*). In prion diseases, amyloid formation is variable and may contribute to pathogenesis (*5*). The host protein involved in misfolding and amyloid formation is PrP (*6*, *7*), and PrP is required for susceptibility to disease as well as replication of infectivity (*8*). After infection, normal protease-sensitive PrP (PrPsen) is converted to an aggregated partially protease-resistant structure (PrPres or PrP^{Sc}) (*9*) associated with brain pathology. Three basic patterns of PrPres deposition are found in prion diseases: diffuse "synaptic" nonamyloid deposits, coarse perivacuolar deposits, and dense plaque-like amyloid deposits (*10*, *11*). However, the relative roles of these PrPres forms in brain tissue damage are unknown.

In most cell types, the majority of PrPsen is expressed as a GPI-linked cell surface glycoprotein (*12*), but the role of this GPI membrane anchor in TSE disease is unclear. In cell-free experiments, PrP lacking the GPI moiety ("anchorless PrP") can be converted to the PrPres form (*13*, *14*). However, in scrapie-infected cells, absence of the GPI moiety reduces conversion (*15*, *16*), which suggests that conversion involves membrane-bound GPI-linked PrP. However, redirecting PrP to clathrin-coated pits on the plasma membrane by fusing PrP to a transmembrane domain blocks conversion to PrPres (*17*). Thus, GPI-negative (GPI^-) PrP might facilitate or inhibit susceptibility to TSE infection in vivo. Here, we tested the role of the PrP GPI anchor in scrapie infection and disease in transgenic mice expressing only GPI^- PrP.

Generation of GPI-negative PrP transgenic mice. The transgene was constructed by modifying the ''half-genomic'' mouse PrP plasmid pHGPrP (fig. S1) (*18*). Two transgenic (Tg) lines expressing the highest amounts of PrP (Tg23 and Tg44) were selected for experiments. In brains of Tg23 and Tg44 lines heterozygous for the transgene, PrP mRNA expression was half that in C57BL/6 control mice. Organ extracts were also analyzed for PrPsen expression. In brain, PrPsen levels were about one-fourth that in controls, and PrP was also noted in several other tissues (Fig. 1A). The protein was mainly in the unglycosylated form. In neurons isolated from Tg44 mice, PrP was not located on the cell surface, as is the case with GPI-linked PrP (Fig. 1B). However, levels of intracellular PrP in these mice were similar to controls, indicating that PrP did not accumulate abnormally in these cells. In floatation gradients using brain tissue, GPI^- PrP did not float with raft fractions, in contrast to wild-type GPI-linked PrP (fig. S2). In cell lines, GPI^- PrP was not detectable on the plasma membrane (fig. S3) but appeared in the endoplasmic reticulum and Golgi complex, and was secreted into the medium (*19*). Thus, GPI^- PrP differed markedly from wild-type PrP in subcellular localization and processing.

Infection with three scrapie strains. To study the susceptibility of GPI^- PrP Tg mice to scrapie infection, we inoculated Tg mice and non-Tg controls intracerebrally at 6 weeks of age with scrapie brain homogenate containing 0.7×10^6 to 1.0×10^6 ID_{50} (where ID_{50} is the dose causing disease in 50% of animals). Three scrapie strains [RML (Chandler), ME7, and 22L] (*20*, *21*) were tested to assess strain-dependent differences. Mice were observed daily for typical clinical signs of scrapie, including altered gait, kyphosis, ataxia, disorientation, somnolence, and wasting (Table 1). Clinical disease occurred within 140 to 160 days in control mice homozygous for endogenous wild-type mouse PrP, and within 240 to 260 days in heterozygous control mice. In contrast, in Tg23 and Tg44 mice, no clinical signs were observed after 600 days with the RML strain or 400 days with the ME7 strain. Two 22L-infected mice from line 23 developed a wasting syndrome without neurological signs and died at 370 days. Two other mice in this group showed no symptoms of disease after more than 550 days (Table 1), whereas 22L-infected mice from line 44 showed no symptoms after more than 440 days. Thus, the wasting syndrome in line Tg23 was unlikely related to scrapie infection. In summary, scrapie infection failed to induce the usual clinical manifestations of prion disease in these Tg mice.

Replication of scrapie agent. The lack of clinical disease raised the issue of whether

[1]Laboratory of Persistent Viral Diseases, Rocky Mountain Laboratories, National Institute of Allergy and Infectious Diseases, Hamilton, MT 59840, USA. [2]Division of Virology, Department of Neuropharmacology, Scripps Research Institute, La Jolla, CA 92037, USA. [3]Departments of Neurosciences and Pathology, University of California, San Diego, La Jolla, CA 92093, USA.

*To whom correspondence should be addressed. E-mail: bchesebro@niaid.nih.gov

these Tg mice could replicate the scrapie agent. Therefore, scrapie-infected and mock-infected Tg mice were killed 20 to 291 days after inoculation, and brain samples were analyzed for infectivity. By titration in C57BL/6 mice, mock-infected Tg mice had no detectable infectivity. Infected Tg mice also had no detectable infectivity in brain (<500 ID_{50} per brain) at 20 to 30 days after infection. In contrast, at 120 to 291 days after infection, scrapie-infected Tg mice had titers ranging from 2×10^6 to 4.6×10^8 ID_{50} per brain (Table 2). This increase represented substantial scrapie replication relative to the amount inoculated (10^6 ID_{50}) and was more than five orders of magnitude higher than the level in brain at 20 to 30 days (Table 2). However, the highest titer seen was still about one-tenth the usual titer in non-Tg mice with clinical scrapie.

Because PrP sequence differences are known to influence relative susceptibility to scrapie infection, we also tested whether titration of infected Tg brain homogenates might be more sensitive if done in Tg mice. However, the Tg mice proved to be less sensitive than wild-type mice in these titrations, because none of the eight mice developed PrPres or became ill during 500 days of observation.

Detection of PrPres. To determine whether disease-associated PrPres was present, we examined brain homogenates of infected Tg mice by immunoblotting after treatment with proteinase K (PK). Mock-infected mice showed no development of PrPres up to 500 days. In contrast, mice infected with RML scrapie had detectable PrPres by immunoblot starting at day 213, and the signal continued to increase over the ensuing months (Fig. 1, C and D). Several Tg mice inoculated with RML scrapie had up to 40% more PrPres than usually found in the brains of clinically sick scrapie-infected non-Tg control mice (Fig. 1C). Thus, the lack of clinical signs of scrapie suggested that PrPres in these mice had a reduced level of toxicity.

Comparison of PrPres from Tg and non-Tg mice revealed similar resistance to PK digestion and a similar decrease in molecular mass of 6 to 7 kD after PK treatment, consistent with cleavage around residue 89 (Fig. 1E) (*7*, *22*, *23*). In some familial human prion diseases, PrP molecules present in PrPres are also truncated at the C terminus (*24*). However, analysis with antibodies directed to C-terminal PrP residues showed no evidence for truncation (Fig. 1F). After removal of carbohydrates with peptide:*N*-glycosidase F (PNGase F), the predominant PrP band seen was a fragment extending approximately between residues 89 and 231.

Detection of PrPres amyloid in brain tissue. In prion diseases, the deposition pattern and location of PrPres in brain are important aspects of the pathogenic process. To assess brain PrPres deposition, we examined scrapie-infected Tg mice histologically. Dense plaque-like PrPres deposits were detected in the corpus callosum as early as 70 days after infection with scrapie strain RML (Fig. 2A). From day 213 onward there was a progressively wider distribution of PrPres deposits extending to the cerebral cortex, hippocampus, fimbria, hypothalamus, and forebrain (Fig. 2, B to D). PrPres was often near blood vessels (Fig. 2B, inset) and accumulated in dense deposits (Fig. 2E, right), unlike the diffuse PrPres seen in scrapie-infected non-Tg mice (Fig. 2E, left). By 419 days after inoculation, vacuolation typical of prion disease was seen in white matter areas (Fig. 2F). After 22L infection, dense PrPres plaques were found not only in the corpus callosum (Fig. 2G) but also in the cerebellum and brainstem (Fig. 2H) (fig. S3). The ability of strain 22L to infect the cerebellum was also noted in non-Tg mice; this appeared to be a strain-specific property (*25*) not altered by the presence or absence of PrP an-

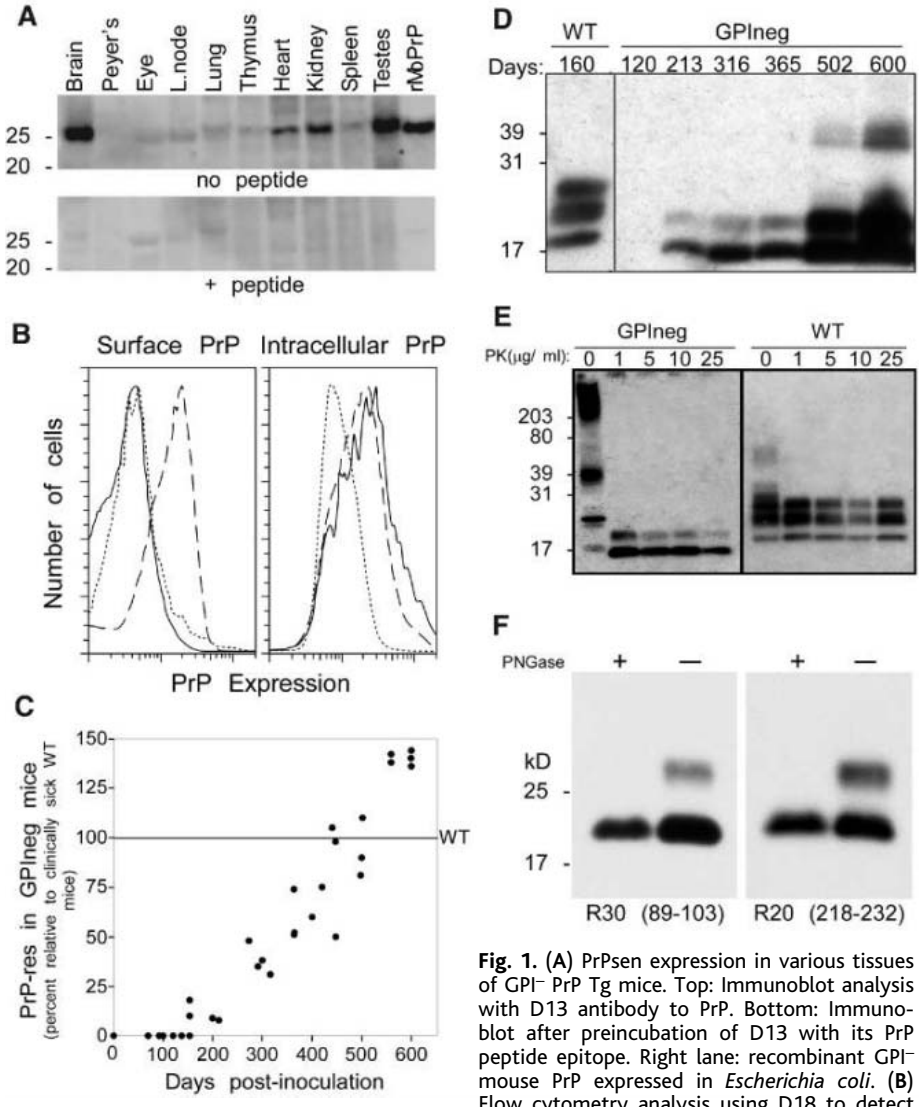

Fig. 1. (**A**) PrPsen expression in various tissues of GPI⁻ PrP Tg mice. Top: Immunoblot analysis with D13 antibody to PrP. Bottom: Immunoblot after preincubation of D13 with its PrP peptide epitope. Right lane: recombinant GPI⁻ mouse PrP expressed in *Escherichia coli*. (**B**) Flow cytometry analysis using D18 to detect cell surface and intracellular PrP in neurons purified from hippocampus (*40*). Solid line, GPI⁻ PrP Tg mouse (Tg44); dashed line, C57BL/6 control mouse; dotted line, PrP null (−/−) mouse. GPI⁻ PrP Tg mice have normal intracellular PrP expression but lack cell surface expression, in agreement with findings that GPI⁻ PrP is secreted from cells (*19*). (**C**) PrPres in brain of scrapie-infected GPI⁻ PrP Tg mice as a percentage of the amount in wild-type mice with clinical scrapie. After 500 days, PrPres in asymptomatic Tg mice exceeded the amount in diseased wild-type mice. (**D**) Immunoblot analysis of PrPres in brains of individual GPI⁻ PrP Tg mice at various days after scrapie inoculation. Brain homogenate from clinically ill wild-type mice is shown for comparison. (**E**) Proteinase K sensitivity of PrPres found in GPI⁻ PrP Tg mice. PrPres in Tg and non-Tg control mice have similar PK sensitivity. Species of higher molecular mass in lanes without PK in brain extracts from Tg mice indicate presence of PrP multimers, not prominent in infected non-Tg control mice. (**F**) Immunoblotting of PrPres from scrapie-infected GPI⁻ PrP Tg mouse before and after treatment with PNGase F to remove carbohydrates. Blotting with antibodies directed to PrP residues 89 to 103 (R30) or 218 to 232 (R20) gave identical patterns; this result indicates that the PrPres is not prematurely truncated at the C terminus, as is PrP amyloid in human familial prion disease.

choring. Strain ME7 was similar to 22L but did not induce PrPres in the cerebellum (table S1).

Because the dense deposits of PrPres appeared to be plaque-like in nature, brains of infected mice were stained with thioflavin S to test for amyloid plaque formation. Tg mice infected with RML, 22L, or ME7 scrapie strains showed very bright staining with thioflavin S in all areas positive for PrPres (Fig. 2, I and J), whereas PrPres in non-Tg mice infected with these same strains was negative. Thus, PrPres in Tg mice appeared predominantly in the form of amyloid plaques, in contrast to PrPres in non-Tg control mice where minimal amyloid was found.

Electron microscopic studies. To confirm that the thioflavin S staining seen by light microscopy was associated with fibrillary protein deposits typical of amyloid, we used electron microscopy to examine brains of scrapie-infected Tg mice. After infection of Tg mice, ultrastructural abnormalities were seen in both gray and white matter, whereas uninfected and mock-infected Tg mice were identical to control mice. Abundant deposition of amyloid fibrils was observed both in and around vascular endothelial cells and was associated with hypertrophic contorted basement membranes (Fig. 3, B and C). Furthermore, in the corpus callosum, swollen dystrophic nonmyelinated axons containing abnormal lysosomes and other electron-dense bodies were found in the plaque regions (Fig. 3E). At the ultrastructural level, these lesions in scrapie-infected Tg mice were similar to lesions found in β-amyloid (Aβ) plaques of human patients with Alzheimer's disease or mouse models of Alzheimer's (*26*, *27*).

Coexpression of wild-type PrP and GPI-negative PrP accelerates scrapie disease. Previously, coexpression of a secreted PrP fusion protein plus wild-type PrP delayed scrapie disease in mice (*28*). Because PrP expressed in GPI$^-$ PrP Tg mice is also secreted from cells and is converted in cell-free reactions (*13*), we tested whether inhibition of scrapie would occur in mice coexpressing wild-type and GPI$^-$ PrP. After infection with strain 22L, non-Tg mice expressing only a single copy of the wild-type PrP gene died within 241 to 257 days. However, mice heterozygous for expres-

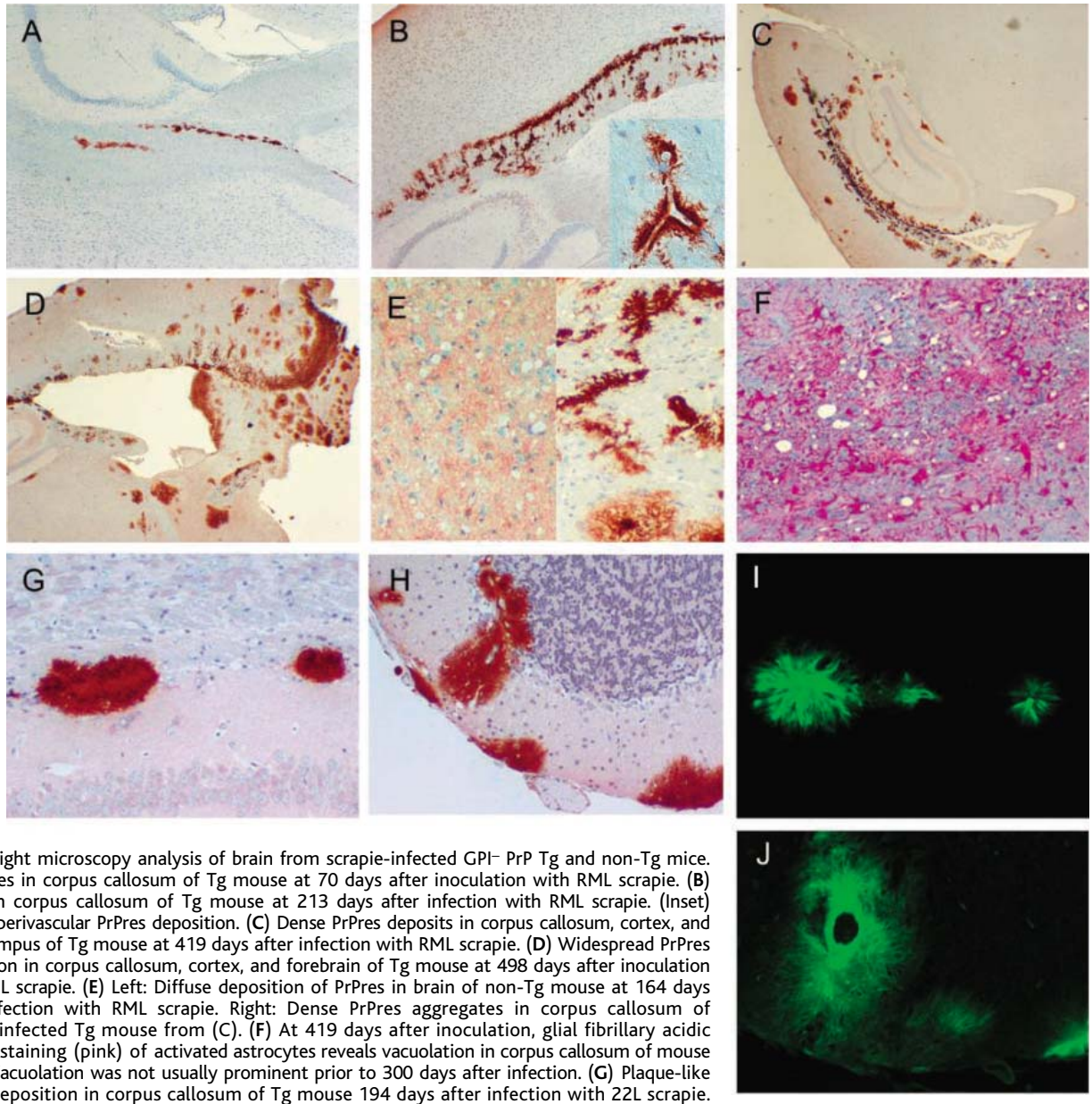

Fig. 2. Light microscopy analysis of brain from scrapie-infected GPI$^-$ PrP Tg and non-Tg mice. (**A**) PrPres in corpus callosum of Tg mouse at 70 days after inoculation with RML scrapie. (**B**) PrPres in corpus callosum of Tg mouse at 213 days after infection with RML scrapie. (Inset) Intense perivascular PrPres deposition. (**C**) Dense PrPres deposits in corpus callosum, cortex, and hippocampus of Tg mouse at 419 days after infection with RML scrapie. (**D**) Widespread PrPres deposition in corpus callosum, cortex, and forebrain of Tg mouse at 498 days after inoculation with RML scrapie. (**E**) Left: Diffuse deposition of PrPres in brain of non-Tg mouse at 164 days after infection with RML scrapie. Right: Dense PrPres aggregates in corpus callosum of scrapie-infected Tg mouse from (C). (**F**) At 419 days after inoculation, glial fibrillary acidic protein staining (pink) of activated astrocytes reveals vacuolation in corpus callosum of mouse in (C). Vacuolation was not usually prominent prior to 300 days after infection. (**G**) Plaque-like PrPres deposition in corpus callosum of Tg mouse 194 days after infection with 22L scrapie. (**H**) Plaque-like PrPres in cerebellum around blood vessels in meninges of Tg mouse 194 days after infection with 22L scrapie. (**I**) Thioflavin S staining of PrPres amyloid in corpus callosum of mouse in (G). (**J**) Thioflavin S staining of PrPres amyloid in cerebellum of mouse in (H). Magnifications: ×20 [(A) and (B)], ×10 [(C) and (D)], ×200 [(E) to (J)].

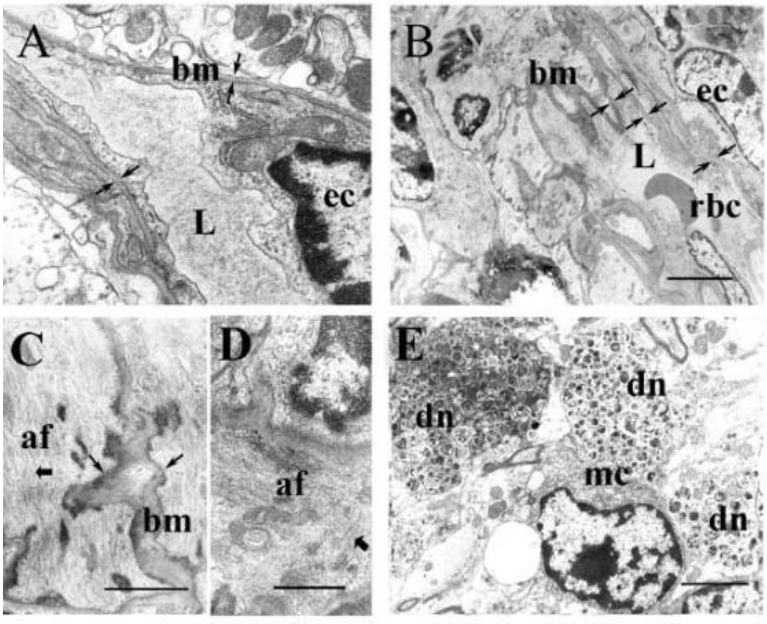

Fig. 3. Ultrastructural analysis of brains of scrapie-infected and uninfected GPI⁻ PrP Tg mice. Electron micrographs were obtained from the deep layers of the neocortex and corpus callosum. Infected mice were 400 days after infection with RML scrapie. (**A**) Low-power view of a normal brain blood vessel in uninfected mouse, showing the lumen (L) and adjacent endothelial cell [nucleus labeled (ec)]. Basement membrane (bm) is identified by arrows. (**B**) Low-power view of an intermediate-size brain blood vessel of scrapie-infected mouse displaying extensive disorganization of cytoarchitecture with distortion of the basement membranes (see arrows). Lumen of the vessel contains a red blood cell (rbc), and an adjacent endothelial cell nucleus is visible. Scale bar, 5 μm. (**C**) At higher magnification, entire perivascular space is packed with hair-like amyloid fibrils (af), and a single fibril is identified by a thick arrow. The basement membrane is irregular and thickened (thin arrows). Scale bar, 2 μm. (**D**) Extracellular amyloid fibrils (thick arrow) in perivascular region. Scale bar, 2 μm. (**E**) Neuritic plaque with microglial cell (mc) and three dystrophic nonmyelinated neurites (dn) containing abundant electron-dense and laminated bodies, similar to damage near Aβ amyloid plaques in human and mouse models of Alzheimer's disease. Scale bar, 4 μm.

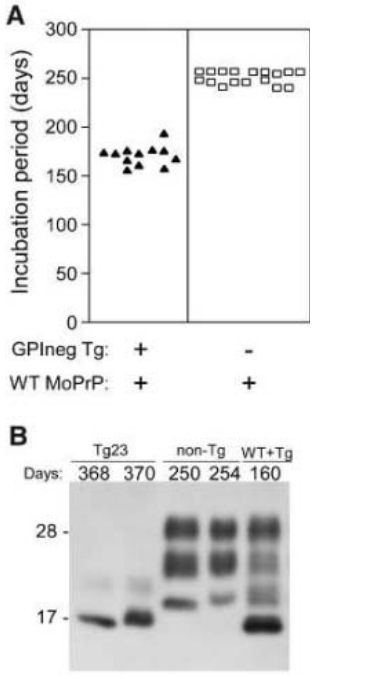

Fig. 4. (**A**) Acceleration of scrapie clinical disease in mice expressing both anchorless PrP and wild-type PrP. GPI⁻ PrP Tg (+/−) mice on the MoPrP (−/−) background were bred with non-Tg C57BL/10 mice previously selected to be heterozygous (+/−) for mouse PrP. Mice were infected with the 22L scrapie strain intracerebrally. All mice used were MoPrP heterozygous (+/−) and were separated into groups that were positive or negative for the GPI⁻ PrP transgene. Mice expressing both wild-type (WT) and GPI⁻ MoPrP developed clinical scrapie about 100 days earlier than mice expressing only WT MoPrP. (**B**) Immunoblot detection of PrPres in scrapie-infected Tg mice and control mice. Starting at left, lanes 1 and 2: Mice from Tg23 line inoculated with 22L scrapie died with wasting syndrome at 368 to 370 days. Lanes 3 and 4: Non-Tg littermate control mice heterozygous for mouse PrP (+/−) infected with 22L scrapie. Clinical disease with typical scrapie neurological signs was seen at 250 to 254 days after infection. Lane 5: Littermate control expressing both GPI⁻ PrP and WT PrP inoculated with 22L scrapie developed clinical disease at 160 days after inoculation. Each lane was loaded with 0.6 mg brain.

sion of both wild-type PrP and GPI⁻ PrP died within 156 to 192 days (Fig. 4A), and brains of these mice appeared to have PrPres generated from both PrP types (Fig. 4B). Thus, anchorless PrP accelerated rather than inhibited scrapie disease. The brains of these mice showed severe vacuolation plus a combination of diffuse PrPres and plaque-like PrPres, with a wider distribution of plaque-like PrPres than in mice expressing only anchorless PrP (fig. S3). The presence of both wild-type and anchorless PrP appeared to enhance the spread of both the amyloid and nonamyloid forms of PrPres.

Discussion. Deletion of the mouse PrP GPI anchor markedly changed the quality of PrPres found in brain, causing a shift from the usual diffuse or punctate nonamyloid pattern to a pattern with thioflavin S–positive PrPres amyloid. Thus, the GPI moiety might interfere with the ability of PrP to form amyloid fibrils. Possibly GPI-mediated PrP membrane attachment might account for this inhibition, or the GPI group might itself block the refolding necessary for amyloid formation. Alternatively, β-sheet structure and amyloid formation might be favored because GPI⁻ PrPsen mostly lacks carbohydrates. PrP amyloid found in humans with familial prion disease also lacks the GPI anchor and carbohydrates, but this amyloid PrP is truncated at both N and C termini, including removal of the entire second and third α helices (*24*, *29*). In contrast, the PrP amyloid found in Tg mice had no evidence for C-terminal truncation (Fig. 1F). Thus, the removal of the residues forming these helices was not as important as lack of the GPI group and the carbohydrates for PrP amyloid formation in vivo.

PrP is a required element for the replication of scrapie infectivity and development of disease (*8*). The present Tg mouse model has separated these aspects, as the GPI group of PrP strongly influenced the development of clinical disease with a lesser impact on agent replication. In GPI⁻ Tg mice, replication of infectivity occurred despite changes in the clinical disease and the type of PrPres deposits. However, relative to clinically ill wild-type mice, the amount of infectivity detected was reduced by nearly a factor of 10. These lower titers were not due to the presence of a new scrapie ''strain'' with a preference for mice expressing GPI⁻ PrP, because attempts to pass scrapie from Tg mice to recipient Tg mice were not successful. Thus, although the GPI anchor was not essential for replication of infectivity, the efficiency of replication in the context of anchorless PrP was reduced.

The lack of clinical disease induced by RML scrapie in the presence of PrPres amyloid and replication of scrapie infectivity is perhaps the most surprising aspect of the current Tg mouse model. PrP amyloid plaques did not cause a rapid fatal clinical disease similar to typical scrapie. Apparently, wild-type diffuse PrPres or its breakdown products are more toxic to brain function than is the amyloid PrPres seen in GPI⁻ PrP Tg mice. A similar hypothesis has been proposed for Alzheimer's disease where smaller Aβ protofibrils or peptides, rather than plaques, are thought by some to be the major pathogenic moieties (*3*, *4*). Alternative-

Table 1. Detection of clinical disease in scrapie-inoculated GPI$^-$ PrP Tg mice and non-Tg control (WT) mice. In proportions shown, the numerator is the number of mice developing clinical disease per total number of mice injected. The denominator represents the total number of mice under observation at the times indicated; this number was decreased at the times when mice were killed and was increased by inoculation of new mice in later experiments. WT non-Tg mice were either C57BL/6 or C57BL/10 mice.

Days	Proportion of positive mice									
	RML scrapie*				22L scrapie			ME7 scrapie		
	Tg23	Tg44	Tg50	WT	Tg23	Tg44	WT	Tg23	Tg44	WT
150	0/35	0/34	0/15	30/30	0/19	0/19	26/26	0/10	0/11	14/14
200	0/33	0/32	0/12		0/19	0/16		0/10	0/9	
250	0/30	0/28	0/10		0/19	0/16		0/10	0/9	
300	0/26	0/25	0/7		0/13	0/15		0/5	0/7	
400	0/13	0/20	0/3		2†/11	0/13		0/1	0/5	
500	0/5	0/2			2/4			0/1		
550	0/3	0/2			2/4			0/1		
600	0/2	0/1			2/4			0/1		

*Mock-infected Tg mice ($N = 8$) developed no clinical disease over a 500-day period. †These two mice developed a wasting syndrome without accompanying neurological signs, and they died at 370 days after inoculation.

Table 2. Titration of infectivity in brain tissue of scrapie-infected GPI$^-$ PrP Tg mice. Titer was calculated as ID_{50} per brain by dividing the 50% end-point dilution (determined by the Spearman-Karber method) by the volume inoculated (30 or 50 μl) and then multiplying by 400 mg, the average mouse brain weight.

Scrapie strain	Number of days after infection	Dilution of brain homogenate	Average incubation period (days)	Proportion of positive mice	Titer (ID_{50}/brain)
RML	20	5×10^1	>400	0/4	$<5.0 \times 10^2$
RML	30	5×10^1	>400	0/4	$<5.0 \times 10^2$
RML	120	5×10^2	180	6/6	
		5×10^4	200	3/3	
		5×10^5	230	3/3	4.6×10^8
		5×10^6	521	2/3	
		5×10^7	507	2/3	
		5×10^8	>550	0/3	
RML	291	5×10^2	160	7/7	
		5×10^3	180	3/3	2.0×10^6
		5×10^4	200	3/3	
		5×10^5	>400	0/3	
22L*	286	10^2	135	4/4†	
		10^3	158	4/4	
		10^4	173	4/4	$>2.4 \times 10^8$
		10^5	184	4/4	
		10^6	193	4/4	
		10^7	215	4/4	
Mock	120	5×10^1	>500	0/5‡	$<5.0 \times 10^2$

*This titration was initiated later and is still in progress. The titer given may be higher if more mice get sick at later times. †C57BL mice inoculated with brain homogenate from this 22L-infected GPI$^-$ PrP Tg mouse developed scrapie pathology and Western blot PrPres patterns similar to that induced by the original 22L scrapie preparation. ‡Single mice were killed at 330 and 500 days after infection and were negative by Western blot for PrPres. Three mice remained alive at 543 days with no signs of disease.

ly, the lack of normal membrane-anchored PrPsen in GPI$^-$ PrP Tg mice might reduce delivery of neurotoxic signals after PrPres formation (*30*, *31*). However, PrP-negative neurons can be damaged and killed indirectly by PrP-expressing astrocytes infected with scrapie strain 263K (*32*), although this process appears to be slower than when PrP-positive neurons are present (*33*).

The localization of the PrPres fibers and plaques around vascular endothelial cells in this model is similar to the PrP145 stop codon familial prion disease (*34*). We found amyloid fibrils both within endothelial cells and in adjacent extracellular locations, accompanied by basement membrane alterations (Fig. 3, B and C). Surprisingly, there was no evidence for increased expression of the transgene in brain endothelial cells (fig. S4). However, proteoglycans derived from endothelial cells might contribute to the observed perivascular deposition of PrPres, because sulfated proteoglycans similar to those present in basement membrane are known to bind PrPsen (*35*) and PrPres (*36*, *37*) and can even potentiate PrP conversion in vitro (*38*, *39*).

Despite the absence of obvious clinical disease, amyloid PrPres in brains of GPI$^-$ PrP Tg mice was associated with definite neuropathological lesions. By electron microscopy, dystrophic neurites were seen in association with amyloid fibrils and plaque-like lesions similar to Alzheimer's disease (*26*) (Fig. 3D). Because lesions were found primarily in the corpus callosum and only later in other areas, the lack of symptoms may be related to the locations of the lesions. Perhaps, beyond our current observation time of more than 600 days, extension of the 22L scrapie-induced lesions in the cerebellum or brainstem might produce more obvious symptomatology.

References and Notes

1. B. Chesebro, *Br. Med. Bull.* **66**, 1 (2003).
2. M. B. Pepys, *Philos. Trans. R. Soc. London Ser. B* **356**, 203 (2001).
3. B. Caughey, P. T. Lansbury, *Annu. Rev. Neurosci.* **26**, 267 (2003).
4. J. P. Cleary *et al.*, *Nat. Neurosci.* **8**, 79 (2005).
5. H. Fraser, M. Bruce, *Lancet* **i**, 617 (1973).
6. B. Chesebro *et al.*, *Nature* **315**, 331 (1985).
7. B. Oesch *et al.*, *Cell* **40**, 735 (1985).
8. H. Bueler *et al.*, *Cell* **73**, 1339 (1993).
9. K. Basler *et al.*, *Cell* **46**, 417 (1986).
10. H. Budka *et al.*, *Brain Pathol.* **5**, 459 (1995).
11. P. Parchi *et al.*, *Ann. Neurol.* **46**, 224 (1999).
12. N. Stahl, D. R. Borchelt, K. Hsiao, S. B. Prusiner, *Cell* **51**, 229 (1987).
13. D. A. Kocisko *et al.*, *Nature* **370**, 471 (1994).
14. V. A. Lawson, S. A. Priola, K. Wehrly, B. Chesebro, *J. Biol. Chem.* **276**, 35265 (2001).
15. B. Caughey, G. J. Raymond, *J. Biol. Chem.* **266**, 18217 (1991).
16. M. Rogers, F. Yehiely, M. Scott, S. B. Prusiner, *Proc. Natl. Acad. Sci. U.S.A.* **90**, 3182 (1993).
17. K. Kaneko *et al.*, *Proc. Natl. Acad. Sci. U.S.A.* **94**, 2333 (1997).
18. M. Fischer *et al.*, *EMBO J.* **15**, 1255 (1996).
19. M. Horiuchi, J. Chabry, B. Caughey, *EMBO J.* **18**, 3193 (1999).
20. R. L. Chandler, *Lancet* **1**, 1378 (1961).
21. M. E. Bruce, I. McConnell, H. Fraser, A. G. Dickinson, *J. Gen. Virol.* **72**, 595 (1991).
22. J. Hope *et al.*, *EMBO J.* **5**, 2591 (1986).
23. P. Parchi *et al.*, *Proc. Natl. Acad. Sci. U.S.A.* **97**, 10168 (2000).
24. F. Tagliavini *et al.*, *EMBO J.* **10**, 513 (1991).
25. M. E. Bruce, H. Fraser, *Curr. Top. Microbiol. Immunol.* **172**, 125 (1991).
26. E. Masliah *et al.*, *J. Neurosci.* **16**, 5795 (1996).
27. E. Masliah, A. Sisk, M. Mallory, D. Games, *J. Neuropathol. Exp. Neurol.* **60**, 357 (2001).
28. P. Meier *et al.*, *Cell* **113**, 49 (2003).
29. B. Ghetti *et al.*, *Brain Pathol.* **6**, 127 (1996).
30. S. Brandner *et al.*, *Nature* **379**, 339 (1996).
31. L. Solforosi *et al.*, *Science* **303**, 1514 (2004).
32. M. Jeffrey, C. M. Goodsir, R. E. Race, B. Chesebro, *Ann. Neurol.* **55**, 781 (2004).
33. G. Mallucci *et al.*, *Science* **302**, 871 (2003).
34. B. Ghetti *et al.*, *Proc. Natl. Acad. Sci. U.S.A.* **93**, 744 (1996).
35. B. Caughey, K. Brown, G. J. Raymond, G. E. Katzenstien, W. Thresher, *J. Virol.* **68**, 2135 (1994).
36. A. D. Snow, R. Kisilevsky, J. Willmer, S. B. Prusiner, S. J. DeArmond, *Acta Neuropathol. (Berlin)* **77**, 337 (1989).
37. P. A. McBride, M. I. Wilson, P. Eikelenboom, A. Tunstall, M. E. Bruce, *Exp. Neurol.* **149**, 447 (1998).
38. C. Wong *et al.*, *EMBO J.* **20**, 377 (2001).
39. O. Ben-Zaken *et al.*, *J. Biol. Chem.* **278**, 40041 (2003).
40. G. F. Rall *et al.*, *Proc. Natl. Acad. Sci. U.S.A.* **94**, 4659 (1997).

41. We thank S. Hughes, H. Lewicki, and K. Wehrly for laboratory technical assistance, and A. Mora and G. Hettrick for graphics assistance. Supported in part by NIH grant AG004342.

Supporting Online Material

www.sciencemag.org/cgi/content/full/308/5727/1435/DC1
Materials and Methods
Figs. S1 to S5

8 February 2005; accepted 4 April 2005
10.1126/science.1110837

Structure of the Ultrathin Aluminum Oxide Film on NiAl(110)

Georg Kresse,[1]* Michael Schmid,[2] Evelyn Napetschnig,[2] Maxim Shishkin,[1] Lukas Köhler,[1] Peter Varga[2]

The well-ordered aluminum oxide film formed by oxidation of the NiAl(110) surface is the most intensely studied metal surface oxide, but its structure was previously unknown. We determined the structure by extensive ab initio modeling and scanning tunneling microscopy experiments. Because the topmost aluminum atoms are pyramidally and tetrahedrally coordinated, the surface is different from all Al_2O_3 bulk phases. The film is a wide-gap insulator, although the overall stoichiometry of the film is not Al_2O_3 but $Al_{10}O_{13}$. We propose that the same building blocks can be found on the surfaces of bulk oxides, such as the reduced corundum (0001) surface.

The detailed study of oxide surfaces is often hampered because many surface-sensitive techniques cannot be applied to bulk oxides, which are almost perfect insulators and are therefore difficult to examine with methods involving charged particles (electrons and ions). Ultrathin oxide films, which are thin enough to avoid charge accumulation, represent an elegant solution to this problem and are now widely used as microscopic model systems. Furthermore, ultrathin oxides are technologically important; their uses range from protective films against corrosion and mechanical wear to insulating films in semiconductor devices. It is thus not unexpected that ultrathin oxides are fascinating researchers worldwide (*1*–*9*).

The ultrathin alumina film formed by oxidation of NiAl(110) is widely used as a model system for technologically important oxide-supported catalysts. Despite enormous effort, its structure has remained unresolved (*10*–*15*), impeding progress in detailed understanding of the influence of the oxide support on the catalytic reactivity. A surface x-ray diffraction (XRD) study recently presented a structural model for this surface (*16*). However, this structure has two bonds with unphysically short lengths (Al-Al, 2.08 Å; Al-O, 1.51 Å) and was revealed to be unstable in our ab initio calculations. Here, we combine atomistic information gained by scanning tunneling microscopy (STM) with ab initio density functional theory (DFT) to produce a structural model, which differs considerably from all previous models based on Al_2O_3 bulk structures. Al_2O_3 commonly crystallizes in the corundum structure (sapphire), adopted by many other trivalent metals as well. In this crystal structure, O atoms are arranged in hexagonal close-packed planes, and the Al atoms occupy two out of three octahedral interstitial sites between the oxygen planes, forming a buckled honeycomb lattice. In the other bulk alumina structures, such as γ and κ alumina, metal atoms are found in octahedral and tetrahedral sites between the close-packed O layers. On the basis of the bulk materials, we would therefore expect that thin films involve hexagonal O planes and octahedrally and tetrahedrally coordinated metal atoms with an overall Al_2O_3 stoichiometry (*17*, *18*).

However, this simple assumption is invalidated by the room-temperature STM measurements (Fig. 1C) (*19*). We observed square features on the surface (marked by green rectangles and squares). We explain them by a square arrangement of oxygen atoms, as shown in the final model (Fig. 1A and table S1). The stacking sequence and stoichiometry of the film is $4(Al_4O_6Al_6O_7)$ and thus also deviates from the commonly assumed Al_2O_3 stoichiometry (*10*, *16*, *17*). The oxide unit cell covers 16 NiAl surface unit cells and is commensurate to the substrate in the direction of the yellow diagonal of the unit cell ("row matching") (*10*–*12*). In the second direction, the film is incommensurate, which necessitates some approximation in the modeling. We chose a parallelogram-shaped supercell with two oxide unit cells placed onto 33 NiAl unit cells to model the interface (*19*). The positions of the 28 O atoms in the surface layer (O_s) are determined by the room-temperature STM images. Almost coplanar with these O atoms, 24 Al surface atoms (Al_s) are arranged in a nearly hexagonal pattern that fits the 24 bright protrusions observed in low-temperature STM images under certain tunneling conditions (Fig. 1E) (*14*, *20*). The

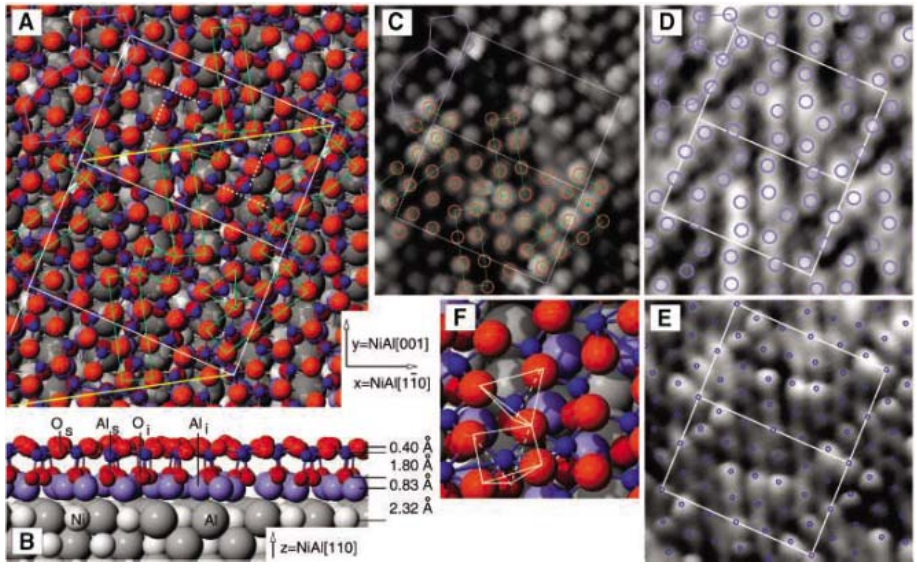

Fig. 1. (**A**) Top and (**B**) side view of the DFT- and STM-based model for the ultrathin aluminum oxide film on NiAl(110). (**C** to **E**) Experimental STM images of the film at [(C) and (D)] room temperature and (E) low temperature. Sample bias voltage and tunneling current values are (C) −2.5 mV/1.4 nA, (D) −0.2 V/0.9 nA, and (E) −0.5 V/0.3 nA. Two oxide unit cells are marked by white rectangles, the diagonal along which the oxide is commensurate is yellow, and the parallelogram enclosed by the yellow and white lines delimits the simulation cell. Green rectangles and squares highlight oxygen atoms in a square arrangement. Circles indicate the Al and O positions from (A) and (B) in the corresponding colors. (**F**) Closeup of the structure.

[1]Institut für Materialphysik and Centre for Computational Materials Science, Universität Wien, A-1090 Wien, Austria. [2]Institut für Allgemeine Physik, Technische Universität Wien, A-1040 Wien, Austria.

*To whom correspondence should be addressed. E-mail: Georg.Kresse@univie.ac.at

surface atoms not only have twofold rotational symmetry but their arrangement also exhibits glide planes (dotted lines in Fig. 1A). Because glide planes imply a rectangular cell (p2gg plane-group symmetry), the symmetry of the cell explains why it is almost perfectly rectangular in spite of its oblique orientation with respect to the substrate.

To determine the structure of the subsurface layers not accessible by STM, we used extensive ab initio modeling. We started with smaller systems well-suited to identify general aspects and possible building blocks. The knowledge gained with these systems enabled us to tackle larger supercells, with the final model (Fig. 1A) consisting of a total of 712 atoms. The initial model systems were based on previous experiments (*14*, *16*) with two hexagonally arranged O layers and Al atoms sandwiched in between the O layers and between the oxide and the NiAl surface (i.e., NiAl-Al_{hex}-O_{hex}-Al_{hex}-O_{hex}). The in-plane packing density of O and Al atoms was chosen to be 24/16 = 1.5 atoms per NiAl unit cell. To determine the most favorable stoichiometry, Al atoms were subsequently removed from the Al layers, and each model was subjected to simulated annealing, in order to determine the global energy minimum for this particular stoichiometry (*19*). The stability of each structure was assessed by calculating the change of the surface energy $\Delta\gamma$ in the grand canonical ensemble

$$\Delta\gamma = (E_{\mathrm{NiAl-slab/oxide}} - E_{\mathrm{NiAl-slab}} - N_{\mathrm{Al}}\,\mu_{\mathrm{Al}} - N_{\mathrm{O}}\,\mu_{\mathrm{O}})/\mathrm{area}$$

where N_O and N_{Al} are the number of O and Al atoms in the oxide film, E are the energies of the corresponding slabs, and μ_O and μ_{Al} are the chemical potentials of O and Al atoms (*21*).

We found that the number of Al atoms at the interface is identical to the number of NiAl unit cells, with a strong preference for the Al atoms to be located above the Ni rows, and that the number of Al atoms in the surface layer is identical to the number of O atoms in each layer. The most stable model determined by this search is shown in Fig. 2A. Compared with the O density in the experimental STM image (Fig. 1C), this model still lacks two surface O atoms, but two voids for these extra O atoms can be spotted in the topmost layer (white circles in Fig. 2A). After adding the additional O atoms and subjecting the model to finite-temperature molecular dynamics, a structure evolves (Fig. 2B) that has square and triangular features similar to those observed in the experimental STM image but that lacks the proper long-range periodicity.

The building blocks (DFT) and the positions of the O_s and Al_s atoms (STM) are unambiguously determined, as well as the position of the second layer O atoms (O_i), which the DFT model suggests to be located below the Al_s atoms (dark red and blue balls in Fig. 2B). Thus, in the final structure, all Al_s atoms are either tetrahedrally or pyramidally coordinated, with the O tip of the tetrahedron and quadratic pyramids pointing toward the substrate (Fig. 1, A and F). These building blocks are responsible for the triangular and square features in the STM images. Considering the many bulk oxide structures with hexagonally close-packed oxygen layers, the existence of square pyramids is at first sight unexpected and has not been considered in previous experimental studies of alumina surfaces. The pyramids can be understood, however, as truncated octahedra; notably, O octahedra with a central metal atom are the most important building blocks of metal oxides.

The positions of the interfacial aluminum atoms (Al_i) were finally determined by placing one Al atom above each Ni atom and subsequent annealing, also allowing for a rearrangement of other atoms in the oxide. This process yields a space-filling arrangement of the Al_i atoms in pentagon-heptagon pairs (blue lines in Fig. 1, A to D). The reason for this particular arrangement is the preferred chemical short-range order; Al atoms prefer Ni neighbors. In corundum, however, the Al atoms are arranged in a honeycomb lattice, which would result in an unfavorably high number of Al-Al neighbors at the interface. The pentagon-heptagon pairs, which are common defects in honeycomb structures, can be considered an ordered "defect" arrangement that allows a decrease in the interface energy. As a result, five rows of Al_i atoms match onto five Ni rows running approximately perpendicular to the yellow diagonal in Fig. 1A. This explains the experimentally observed row matching in the $[1\bar{1}0]$ direction. The O_s atoms above the Al_i atoms become brighter in the STM images at larger bias voltages (*20*). Figure 1D therefore shows that the interface structure has been correctly determined.

A further important property of the Al_i atoms is that they bind by means of the p_z orbital and one of their electrons to the underlying Ni row. The two remaining Al valence electrons are involved in anchoring the oxide film. Thus, in spite of the unusual stoichiometry, $4(Al^{+2}{}_4O^{-2}{}_6Al^{+3}{}_6O^{-2}{}_7)$, the formal ionicities multiplied by the number of ions sum to zero. The calculations also show a wide electronic gap in agreement with the experimental observation that the film is insulating (fig. S1). Finally, we note that among all the systems considered, our model results in the lowest surface energy. The structure previously suggested by Stierle *et al*. (*16*) undergoes massive changes upon relaxation with DFT, and even after relaxation, the surface energy per NiAl(110) unit cell remains about 2.5 eV less favorable than for the present model.

As a further confirmation of the structural model, we calculated the binding energies of the O 1s and Al 2p core electrons and, when we compared them with experimental data (*10*), found excellent agreement. However, a more convincing validation is supplied by the measured high-resolution electron energy-loss spectrum (*13*) shown alongside the simulated spectrum in Fig. 3. The simulated vibrational spectrum shows a slight redshift of approximately 10 to 20 cm^{-1}, which is most likely related to the density functional approximation. Otherwise, the positions of the peaks as well as the intensity distribution are in excellent agreement with experiment. Considering that we did not perform a structural refinement, we

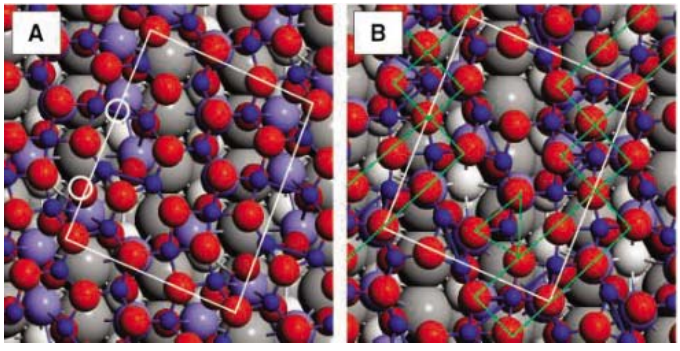

Fig. 2. Energetically favorable models for smaller oxide unit cells with stoichiometries (**A**) $2(Al_4O_6Al_6O_6)$ and (**B**) $2(Al_4O_6Al_6O_7)$ on a $\begin{pmatrix} 2 & -1 \\ 1 & 3 \end{pmatrix}$ NiAl unit cell (white rectangle). Green lines mark local square and hexagonal arrangements of oxygen atoms, and white circles indicate voids where extra oxygen atoms can be added.

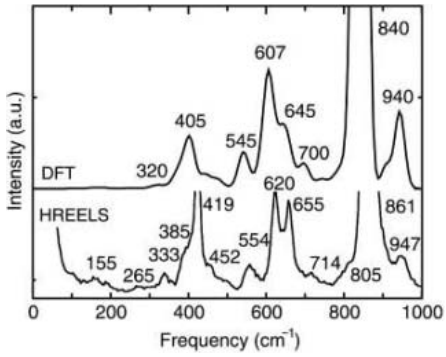

Fig. 3. Infrared-active modes as calculated (*19*) by DFT (broadened by a Gaussian with a width of 20 cm^{-1}) and high-resolution electron energy-loss spectrum (HREELS) from (*13*). a.u., arbitrary units.

also found good agreement with the published XRD data (*16*) (supporting online material text, figs. S2 and S3).

With 12 Al_s atoms in pyramids and 12 in tetrahedra and the nonhexagonal oxygen layer, the film is neither related to bulk corundum nor to bulk γ or κ alumina. This result shows that extrapolation from bulk materials to thin films, even if supplemented by chemical intuition, is often insufficient for the correct determination of complex structures. However, by applying the experiment and theory in a closely coupled manner, very complex structures—here, 92 atoms in the unit cell—can be solved unambiguously.

Finally, the structure of the ultrathin alumina film on NiAl(110) will provide a good starting point for understanding the structures of other oxide surfaces, especially those of Al_2O_3. For instance, the average Al-Al in-plane distance in the surface layer of the complex $\sqrt{31} \times \sqrt{31}$ surface reconstruction of corundum (0001) is 3.03 Å (*22*, *23*), exactly the same value as in the first Al layer of the ultrathin oxide on NiAl(110). This similarity suggests that the reduced corundum surface is built in a manner similar to the current structure, with exactly the same structural elements, resulting in an oxygen layer with square and hexagonal arrangements at the top and a distorted hexagonal Al layer slightly below.

References and Notes

1. H. Over *et al.*, *Science* **287**, 1474 (2000).
2. C. I. Carlisle *et al.*, *Phys. Rev. Lett.* **84**, 3899 (2000).
3. E. Lundgren *et al.*, *Phys. Rev. Lett.* **88**, 246103 (2002).
4. B. L. Hendriksen, J. W. Frenken, *Phys. Rev. Lett.* **89**, 046101 (2002).
5. N. Nilius, T. M. Wallis, W. Ho, *Phys. Rev. Lett.* **90**, 046808 (2003).
6. X. H. Qiu, G. V. Nazin, W. Ho, *Science* **299**, 542 (2003).
7. E. Lundgren *et al.*, *Phys. Rev. Lett.* **92**, 046101 (2004).
8. J. Gustafson *et al.*, *Phys. Rev. Lett.* **92**, 126102 (2004).
9. W. X. Li *et al.*, *Phys. Rev. Lett.* **93**, 146104 (2004).
10. R. M. Jaeger *et al.*, *Surf. Sci.* **259**, 235 (1991).
11. J. Libuda *et al.*, *Surf. Sci.* **318**, 61 (1994).
12. F. Winkelmann *et al.*, *Surf. Sci.* **307–309**, 1148 (1994).
13. M. Frank *et al.*, *Surf. Sci.* **492**, 270 (2001).
14. M. Kulawik, N. Nilius, H.-P. Rust, H.-J. Freund, *Phys. Rev. Lett.* **91**, 256101 (2003).
15. X. Torrelles *et al.*, *Surf. Sci.* **487**, 97 (2001).
16. A. Stierle *et al.*, *Science* **303**, 1652 (2004).
17. D. R. Jennison, A. Bogicevic, *Surf. Sci.* **464**, 108 (2000).
18. X.-G. Wang *et al.*, *Phys. Rev. Lett.* **84**, 3650 (2000).
19. Materials and methods are available as supporting material on *Science* Online.
20. STM simulations based on the Tersoff-Hamann approach [local density of states (LDOS) near the Fermi edge] show the O_s atoms as protrusions. At larger tip-surface distances, O_s atoms with Al_i atoms below become progressively brighter, because the tails of the NiAl states can more easily penetrate into the vacuum through the Al_i atoms. This is in agreement with the experimental observation that only these O_s atoms are visible for larger bias voltages, where the tip-surface distance is relatively large. Obtaining atomic resolution in the low-temperature STM at moderately high tunneling voltages as well as the appearance of the STM images in (*14*) indicate that the contrast observed in the low-temperature images is not due to simple LDOS but rather due to an adsorbate at the tip interacting with the surface Al atoms, similar to the process discussed for chemical contrast on alloys (*24*). This type of image was not observed at room temperature, indicating that the adsorbate is not stable at the tip at room temperature.
21. At typical growth conditions, the chemical potentials μ_{Al} and μ_O can be estimated to be roughly 1 eV smaller than the formation energy of bulk face-centered cubic Al and O_2, respectively (*25*, *26*).
22. G. Renaud, B. Villette, I. Vilfan, A. Bourret, *Phys. Rev. Lett.* **73**, 1825 (1994).
23. C. Barth, M. Reichling, *Nature* **414**, 54 (2001).
24. M. Schmid, H. Stadler, P. Varga, *Phys. Rev. Lett.* **70**, 1441 (1993).
25. M. Hagen, M. W. Finnis, *Philos. Mag. A* **77**, 447 (1998).
26. K. Reuter, M. Scheffler, *Phys. Rev. B* **65**, 035406 (2002).

27. We thank H.-J. Freund for helpful discussions and for lending an NiAl single crystal to us. This work was supported by the Austrian Fonds zur Förderung der wissenschaftlichen Forschung.

Supporting Online Material

www.sciencemag.org/cgi/content/full/308/5727/1440/DC1
Materials and Methods
SOM Text
Figs. S1 to S3
Table S1

22 November 2004; accepted 7 April 2005
10.1126/science.1107783

Directed Assembly of Block Copolymer Blends into Nonregular Device-Oriented Structures

Mark P. Stoykovich,[1] Marcus Müller,[2] Sang Ouk Kim,[3] Harun H. Solak,[4] Erik W. Edwards,[1] Juan J. de Pablo,[1] Paul F. Nealey[1]†

Self-assembly is an effective strategy for the creation of periodic structures at the nanoscale. However, because microelectronic devices use free-form design principles, the insertion point of self-assembling materials into existing nanomanufacturing processes is unclear. We directed ternary blends of diblock copolymers and homopolymers that naturally form periodic arrays to assemble into nonregular device-oriented structures on chemically nanopatterned substrates. Redistribution of homopolymer facilitates the defect-free assembly in locations where the domain dimensions deviate substantially from those formed in the bulk. The ability to pattern nonregular structures using self-assembling materials creates new opportunities for nanoscale manufacturing.

One of the challenges in nanofabrication is the integration of self-assembling materials into existing manufacturing strategies to achieve molecular-level process control and the ability to produce useful architectures. Previous reports of block copolymer lithography described an inexpensive, parallel, and scalable technique for patterning dense periodic arrays of nanostructures (*1*) that are suited for a number of applications such as nanowires (*2*, *3*), quantum dots (*1*, *4*), magnetic storage media (*5*), flash memory devices (*6*), photonic crystals (*7*), and silicon capacitors (*8*). Diblock copolymers consist of two chemically connected polymer chains. Because of their different properties, the chain segments tend to spontaneously form ordered nanostructures, including spheres, cylinders, and lamellae, whose shape and dimensions depend on the molecular weight and composition of the polymer (*9*). Block copolymer lithography refers to the use of these ordered structures in the form of thin films as patterning templates. Varying degrees of long-range order and substrate registration of the periodic arrays are achieved by using strategies such as electric fields (*2*, *10*), chemically (*11–13*) and topographically (*14–16*) patterned substrates, and shear (*17*). We demonstrate that, by directing the assembly of blends of block copolymers and homopolymers on chemically nanopatterned substrates, it is possible to pattern nonregular-shaped structures aided by a nonuniform distribution of homopolymers across the patterns. The technological implication of this approach is that the fine control of structure dimensions afforded by self-assembling block copolymer materials may be harnessed for applications such as the production of nanoelectronic devices that require patterns more complex than simple periodic arrays.

Current commercial lithographic processes can generate patterns with perfection over macroscopic areas and with dimensional control of features, registration, and overlay within exacting tolerances and margins. In the past decade, considerable resources have been

[1]Department of Chemical and Biological Engineering and Center for Nanotechnology, University of Wisconsin (UW), Madison, WI 53706, USA. [2]Department of Physics, University of Wisconsin, Madison, WI 53706, USA. [3]Department of Materials Science and Engineering, Korea Advanced Institute of Science and Technology, Daejeon 305-701, Republic of Korea. [4]Laboratory for Micro- and Nanotechnology, Paul Scherrer Institute, CH-5232 Villigen PSI, Switzerland.

†To whom correspondence should be addressed. E-mail: nealey@engr.wisc.edu

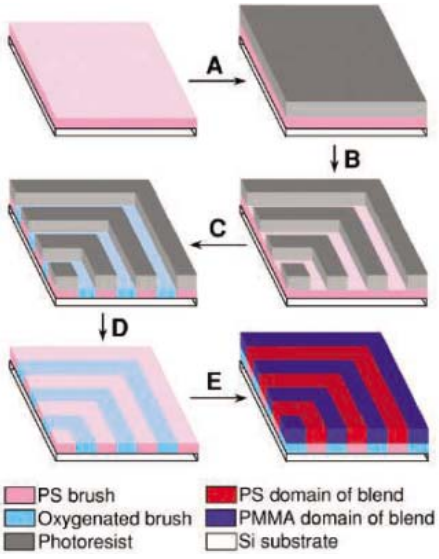

Fig. 1. Schematic of the process used to fabricate chemically nanopatterned surfaces that direct the self-assembly of ternary blends in linear and bend geometries. (**A**) A photoresist was spin-coated on a PS brush that was grafted to a Si substrate and (**B**) patterned by using advanced lithography to produce line and space features of period L_S. (**C**) Oxygen plasma etching was used to chemically modify the exposed regions of the PS brush and to convert the topographic photoresist pattern into a chemical surface pattern. (**D**) The photoresist was removed by solvent treatment, and (**E**) a ternary block copolymer–homopolymer blend was coated and annealed on the chemical surface pattern.

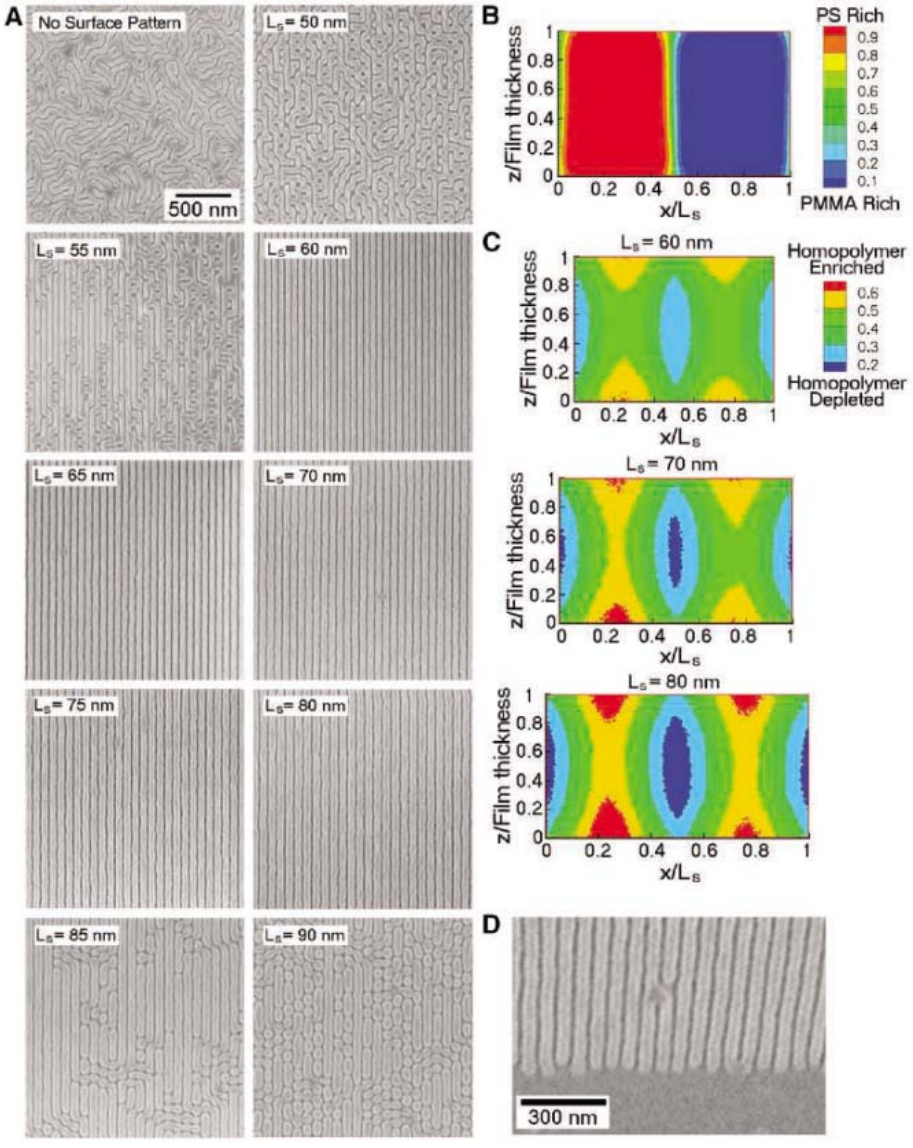

Fig. 2. Behavior of ternary blends on chemical surface patterns with linear geometries. (**A**) Top-down SEM images of the ternary PS-b-PMMA/PS/PMMA blend (L_B = 70 nm) on an unpatterned neutral surface of PS-r-PMMA and on chemically striped PS surfaces. The chemical surface patterns have a period, L_S, ranging from 50 to 90 nm. Each micrograph depicts a 2 μm by 2 μm area. The bright and dark regions correspond to the PS and PMMA domains, respectively, and the dimensions of the PS domains appear artificially large because of the SEM imaging. (**B**) Contour plot of the relative composition of PS segments in a single lamellar period (L_S = L_B = 70 nm) as obtained from two-dimensional SCMF simulations. The PS- and PMMA-rich domains are shown in red and blue, respectively. (**C**) Contour plots of the relative concentration of both homopolymers, PS and PMMA, from SCMF simulations of defect-free morphologies of the ternary blend on linear surface patterns with L_S of 60, 70, and 80 nm. The centers of the lamellar domains are enriched in homopolymers (shown in red), whereas the domain interfaces are depleted of homopolymers (shown in blue). The contour plots of (B) and (C) are displayed as a cross section of the thin film, where *x* is the direction normal to the lamellae and *z* is the direction normal to the substrate (z/film thickness = 0) and free surface (z/film thickness = 1). The data have been averaged in the direction parallel to the lamellae. (**D**) Top-down SEM image of the ends of line structures. The perpendicular lamellar domains (top portion) terminate at a boundary with lamellae oriented parallel to the substrate (bottom portion). The end of the chemical surface pattern has a period of L_S = 60 nm, whereas at the top of the image $L_S \approx$ 63 nm.

allocated to the development of exposure tools capable of resolving nanoscale patterns (< 30 nm) with the required registration and overlay capabilities, but relatively modest investments have been made in the development of suitable imaging materials at this length scale (*18*). Currently chemically amplified photoresists are used in manufacturing processes to pattern features with dimensions as small as 50 to 70 nm but may not be extendable as feature dimensions shrink to 30 nm and below. Other types of photoresists and electron beam lithography have been used to fabricate proof-of-principle devices with features below 10 nm (*19*, *20*). Although these demonstrations provide motivation for continuing to push the limits of nanomanufacturing, the materials and processes themselves are not amenable for production purposes in their present form (*20*). Self-assembling materials used in conjunction with the most advanced exposure tools may enable extension of current manufacturing practices to dimensions of 10 nm and less. Recently we demonstrated that the domains of block copolymer films could be directed to assemble into defect-free periodic patterns over arbitrarily large areas in registry with lithographically defined chemical surface patterns (*11*, *21*) and with nanometer precision over the lateral dimensions of the domains (*22*). We now extend the capabilities of block copolymer lithography to include patterns of line segments and nested arrays of lines with sharp bends by using ternary blends of diblock copolymers and homopolymers.

The schematic in Fig. 1 illustrates the process used to fabricate chemically nanopatterned surfaces that subsequently direct the assembly of films of ternary block copolymer-homopolymer blends (*11*, *22*). Hydroxy-terminated polystyrene (PS) was

grafted to a silicon substrate, resulting in a PS brush layer (*22*–*24*). The PS brush was then coated with a thin film of photoresist. Advanced lithography was used to pattern the photoresist with arrays of roughly equal lines and spaces having periods between 50 and 90 nm and bends with angles from 45° to 135°. Patterning was performed by electron beam lithography for all features with periods ≥ 60 nm and by extreme ultraviolet interference lithography (*25*) for features with periods < 60 nm (*24*). The sample was then subjected to an oxygen plasma. The surface was chemically modified and rendered strongly hydrophilic or polar only in areas where the photoresist did not cover the PS brush (*24*). The remaining photoresist was removed by solvent rinses, leaving behind the chemically nanopatterned surface. A ~43-nm film of a ternary block copolymer–homopolymer blend was subsequently spin-coated and annealed on the patterned surface at 193°C for 7 days (*24*). These block copolymer films have an adequate thickness to act as templates for patterning through selective etching or deposition processes (*1*, *3*, *5*, *8*) and are sufficiently thin for the surface interactions to stabilize the perpendicular morphology (*21*). The ternary blend consisted of 60 weight % (wt. %) symmetric polystyrene-block-poly(methyl methacrylate) (PS-b-PMMA, 104 kg mol^{-1}, bulk lamellar period of L_O = 49 nm), 20 wt. % polystyrene homopolymer (PS, 40 kg mol^{-1}), and 20 wt. % poly(methyl methacrylate) homopolymer (PMMA, 41 kg mol^{-1}). On homogeneous neutral wetting surfaces, the blend formed a lamellar phase with a period, L_B, of 70 nm (Fig. 2A) (*26*). The PS domain of the ternary blend preferentially wet the unmodified PS brush, and the PMMA domain preferentially wet the regions of the brush that were chemically modified by the oxygen plasma. Scanning electron microscopy (SEM) was used to image the domain structure of the block copolymer blend after annealing.

Top-down SEM images of the domain structure of the ternary blend with L_B = 70 nm on surfaces with striped chemical nanopatterns of period L_S between 50 to 90 nm are shown in Fig. 2A. Lamellae were perfectly ordered and registered on surfaces having L_S ranging from 60 to 80 nm. For L_S < 60 nm, compression of the lamellar domains led to the formation of bridges between domains that were predominately oriented perpendicular to the surface pattern. For L_S > 80 nm, the lamellar structures appeared to be pinched off into small, circular domains of PS or PMMA. For L_S = 85 nm, the circular domains, although remaining centered and registered with the underlying chemical pattern, had an increased propensity to merge with neighboring domains on adjacent surface stripes. For L_S = 90 nm there were few aligned lamellae and more circular domains. These defect structures in the blends are distinctly different than the dislocations and disclinations observed at incommensurate values of L_S and L_O for pure block copolymers (*11*, *22*). The range of L_S over which perfect directed assembly was achieved with the blends, however, is consistent with previous results using pure block copolymers (*22*).

Single chain in mean field (SCMF) simulations, a particle-based self-consistent field method, were performed to calculate the molecular-level distribution of homopolymers within the lamellar domains as a function of L_S (*24*, *27*). Self-consistent field techniques (*28*) have been shown to accurately describe the self-assembly of block copolymers in the bulk (*29*) and under confinement (*30*). The calculations use values of χN, where χ is the Flory-Huggins interaction parameter taken from the literature and N is the degree of polymerization, and the length scale as determined from the lamellar period of the blend, L_B, on unpatterned surfaces. Figure 2B presents a contour plot of the composition of perfectly aligned ternary blend domains on a chemically striped surface (L_S = L_B = 70 nm). The interfaces between the PS and PMMA domains are found to be sharp for 60 nm ≤ L_S ≤ 80 nm. However, the distribution of homopolymer in the domains varies with L_S (Fig. 2C). In defect-free lamellae with $L_S \geq L_B$, the homopolymers are concentrated primarily at the center of the domains, and an absence of homopolymer is observed near the domain interfaces. The degree of homopolymer segregation to the center of the domains increases with increasing period mismatch, L_S/L_B. Surface patterns with $L_S < L_B$ induce a spatially more uniform homopolymer distribution within the domains. Moreover, the homopolymer within the lamellar domains exhibits a tendency to segregate toward the substrate interface and the free surface because of its lower molecular weight.

A representative image of the ends of line structures is shown in Fig. 2D. Here, perpendicular lamellar domains on underlying chemical patterns terminate at a boundary with lamellae oriented parallel to the substrate assembled on a chemically homogeneous (PS brush) region of the surface. These structures form templates for patterning line segments that terminate at precise locations.

Nested arrays of lines with sharp bends represent model test features for the type of patterns currently used in the free-form logic devices of microprocessors and integrated circuits. Figure 3 shows the directed assembly of nested arrays of lines with different bend geometries. Periods in the linear sections of the chemical surface pattern, L_S, ranged from 65 to 80 nm such that $L_S \sim L_B$ = 70 nm. The linear portions of the blend lamellae were defect-free for all of the examined periods. In addition, the ternary blend formed defect-free lamellae on surface patterns of 45°, 90°, and 135° bends. Perfect assembly was observed on the 45° bends for all examined L_S, but perfect structures were formed on the 90° and 135° bends only for patterns of $L_S \leq$ 70 nm and $L_S \leq$ 65 nm, respectively.

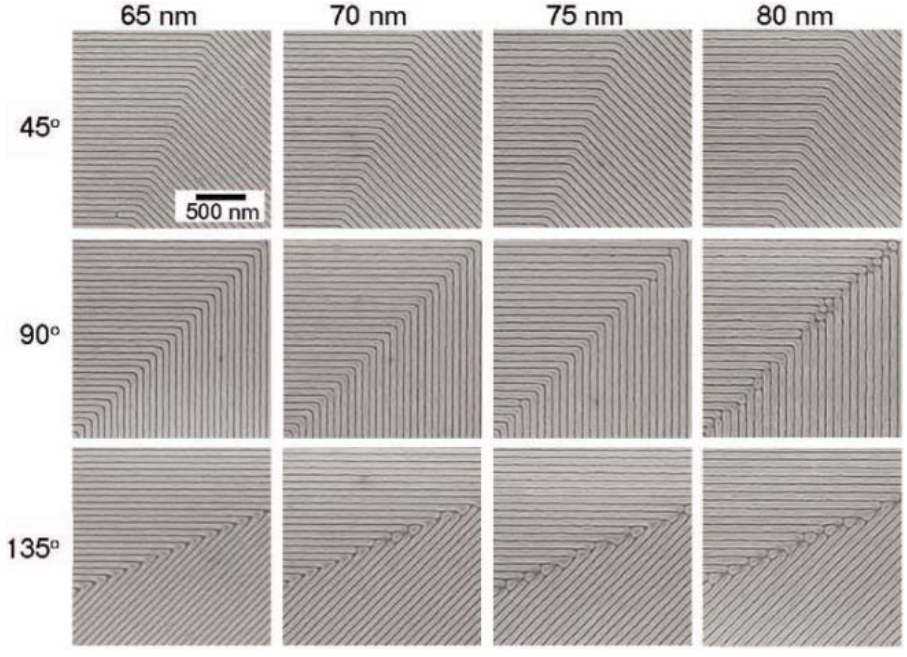

Fig. 3. Top-down SEM images of angled lamellae in a ternary PS-b-PMMA/PS/PMMA blend (L_B = 70 nm). The chemical surface patterns are fabricated with L_S values of 65, 70, 75, and 80 nm, and the lamellar domains of the block copolymer blend are self-assembled and registered around 45°, 90°, and 135° bends. Perfect long-range order was achieved in the linear portions for all L_S, whereas defects arose at the corners of the 90° bends for $L_S \geq$ 75 nm and the 135° bends for $L_S \geq$ 70 nm. The micrographs each depict a 2 μm by 2 μm area.

The differences in domain structure and the formation of defects at the corners of the 45°, 90°, and 135° bends (Fig. 3) depend on the bend angle, θ, and the corner-to-corner lamellar period, L_C (Fig. 4A). Lamellae in the corners of the L_S = 80 nm and 90° bends began to connect with adjacent lamellar domains. For $L_S \geq 70$ nm and 135° bends, the corners were primarily occupied by isolated, round PS domains. These types of defects are similar to those observed on linear chemical surface patterns with $L_S > 80$ nm (Fig. 2A). To a first approximation, one expects the defect-free ordering of lamellae if the corner-to-corner period, $L_C = L_S/\cos(\theta/2)$, is smaller than the largest period [80 nm (compare with Fig. 2A)] of chemical surface stripes on which perfect ordering was observed. For L_S = 70 nm and θ = 90°, however, L_C was 99 nm (≫ 80 nm), but corner defects were not observed experimentally. The underestimation of the stability of defect-free bends by this simple geometric argument suggests that localized redistribution of homopolymer must occur at the bend corners.

SCMF simulations of the directed assembly of ternary blends on surfaces chemically patterned with bend geometries ($L_S = L_B$ = 70 nm) confirm the presence of homopolymer-rich material in the bend corners. Similar to the experimental results, defect-free ordering is observed in the SCMF results for θ values of 45° and 90° (Fig. 4B), and defects arise for the largest bend angle, θ = 135°. The SCMF results in Fig. 4C reveal that the local concentration of homopolymers is greatest in the middle of the corners. For the plots of homopolymer–block copolymer concentration as a function of position (Fig. 4C), the periodicity of the apparent pattern is twice that of the pattern of PS and PMMA domains (Fig. 4B), indicative of alternating regions rich in PS homopolymer and in PMMA homopolymer (both shown in red) separated by block copolymer–rich interfaces (shown in blue). This local redistribution of homopolymer is more pronounced on the 90° bends than on the 45° bends. Figure 4D shows that the concentration profile of homopolymer decays along a line moving away from the corners. The length scale over which homopolymers are recruited to the corners is large, and there is a noticeable depletion of the homopolymers in the linear portions of the domains away from the corners. Although the 45° bends have a nearly bulk homopolymer concentration of ~40 volume % (vol. %) in the linear portions, the 90° bends display a uniformly reduced homopolymer concentration of ~39 vol. % throughout the examined linear region.

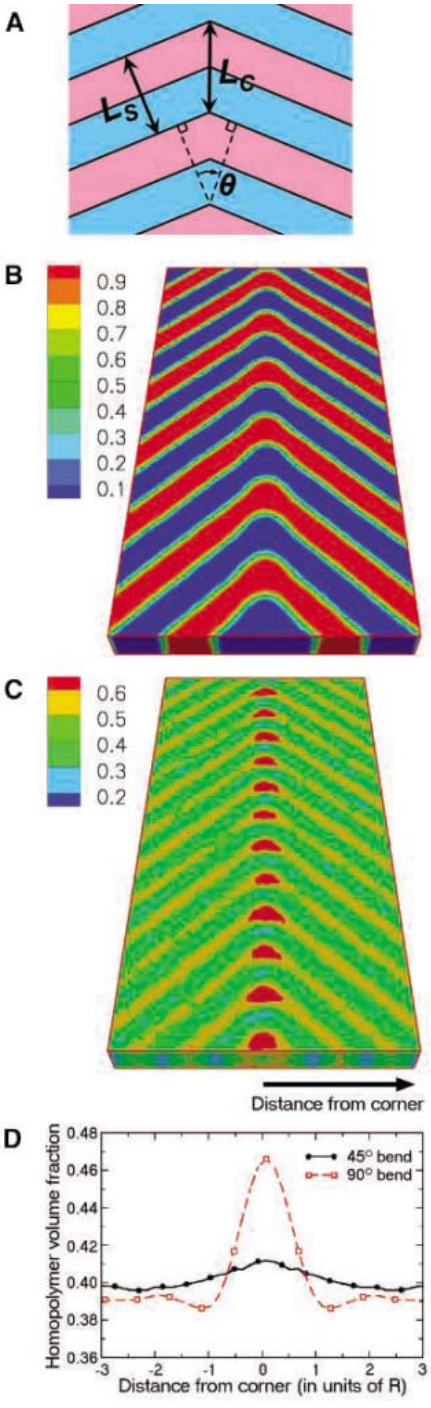

Fig. 4. (**A**) Schematic of the increased lamellar period at the corners of the bends. The linear structures have a lamellar period of L_S, whereas the corner-to-corner lamellar period is L_C such that $L_C > L_S$. Three-dimensional contour plots of (**B**) the PS concentration and (**C**) the total homopolymer concentration obtained from SCMF simulations for $L_S = L_B$ = 70 nm show the segregation of homopolymers to the 90° bend corners (contour levels identical to those in Fig. 2). In (B), the red and blue areas represent PS- and PMMA-rich domains, respectively. In (C), the periodic red areas are enriched alternatively in PS and PMMA homopolymers, whereas the blue stripes represent the domain interfaces that are depleted of homopolymers. The images display the simulated system of area 9.63*R* by 19.26*R* (0.3 μm by 0.6 μm), where $R \approx 31$ nm is the magnitude of the diblock copolymer's end-to-end vector. (**D**) Averaged total homopolymer concentration as a function of the distance from the line of corners for 45° and 90° bends. Upon increasing the bend angle, we observed an increased segregation of the homopolymers to the corners. The enrichment zone is of comparable width to the lamellar spacing and is followed by a depletion zone further away from the corners.

Nested arrays of bent lines are used routinely to benchmark photoresists, but these structures are also reminiscent of metastable defects formed at tilt grain boundaries in the bulk (*31*–*33*). The presence of homopolymer in block copolymer–homopolymer blends mitigates the free energy cost and changes the type of defect observed as a function of tilt angle (*32*, *33*). In contrast to these metastable defects at grain boundaries, the chevron-like structures formed on chemically patterned surfaces are in thermodynamic equilibrium, and structures analogous to omega and T-junction grain boundary defects are not observed at any bend angle. This analysis highlights the relatively large contribution of the polymer-substrate interfacial energy to the overall free energy of sufficiently thin films, which enables the directed assembly of block copolymer domains into structures that do not exist in the bulk [Supporting Online Material (SOM) Text].

The extension of block copolymer lithography to pattern features more complex than simple periodic arrays creates opportunities for widespread use of these nontraditional imaging materials in nanofabrication. Because pattern formation was facilitated through enriched or depleted concentrations of homopolymer depending on the local dimensions of the structures, it may be possible to create relatively high densities of many different types of nonregular shaped structures used in device manufacturing by optimizing blend compositions, polymer chemistry, and interfacial interactions. Our approach retains the essential attributes of current lithographic materials and processes, including pattern perfection and registration, but may be scaled to dimensions of 10 nm or below with precise control over feature size and shape.

References and Notes

1. M. Park, C. Harrison, P. M. Chaikin, R. A. Register, D. H. Adamson, *Science* **276**, 1401 (1997).
2. T. Thurn-Albrecht *et al.*, *Science* **290**, 2126 (2000).
3. W. A. Lopes, H. M. Jaeger, *Nature* **414**, 735 (2001).
4. R. R. Li *et al.*, *Appl. Phys. Lett.* **76**, 1689 (2000).
5. J. Y. Cheng *et al.*, *Adv. Mater.* **13**, 1174 (2001).
6. K. W. Guarini *et al.*, in *International Electron Devices Meeting Technical Digest* (IEEE, Piscataway, NJ, 2003), pp. 541–544.
7. A. Urbas *et al.*, *Adv. Mater.* **12**, 812 (2000).
8. C. T. Black *et al.*, *Appl. Phys. Lett.* **79**, 409 (2001).
9. F. S. Bates, G. H. Fredrickson, *Annu. Rev. Phys. Chem.* **41**, 525 (1990).
10. T. L. Morkved *et al.*, *Science* **273**, 931 (1996).
11. S. O. Kim *et al.*, *Nature* **424**, 411 (2003).
12. L. Rockford *et al.*, *Phys. Rev. Lett.* **82**, 2602 (1999).
13. X. M. Yang, R. D. Peters, P. F. Nealey, H. H. Solak, F. Cerrina, *Macromolecules* **33**, 9575 (2000).
14. R. A. Segalman, H. Yokoyama, E. J. Kramer, *Adv. Mater.* **13**, 1152 (2001).

15. J. Y. Cheng, A. M. Mayes, C. A. Ross, *Nat. Mater.* **3**, 823 (2004).
16. D. Sundrani, S. B. Darling, S. J. Sibener, *Nano. Lett.* **4**, 273 (2004).
17. D. E. Angelescu *et al.*, *Adv. Mater.* **16**, 1736 (2004).
18. D. J. C. Herr, in *Future Fab International*, B. Dustrud, Ed. (Montgomery Research Incorporated, San Francisco, CA, 2005), issue 18, chap. 5.
19. J. Fujita, Y. Ohnishi, Y. Ochiai, S. Matsui, *Appl. Phys. Lett.* **68**, 1297 (1996).
20. K. E. Gonsalves, L. Merhari, H. Wu, Y. Hu, *Adv. Mater.* **13**, 703 (2001).
21. Q. Wang, S. K. Nath, P. F. Nealey, J. J. de Pablo, *J. Chem. Phys.* **112**, 9996 (2000).
22. E. W. Edwards, M. F. Montague, H. H. Solak, C. J. Hawker, P. F. Nealey, *Adv. Mater.* **16**, 1315 (2004).
23. P. Mansky, Y. Liu, E. Huang, T. P. Russell, C. Hawker, *Science* **275**, 1458 (1997).
24. Additional materials and methods information is available on *Science* Online.
25. H. H. Solak *et al.*, *Microelectron. Eng.* **67–68**, 56 (2003).
26. The lamellar spacing of the ternary block copolymer–homopolymer blends can be controlled over a wide range of values by changing the volume fraction of homopolymer. Little is known about their behavior in the form of thin films, but previous studies of phase diagrams and morphology in the bulk (*34*, *35*) provide useful insights.
27. M. Müller, G. D. Smith, *J. Polym. Sci. B* **43**, 934 (2005).
28. G. H. Fredrickson, V. Ganesan, F. Drolet, *Macromolecules* **35**, 16 (2002).
29. M. W. Matsen, F. S. Bates, *Macromolecules* **29**, 1091 (1996).
30. A. Knoll *et al.*, *Nat. Mater.* **3**, 886 (2004).
31. S. P. Gido, E. L. Thomas, *Macromolecules* **27**, 6137 (1994).
32. E. Burgaz, S. P. Gido, *Macromolecules* **33**, 8739 (2000).
33. D. Duque, K. Katsov, M. Schick, *J. Chem. Phys.* **117**, 10315 (2002).
34. F. S. Bates *et al.*, *Phys. Rev. Lett.* **79**, 849 (1997).
35. D. Broseta, G. H. Fredrickson, *J. Chem. Phys.* **93**, 2927 (1990).
36. This research was supported by the Semiconductor Research Corporation (SRC) (2002-MJ-985), NSF through the Nanoscale Science and Engineering Center (DMR-0425880), and the Camille Dreyfus Teacher-Scholar Award. This work made use of the facilities and staff at the UW Center for Nanotechnology, the Synchrotron Radiation Center at UW Madison (NSF DMR-0084402), and the Swiss Light Source at the Paul Scherrer Institute. The authors thank the John von Neumann-Institute for Computing, Jülich, Germany, for central processing unit time on the IBM p690-cluster. M.P.S. acknowledges a research fellowship from the SRC Graduate Fellowship Program.

Supporting Online Material
www.sciencemag.org/cgi/content/full/308/5727/1442/DC1
Materials and Methods
SOM Text
Fig. S1

14 February 2005; accepted 18 April 2005
10.1126/science.1111041

Production of Liquid Alkanes by Aqueous-Phase Processing of Biomass-Derived Carbohydrates

George W. Huber, Juben N. Chheda, Christopher J. Barrett, James A. Dumesic*

Liquid alkanes with the number of carbon atoms ranging from C_7 to C_{15} were selectively produced from biomass-derived carbohydrates by acid-catalyzed dehydration, which was followed by aldol condensation over solid base catalysts to form large organic compounds. These molecules were then converted into alkanes by dehydration/hydrogenation over bifunctional catalysts that contained acid and metal sites in a four-phase reactor, in which the aqueous organic reactant becomes more hydrophobic and a hexadecane alkane stream removes hydrophobic species from the catalyst before they go on further to form coke. These liquid alkanes are of the appropriate molecular weight to be used as transportation fuel components, and they contain 90% of the energy of the carbohydrate and H_2 feeds.

The production of liquid fuels from renewable biomass resources is particularly attractive because gasoline- and diesel-powered hybrid electric vehicles are being developed that have overall energy efficiencies comparable to those of vehicles powered by fuel cells based on current technologies (*1*). Approximately 75% of the dry weight of herbaceous and woody biomass is composed of carbohydrates (*2*). Several processes currently exist to convert carbohydrates to liquid fuels, including the formation of bio-oils by liquefaction or pyrolysis of biomass (*3*), the production of alkanes or methanol by Fischer-Tropsch synthesis from biomass-derived CO:H_2 gas mixtures (*2*), and the conversion of sugars and methanol to aromatic hydrocarbons over zeolite catalysts (*4*, *5*).

However, the conversion of glucose to ethanol is the most widely practiced process (*6*) for producing liquid fuels from biomass, with an overall energy efficiency from corn (the heating value of ethanol divided by the energy required to produce ethanol from corn) equal to about 1.1 without coproduct energy credits (*7*). Approximately 67% of the energy required for ethanol production is consumed in the fermentation/distillation process, of which over half is used to distill ethanol from water (*7*, *8*).

In comparison, the production of alkanes from aqueous carbohydrate solutions would involve the spontaneous separation of the alkanes from water. Accordingly, we estimate that the overall energy efficiency for alkane production from corn would be increased to approximately 2.2, if we assume that this process eliminates the energy-intensive distillation step but still requires all of the remaining energy inputs needed for the production of ethanol from corn (*9*).

We have recently shown how an aqueous solution of sorbitol (the sugar-alcohol of glucose) can be converted to hexane (Eq. 1) with a catalyst containing both acid (e.g., SiO_2-Al_2O_3) and metal (e.g., Pt or Pd) sites to catalyze dehydration and hydrogenation reactions, respectively (*10*). Hydrogen for this reaction can be produced from the aqueous-phase reforming of sorbitol (Eq. 2) in the same reactor or in a separate reactor with a nonprecious metal catalyst (*11*). The net reaction (Eq. 3) is an exothermic process in which approximately 1.5 mol of sorbitol produce 1 mol of hexane.

$$C_6O_6H_{14} + 6H_2 \rightarrow C_6H_{14} + 6H_2O \quad (1)$$

$$C_6O_6H_{14} + 6H_2O \rightarrow 6CO_2 + 13H_2 \quad (2)$$

$$\frac{19}{13}C_6O_6H_{14} \rightarrow C_6H_{14} + \frac{36}{13}CO_2 + \frac{42}{13}H_2O \quad (3)$$

Alkanes produced in the aqueous-phase dehydration/hydrogenation (APD/H) of carbohydrates would provide a renewable source of transportation fuel to complement the rapidly growing production of biodiesel from vegetable oils and animal fats (*12*). Unfortunately, the high volatility of hexane makes this compound of low value as a fuel additive (*13*). Thus, the production of high-quality liquid fuels from carbohydrates requires the formation of larger alkanes, and this production can be accomplished by first linking carbohydrate-derived moieties through the formation of C-C bonds before APD/H processing. Here we present a catalytic process for the conversion of biomass-derived carbohydrates to liquid alkanes in the higher mass ranges (from C_7 to C_{15}) that can be used as sulfur-free fuel components. We note that C-O-C linkages (as found in disaccharides) are broken under APD/H reaction conditions. The formation of C-C bonds between carbohydrate-derived moieties can be carried out by a variety of chemical routes, and we have chosen a dehydration step (acid-catalyzed) followed by an aldol-condensation (base-catalyzed) step (Fig. 1).

Our current APD/H process cannot be used to produce alkanes from large water-soluble organic compounds because extensive amounts of coke form on the catalyst surface (between

Department of Chemical and Biological Engineering, University of Wisconsin at Madison, Madison, WI 53706, USA.

*To whom correspondence should be addressed. E-mail: dumesic@engr.wisc.edu

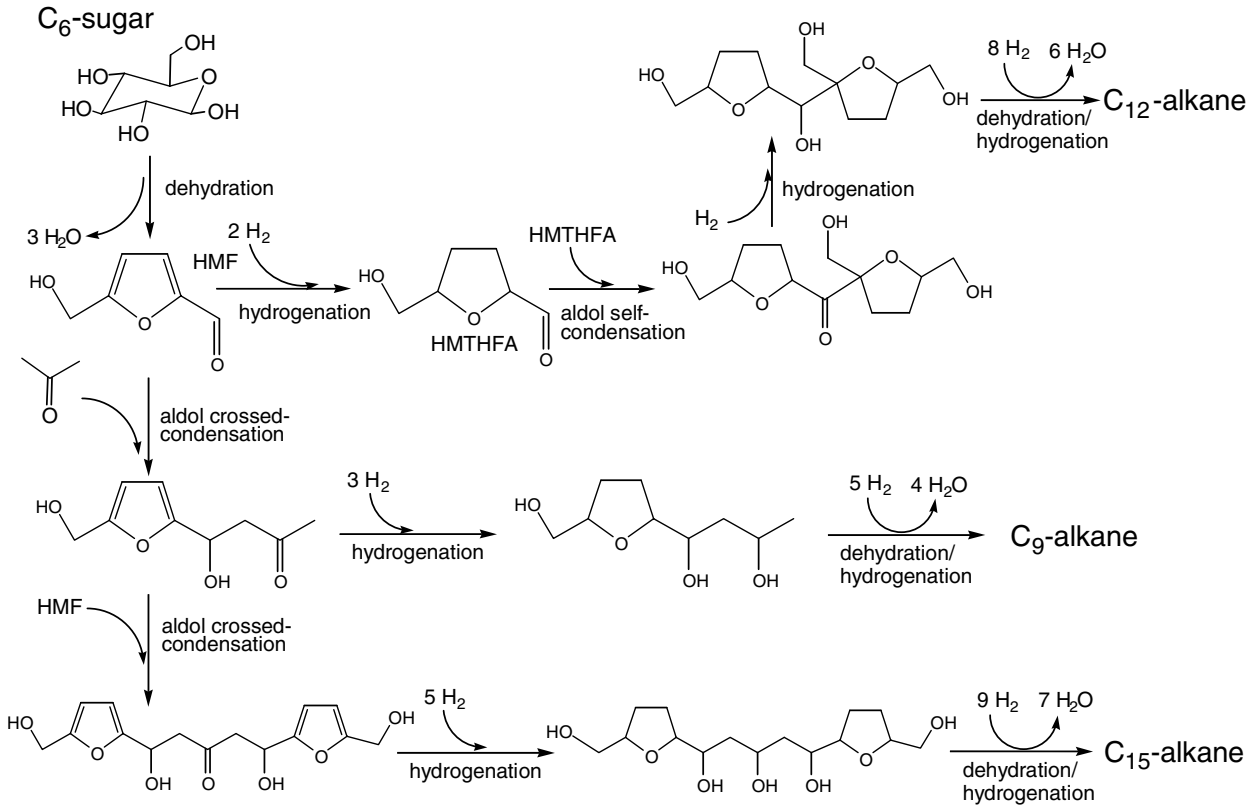

Fig. 1. Reaction pathways for the conversion of biomass-derived glucose into liquid alkanes.

20 and 50% of the reactant converts to coke). Accordingly, we have modified our reactor system to carry out dehydration/hydrogenation reactions in a four-phase reactor system consisting of (i) an aqueous inlet stream, which contains the large water-soluble organic reactant; (ii) a hexadecane alkane inlet stream; (iii) an H_2 inlet gas stream; and (iv) a solid catalyst (Pt/SiO_2-Al_2O_3). As dehydration/hydrogenation takes place, the aqueous organic reactant becomes more hydrophobic, and the hexadecane alkane stream removes hydrophobic species from the catalyst before they go on further to form coke. In an industrial setting, the alkanes produced from the reaction would be recycled to the reactor and used for the alkane feed. Reaction kinetics experiments conducted with pure water as the aqueous feed showed that only a small amount of hexadecane was converted to lighter alkanes in the four-phase dehydration/hydrogenation (4-PD/H) reactor system (0.007 $\mu mol\ min^{-1}\ g_{catalyst}{}^{-1}$), and this low reactivity was subtracted from all of our subsequent experimental data.

To benchmark the performance of our 4-PD/H reactor, we studied the conversion of a 5 weight percent (wt %) aqueous solution of sorbitol for different feed rates of the hexadecane alkane stream. Results for these measurements showed that increasing the hexadecane flow rate decreased the conversion of sorbitol (table S3, entries S1 to S3). No major differences were observed in the selectivity of the reaction when the hexadecane-to-water flow rate ratio was increased (table S4, entries S1 to S3). Here we report only data collected from the 4-PD/H reactor at high conversion (>70%), so that alkanes are the primary product. At these high conversions and slow liquid flow rates, it is probable that transport limitations occur that decrease the reaction rates (*14*).

Furoin [purchased from Aldrich, St. Louis, Missouri, and prepared from furfural by the Pinnacol coupling reaction (*15*)], furfural-acetone (1:1) (purchased from Aldrich and

Table 1. Selected values for conversion and process conditions for 4-PD/H of biomass-derived molecules. The full table is available in (*16*). All 4-PD/H reactions were carried out at 523 to 538 K, 52 to 60 bars, and H_2 gas hourly space velocities (cm^3 of H_2/cm^3 of catalyst) of 1000 to 3000 $hour^{-1}$. A 4 wt % Pt/SiO_2-Al_2O_3 catalyst was used for these reactions. Each experimental point was collected after 20 hours on stream. Condensed feeds were prepared by aldol condensation at room temperature using Mg-Al–oxide and NaOH catalysts. SC, self-condensed; Fur, furfural; Ace, acetone; org, organic. Numbers listed in parentheses indicate the molar ratio of feeds. All feeds were hydrogenated in a Parr reactor with a Pd/Al_2O_3 catalyst before conversion in the 4-PD/H reactor. Entries 1 to 3 and 5 to 7 were hydrogenated in methanol or a methanol/water mixture, with all other feeds being hydrogenated in H_2O. wt (%) refers to wt % organics in aqueous feed solution. WHSV is weight hourly space velocity, which is the mass of aqueous feed solution per mass of catalyst per hour. Org/Aq is the organic (hexadecane)–to–aqueous volumetric feed ratio.

Entry	Feed	wt (%)	WHSV ($hour^{-1}$)	Org/Aq	% Carbon in phase		
					Org	Gas	Aq
1	Furoin	2.0	0.26	3.0	69.2	18.5	2.3
2	Fur:Ace (1:1)-1	1.9	0.26	3.0	100.0	6.3	1.6
3	Fur:Ace (1:1) org*	5.0	0.51	∞	73.2	7.8	NA
4	Fur:Ace (1:1)-3	12.5	0.29	3.0	91.2	4.1	0.7
5	Fur:Ace (2:1)	1.0	0.29	3.0	79.0	2.4	0.8
6	HMF:Ace (1:1)-1	1.8	0.25	3.0	66.1	15.7	1.5
7	HMF:Ace (1:1)-2†	1.9	0.26	3.0	69.5	7.7	0.9
8	HMF:Ace (1:1)-3	1.8	0.29	3.0	53.3	31.1	2.3
9	HMF:Ace (1:10)	9.5	0.35	0.7	77.2	10.3	20.0
10	HMF:Fur:Ace (1:1:2)	1.9	0.29	3.0	48.5	27.8	3.1
11	SC THF3A	5.0	0.35	0.7	53.2	44.1	4.2
12	SC THF2A	3.9	0.35	0.7	47.9	20.8	13.0

*Fur:Ace (1:1) org was added to the hexadecane feed, and no aqueous flow was used for this feed. †This feed was condensed with twice the amount of Mg-Al–oxide than was the feed above it (entry 6).

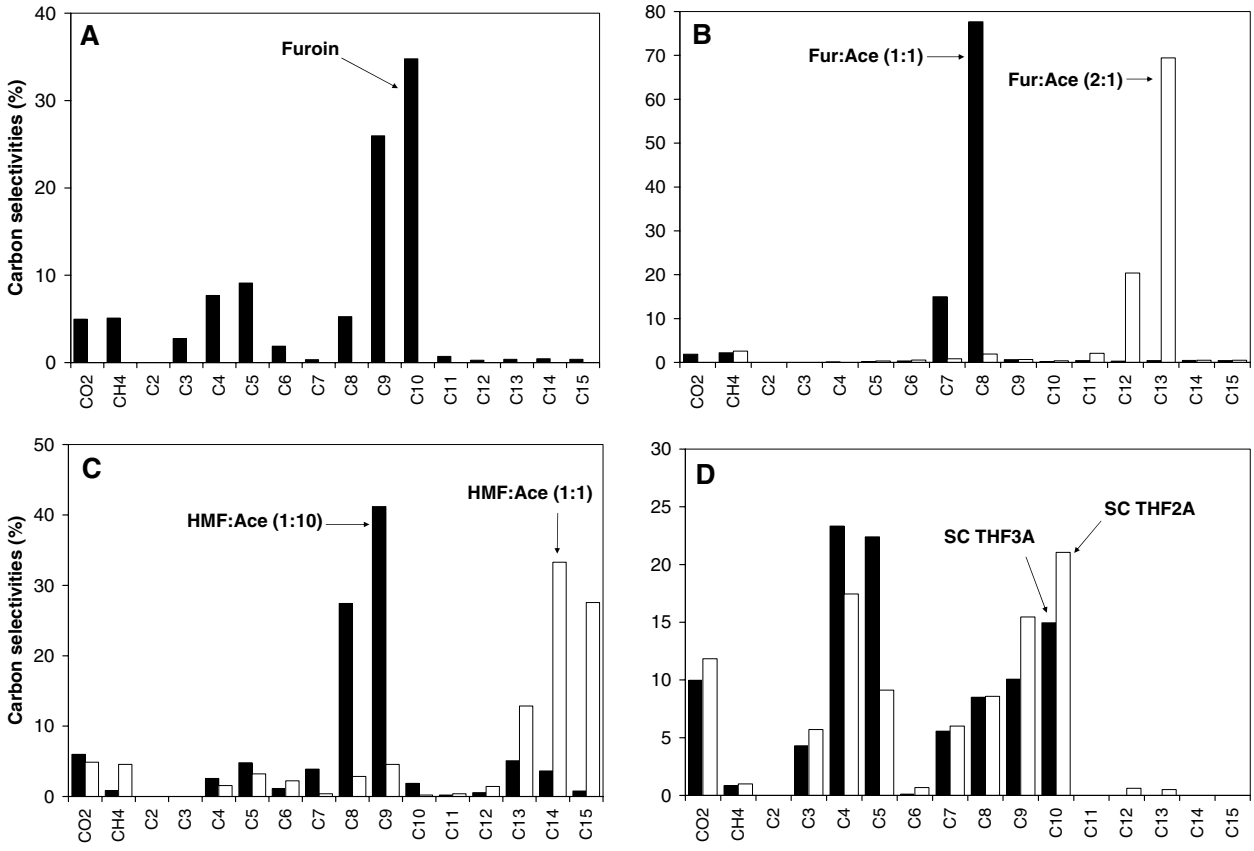

Fig. 2. Carbon selectivities from 4-PD/H processing of various condensed feeds. See Table 1 for the feed key. (**A**) Furoin (Table 1, entry 1). (**B**) Furfural (Fur):acetone (Ace) (1:1)-1 (entry 2), black; Fur:Ace (2:1) (entry 5), white. (**C**) HMF:Ace (1:10) (entry 9), black; HMF:Ace (1:1)-2 (entry 7), white. (**D**) Self-condensed (SC) THF3A (entry 11), black; SC THF2A (entry 12), white.

prepared by aldol condensation of furfural and acetone), and furfural-acetone (2:1) [prepared by aldol condensation of furfural-acetone with furfural and NaOH (*16*)] were hydrogenated in methanol in a stainless-steel batch reactor (Parr Instruments, Moline, Illinois, at 55 bars of H_2 pressure and 393 K) with a Pd/Al_2O_3 catalyst. This hydrogenation step was carried out to minimize possible coking reactions that may take place from unsaturated molecules on the Pt/SiO_2-Al_2O_3 catalyst in the 4-PD/H reactor and to increase the solubility of the condensed products in water. These hydrogenated compounds were then dissolved in water and converted to alkanes in the 4-PD/H reactor. The main products of the hydrogenated furoin were C_9 and C_{10} alkanes (Fig. 2A).

The hydrogenated furfural-acetone (1:1) was added to both water and hexadecane, and both feeds produced mainly C_7 and C_8 alkanes in the 4-PD/H process (Tables 1 and 2, entries 2 and 3). Hydrogenated furfural-acetone (2:1) produced primarily C_{11} to C_{13} alkanes from the 4-PD/H reactor (Fig. 2B).

Furfural-acetone (1:1) could also be hydrogenated in water without using methanol as a solvent (Tables 1 and 2, entry 4). In this step, we added the furfural-acetone (1:1) adduct, Pd/Al_2O_3, and water into a Parr reactor, which was subsequently pressurized with H_2 (at 55 bars) and heated to 393 K. As shown in entry 4 of Tables 1 and 2, we could prepare an aqueous solution of 12.5 wt % hydrogenated furfural-acetone (1:1), and this feed produced primarily C_7 and C_8 alkanes in the 4-PD/H reactor. The results from these experiments indicate that our process for producing liquid alkanes from biomass-derived resources does not require the use of alcohol solvents, and it is not limited to dilute aqueous feeds (*17*).

Aldol-condensation reactions are particularly relevant for the production of large organic compounds from biomass, because various species containing carbonyl groups can be formed from carbohydrates, including furfurals, dihydroxyacetone, and acetone. For example, glucose and xylose do not undergo aldol-condensation reactions because the carbonyl group undergoes intramolecular reactions to form ring structures (*18*), but dehydrating glucose and xylose yields 5-hydroxymethylfurfural (HMF) and furfural, respectively, with mineral or solid acid catalysts (Fig. 1) (*2*, *19*–*22*). Both HMF and furfural have an aldehyde group, and although they cannot undergo self-condensation because they do not have an α-H atom, they can condense with other molecules that can form carbanion species such as acetone, dihydroxyacetone, or glyceraldehyde (Fig. 1) (*23*). Acetone can be produced from the fermentation of glucose (*2*), and dihydroxyacetone and glyceraldehyde can be produced from the retro–aldol condensation of glucose (*18*, *24*).

Crossed aldol condensation of HMF with acetone was carried out with HMF:acetone molar ratios of 1:1 and 1:10 by using a mixed Mg-Al–oxide catalyst at room temperature (Tables 1 and 2, entries 6 to 9). The Mg-Al–oxide catalyst was prepared by coprecipitation (*16*) similar to the method reported elsewhere (*25*–*27*). The condensed molecules were then hydrogenated in a batch reactor in a methanol/H_2O solvent for the HMF:acetone (1:1)-1 and (1:1)-2 feeds, followed by the conversion to alkanes in the 4-PD/H reactor. All other feeds discussed in this paper were batch hydrogenated in H_2O. As shown in Fig. 2C, the condensed HMF:acetone feeds produced mainly C_8 to C_{15} alkanes in the 4-PD/H reactor, depending on the HMF:acetone ratio used in the aldol-condensation step. When the HMF:acetone ratio decreases, the alkane distribution shifts to lighter alkanes (Fig. 2C). The selectivity can also be shifted to heavier alkanes by increasing the extent of conversion for the aldol condensation step of HMF:acetone (Table 2, entries 6 and 7).

To improve the potential practical utility of our process, we studied whether hydrogenation of the HMF:acetone adduct could be accomplished without using methanol as a

Table 2. Selected values for alkane and CO_2 selectivities from 4-PD/H of biomass-derived molecules. The full table is available in (*16*). Table 1 contains relevant process conditions, the feed key, and the conversion data. Selectivity is defined as (moles of product × number of carbon atoms in product)/(total moles of carbon atoms in products) × 100. The selectivity takes into account only the products in the organic and gas phases. Alkane products are mostly straight chain in form, except for the SC THF3A and SC THF2A feeds. At lower conversions, small amounts of alcohols (<10% of total products) are also observed in the organic phase.

Entry	Feed	Alkane and CO_2 selectivities (%)															
		CO_2	C_1	C_2	C_3	C_4	C_5	C_6	C_7	C_8	C_9	C_{10}	C_{11}	C_{12}	C_{13}	C_{14}	C_{15}
1	Furoin	5.2	5.2	0.0	2.8	8.0	9.2	1.8	0.3	5.4	26.2	34.0	0.7	0.3	0.3	0.4	0.2
2	Fur:Ace (1:1)-1	1.8	2.2	0.0	0.0	0.1	0.2	0.3	15.0	77.7	0.6	0.2	0.4	0.3	0.4	0.4	0.4
3	Fur:Ace (1:1) org	0.0	4.7	0.2	1.7	1.8	2.0	1.9	4.5	71.4	2.4	2.2	2.2	2.1	2.4	0.6	0.0
4	Fur:Ace (1:1) -3	1.7	0.4	0.0	0.1	0.1	0.1	0.2	17.1	64.4	7.4	5.8	2.5	0.1	0.1	0.1	0.0
5	Fur:Ace (2:1)	0.0	3.0	0.0	0.0	0.0	0.4	0.7	1.0	2.1	0.8	0.5	2.1	19.7	68.6	0.6	0.5
6	HMF:Ace (1:1)-1*	6.8	3.3	0.0	0.0	6.0	14.6	9.3	0.4	6.8	9.5	0.0	0.0	0.7	8.5	19.5	14.5
7	HMF:Ace (1:1)-2*	5.0	4.0	0.0	0.0	1.5	3.2	2.2	0.4	2.9	4.6	0.2	0.4	1.5	13.5	32.9	27.6
8	HMF:Ace (1:1)-3	5.7	3.5	0.0	23.5	3.8	10.0	7.0	0.7	5.9	6.9	0.1	0.3	1.0	6.2	14.5	10.9
9	HMF:Ace (1:10)†	6.0	0.9	0.0	0.0	2.6	4.8	1.1	3.9	27.4	41.2	1.9	0.2	0.5	5.1	3.6	0.8
10	HMF:Fur:Ace (1:1:2)	4.0	3.0	0.0	25.3	3.8	7.2	3.3	2.5	10.2	5.6	0.0	1.0	4.8	14.3	10.8	4.4
11	SC THF3A‡	9.4	0.7	0.0	4.2	23.4	25.1	0.1	3.4	6.7	11.6	14.3	0.1	0.9	0.0	0.0	0.0
12	SC THF2A§	11.4	1.3	0.0	5.1	15.1	9.9	0.5	5.2	13.0	17.7	19.4	0.3	0.9	0.3	0.0	0.0

*C_3 selectivity is zero because acetone was removed during the separation of hydrogenated products from methanol-water solution. †Propane is not included in the alkane selectivity calculation for this feed. ‡Liquid alkanes produced in this feed were mostly branched. The C_{10} alkane was 3-methyl-5-dimethyl-heptane. §Liquid alkanes produced in this feed were mostly branched. The C_{10} alkane was 4-methylnonane.

solvent. For this case, we first carried out the aldol condensation of HMF:acetone (1:1) in water over the Mg-Al–oxide catalyst, and we then added Pd/Al_2O_3 to the reaction slurry, followed by treatment with H_2 (at 55 bars) at 393 K in the Parr reactor. Similar to hydrogenation of furfural:acetone in water, we found that the hydrogenation of the HMF:acetone adduct increases its solubility in water, and the aqueous solution from this hydrogenation step produced significant amounts of C_{14} and C_{15} alkanes from the 4-PD/H reactor (Table 2, entry 8). The results in Tables 1 and 2 also show that mixtures of HMF and furfural (Tables 1 and 2, entry 10) can be condensed with acetone to form alkanes ranging from C_7 to C_{15}. Unlike the production of ethanol by fermentation, cellulose and hemicellulose need not be separated for the effective production of liquid alkanes by 4-PD/H processing.

Results for crossed aldol condensation of furfural and HMF with dihydroxyacetone and glyceraldehyde are summarized in entries S15 to S20 of tables S3 and S4. These condensation reactions over a Mg-Al–oxide catalyst showed a large disappearance of furfural and HMF based on high-performance liquid chromatography (table S1); however, as shown in table S4, fewer than 30% of the alkane products are heavier than the C_5 and C_6 reactants (for reactions of furfural and HMF, respectively). Condensing furfural with hydroxyacetone gave an alkane distribution similar to that produced from the condensation of furfural with dihydroxyacetone (table S4, entry S18). Thus, although it is possible to make heavier liquid alkanes by crossed aldol condensation of furfural and HMF with dihydroxyacetone, hydroxyacetone, or glyceraldehydes, the selectivities of these processes will need to be improved.

Another route to make large water-soluble organic compounds is to selectively hydrogenate the C=C double bonds of HMF and furfural, producing 5-hydroxymethyl-tetrahydrofurfural (HMTHFA) and tetrahydrofuran-2 carboxyaldehyde (THF2A), respectively. These species can form carbanion species and undergo self-aldol-condensation reactions (Fig. 1). The results in Fig. 2D show that the self-aldol condensation of tetrahydrofuran-3 carboxyaldehyde (THF3A, purchased from Aldrich) and THF2A produced liquid hydrocarbons ranging from C_8 to C_{10} from the 4-PD/H reactor. THF2A was produced by the dehydrogenation of tetrahydrofurfuryl alcohol in the gas phase over a Cu/SiO_2 catalyst (*16*).

The conversion of carbohydrates to liquid alkanes requires the storage of a considerable amount of hydrogen in the fuel (i.e., essentially one molecule of H_2 is used to convert each carbon atom in the carbohydrate reactant to an alkane moiety). The liquid alkanes retain 90% of the energy content of the carbohydrate and H_2 reactants. Thus, the carbon in the carbohydrates serves as an effective energy carrier for transportation vehicles, which is analogous to the role of carbohydrates as energy storage compounds for living organisms. We have demonstrated the feasibility of producing liquid alkanes from biomass-derived compounds, but future research is needed to determine how to minimize undesired coking reactions and to develop new catalysts that exhibit long-term stability under aqueous-phase reaction conditions [see (*16*) for a brief discussion of the stability of solid base catalysts under our reaction conditions].

References and Notes

1. M. A. Weiss, J. B. Heywood, A. Schafer, V. K. Natarajan, *Comparative Assessment of Fuel Cell Cars* (publication no. LFEE 2003-001 RP, MIT Laboratory for Energy and the Environment, 2003; available at http://lfee.mit.edu/public/LFEE_2003-001_RP.pdf).
2. D. L. Klass, *Biomass for Renewable Energy, Fuels and Chemicals* (Academic Press, San Diego, CA, 1998).
3. D. C. Elliott *et al.*, *Energy Fuels* **5**, 399 (1991).
4. N. Y. Chen, J. T. F. Degnan, L. R. Koenig, *Chemtech* **16**, 506 (1986).
5. P. B. Weisz, W. O. Haag, P. G. Rodewald, *Science* **206**, 57 (1979).
6. R. Katzen, G. T. Tsao, *Adv. Biochem. Eng. Biotechnol.* **70**, 77 (2000).
7. H. Shapouri, J. A. Duffield, M. Wang, *The Energy Balance of Corn Ethanol: An Update* (report no. 814, Office of the Chief Economist, U.S. Department of Agriculture, 2002; available at www.usda.gov/oce/oepnu/aer-814.pdf).
8. R. Katzen *et al.*, in *Fuels from Biomass and Wastes*, D. L. Klass, G. H. Emert, Eds. (Ann Arbor Science, Ann Arbor, MI, 1981), pp. 393–402.
9. In these calculations, we used values of the energy required for corn production, corn transportation, ethanol conversion, and ethanol transportation reported by Shapouri *et al.* (*7*); we used yields for sugar and ethanol production reported by Klass (*2*); and we assumed that sugars were converted to alkanes as given by a stoichiometry analogous to Eq. 3. (*16*).
10. G. W. Huber, R. D. Cortright, J. A. Dumesic, *Angew. Chem. Int. Ed. Engl.* **43**, 1549 (2004).
11. G. W. Huber, J. W. Shabaker, J. A. Dumesic, *Science* **300**, 2075 (2003).
12. F. Ma, M. A. Hanna, *Bioresour. Technol.* **70**, 1 (1999).
13. K. Owen, T. Coley, *Automotive Fuels Handbook* (Society of Automotive Engineers, Warrendale, PA, 1990).
14. J. W. Shabaker, R. R. Davda, G. W. Huber, R. D. Cortright, J. A. Dumesic, *J. Catal.* **215**, 344 (2003).
15. W. C. Zhang, C. J. Li, *J. Chem. Soc., Perkin Trans.* **1**, 3131 (1998).
16. Materials and methods are available as supporting material on *Science* Online.
17. Whereas the solubility of furfural-acetone (1:1) is low in water, we have determined that hydrogenation of the furan ring in the adduct increases the solubility in water to values higher than 35 wt %.
18. P. Collins, R. Ferrier, *Monosaccharides* (Wiley, West Sussex, UK, 1995).
19. C. Moreau, R. Durand, D. Peyron, J. Duhamet, P. Rivalier, *Ind. Crop. Prod.* **7**, 95 (1998).
20. C. Moreau *et al.*, *Appl. Catal. A* **145**, 211 (1996).
21. K. Lourvanij, G. L. Rorrer, *Ind. Eng. Chem. Res.* **32**, 11 (1993).
22. J. Lewkowski, *ARKIVOC* **2001**, 17 (2001), available at www.arkat-usa.org/ark/journal/2001/I01_General/403/0113_index.asp.
23. Aqueous-phase aldol condensation reactions have previously been carried out with glyceraldehyde, dihydroxyacetone, formaldehyde, and butyraldehyde using both homogeneous and heterogeneous base catalysts (*24, 28*). Cross-condensation of furfural with acetone has been conducted using amino-functionalized mesoporous base catalysts (*29*). Mixed Mg-Al–oxides have previously been used as solid base catalysts for liquid-phase aldol-condensation reactions (*25–27*).
24. C. D. Gutsche *et al.*, *J. Am. Chem. Soc.* **89**, 1235 (1967).
25. M. Sasaki, K. Goto, K. Tajima, T. Adschiri, K. Arai, *Green Chem.* **4**, 285 (2002).
26. M. J. Climent, A. Corma, S. Iborra, K. Epping, A. Velty, *J. Catal.* **225**, 316 (2004).

27. K. K. Rao, M. Gravelle, J. S. Valente, F. Figueras, *J. Catal.* **173**, 115 (1998).
28. V. Serr-Holm *et al.*, *Appl. Catal. A* **198**, 207 (2000).
29. B. M. Choudary *et al.*, *J. Mol. Catal. A* **142**, 361 (1999).
30. Supported by the U.S. Department of Energy Office of Basic Energy Sciences, NSF Chemical and Transport Systems Division of the Directorate for Engineering, and Conoco-Phillips. We thank M. Mavrikakis and R. Cortright for ongoing discussions, Y.-Y. Luk for help with aldol-condensation reactions, and E. L. Sughrue (Conoco-Phillips) and D. E. Resasco (University of Oklahoma) for helpful discussions about diesel fuel.

Supporting Online Material
www.sciencemag.org/cgi/content/full/308/5727/1446/DC1
Materials and Methods
Fig. S1
Tables S1 to S4
References

16 February 2005; accepted 15 April 2005
10.1126/science.1111166

Kinetic Evidence for Five-Coordination in $AlOH(aq)^{2+}$ Ion

Thomas W. Swaddle,[1] Jörgen Rosenqvist,[2] Ping Yu,[3] Eric Bylaska,[6] Brian L. Phillips,[7] William H. Casey[2,4,5]*

Trivalent aluminum ions are important in natural bodies of water, but the structure of their coordination shell is a complex unsolved problem. In strong acid (pH < 3.0), Al^{III} exists almost entirely as the octahedral $Al(H_2O)_6^{3+}$ ion, whereas in basic conditions (pH > 7), a tetrahedral $Al(OH)_4^-$ structure prevails. In the biochemically and geochemically critical pH range of 4.3 to 7.0, the ion structures are less clear. Other hydrolytic species, such as $AlOH(aq)^{2+}$, exist and are traditionally assumed to be hexacoordinate. We show, however, that the kinetics of proton and water exchange on aqueous Al^{III}, coupled with Car-Parrinello simulations, support a five-coordinate $Al(H_2O)_4OH^{2+}$ ion as the predominant form of $AlOH(aq)^{2+}$ under ambient conditions. This result contrasts Al^{III} with other trivalent metal aqua ions, for which there is no evidence for stable pentacoordinate hydrolysis products.

Aluminum is the third most abundant element in Earth's crust, after oxygen and silicon, and its chemistry in water is central to geochemistry, environmental science, and medicine (*1*, *2*). In particular, the speciation (*3*) and ligand substitution kinetics (*4*) of the Al^{III} ions in the pH range 3 to 7 govern its toxicity toward plants, fish, and humans, yet the hydrolytic chemistry of Al^{III} remains poorly understood. The structures of the octahedral ion $Al(H_2O)_6^{3+}$, which dominates at pH < 3.0, and the tetrahedral aluminate ion $Al(OH)_4^-$, which dominates at pH > 7, are well established (*5*). The first hydrolysis product, $Al(H_2O)_{n-1}OH^{2+}$, where n is the coordination number, becomes important at 3.0 < pH < 4.3. It coexists with $Al(H_2O)_{n-2}(OH)_2^+$ above pH 4.3 and with $Al(OH)_4^-$ at 5.2 < pH < 6.7 (*3*, *5*–*7*). At high Al^{III} concentrations (> 0.05 mol L^{-1}), oligomers such as $(H_2O)_4Al(OH)_2Al(OH_2)_4^{4+}$ and the Keggin ion $AlO_4(Al(OH)_2)_{12}(H_2O)_{12}^{7+}$ (which contains one four-coordinate and twelve six-coordinate Al^{III} atoms) appear around pH 5 (*5*, *6*, *8*, *9*). Thus, not only is the speciation of $Al^{III}(aq)$ complicated in the pH range 4.3 to 7.0, rendering quantitative studies difficult, but there is a shift from dominant six- to four-coordination over this range.

It is generally assumed (*5*, *6*) by analogy with several other trivalent metals but without experimental justification that octahedral coordination is retained in $Al(H_2O)_{n-1}OH^{2+}$ and most other hydrolytic species. Martin (*3*, *7*) pointed out that the remarkable closeness of the acid dissociation constants K_a of $Al(H_2O)_6^{3+}$, $Al(H_2O)_{n-1}OH^{2+}$, $Al(H_2O)_{n-2}(OH)_2^+$, and $Al(H_2O)_{n-3}(OH)_3$ ($pK_a = -\log K_a$ = 5.5, 5.8, 6.0, and 6.2, respectively, in dilute solution) could be explained by a progressive reduction of coordination number n from 6 toward 4 across this sequence: Decreasing n shortens Al-O bond lengths, increasing the polarization and hence the acidity of the remaining aqua ligands.

We report high-pressure ^{17}O-nuclear magnetic resonance (NMR) data that support Martin's basic hypothesis. We have studied the hydrogen-ion dependence of the rate of exchange of water ligands bound to the $Al(H_2O)_6^{3+}$ with free solvent, and our results are consistent with coupling of proton and water dissociation from $Al(H_2O)_6^{3+}$ via a five-coordinate $Al(H_2O)_4OH^{2+}$ ion.

$$Al(H_2O)_6^{3+} \rightleftharpoons Al(H_2O)_4OH^{2+} + H^+ + H_2O \quad (1)$$

The key data are volumes of activation $\Delta V_M^{\ddagger}$ [$-RT(\partial \ln k_M/\partial P)_T$, where k_M is the corresponding rate constant for water exchange on aqueous metal ions $M(aq)^{z+}$], because they are considered to be diagnostic of the reaction mechanism (*10*). These $\Delta V_M^{\ddagger}$ parameters are extracted from the pressure dependence of the measured rate constants. Formation of an intermediate in which the coordination number n is reduced is termed a dissociative (**D**) mechanism, for which $0 \ll \Delta V_M^{\ddagger} \leq +14$ cm^3 mol^{-1}, whereas formation of an intermediate of expanded n is called an associative (**A**) mechanism and shows $0 \gg \Delta V_M^{\ddagger} \geq -14$ cm^3 mol^{-1} (*11*). Cases in which the entry and departure of water molecules are coupled (no long-lived intermediates) are called interchange mechanisms: dissociative interchange ($\mathbf{I_d}$) for which, operationally, $\Delta V_M^{\ddagger}$ is positive, and associative interchange ($\mathbf{I_a}$), for which it is negative. For the acid-independent water-exchange pathway on $Al(H_2O)_6^{3+}$ (i.e., for the direct exchange of H_2O with $Al(H_2O)_6^{3+}$), $\Delta V_{Al}^{\ddagger}$ is +5.7 cm^3 mol^{-1} (*12*), indicating a dissociatively activated mechanism, in agreement with the results of ab initio calculations (*13*). The $\Delta V^{\ddagger}$ value and mechanism for the first hydrolyzed complex, $AlOH(aq)^{2+}$, is reported here.

The standard model (*10*) for water exchange via conjugate-base species $[MOH(aq)^{(z-1)+}]$ holds that proton exchange is much more rapid than oxygen exchange, and that a preequilibrium state is established with retention of the first coordination sphere, characterized by an equilibrium constant, K_a, and an equilibrium pressure dependence described by a volume of reaction, $\Delta V_a^0 = -RT(\partial \ln K_a/\partial P)_T$:

$$M(H_2O)_n^{z+} \overset{K_a,\ \Delta V_a^0}{\rightleftharpoons} M(H_2O)_{n-1}OH^{(z-1)+} + H^+ \quad (2)$$

The rate-determining step is then water exchange on the $M(H_2O)_{n-1}OH^{(z-1)+}$ ion (rate constant k_{MOH}). Experiments support this mechanism for a wide range of metal ions (*5*).

From ^{17}O-NMR data in aqueous $AlCl_3$, we obtained rate constants k_{obs} for water exchange on aluminum species (Fig. 1A), and they vary inversely with $[H^+]$, as expected [e.g., (*14*)].

$$k_{obs} = (k_1 + k_2/[H^+]) \times X_1 \quad (3)$$

X_1 is the mole fraction of Al^{III} present as $Al(H_2O)_6^{3+}$ (the calculated pressure depen-

[1]Department of Chemistry, University of Calgary, Calgary, AB T2N 1N4, Canada. [2]Department of Land, Air, and Water Resources, [3]Nuclear Magnetic Resonance Facility, [4]Department of Geology, [5]Department of Chemistry, University of California, Davis, CA 95616, USA. [6]Fundamental Sciences, Pacific Northwest Laboratory, P.O. Box 999, Richland, WA 99352, USA. [7]Department of Geosciences, State University of New York, Stony Brook, NY 11794, USA.

*To whom correspondence should be addressed. E-mail: whcasey@ucdavis.edu

dence of which is negligible, regardless of the assumed value of ΔV_a^0). The very small contribution k_1 is k_{Al}, the rate coefficient for competing direct exchange at $Al(H_2O)_6^{3+}$, without the intermediacy of the conjugate base. If the standard model applies, then $k_2 = k_{AlOH} \times K_a$ (ignoring activity coefficients), and the corresponding $\Delta V_2^{\ddagger} = -RT(\partial \ln k_2/\partial P)_T = \Delta V_{AlOH}^{\ddagger} + \Delta V_a^0$. In other words, according to the standard model, the overall activation volume for the conjugate-base mechanism is the sum of the volume change to form the base, $Al(OH)(H_2O)_{n-1}^{2+}$ (ΔV_a^0) and the activation volume for water exchange at the base ($\Delta V_{AlOH}^{\ddagger}$). Our data at both 333 K and 348 K (Fig. 1B) afford a value for $\Delta V_2^{\ddagger}$ of –0.7 cm^3 mol^{-1} (Fig. 1B). Thus

$$\Delta V_{AlOH}^{\ddagger} = -0.7 - \Delta V_a^0 \text{ cm}^3 \text{ mol}^{-1} \quad (4)$$

Observation of $\Delta V_2^{\ddagger} \sim 0$ is anomalous. There are two opposed explanations for this low value that hinge upon the value assigned to ΔV_a^0. For $Al(H_2O)_6^{3+}$, ΔV_a^0 has not been measured (*15*), but the simple yet effective empirical Eq. 5 (*11*) permits calculation of the absolute volumes V^0_{abs} of aqueous metal ions $M(aq)^{z+}$ at 298 K

$$V^0_{abs}/\text{cm}^3 \text{ mol}^{-1} = 2.523 \times 10^{-6}(r + 238.7)^3 - 18.07n - 417.5z^2/(r + 238.7) \quad (5)$$

where r is the radius of the metal ion in pm. Equating the volumes of coordinated H_2O and OH^-, setting V^0_{abs} for $H^+(aq)$ = –5.4 cm^3 mol^{-1} (*16*), and assuming no change in n, one can calculate values of ΔV_a^0 for other trivalent metals that reproduce the experimental values (table S1) to within ±2 cm^3 mol^{-1}. We calculate the volumes of reaction, below, for species with different numbers of oxygens coordinated to aluminum.

$$Al(H_2O)_6^{3+} \rightarrow Al(H_2O)_5OH^{2+} + H^+ \quad \Delta V_{a(n=6)}^0 = +1.7 \pm 2 \text{ cm}^3 \text{ mol}^{-1} \quad (6)$$

$$Al(H_2O)_5^{3+} \rightarrow Al(H_2O)_4OH^{2+} + H^+ \quad \Delta V_{a(n=5)}^0 = +1.9 \pm 2 \text{ cm}^3 \text{ mol}^{-1} \quad (7)$$

$$Al(H_2O)_6^{3+} \rightarrow \{Al(H_2O)_4OH^{2+} + H_2O\} + H^+ \quad \Delta V_{a(n=6\rightarrow5)}^0 = +16.2 \pm 2 \text{ cm}^3 \text{ mol}^{-1} \quad (8)$$

Thus, ΔV_a^0 is close to zero for any n if n does not change (Eqs. 6 and 7) but becomes strongly positive if n decreases concomitantly with proton loss (Eq. 8). A value of +1 ± 2 cm^3 mol^{-1}, similar to those for hydrolyses of other trivalent metal ions (table S1), may be assigned to $\Delta V_{a(n=6)}^0$.

If the exchanging conjugate-base species were $Al(H_2O)_5OH^{2+}$, Eq. 4 would indicate $\Delta V_{AlOH}^{\ddagger} \approx -2$ cm^3 mol^{-1}, which implies an associatively activated $\mathbf{I_a}$ mechanism (*10–12*, *17*). Such a mechanism is extremely unlikely for sterically crowded six-coordinate Al^{3+}, the extraordinarily small ionic radius of which (53 pm, the smallest of all 3+ ions) (*18*) makes expansion of the coordination number highly unlikely (*5*, *19*). Indeed, no minerals or coordination compounds are known in which Al^{3+} is seven-coordinate, and ab initio calculations by Kowall *et al.* (*13*) confirm that $Al(H_2O)_6^{3+}$ has no tendency to increase its coordination number beyond six. Moreover, the implication of a more associative mode of activation for $Al(H_2O)_5OH^{2+}$ than for $Al(H_2O)_6^{3+}$ runs counter to the literature (*10*). For other metals M, $\Delta V_{MOH}^{\ddagger}$ is invariably more positive than $\Delta V_M^{\ddagger}$ for a given hexaaqua trivalent metal ion (Table 1). Thus, the standard model is unrealistic for Al^{III} but would be consistent with water exchange via a five-coordinate $Al(H_2O)_4OH^{2+}$ ion, as in reaction 1; this ion would give a large positive value of ΔV_a^0 (Eq. 8) but would be open to facile water exchange by an associative mechanism (reverse of reaction 1) with a strongly negative value of $\Delta V_{AlOH}^{\ddagger}$, resulting in $\Delta V_2^{\ddagger} \sim 0$ (Eq. 4) as observed. For comparison with the standard model, reaction 1 may be viewed as a two-step process (Eqs. 9 and 10; $k_a/k_{-a} = K_a$) that differs from the standard model in that $Al(H_2O)_4OH^{2+}$ is now a stable entity rather than a high-energy intermediate in a **D** mechanism.

$$Al(H_2O)_6^{3+} \underset{k_{-a}}{\overset{k_a}{\rightleftharpoons}} Al(H_2O)_5OH^{2+} + H^+ \quad (9)$$

$$Al(H_2O)_5OH^{2+} \underset{k_{-b}}{\overset{k_b}{\rightleftharpoons}} Al(H_2O)_4OH^{2+} + H_2O \quad (10)$$

Closer consideration of Eqs. 9 and 10, however, reveals a further departure from the standard model in that k_a in Eq. 9 must be rate determining for both proton and water exchange. According to the combined Eq. 1, three protons ($\boldsymbol{H^+ + H_2O}$) are exchanged with the bulk medium for every exchanged oxygen atom. Thus, if the overall process represented by Eq. 1 is the only one contributing measurably to the rate of water exchange via

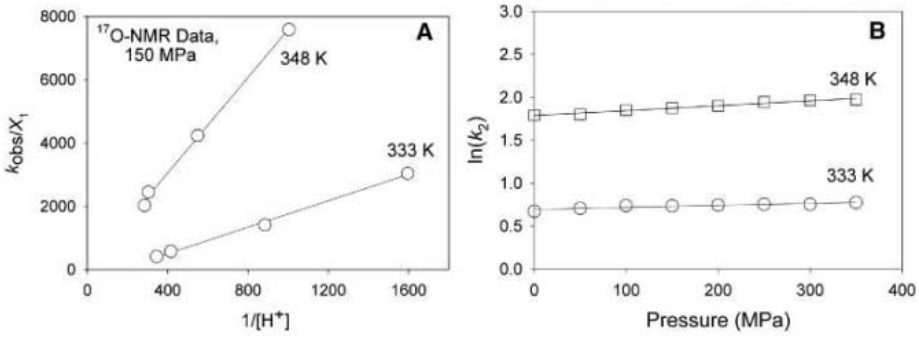

Fig. 1. (**A**) Typical high-pressure kinetic data (150 MPa) obtained from ^{17}O-NMR spectra. Regression of the apparent rate coefficients (k_{obs}), divided by the fraction (X_1) of dissolved aluminum as the $Al(H_2O)_6^{3+}$, as a function of hydrogen-ion concentration yields values for k_2 at each temperature via Eq. 3. (**B**) Regression of ln(k_2) as a function of pressure. The lines correspond to linear-least-squares fits to the data, and the corresponding slopes are 2.4 (±0.4) × 10^{-4} and 2.6 (±0.3) × 10^{-4} MPa^{-1} at 333K and 348 K, respectively, both of which yield $\Delta V_2^{\ddagger}$ = –0.7 cm^3 mol^{-1} to within experimental uncertainty.

Table 1. Kinetic parameters for exchange of water molecules from the inner coordination sphere of octahedral complexes of some trivalent metals and their conjugate bases (*12–14*). The ionic radii are for hexacoordinate M^{3+} (*18*).

Complex	k_M^{298} (s^{-1})	$\Delta V_M^{\ddagger}$ (cm^3 mol^{-1})	Mechanism	Ionic radius (pm)
$Ga(H_2O)_6^{3+}$	4.0 × 10^2	+5.0 ± 0.5	$\mathbf{I_d}$	62
$Ga(H_2O)_5OH^{2+}$	1.1 × 10^5	+6.2	$\mathbf{I_d}$	
$Fe(H_2O)_6^{3+}$	1.6 × 10^2	–5.4 ± 0.4	$\mathbf{I_a}$	64.5
$Fe(H_2O)_5OH^{2+}$	1.2 × 10^5	+7.0 ± 0.5	$\mathbf{I_d}$	
$Al(H_2O)_6^{3+}$	1.3	+5.7 ± 0.2	$\mathbf{I_d}$ or **D**	53.5
$Al(H_2O)_{n-1}OH^{2+}$	3.1 × 10^4	this paper		
$Cr(H_2O)_6^{3+}$	2.4 × 10^{-6}	–9.6 ± 0.1	$\mathbf{I_a}$	61.5
$Cr(H_2O)_5OH^{2+}$	1.8 × 10^{-4}	+2.7 ± 0.5	$\mathbf{I}$	
$Ru(H_2O)_6^{3+}$	3.5 × 10^{-6}	–8.3 ± 2.1	$\mathbf{I_a}$	68
$Ru(H_2O)_5OH^{2+}$	5.9 × 10^{-4}	+0.9	$\mathbf{I}$	
$Rh(H_2O)_6^{3+}$	2.2 × 10^{-9}	–4.1 ± 0.6	$\mathbf{I_a}$	66.5
$Rh(H_2O)_5OH^{2+}$	4.2 × 10^{-5}	+1.5	$\mathbf{I}$	
$Ir(H_2O)_6^{3+}$	1.1 × 10^{-10}	–5.7 ± 0.5	$\mathbf{I_a}$	68
$Ir(H_2O)_5OH^{2+}$	5.6 × 10^{-7}	+1.3	$\mathbf{I}$	

$AlOH^{2+}$(aq), the rate constant for proton exchange $k_{H(Al)}$ on $Al(H_2O)_6^{3+}$ at low pH should equal $3 \times k_{AlOH}$ for oxygen exchange via $AlOH^{2+}$(aq), or 9.3×10^4 s^{-1} at 298 K (*14*). Indeed, Fong and Grunwald (*20*, *21*) found by ^{1}H-NMR that $k_{H(Al)} = 7.9 \times 10^4$ s^{-1} at 298 K, whereas Eyring and colleagues (*22*) obtained 10.9×10^4 s^{-1} by dielectric relaxation. Reprotonation of $AlOH^{2+}$ is very fast, approaching the diffusion-controlled rate (*20*, *22*).

In terms of Eqs. 9 and 10, these observations imply that, unusually, k_a determines the rate of water exchange on Al^{III}(aq) by the conjugate-base pathway, reaction 10 being relatively fast because of the ease of associative water attack on $Al(H_2O)_4OH^{2+}$ [and, conversely, of dissociative water loss from $Al(H_2O)_5OH^{2+}$]. In other words, water dissociation follows promptly on proton loss, so that Eqs. 9 and 10 reduce to a single process, Eq. 1, on NMR time scales. It follows that $\Delta V_2^{\ddagger}$ (-0.7 cm^3 mol^{-1}) is actually the volume of activation $\Delta V_a^{\ddagger}$ for proton dissociation (Eq. 9). In contrast, in the standard model, k_b is rate determining, but this is evidently not the case for Al^{III}. The dimer $(H_2O)_4Al(OH)_2Al(OH_2)_4^{4+}$, in which the Al^{III} centers are coordinatively saturated, would be unlikely to contribute to the water exchange rate and, besides, is undetectable in dilute Al^{III} solutions (*7*). Water exchange on $Al(H_2O)_6^{3+}$ without deprotonation is too slow [1.29 s^{-1} at 298 K (*12*)] to affect the proton exchange rate.

To test this proposed mechanism, we conducted Car-Parrinello molecular-dynamics (CPMD) simulations of Al^{III} with 64 water molecules (*23*–*29*). We formed a six-coordinate $AlOH^{2+}$ ion by removing a single H^+ from an equilibrated $Al(H_2O)_6^{3+}$ + 58 H_2O CPMD simulation and found that the $Al(H_2O)_5OH^{2+}$ converted to a persistent five-coordinate structure within 0.8 ps (Fig. 2).

Beyond these data and simulations, confirmatory evidence for the existence of five-coordinate $AlOH^{2+}$ in solution is elusive. ^{27}Al-NMR might seem promising, because it is known that, in solids, five-coordinate $Al^{III}O_5$ sites can be observed at chemical shift $\delta \sim +35$ parts per million (ppm) relative to $Al(H_2O)_6^{3+}$ (*30*). In ^{27}Al-NMR, however, rapid quadrupolar relaxation of the nucleus causes line widths to be broad unless the Al^{III} atom occupies a site of high local symmetry such as O_h in $Al(H_2O)_6^{3+}$; extreme broadening of ^{27}Al resonances from sites of low symmetry may result in their being lost into baseline noise (*8*). In studying $Al(H_2O)_6^{3+}$ hydrolysis at 298 K with low, geochemically relevant concentrations (10 μmol L^{-1}), Faust *et al.* (*31*) could not account for the loss of ^{27}Al "monomer" intensity as the degree of hydrolysis increased, because no other ^{27}Al resonances were detectable. They suggested that the $AlOH(aq)^{2+}$ and $Al(OH)_2(aq)^+$ resonances occurred at $\delta = +3.5$ and $+3.7$ ppm (respectively) relative to $Al(H_2O)_6^{3+}$, that they are in rapid exchange equilibrium with the $Al(H_2O)_6^{3+}$ line, and that the missing ^{27}Al intensity could be attributed to oligomeric hydrolysis products. Missing ^{27}Al intensity was noted and similarly explained in Al^{III} hydrolysis studies by Akitt and Elders (*6*) and Kloprogge *et al.* (*9*).

Öhman (*32*), however, has pointed out that the $AlOH(aq)^{2+}$ and $Al(OH)_2(aq)^+$ chemical shifts inferred by Faust *et al.* (*31*) are inconsistent with the general observation that ^{27}Al δ values for successive complexation steps at Al^{III} are additive and also that oligomerization is known from well-established pH titrimetric evidence to be negligible at the very low $[Al]_{total}$ used. $[Al]_{total}$ was much higher in the studies by Akitt and Elders (*6*) and Kloprogge *et al.* (*9*). Öhman (*32*) suggested that the missing ^{27}Al intensity might be due to unspecified adsorption phenomena.

We suggest instead that the missing ^{27}Al intensity in the study of Faust *et al.* (*31*), and to some degree in those of Akitt and Elders (*6*) and Kloprogge *et al.* (*9*), was due to an undetectably broadband arising from $Al(H_2O)_4OH^{2+}$, centered near $\delta = +35$ ppm relative to $Al(H_2O)_6^{3+}$, and owing its breadth to a combination of rapid quadrupolar relaxation associated with the low-symmetry ^{27}Al environment (at most, C_{4v}) and chemical exchange broadening (Eq. 1). In this interpretation, the single Al^{III} "monomer" resonance of Faust *et al.* (*31*) would be exclusively due to $Al(H_2O)_6^{3+}$, its broadening and increase in δ with increasing pH arising from chemical exchange with unseen $Al(H_2O)_4OH^{2+}$, according to Eq. 1. The deficit in ^{27}Al intensity is close to that expected from $AlOH^{2+}$(aq) concentrations calculated from the data of Palmer and Wesolowski (*33*).

Solvent exchange on Al^{III} by the conjugate-base pathway is thus distinct among the trivalent metals, either because the purported $Al(H_2O)_5OH^{2+}$ complex resulting from a rapid preequilibrium (Eq. 9) undergoes associatively activated water exchange (which we dismiss as unreasonable), or, as we propose, because it promptly loses water dissociatively to form $Al(H_2O)_4OH^{2+}$, leaving deprotonation of $Al(H_2O)_6^{3+}$ as the rate-determining step (k_a). The standard model for water exchange via a conjugate base, although successful for all other M^{III}, accounts poorly for Al^{III} chemistry.

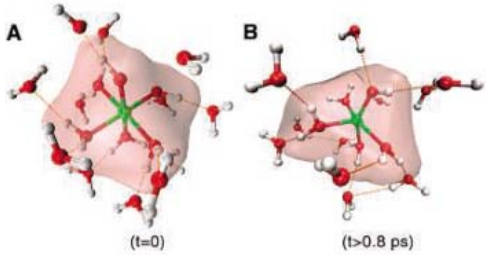

Fig. 2. Snapshot of the initial $Al(H_2O)_6^{3+}$ geometry (**A**) and the five-coordinate $AlOH^{2+}$ ion (**B**) that forms in the CPMD simulations. The surface identifies the inner-coordination spheres, and dashed orange lines show the treelike array of hydrogen bonds that stabilizes the structure. The $AlOH^{2+}$ ion was initially formed by removing an H^+ from an $Al(H_2O)_6^{3+}$ equilibrated with 58 H_2O molecules (for clarity, most are not shown) in a cubic cell (12.4 Å). It converted within 0.8 ps to a five-coordinate structure that persisted for the length of the simulations (10 ps).

References and Notes

1. R. A. Yokel, in *Elements and their Compounds in the Environment: Occurrence, Analysis, and Biological Relevance*, E. Merian, M. Anka, M. Ihnat, M. Stoeppler, Eds. (Wiley, New York, ed. 2, 2004), vol. 2, pp. 635–658.
2. H. Sigel, A. Sigel, Eds., *Aluminum and its Role in Biology* (*Metal Ions Biol. Systems 24*) (Marcel Dekker, New York, 1988).
3. R. B. Martin, *Met. Ions Biol. Syst.* **24**, 1 (1988).
4. R. W. Smith, *Coord. Chem. Rev.* **149**, 81 (1996).
5. D. T. Richens, *The Chemistry of Aqua Ions* (Wiley, New York, 1997), pp. 143–146.
6. J. W. Akitt, J. M. Elders, *J. Chem. Soc. Faraday Trans. I* **81**, 1923 (1985).
7. R. B. Martin, *J. Inorg. Biochem.* **44**, 141 (1991).
8. J. W. Akitt, *Progr. NMR Spectrosc.* **21**, 1 (1989).
9. J. T. Kloprogge, D. Seykens, J. B. H. Jansen, J. W. Geus, *J. Non-Cryst. Solids* **152**, 207 (1993).
10. L. Helm, A. E. Merbach, *Coord. Chem. Rev.* **187**, 151 (1999).
11. T. W. Swaddle, *Inorg. Chem.* **22**, 2663 (1983).
12. D. Hugi-Cleary, L. Helm, A. E. Merbach, *Helv. Chim. Acta* **68**, 545 (1985).
13. T. Kowall *et al.*, *J. Am. Chem. Soc.* **120**, 6569 (1998).
14. J. P. Nordin, D. J. Sullivan, B. L. Phillips, W. H. Casey, *Inorg. Chem.* **37**, 4760 (1998).
15. The absence of ΔV_a^o values for Al^{III} is partly because sensitive techniques such as ultraviolet-visible spectroscopy [used, for example, to determine K_a and ΔV_a^o for $Fe(H_2O)_6^{3+}$ (*17*)] are inapplicable to Al^{III} but also because, for alternative techniques such as densimetry, sufficiently high concentrations of $AlOH^{2+}$ cannot be realized without interference from other hydrolytic species and oligomers (*6*, *8*, *9*).
16. F. J. Millero, in *Water and Aqueous Solutions: Structure, Thermodynamics, and Transport Processes*, R. A. Horne, Ed. (Wiley, New York, 1972), chap. 13.
17. T. W. Swaddle, A. E. Merbach, *Inorg. Chem.* **20**, 4212 (1981).
18. R. D. Shannon, *Acta Crystallogr.* **A32**, 751 (1976).
19. T. W. Swaddle, *Inorg. Chem.* **19**, 3203 (1980).
20. D.-W. Fong, E. Grunwald, *J. Am. Chem. Soc.* **91**, 2413 (1969).
21. Fong and Grunwald (*20*) also found a pH-dependent proton exchange (linearly dependent on $[H^+]^{-1}$ at moderately low pH, rate coefficient j_2 in their nomenclature) that, in the scenario presented here, may be taken to measure the rate of direct exchange of proton between $AlOH^{2+}$ and solvent water via $Al(OH)_2^+$.
22. L. P. Holmes, D. L. Cole, E. M. Eyring, *J. Phys. Chem.* **72**, 301 (1968).
23. CPMD simulations were performed using the PSPW module in NWChem, separable Hamann pseudopotentials, the PBE96 exchange-correlation functional, and a wavefunction cutoff of 72 Ry. Simulations were equilibrated for 2 ps in the presence of a thermostat (T = 400 K) before data were collected for 10 ps at constant energy.
24. R. Car, M. Parrinello, *Phys. Rev. Lett.* **55**, 2471 (1985).

25. E. Apra *et al.*, NWChem, version 4.7 (Pacific Northwest National Laboratory, Richland, WA, 2005).
26. D. R. Hamann, *Phys. Rev. B* **40**, 2980 (1989).
27. L. Kleinman, D. M. Bylander, *Phys. Rev. Lett.* **48**, 1425 (1982).
28. J. P. Perdew, K. Burke, M. Ernzerhof, *Phys. Rev. Lett.* **77**, 3865 (1996).
29. Materials and methods are available as supporting material on *Science* Online.
30. M. C. Cruickshank, L. S. Dent Glasser, S. A. I. Barri, I. J. F. Poplett, *J. Chem. Soc. Chem. Commun.* **23**, 23 (1986).
31. B. C. Faust *et al.*, *Geochim. Cosmochim. Acta* **59**, 2651 (1995).
32. L.-O. Öhman, *Geochim. Cosmochim. Acta* **61**, 3257 (1997).
33. D. A. Palmer, D. J. Wesolowski, *Geochim. Cosmochim. Acta* **57**, 2929 (1993).
34. We thank J. Weare for helping to develop the simulations. The research was supported by separate grants from the Office of Basic Energy Science of the U.S. Department of Energy to W.H.C. and E.B., from the U.S. NSF to B.L.P. and W.H.C., and from the Natural Sciences and Engineering Research Council of Canada to T.W.S.

Supporting Online Material
www.sciencemag.org/cgi/content/full/1110231/DC1
Materials and Methods
Fig. S1
Tables S1 and S2
References

25 January 2005; accepted 18 April 2005
Published online 28 April 2005;
10.1126/science.1110231
Include this information when citing this paper.

An Observation of PKJKP: Inferences on Inner Core Shear Properties

Aimin Cao,[1]* Barbara Romanowicz,[1] Nozomu Takeuchi[2]

The seismic phase PKJKP, which traverses the inner core as a shear wave and would provide direct evidence for its solidity, has been difficult to detect. Using stacked broadband records from the Gräfenberg array in Germany, we documented a high signal-to-noise phase, the arrival time and slowness of which agree with theoretical predictions for PKJKP. The back azimuth of this arrival is also consistent with predictions for PKJKP, as is the comparison with a pseudoliquid inner core model. Envelope modeling of the PKJKP waveform implies a shear velocity gradient with depth in the inner core that is slightly larger than that in the preliminary reference Earth model.

Soon after Lehmann (*1*) discovered Earth's inner core in 1936 through the analysis of travel times of teleseismic body waves, Birch (*2*) suggested that the inner core should be solid as a result of freezing of liquid iron. Thirty years later, indirect evidence of the solidity of the inner core was documented by means of seismic normal mode eigenfrequency measurements (*3*). However, the observation of the phase PKJKP, which traverses the inner core as a shear wave (Fig. 1A), has been a controversial issue. Julian *et al.* (*4*) and Okal and Cansi (*5*) each suggested the detection of PKJKP on the basis of data from short-period seismic arrays at frequencies of ~1.0 Hz and 0.1 to 0.5 Hz, respectively. Deuss *et al.* (*6*) argued that these two claims were misidentifications, and instead proposed an observation of pPKJKP+SKJKP between 0.01 and 0.1 Hz.

PKIKP, which traverses the inner core as a compressional wave (Fig. 1A), is routinely observed. It should be observed simultaneously with PKJKP in the epicentral distance range 116° to 180°, according to the seismic preliminary reference Earth model (PREM) (*7*). The relative amplitude of PKJKP varies strongly with frequency (Fig. 1B). Although we cannot rule out the possibility of observing PKJKP at frequencies of 0.1 to 0.5 Hz (*5*), it is more likely to be found at lower frequencies (*6*).

Here, we used data from the broadband Gräfenberg Seismic Array (GRF) in Germany to detect PKJKP (Fig. 1C). With an aperture of ~100 × 50 km, GRF has provided continuous records at 13 stations since 1980. Its location with respect to frequent large events (moment magnitude M_w > 7.0) in the south Pacific Ocean at distances of ~140° makes it an ideal broadband seismic array to study PKJKP. We studied ~20 large events in the vicinity of Tonga and Santa Cruz islands occurring from 1980 to 1999 (*8*). One of the events (M_w = 7.3, depth = 76 km, 6 February 1999) is uniquely favorable to the observation of PKJKP (Fig. 1C). We chose the band measuring 0.06 to 0.1 Hz for our analysis (*9*).

We aligned the seismograms with respect to the origin time of the event and made an array-sided travel time correction (fig. S1A) (*10*), filtered the data with a band-pass filter, normalized the seismograms with respect to the first arrival (PKIKP+PKiKP), and stacked them using the phase-weighted stack (PWS) technique (*11*). We computed two vespagrams. The first one (Fig. 2A) corresponds to the time and slowness window within which we expect to find the group PKIKP/PKiKP and their depth phases. The second one (Fig. 2C) corresponds to the predicted window for PKJKP, according to the PREM model (*7*). We observe clear energy maxima in both windows. We also observe a clean stacked waveform corresponding to the energy maximum in the PKJKP window (Fig. 2D). We verified that this phase arrives within 5° of the great circle path from the source, ruling out a scattered near-array phase (Fig. 2E). We further investigated whether this phase could be a mantle, outer core, or even crust phase, by considering for reference a model with a liquid inner core, as was done by Deuss *et al.* (*6*). In such a model, there would not be a PKJKP phase. We constructed synthetic vespagrams using the direct-solution method (DSM) (*12*, *13*).

Consideration of near source local structure, as well as moment tensor information (*13*) allowed us to model both the waveform of PKIKP+PKiKP and its depth phase, pPKIKP+pPKiKP (Fig. 3A) for both solid and liquid inner cores, providing accurate source-time functions for the synthetic calculations. It is not possible to discern PKJKP in an individual synthetic trace, because PKJKP is so weak that it is deeply hidden behind unidentifiable mantle, outer core, and crust phases. To extract the PKJKP phase, we generated synthetic differential seismograms between solid inner core and liquid inner core (Fig. 3B). However, even when we chose a shear-wave quality factor Q_β = 300 for the solid inner core, PKJKP and pPKJKP were not prominent enough. This is because transmission coefficients of the inner core *P*-wave phases (PcPPKIKP, pPcPPKIKP, sPcPPKIKP, and PKKPdf; fig. S4) are artificially increased in the case of the liquid inner core, compared with the real earth. This artificial energy is weak, but stronger than that of the potential PKJKP.

The liquid inner core model serves to remove the inner core shear-wave energy from the time window shown in Fig. 3B, so as to better extract PKJKP and pPKJKP in the differential seismogram. We can also achieve this by reducing the shear-wave velocity in the inner core by 8% compared with the PREM model. In this case, the inner core shear-wave energy moves beyond the appropriate time window (PKJKP and pPKJKP are moved backward by ~50 s). Meanwhile, the artificial compressional energy is considerably reduced (Fig. 3C) and both PKJKP and pPKJKP phases are present in the synthetic differential seismogram. pPKJKP is ~2.2 times as weak as PKJKP. If we also take the background noise into account, the amplitude ratio of PKJKP to pPKJKP may be as large as ~4.8 (fig. S2). Therefore, it is not surprising that we do not observe pPKJKP for this event. We thus only discuss PKJKP. Synthetic vespagrams for this pseudoliquid inner core (Fig. 4A) show that there is no energy maximum corresponding to waves with negative slowness, confirming that the target phase observed in Fig. 2, C, D, and E, is not a crust, mantle, or outer core phase (*14*).

[1]Seismological Laboratory, University of California, Berkeley. [2]Earthquake Research Institute, University of Tokyo, Japan.

*To whom correspondence should be addressed. E-mail: acao@seismo.berkeley.edu

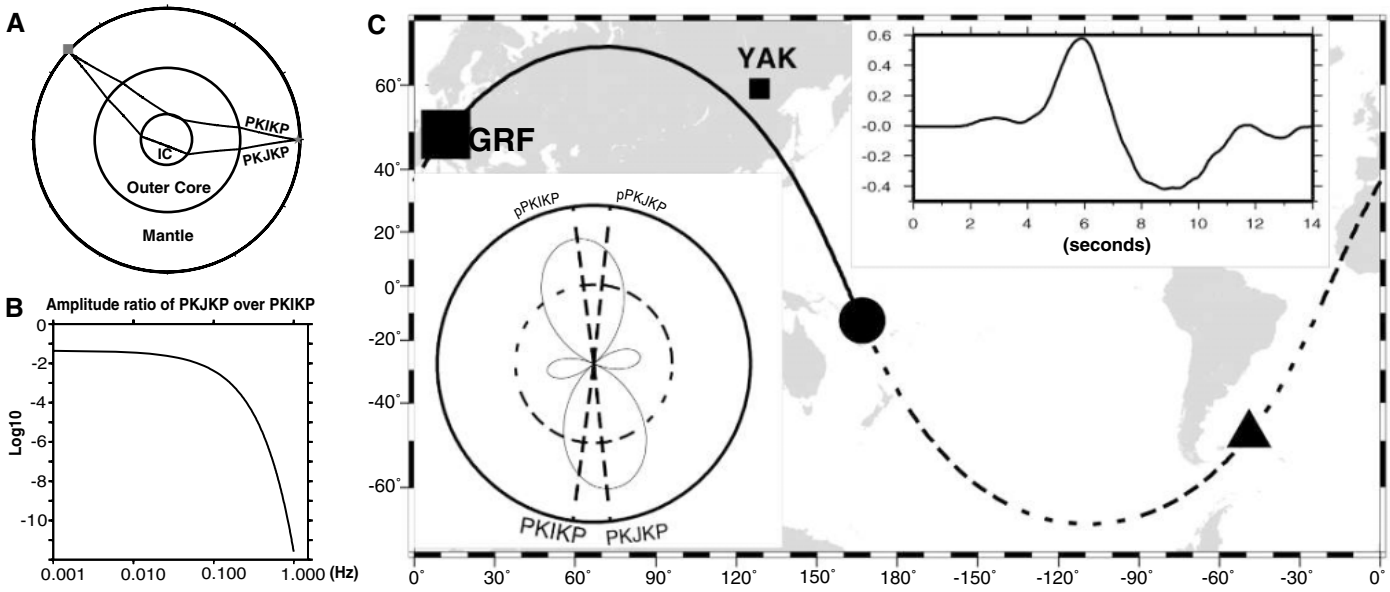

Fig. 1. (**A**) Ray paths of PKJKP and PKIKP. The point on the right and square on the left indicate the source and GRF array locations, respectively. IC, inner core. (**B**) The theoretical amplitude ratio of PKJKP over PKIKP as a function of frequency based on the reference model PREM (*7*), after correcting for transmission and geometrical spreading (*16*). The reference epicentral distance is 138°. Given the dynamic range of present seismometers, it is unlikely that one could observe PKJKP (or pPKJKP) in the frequency range ~1.0 Hz (*4*). (**C**) Geographical setting of the event (dot) and GRF seismic array (square). The solid line is the ray path of PKIKP and the dashed line is the ray path of PKJKP projected on Earth's surface. The triangle marks the location of the bottoming point of PKJKP in the inner core. The upper right inset shows the source-time history of the event characterized by a *P* phase recorded at a broadband station (YAK, distance = 80.1°) of the Global Seismographic Network, located in a similar azimuth as GRF. The lower left inset illustrates the *P*-wave radiation pattern in the vertical plane of the great circle. This event is exceptional: (i) The source duration is less than 9 s; (ii) the expected PKJKP is emitted from the top of the lobe of the *P*-wave radiation pattern; and (iii) the potential interfering phases identified in previous studies (*4*, *5*), such as PcPPKIKP, pPcPPKIKP, sPcPPKIKP, and PKKPdf, are at least 17 s away from the predicted PKJKP arrival time (according to PREM).

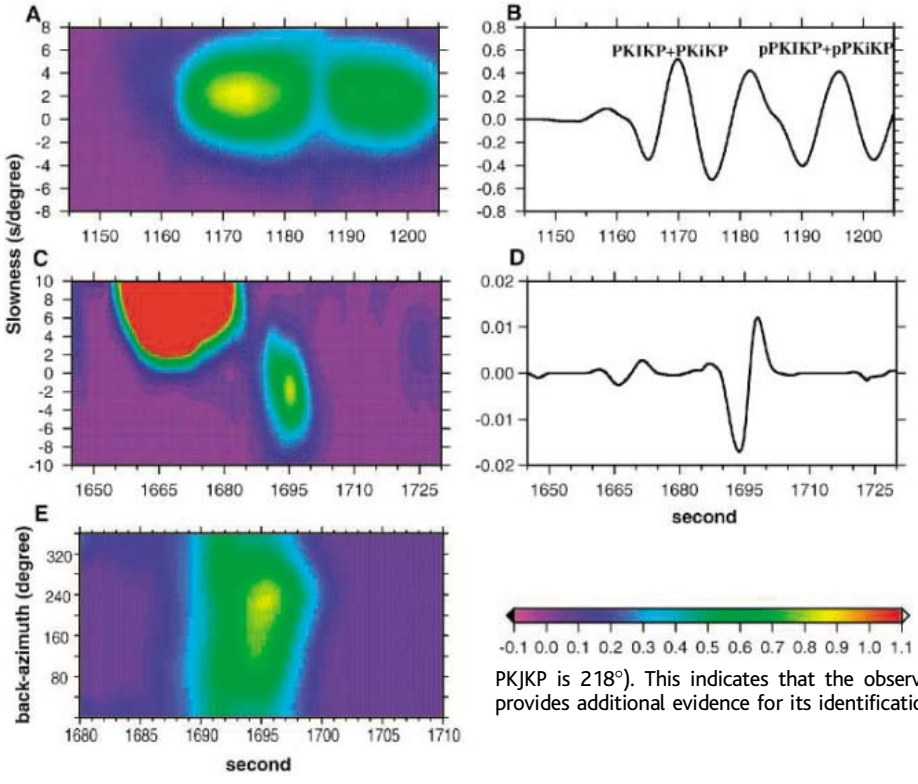

Fig. 2. (**A**) Observed vespagram for PKIKP+PKiKP and their depth phases (the energy level is amplified 1.6 times). The center of the energy maximum is for a slowness of ~1.9 s/degree, which is the average of slownesses of PKIKP (1.85 s/degree) and PKiKP (2.04 s/degree) predicted from PREM (*7*). The following weaker energy maximum corresponds to pPKIKP+pPKiKP and has the same slowness, as predicted from PREM. (**B**) Stacked waveforms for PKIKP+PKiKP and their depth phases for the energy maximum in (A). (**C**) Observed vespagram for the potential PKJKP (energy level is amplified 40 times). The slowness of the energy maximum is ~−1.6 s/degree, close to the PREM prediction of –1.43 s/degree. The arrival time is also compatible with PREM (1695 s for the maximum energy, compared with a prediction of 1690 s for the high-frequency onset of the pulse). (**D**) Stacked waveform corresponding to the energy maximum in (C). (**E**) Vespagram in the back azimuth and travel time domain. This shows the direction of arrival of the detected energy, which we identify as PKJKP, in the negative slowness range of (C). The estimated back azimuth is ~223°, which shows that the observed energy propagates along the major arc from the source (the expected back azimuth of PKJKP is 218°). This indicates that the observed phase is not a near-array scattered phase and provides additional evidence for its identification as PKJKP.

The PKJKP waveform (Fig. 2D) allows us to estimate the shear-wave velocity in the inner core by envelope-function modeling. Synthetic envelope functions of PKJKP are computed from the synthetic differential seismograms between the solid inner core and the pseudoliquid inner core (*13*). We process the synthetic differential seismograms in the same way as the observed seismogram and compare the envelope with the observed one (fig. S2). The envelope-function modeling suggests that the observed PKJKP is about 9.0 s faster than the

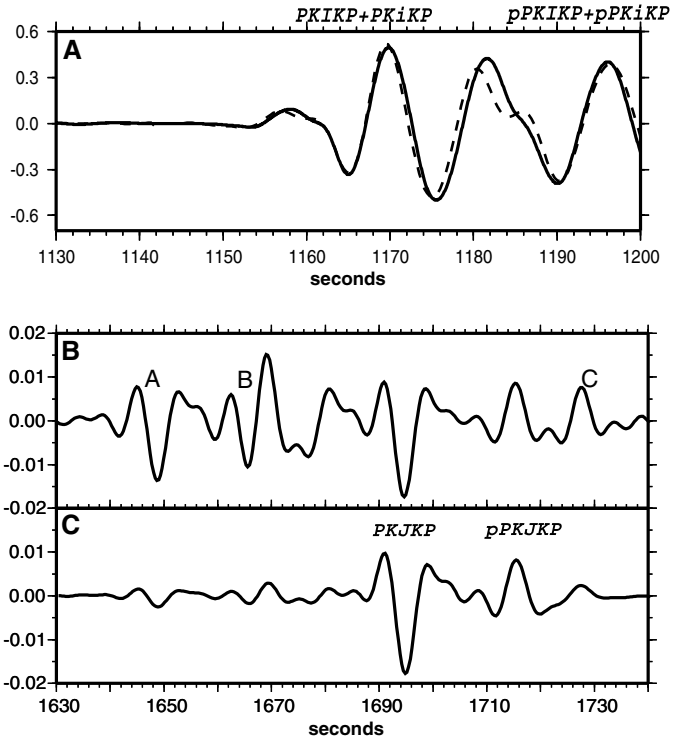

Fig. 3. Synthetic modeling. (**A**) Waveform modeling of PKIKP+PKiKP as well as pPKIKP+pPKiKP based on U.S. Geological Survey Preliminary Determination of Epicenters moment tensor. Both the observed (dashed line) and the synthetic (solid line) seismograms are normalized after applying the band-pass filter (0.06 to 0.1 Hz). Synthetics are obtained with DSM (*12*). (**B**) Synthetic differential seismogram for the PREM model compared with a true liquid inner core, for which the shear-wave velocity is equal to zero. A (PcPPKIKP), B (pPcPPKIKP+sPcPPKIKP), and C (PKKPdf) are artificially enhanced by the assumption of liquid inner core. (**C**) Synthetic differential seismogram based on the pseudoliquid inner core used in this Report. We now can clearly see both PKJKP and pPKJKP phases. The amplitude of PKJKP is approximately 2.2 times as large as that of pPKJKP.

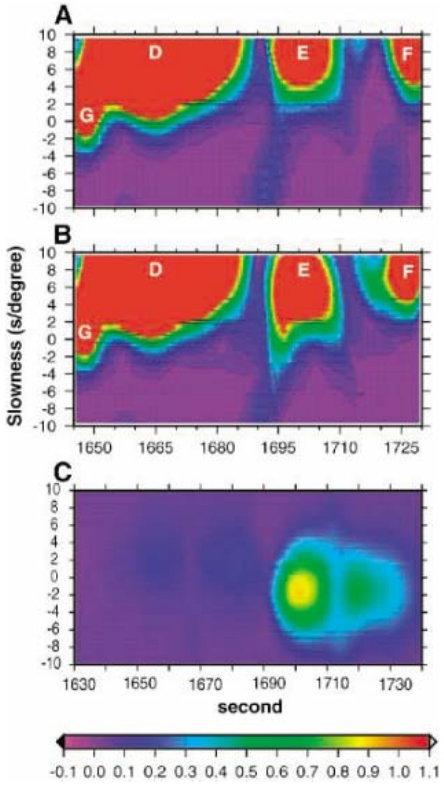

Fig. 4. Synthetic vespagrams. (**A**) Pseudoliquid inner core model. Time windows are identical to those in Fig. 2C. Energy level is amplified 40 times, as in Fig. 2C. D, E, and F are crust, mantle, or outer core phases, and G is PcPPKIKP. See fig. S3 for a plot with energy level amplified only 20 times to bring out the relative strength of these phases. (**B**) Solid inner core model, assuming $Q_\beta = 300$. Because the strong mantle phase E in the synthetic model arrives at the same time as PKJKP, the dominant energy of phase E hides the much weaker PKJKP, which only slightly distorts the pattern of phase E. Likewise, pPKJKP slightly distorts the pattern of phase F. Phases E and F are not present in the observed stacks. Therefore, we cannot directly use the comparison of observed vespagram to that predicted by the solid inner core model; instead, we use a differential seismogram modeling approach, in which the energy from phases E and F is removed. (**C**) Synthetic differential vespagram in the slowness-time domain. This vespagram is calculated for the solid inner core minus the pseudoliquid inner core models. The time window is the same as that in Fig. 3C. The estimated slownesses of the energy maxima are both −1.4 s/degree, as are the predictions based on PREM. This identifies the two phases in the differential seismogram (Fig. 3C) as PKJKP and pPKJKP.

synthetic PKJKP. It implies that the shear-wave velocity in the inner core may be ~1.5% faster than that for the PREM model (*7*). PREM is primarily based on normal mode data, which mainly sample the shallow portion of the inner core, whereas here, PKJKP samples the central part (Fig. 1A). Thus, it is in agreement with previous results if one allows for a slight increase in shear velocity with depth in the inner core. The use of GRF array data was key to this study (*15*).

References and Notes

1. I. Lehmann, *Bur. Centr. Seismol. Int. A.* **14**, 87 (1936).
2. F. Birch, *Am. J. Sci.* **238**, 192 (1940).
3. A. M. Dziewonski, F. Gilbert, *Nature* **234**, 465 (1971).
4. B. R. Julian, D. Davies, R. M. Sheppard, *Nature* **235**, 317 (1972).
5. E. A. Okal, Y. Cansi, *Earth Planet. Sci. Lett.* **164**, 23 (1998).
6. A. Deuss, J. H. Woodhouse, H. Paulssen, J. Trampert, *Geophys. J. Int.* **142**, 67 (2000).
7. A. M. Dziewonski, D. L. Anderson, *Phys. Earth Planet. Inter.* **25**, 297 (1981).
8. The relocated catalog by Engdahl *et al.* is available for this time period; E. R. Engdahl, R. D. van der Hilst, R. P. Buland, *Bull. Seismol. Soc. Am.* **88**, 722 (1998).
9. From 100 s before PKIKP and 200 s after PKJKP, the amplitude spectrum (fig. S1B) indicates that the amplitude decays significantly at periods longer than 0.06 Hz. Only in the frequency range 0.06 to 0.1 Hz is the amplitude relatively constant.
10. The GRF seismic array has a relatively small aperture, but there is still noticeable variation of differential travel times of PKIKP, which can be as large as 0.6 s across the array. This variation is presumed to be primarily related to crust and/or uppermost mantle heterogeneity just beneath the array. This heterogeneity should also influence PKJKP at a similar level, because the two ray paths are very close in this region (Fig. 1A). GRB2, which is at the center of this broadband seismic array, is chosen as the reference station.
11. M. Schimmel, H. Paulssen, *Geophys. J. Int.* **130**, 497 (1997).
12. N. Takeuchi, R. J. Geller, P. R. Cummins, *Geophys. Res. Lett.* **23**, 1175 (1996).
13. Materials and methods are available as supporting material on *Science* Online.
14. The phase observed in Fig. 2, C and D, cannot be due to random noise. (i) The PWS stacking technique (*11*) is designed specifically to remove the influence of the background incoherent noise. (ii) If what we observed had been random noise, the energy extrema should have also distributed randomly in the observed vespagram.
15. Compared with global broadband seismic networks (*6*), GRF has a number of distinct advantages: (i) We can examine all potential interfering phases, which are expected to appear in the time window of our study, to make sure they arrive sufficiently far away in time and/or slowness from PKJKP. When global networks are used, the number of identifiable interfering phases is much larger. As a result, it seems more difficult to prevent the relatively strong phase(s) from appearing close to PKJKP (or pPKJKP). Usually, the stacking technique cannot suppress this kind of energy completely and thus cannot prevent these phases from interfering with the very weak PKJKP (or pPKJKP) energy (*11*). (ii) We can expect that the presumed PKJKP phases recorded at every station in GRF are coherent. When using global networks, one must correct for polarities of the expected PKJKP (or pPKJKP) phases in different quadrants if they are opposite. (iii) GRF stations use identical seismometers. We can directly process the data without removing instrument responses as we adopt normalized traces to constrain Q_β. Although the aperture of GRF seismic array is relatively small for this very sharp large event, it is sensitive to small perturbations in arrival times (as low as ~0.3 s) using vespagrams. This is also the reason that the array-sided travel time correction is necessary.
16. A. Cao, B. Romanowicz, *Earth Planet. Sci. Lett.* **228**, 243 (2004).

17. We thank the Gräfenberg Array operators for the long-term high-quality maintenance of their array. This work was supported by NSF grant EAR-0308750. This is Berkeley Seismological Laboratory contribution 05-08.

Supporting Online Material

www.sciencemag.org/cgi/content/full/1109134/DC1
Materials and Methods
Figs. S1 to S4
References and Notes

27 December 2004; accepted 30 March 2005
Published online 14 April 2005;
10.1126/science.1109134
Include this information when citing this paper.

Gender-Specific Reproductive Tissue in Ratites and *Tyrannosaurus rex*

Mary H. Schweitzer,[1,2,3]* Jennifer L. Wittmeyer,[1] John R. Horner[3]

Unambiguous indicators of gender in dinosaurs are usually lost during fossilization, along with other aspects of soft tissue anatomy. We report the presence of endosteally derived bone tissues lining the interior marrow cavities of portions of *Tyrannosaurus rex* (Museum of the Rockies specimen number 1125) hindlimb elements, and we hypothesize that these tissues are homologous to specialized avian tissues known as medullary bone. Because medullary bone is unique to female birds, its discovery in extinct dinosaurs solidifies the link between dinosaurs and birds, suggests similar reproductive strategies, and provides an objective means of gender differentiation in dinosaurs.

A relatively small (femur length, 107 cm) *Tyrannosaurus rex* [Museum of the Rockies (MOR) specimen number 1125] was discovered at the base of the Hell Creek Formation (dated at ~70 million years ago) as an association of disarticulated elements with excellent preservation (*1*). At death, MOR 1125 was estimated to be 18 ± 2 years (*2*), on the basis of lines of arrested growth (LAG).

Interior femur fragments from MOR 1125 were reserved without preservatives for chemical and molecular analyses. Gross examination revealed a thin layer of bone tissue lining the inner (medullary) surfaces of the bone fragments that was structurally distinct from other described bone types (Fig. 1D) but possessed characteristics in common with avian medullary bone (MB).

MB is an ephemeral tissue, deposited on the endosteal surface of avian long bones (*3*–*10*). Its formation in female birds is triggered by increasing levels of gonadal hormones produced upon ovulation (*4*, *10*, *11*), but it can also be artificially induced in male birds by the administration of estrogen (*3*, *4*, *12*). Because MB is densely mineralized and extremely well vascularized, it provides an easily mobilized source of calcium necessary for the production of calcareous eggshells (*13*). We compare MB from emu and ostrich (*14*) at different stages of the laying cycle with newly identified dinosaur tissues, because these basal birds share more primitive features with nonavian dinosaurs than do extant neognaths (*15*–*18*).

Our investigations show that ratite MB differs from that seen in better-studied neognaths. We observed substantial variation between emu and ostrich MB tissues and between both ratites and reported neognath tissues (Fig. 1 and fig. S1). MB (Fig. 1) may be thick (chicken and ostrich) or quite thin (emu) at midshaft; and it may be separated by a distinct layer of endosteal laminar bone

[1]Department of Marine, Earth, and Atmospheric Sciences, North Carolina State University, Raleigh, NC 27695, USA. [2]North Carolina State Museum of Natural Sciences, Raleigh, NC 27601, USA. [3]Museum of the Rockies, Montana State University, Bozeman, MT 59717, USA.

*To whom correspondence should be addressed. E-mail: schweitzer@ncsu.edu

Fig. 1. Extant avian MB and homologous dinosaurian bone tissues. (**A**) Domestic laying hen, midshaft femur cross section showing the extension of spongy MB deep into the marrow cavity and surrounding preexisting trabeculae (T). (**B**) Laying emu, midshaft cross section, with a thin layer of MB on the endosteal bone surface, separated from overlying CB by ELB. (**C**) Ostrich MB arising from CB. Convoluted bony projections surround large cavities and form by continued deposition on hairlike spicules of calcified bone (S). (**D**) MB on endosteal surface of MOR 1125 femur fragment delineated from overlying CB by large vascular sinuses and change in color, texture, and density. (**E**) Emu and (**F**) ostrich bone taken at same aspect as (D), showing morphological distinction between bone types. (**G**) Higher magnification of dinosaur femur fragment in oblique view shows dense CB lined with newly described bone tissue, also seen in oblique view of emu (**H**) and ostrich (**I**) tibia. Ostrich MB is apparently unique in forming longitudinal tubules.

(ELB) as described by Chinsamy *et al*. (*19*) (chicken and emu), or not (ostrich). The innermost layer of MB in the ostrich [adjacent to the endosteal surface of cortical bone (CB)] appears to arise from dense sheets to form tubular structures that parallel the long axis of the bone (Fig. 1I). Thin hairlike spicules (Fig. 1C) of mineralized bone protrude from the tubes and may be intimately involved in their formation from the basal layer. Mineralized spicules were also noted arising from emu MB (fig. S2), but the tubelike structures were not so apparent or distinct. The MB tissues are morphologically distinct from overlying CB and are similarly distributed in both dinosaur (Fig. 1D) and ratite (Fig. 1, E and F) samples. Higher magnifications of *T. rex* (Fig. 1G) and ratite (Fig. 1, H and I) tissues show the open, crystalline, and fibrous structure of these highly vascular tissues, in contrast to the denser CB.

In a fresh fracture, dense and relatively homogenous dinosaur CB is distinct from the loosely organized and highly vascular MB internal to it (Fig. 2A). A distinct layer corresponding to ELB (*19*) separates the two bone types. A large erosion room is visible at this boundary, lined with laminar tissue. An emu bone fragment (Fig. 2B) in similar orientation shows MB tissues with a distinctive, less organized and "crumbly" texture relative to overlying CB. It is interspersed with or laid down between large erosion rooms within the deep cortex and ELB of the tibial shaft. The dense cortex and laminar structure of the ELB are easily distinguished from surrounding MB. The ostrich MB (Fig. 2C) differs in both texture and orientation, with open cavities that are bordered by tubelike bone spicules.

The lacy vascularity of the *T. rex* tissues (Fig. 2D) is consistent with the larger vascular canals and whorled pattern of the emu (Fig. 2E) and especially with the ostrich (Fig. 2F), where wide blood-filled sinuses separate forming bone spicules. In ground section (Fig. 2G), MOR 1125 femur cortical bone is characterized by well-developed multigeneration Haversian systems with obvious and defined cement lines, supporting a mature status for this dinosaur (*2*). A region of decreased vascularity and laminar structure marks the ELB. In contrast, the medullary tissues arising from the ELB are densely vascularized but show no evidence of Haversian remodeling or cement lines, indicating that this tissue is newly deposited, or younger bone. A fresh cut section of emu bone (Fig. 2H) in comparable orientation shows dense CB and vascular, crystalline, and loosely organized MB, separated by a thin, dense, and less vascular ELB. MB in the ostrich (Fig. 2I) is more extensive than in the emu samples, most likely because shelling had not yet begun (*14*). No distinct ELB is visible. MB appears laminar rather than spiculated in Fig. 2I, because the tubules formed by bony spicules are oriented longitudinally rather than in cross section as in Fig. 2F, but it is the same tissue.

Additional pattern similarities are seen in demineralized (*14*) ratite (Fig. 3, B and C) and *T. rex* (Fig. 3A) medullary tissues. In all cases, the matrix is fibrous and randomly organized. The reddish color in extant tissues is due to blood retained in sinuses that separate the bone spicules. The *T. rex* tissues are similarly pigmented, due either to diagenetic alteration or to close association of bony tissues with blood-producing marrow during the life of the dinosaur.

In all MB tissues shown, large vascular sinuses are easily discerned (Fig. 3, D to F), but in the *T. rex*, vascular openings are surrounded by circumferentially oriented matrix

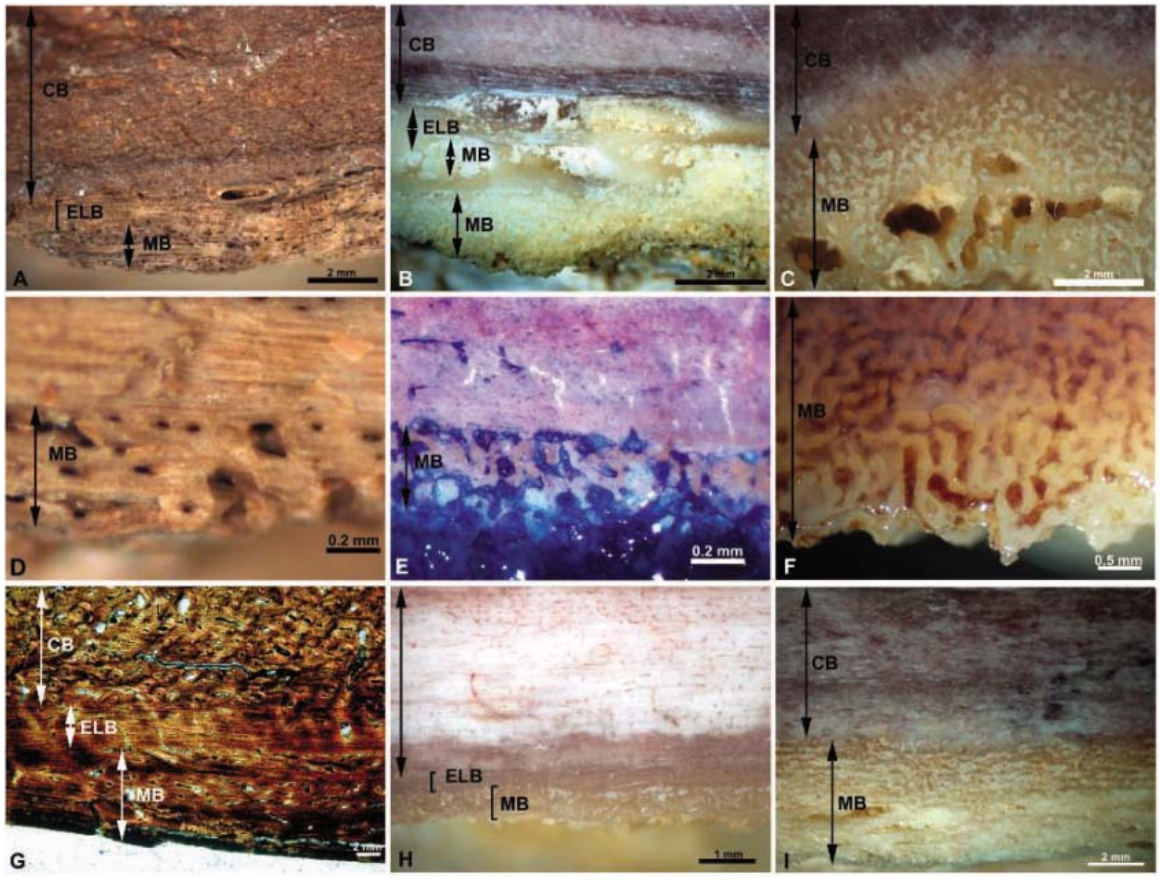

Fig. 2. Dinosaur and ratite comparative views. (**A**) Freshly broken fragment of MOR 1125 shows laminar ELB separating CB and MB. Bone tissues decrease in density internal to the ELB, because of increased vascularity. (**B**) Emu tibia, midshaft section. Erosion rooms extending into ELB are secondarily filled by MB. (**C**) Ostrich bone, midshaft. MB is distinct from CB, but no obvious ELB is visible and several large vascular sinuses are seen. (**D**) Higher magnification of MB region of MOR 1125, showing increased porosity and more random orientation of MB than CB or ELB. (**E**) Emu, stained (*14*) to distinguish bone from infiltrating marrow fat. MB is more vascular than overlying CB and exhibits a random, whorled pattern. (**F**) Ostrich MB, showing relationship of bony spicules to invading blood sinuses, colored red from remnant blood. (**G**) Ground section of MOR 1125. Dense cortical Haversian bone shows second- and third-generation remodeling. ELB separates Haversian bone from more vascular MB. (**H**) Similar orientation of emu femur shows dense CB, distinct ELB, and a thin layer of MB. (**I**) Ostrich MB appears more laminar than in (C) or (F) because of the longitudinal orientation of tubelike medullary spicules.

fibers (Fig. 3D) that are less apparent in extant bone. The ostrich medullary tissues are denser than either the emu (Fig. 3E) or *T. rex* samples, particularly closer to the cortex, but the variation in the size and density of vascular sinuses (Fig. 3F) is similar to that seen in the *T. rex* tissues. In planar view, MOR 1125 undemineralized tissues show a random orientation of fibers, and vascular openings penetrate deep into the tissues (Fig. 3G, inset) and exhibit an unusual doublet or triplet pattern, where multiple vessels penetrate an osteonlike core (arrows), also seen in the emu (Fig. 3H, arrows). The ostrich medullary tissues (Fig. 3I) are more variable, denser, and less random in appearance than those of the emu, but the morphology changes as the tissues extend into the medullary cavity. Close to the cortex (Fig. 3I, inset, and fig. S3), the bone is sheetlike, relatively dense, and punctured by vascular sinuses exhibiting the doublet pattern (arrows) noted above. As tissues extend into the medullary cavity (Fig. 3I), this pattern becomes obscured. Inset bone has been stained (*14*) for better contrast.

In regions of MOR 1125 bone where most of the medullary tissues have eroded (Fig. 3J), patches of denser CB can be seen, emphasizing the random mazelike pattern and large vascular sinuses of medullary tissues, a pattern also seen in the emu bone (Fig. 3K). The ostrich MB shows a similar pattern of bony spicules surrounding large and small blood sinuses (Fig. 3L).

Scanning electron micrographs (*14*) reveal the distinctive grainy texture and disorganized morphology of demineralized *T. rex* and avian MB (Fig. 4). This contrasts with the smooth and fibrous texture of demineralized CB from the same specimens (Fig. 4, E to H). Higher magnifications of demineralized CB (Fig. 4, I to K) emphasize the smooth, fibrous, and more ordered nature of all specimens, although in MOR 1125 (Fig. 4I), degradation is apparent.

MB occurs naturally only in extant female birds, although it varies in amount and distribution among taxa and with ovulatory phase (*5*, *20*). It is chemically, functionally, and structurally distinct from both overlying CB and internal trabecular bone (*21*, *22*). Although "medullary" and "trabecular" bone are terms often used interchangeably in the literature, MB has a larger surface area and is more vascular than other bone types, allowing rapid calcium mobilization (*5*). It is more highly mineralized, with a greater apatite-to-collagen ratio (*5*, *7*, *20*–*22*), and incorporates acidic mucopolysaccharides and glycosaminoglycans that are not present in CB (*5*, *11*). Additionally, the matrix of MB is higher in noncollagenous proteins and lower in collagen, and has a higher collagen III–to–collagen I ratio (*22*) relative to other bone types. If preservation allows, these characteristics will be used as part of ongoing research to chemically distinguish the two bone types in this dinosaur.

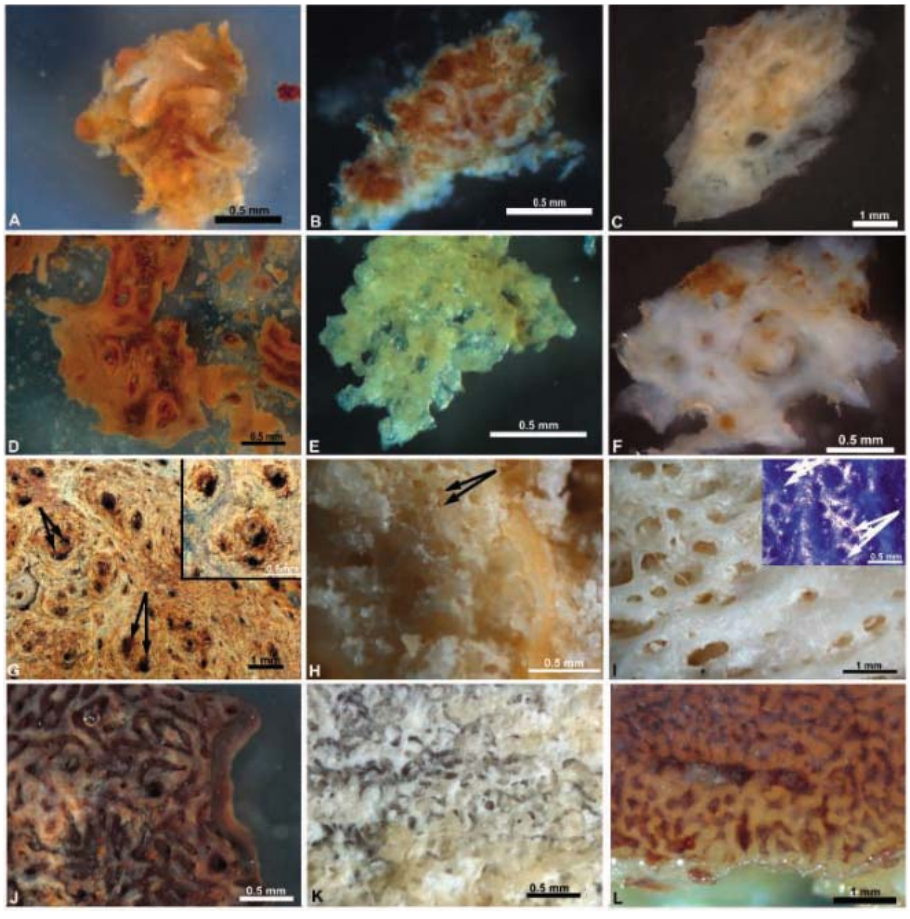

Fig. 3. Dinosaur and ratite MB. (**A**) MOR 1125, (**B**) emu, and (**C**) ostrich demineralized (*14*) MB. The coloration in (B) and (C) results from infiltration of tissues with blood sinuses. (**D**) MOR 1125, partially demineralized, showing enlarged, randomly arranged vascular openings surrounded by circumferential matrix fibers. Partially demineralized (**E**) emu and (**F**) ostrich medullary tissues show extensive vascular penetration, with randomly spaced and varyingly sized vessel openings. (**G**) Plane view of undemineralized dinosaur tissues shows fibrous matrix and an unusual pattern of vascular doublets or triplets within osteonlike structures (arrows). The inset shows variation in depth and diameter of vascular sinuses. (**H**) Undemineralized emu MB shows similar doublet pattern (arrows) and fibrous matrix. The greater depth of field makes focusing difficult. (**I**) Ostrich MB is denser closer to the cortex (inset), where the doublet/triplet pattern of vessels (arrows) is evident, but this becomes obscured by the increasing development of bony tubes and spicules as bone extends further into the medullary cavity. (**J**) Plane view of MOR 1125 shows the partially eroded, fibrous MB distributed across the cortex in a mazelike fashion. (**K**) Emu MB shows white (chloroform-altered) and cream-colored MB in the same mazelike pattern. (**L**) Thicker, randomly oriented tubular spicules of ostrich MB, showing deep penetration and intimate association of blood-containing sinuses.

The existence of avian-type MB in dinosaurs has been hypothesized (*9*, *23*) but not identified. In part, this could be because of taphonomic bias, because the death and fossilization of an ovulating dinosaur would be comparatively rare. Additionally, MB in extant birds is fragile, the spicules separating easily from the originating layer (fig. S1). Dinosaur MB may separate and be lost from overlying CB in a similar manner during diagenesis.

The location, origin, morphology, and microstructure of the new *T. rex* tissues support homology with ratite MB. The *T. rex* tissues line the medullary cavities of both femora of MOR 1125, suggesting an organismal response. The tissues are similar in distribution to those of extant ratites, being more extensive in proximal regions of the bone. They are clearly endosteal in origin, and the microstructure with large vascular sinuses is consistent with the function of MB as a rapidly deposited and easily mobilized calcium source. The random, woven character indicates rapidly deposited, younger bone. Finally, the robustly supported relationship between theropods and extant birds (*15*–*18*, *24*, *25*) permits the application of phylogenetic inference to support the identification of these tissues (*26*, *27*).

The morphology of these dinosaur tissues is not identical to that of extant neognaths

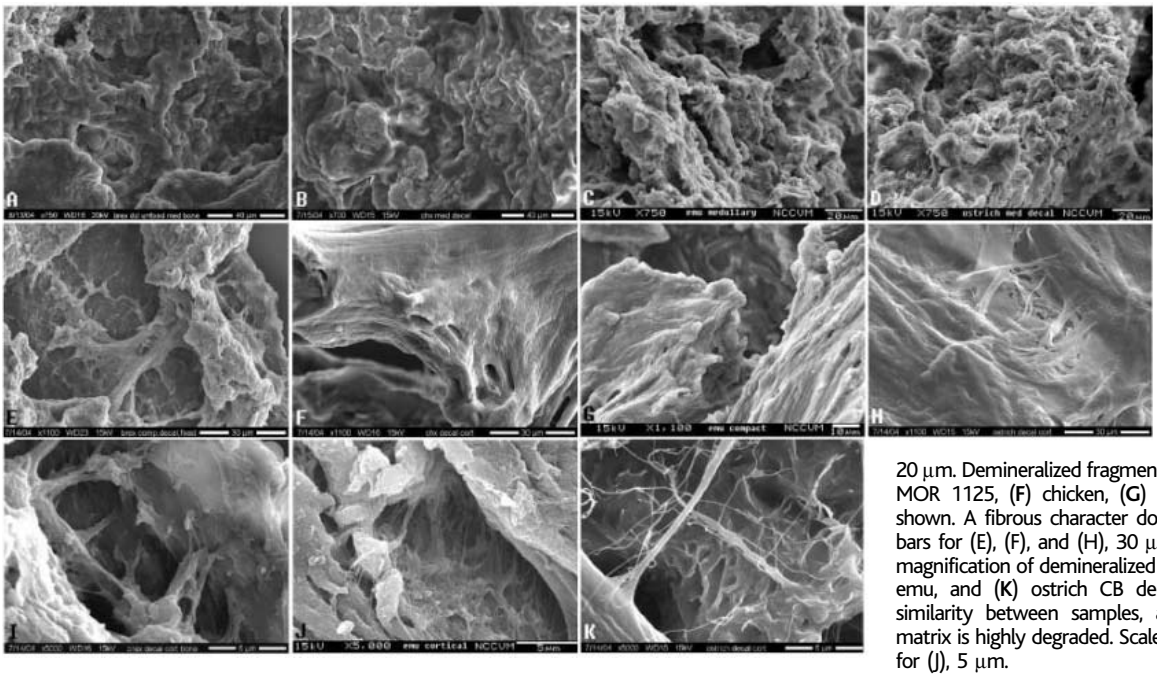

Fig. 4. Scanning electron microscope images of demineralized MB [(A) to (D)] and CB [(E) to (K)]. Demineralized, aldehyde-fixed (*14*) MB tissues from (**A**) MOR 1125, (**B**) extant laying hen, (**C**) emu, and (**D**) ostrich show random, crumbly texture. Organized collagen fiber bundles are not distinct in any sample because of rapid deposition and woven character. Scale bars for (A) and (B), 40 μm; for (C) and (D), 20 μm. Demineralized fragments of cortical bone from (**E**) MOR 1125, (**F**) chicken, (**G**) emu, and (**H**) ostrich are shown. A fibrous character dominates all samples. Scale bars for (E), (F), and (H), 30 μm; for (G), 10 μm. Higher magnification of demineralized CB from (**I**) MOR 1125, (**J**) emu, and (**K**) ostrich CB demonstrates the structural similarity between samples, although the MOR 1125 matrix is highly degraded. Scale bars for (I) and (K), 6 μm; for (J), 5 μm.

(fig. S1), but is more similar to that seen in ratites. *T. rex* medullary tissues are less extensive than those reported for neognaths, which may be explained by many factors. First, there is a wide range of MB morphologies in extant taxa (*20*), varying with both reproductive phase and the position of the egg within the reproductive tract (*6*). Medullary tissues become thinner as shelling progresses and disappear completely with deposition of the last egg. If the same was true of dinosaurs, MOR 1125 may have died toward the end of the laying cycle. Second, MB in extant birds is hypothesized to provide a buffer against excessive and debilitating bone resorption during shelling (*4*, *28*). It is most extensive in smaller taxa with high reproductive rates, because of the demand for rapid mobilization of skeletal calcium for shelling. Extinct theropods produced hard-shelled eggs, as did other dinosaurs and all extant birds (*29*, *30*). Although egg size is not known, eggs were most likely smaller relative to overall body size than in extant birds, resulting in less demand for bone calcium reserves and reducing the need to offset resorption. These factors may also contribute to the smaller ratio of medullary to cortical thickness in theropods than in extant birds. Finally, *T. rex*, although phylogenetically close to extant birds (*15*–*18*, *24*, *25*), was distinct in size, biomechanical constraints, and, to some degree, physiology (*31*); therefore, slight variations in bone and tissue types would be expected.

MB most likely first evolved within the lineage in early, small theropods with high productivity. A relatively thicker tyrannosaur bone cortex would reduce the need for MB, and its presence in MOR 1125 may reflect the retention of a primitive trait. This hypothesis may be tested by examination of the limb bones of the recently reported oviraptor containing eggs in the reproductive tract (*32*).

The existence of MB in crocodiles has been referred to anecdotally (*3*, *21*), but although they do resorb CB during shelling, experimental evidence suggests that they do not form MB (*6*, *9*, *11*, *12*), even after stimulation with estrogen (*33*). The identification of medullary tissues in dinosaurs supports a closer relationship to birds than to other extant archosaurs, sheds light on reproductive strategies of nonavian theropods, and provides an objective means of gender determination in extinct dinosaurs.

References and Notes

1. M. H. Schweitzer, J. L. Wittmeyer, J. R. Horner, J. A. Toporski, *Science* **307**, 1952 (2005).
2. J. R. Horner, K. Padian, *Proc. R. Soc. London Ser. B* **271**, 1875 (2004).
3. T. Yamamoto, H. Nakamura, T. Tsuji, A. Hirata, *Anat. Rec.* **264**, 25 (2001).
4. S. C. Miller, B. M. Bowman, *Dev. Biol.* **87**, 52 (1981).
5. C. G. Dacke *et al.*, *J. Exp. Biol.* **184**, 63 (1993).
6. M. A. Bloom, L. V. Domm, A. V. Nalbandov, W. Bloom, *Am. J. Anat.* **102**, 411 (1958).
7. T. G. Taylor, K. Simkiss, D. A. Stringer, in *Physiology and Biochemistry of the Domestic Fowl (Volume 2)*, D. J. Bell, B. M. Freeman, Eds. (Academic Press, London, 1971), pp. 621–640.
8. E. Bonucci, G. Gherardi, *Cell Tissue Res.* **163**, 81 (1975).
9. A. Chinsamy, P. M. Barrett, *J. Vertebr. Paleontol.* **17**, 450 (1997).
10. A. Ascenzi, C. Francois, D. S. Bocciarelli, *J. Ultrastruct. Res.* **8**, 491 (1963).
11. T. Sugiyama, S. Kusuhara, *Asian-Australas. J. Anim. Sci.* **14**, 82 (2001).
12. T. Ohashi, S. Kusuhara, K. Ishida, *Br. Poult. Sci.* **28**, 727 (1987).
13. J. L. Arias, M. S. Fernandez, *World's Poult. Sci. J.* **57**, 349 (2001).
14. Materials and methods are available as supporting material on *Science* Online.
15. J. A. Gauthier, *Mem. Calif. Acad. Sci.* **8**, 1 (1986).
16. L. M. Chiappe, *Nature* **378**, 349 (1995).
17. K. Padian, L. M. Chiappe, *Sci. Am.* **278**, 38 (1998).
18. J. Cracraft, J. A. Clarke, in *New Perspectives on the Origin and Early Evolution of Birds. Proceedings of the International Symposium in Honor of J. H. Ostrom*, J. Gauthier, L. F. Gall, Eds. (Special Publication of the Peabody Museum of Natural History, New Haven, CT, 2001), pp. 143–147.
19. A. Chinsamy, L. M. Chiappe, P. Dodson, *Paleobiology* **21**, 561 (1995).
20. H. Schraer, S. J. Hunter, *Comp. Biochem. Physiol. A* **82**, 13 (1985).
21. C. C. Whitehead, *Poult. Sci.* **83**, 193 (2004).
22. L. Knott, A. J. Bailey, *Br. Poult. Sci.* **40**, 371 (1999).
23. D. M. Martill, M. J. Barker, C. G. Dacke, *Nature* **379**, 778 (1996).
24. C. A. Forster, S. D. Sampson, L. M. Chiappe, D. W. Krause, *Science* **279**, 1915 (1998).
25. P. C. Sereno, *Annu. Rev. Earth Planet. Sci.* **25**, 435 (1997).
26. H. N. Bryant, A. P. Russell, *Philos. Trans. R. Soc. London Ser. B* **337**, 405 (1992).
27. L. M. Witmer, in *Functional Morphology in Vertebrate Paleontology*, J. J. Thomason, Ed. (Cambridge Univ. Press, New York, 1995), pp. 19–33.
28. S. Wilson, B. H. Thorpe, *Calcif. Tissue Int.* **62**, 506 (1998).
29. K. Carpenter, Ed., *Eggs, Nests, and Baby Dinosaurs: A Look at Dinosaur Reproduction* (Indiana Univ. Press, Bloomington, IN, 1999).
30. K. E. Mikhailov, *Spec. Pap. Palaeontol.* **56**, 1 (1997).
31. M. H. Schweitzer, C. L. Marshall, *J. Exp. Zoolog. Part B Mol. Dev. Evol.* **291**, 317 (2001).
32. T. Sato, Y. Chang, X. Wu, D. Zelenitsky, Y. Hsiao, *Science* **308**, 375.
33. R. M. Elsey, C. S. Wink, *Comp. Biochem. Biophys.* **84A**, 107 (1986).

34. We thank C. Ancell, J. Barnes, D. Enlow, J. Flight, A. Friederichs, B. Harmon, L. Knott, E. Lamm, N. Myrhvold, A. de Ricqles, A. Steele, and T. Sugiyama for insight and assistance, and D. Brown (Carlhaven Farms) and J. Perkins (Perkins Ostrich) for ratite specimens. R. Avci (Image and Chemical Analysis Laboratory, Montana State University) and M. Dykstra [Laboratory for Advanced Electron and Light Optical Methods, North Carolina State University (NCSU) College of Veterinary Medicine] provided scanning electron micro-

scope access. We also thank J. Fountain and K. Padian for editorial advice. The ground section of MOR 1125 was provided by Quality Thin Sections, and the laying hen demineralized thin sections were provided by J. Barnes (NCSU College of Veterinary Medicine). Site access was provided by the Charles M. Russell National Wildlife Refuge. The research was funded by NCSU as well as by grants from N. Myhrvold (J.R.H.) and NSF (M.H.S.).

Supporting Online Material
www.sciencemag.org/cgi/content/full/308/5727/1456/DC1
Materials and Methods
Figs. S1 to S3

11 March 2005; accepted 21 April 2005
10.1126/science.1112158

Ivory-billed Woodpecker (*Campephilus principalis*) Persists in Continental North America

John W. Fitzpatrick,[1]* Martjan Lammertink,[1,2] M. David Luneau Jr.,[3] Tim W. Gallagher,[1] Bobby R. Harrison,[4] Gene M. Sparling,[5] Kenneth V. Rosenberg,[1] Ronald W. Rohrbaugh,[1] Elliott C. H. Swarthout,[1] Peter H. Wrege,[1] Sara Barker Swarthout,[1] Marc S. Dantzker,[1] Russell A. Charif,[1] Timothy R. Barksdale,[6] J. V. Remsen Jr.,[7] Scott D. Simon,[8] Douglas Zollner[8]

The ivory-billed woodpecker (*Campephilus principalis*), long suspected to be extinct, has been rediscovered in the Big Woods region of eastern Arkansas. Visual encounters during 2004 and 2005, and analysis of a video clip from April 2004, confirm the existence of at least one male. Acoustic signatures consistent with *Campephilus* display drums also have been heard from the region. Extensive efforts to find birds away from the primary encounter site remain unsuccessful, but potential habitat for a thinly distributed source population is vast (over 220,000 hectares).

The ivory-billed woodpecker is one of seven North American bird species that are suspected or known to have become extinct since 1880 (*1*). One of the world's largest woodpeckers, this species of considerable beauty and lore was uncommon but widespread across lowland primary forest of the southeastern United States until midway through the 19th century (*2*, *3*). Its disappearance coincided with the systematic annihilation of virgin tall forests across the southeastern United States between 1880 and the 1940s. Relentless pursuit by professional collectors accelerated the species' decline from 1890 to the early 1920s. The last well-documented population occupied a stand of old-growth bottomland hardwood forest in northeastern Louisiana (the Singer Tract) during the late 1930s (*3*–*6*). That population disappeared as the Singer Tract was logged amid cries for protection of both forest and bird. The final individual in the Singer Tract, an unpaired female, was last seen in cut-over forest remnants in 1944 (*7*).

A resident subspecies of ivory-billed woodpecker (*Campephilus principalis bairdii*) occupied tall forests throughout Cuba, and a small population was mapped and photographed in eastern Cuba as late as 1956 (*8*). Fleeting observations of at least two individuals in 1986 and 1987 by several experts are widely accepted as valid (*9*), but repeated efforts to confirm the continued existence of that population have failed (*10*).

Anecdotal reports of ivory-billed woodpeckers in the southern United States continue to this day. Such reports are suspect because of the existence and relative abundance throughout this region of the superficially similar pileated woodpecker (*Dryocopus pileatus*). Three reports were accompanied by physical evidence, but their veracity continues to be questioned [supporting online material (SOM) text]. Thus, no living ivory-billed woodpecker has been conclusively documented in continental North America since 1944.

At approximately 13:30 Central Standard Time (CST) on 11 February 2004, while kayaking alone on a bayou in the Cache River National Wildlife Refuge, Monroe County, Arkansas, G. Sparling spotted an unusually large red-crested woodpecker flying toward him and landing near the base of a tree about 20 m away. Several field marks suggested that the bird was a male ivory-billed woodpecker (SOM text), and Sparling hinted at his sighting on a Web site. T. Gallagher and B. Harrison were struck by the apparent authenticity of this sighting and arranged to be guided through the region by Sparling. At 13:15 CST on 27 February 2004, within 0.5 km of the original sighting, an ivory-billed woodpecker (sex unknown) flew directly in front of their canoe with the apparent intention of landing on a tree near the canoe, thereby fully revealing its dorsal wing pattern. The bird instead veered into the forest, apparently landed briefly several times (each time blocked from the observers' sight by trees), and then flew off (SOM text and fig. S1). Efforts to locate the bird over the next several days failed, but subsequent surveys by teams of experienced observers yielded a minimum of five additional visual encounters between 5 April 2004 and 15 February 2005 (SOM text). All seven convincing sightings were within 3 km of one another.

At 15:42 Central Daylight Time on 25 April 2004, M. D. Luneau secured a brief but crucial video of a very large woodpecker perched on the trunk of a water tupelo (*Nyssa aquatica*), then fleeing from the approaching canoe (fig. S2 and movie S1). The woodpecker remains in the video frame for a total of 4 s as it flies rapidly away. Even at its closest point, the woodpecker occupies only a small fraction of the video. Its images are blurred and pixilated owing to rapid motion, slow shutter speed, video interlacing artifacts, and the bird's distance beyond the video camera's focal plane. Despite these imperfections, crucial field marks are evident both on the original and on deinterlaced and magnified video fields (*11*) (fig. S3). At least five diagnostic features allow us to identify the subject as an ivory-billed woodpecker.

1) Size. When the woodpecker first begins to take flight from the left side of a tupelo trunk, two video fields reveal the dorsal surface of the right wing and a large black tail (Fig. 1). The minimum distances between the "wrist" and the tip of its tail—measured independently on each of the two video fields and compared to known scales (the diameter of the tupelo trunk at two places)—are 34 to 38 cm. These values exceed comparable values for the pileated woodpecker and correspond to the upper range for the ivory-billed woodpecker (fig. S4).

[1]Cornell Laboratory of Ornithology, Cornell University, 159 Sapsucker Woods Road, Ithaca, NY 14850, USA. [2]Institute for Biodiversity and Ecosystem Dynamics, Universiteit van Amsterdam, Mauritskade 61, 1092 AD Amsterdam, Netherlands. [3]Department of Engineering Technology and Department of Information Technology, University of Arkansas at Little Rock, Little Rock, AR 72204, USA. [4]Department of Communications, Oakwood College, Huntsville, AL 35896, USA. [5]107 Stillmeadow Lane, Hot Springs, AR 71913, USA. [6]Birdman Productions, Post Office Box 1124, 65 Mountain View Drive, Choteau, MT 59422, USA. [7]Museum of Natural Science, Louisiana State University, Baton Rouge, LA 70803, USA. [8]The Nature Conservancy, Arkansas Chapter, 601 North University Avenue, Little Rock, AR 72205, USA.

*To whom correspondence should be addressed. E-mail: jwf7@cornell.edu

2) Wing pattern at rest. These same two video fields (Fig. 1) reveal an extensive posterior white region on the opening wing, sharply bordered by an anterior black patch that corresponds to upper wing coverts and wrist area. Such extensive white on the secondary flight feathers is consistent with both sexes of ivory-billed woodpecker. The only comparably large white patch anywhere on a pileated woodpecker is the underwing lining, which would be obscured at this early stage of wing extension, and any barely visible portion of the white underwing should appear anteriorly, not posteriorly, on the wing.

3) Wing pattern in flight. During the first 1.2 s of flight, the fleeing woodpecker completes 10 full wingbeats before being obscured temporarily by a tupelo trunk (fig. S3). All visible wingbeats reveal extensive white patches on the posterior dorsal and ventral wing surfaces, representing entirely white secondary and innermost primary flight feathers. Body and wing tips are black. Video images of flying pileated woodpeckers, including our model during reenactment (*11*), consistently reveal a different pattern: Ventrally, white wing-linings are bordered by a dark trailing edge. Dorsally, a white band (proximally narrow, distally broadening into a wide spot along the base of the inner primaries) is surrounded by an otherwise all-dark upper wing surface (Fig. 2).

4) White plumage on dorsum. As the fleeing woodpecker gains elevation (video fields 966.7 to 1016.7 in fig. S3), white plumage is clearly evident on the back between the wings. Ivory-billed woodpeckers have a pair of longitudinal dorsal stripes that approach one another on the middle and lower back (Fig. 2), producing a white area that is visible on a dorsal view of a fleeing bird. Pileated woodpeckers have lateral white marks on the sides of the head and neck but lack any trace of white on the dorsum.

5) Black-white-black pattern of the perched bird. In the Luneau video (26 to 21 s before the zero point in fig. S3), a blurry white object bordered above and below by black is visible on a distant tupelo trunk (fig. S5). The object was not present during subsequent inspections of the site, when we determined that it had been situated 4 m above the water, on a tree located 3 m from the trunk from which the woodpecker flew 21 s later. We interpret the object to be a large perched woodpecker. Among candidate species, the observed pattern fits only that of the ivory-billed woodpecker. Placing a life-sized model on the same tree trunk produced a similar image (fig. S5).

Two other features suggesting the ivory-billed woodpecker are evident on the Luneau video, but we do not currently regard them as diagnostic, in part because we lack suf-

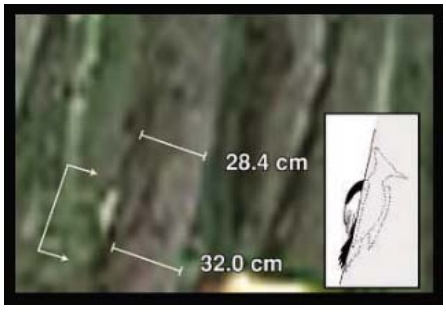

Fig. 1. Zoomed segment of frame 33.3 from the Luneau video (fig. S3), one of two consecutive frames in which the woodpecker's right wing is revealed immediately before flight. The large white area represents a dorsolateral view of the secondary flight feathers. Bracketed arrows mark the exposed distance between a spot near the bird's wrist and the tip of its tail, which is thrusting laterally upon takeoff. Parallel white bars identify two diameters of the tree trunk, measured later for scale. The inset sketch (by J. Fitzpatrick) interprets the approximate position of the bird, including unrevealed portions (dotted lines and shaded background).

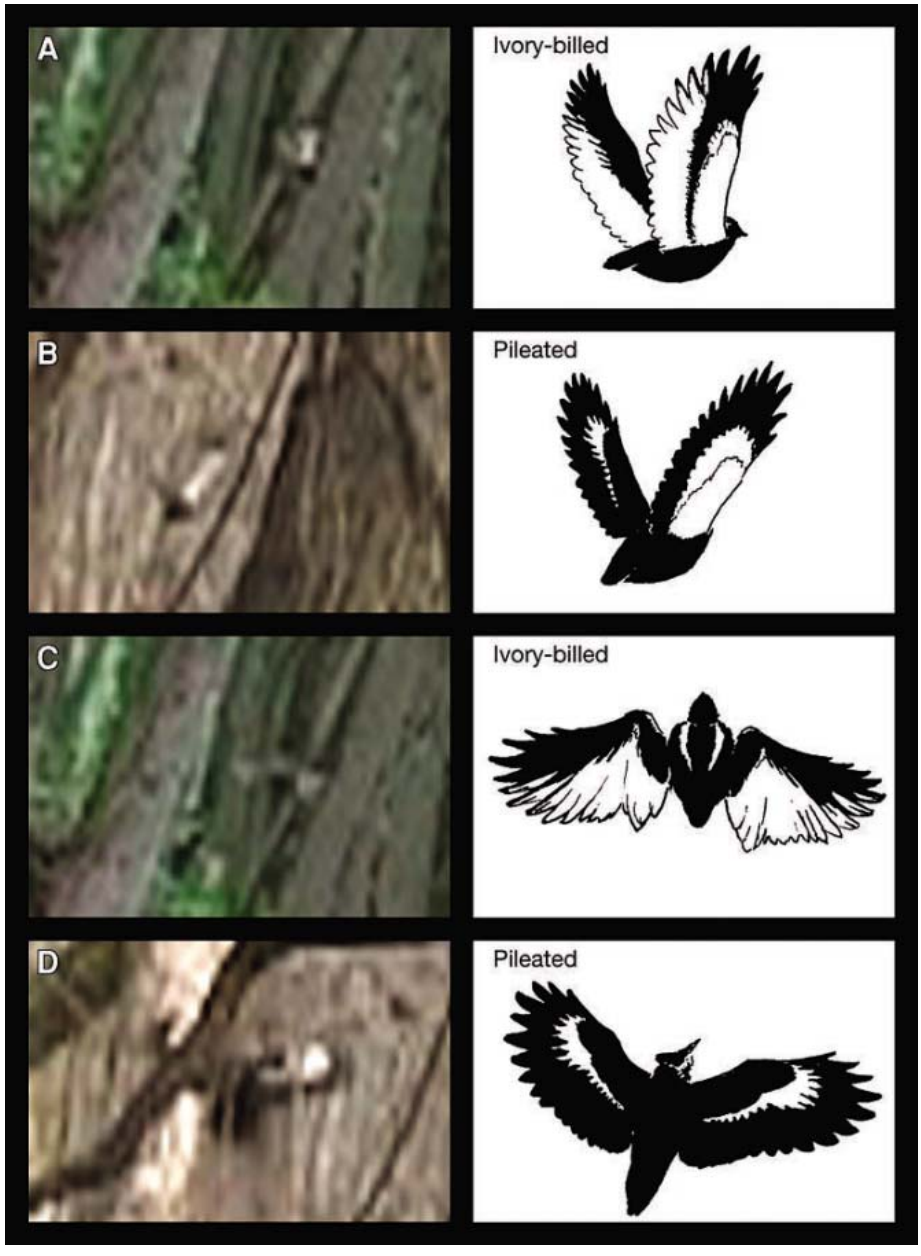

Fig. 2. Selected video frames of the woodpecker in the Luneau video [(**A** and **C**), left column], comparably distant and imperfect video frames of a pileated woodpecker recorded in the study area in similar postures [(**B** and **D**), left column], and interpretative sketches by J. Fitzpatrick (right column). With these distances and light conditions, bleeding tends to exaggerate the apparent extent of white in the wings. However, careful study of these and numerous other video examples consistently reveals dark trailing edges on both upper and lower wing surfaces of pileated woodpeckers—features not present on the bird in the Luneau video.

ficiently comparable data for objective comparison with the pileated woodpecker. First, the estimated wingspan of the fleeing woodpecker exceeds 71 cm (*11*), a value that is within the published range for the ivory-billed woodpecker and at or above the maximum published wingspan of the pileated woodpecker. Second, the video shows a woodpecker on a sustained escape flight that is rapid (nine wingbeats per second) and direct for at least 4 s. This flight pattern matches many anecdotal descriptions of the ivory-billed woodpecker (*2*–*5*) and is atypical for the pileated woodpecker.

We considered and rejected the hypothesis that the sightings and video can be explained by a "piebald" or partially leucistic pileated woodpecker with symmetric white patches on wings and back approximately matching the pattern of an ivory-billed woodpecker. Several observers described the bird they saw as conspicuously larger than a pileated woodpecker, and the video bears this out (fig. S4). We are unaware of any examples of extensively and symmetrically piebald pileated woodpeckers in museum collections or the literature (*12*, *13*). During 14 months of nearly continuous fieldwork by dozens of observers, pileated woodpeckers were encountered virtually daily throughout the study region, where they are common and noisy residents occupying permanent territories. We would expect any strikingly plumaged leucistic individual in the study area to have been observed regularly.

Despite substantial survey efforts by skilled observers after the original sightings, we obtained minimal acoustic evidence of the ivory-billed woodpecker in the region. Distinctive "double-knock" display drums characteristic of most members of the genus *Campephilus*, including the ivory-billed woodpecker, were heard sporadically by seven different observers between March 2004 and March 2005, and series of these display drums were heard on three occasions (SOM text). No observer has positively heard or recorded nasal "kent" notes that are typical of the species (*5*). During late spring 2004, and again from 16 December 2004 through the present, we acoustically monitored a 20-km^2 region of forest in the vicinity of the sightings and potential habitat elsewhere in the White River and Cache River refuge complex (*11*). Recordings of series of "kent" notes exist in these data but cannot be positively distinguished from exceptional calls by blue jays (*Cyanocitta cristata*).

Our field surveys (*11*) to date have revealed little about population size or breeding. Work covering substantial portions of the Cache River and White River National Wildlife Refuges from December 2004 through April 2005 yielded remarkably few encounters. Except for the flurry of sightings and the video in April 2004, our surveys have provided no evidence for the predictable occurrence of ivory-billed woodpeckers in a localized area and no evidence of a mated pair. Indeed, we cannot rule out the possibility that all of our fleeting encounters involved the same bird. In three sightings (including the initial one of a perched bird), the observer saw red on the hindcrest, which indicates that at least one male exists (the female's crest is all black). The life spans of large woodpeckers rarely exceed 15 years (*14*). Hence, the individual(s) documented here probably hatched no earlier than the 1990s and could even represent dispersing nonbreeders hatched in the 21st century.

The difficulty of detecting ivory-billed woodpeckers in the Big Woods may be a consequence of extremely low population density. In the Singer Tract's mature bottomland hardwoods, Tanner documented only one pair per 16 km^2 of forest (*5*). The present Big Woods landscape consists of patches of mature forest amid a matrix of regenerating trees of various ages; its resource base for ivory-billed woodpeckers is much reduced as compared to that of the Singer Tract. Although we failed to find occupied roost holes in an intensive search of over 41 km^2 of forest around the sighting area (*11*), we have covered only a small part of the available potential habitat. Individuals may roost far from where our encounters have been concentrated. Large woodpeckers are known to adapt to fragmented forest landscapes by expanding their home range sizes (*15*, *16*) (SOM text). Ivory-billed woodpeckers are capable of rapid and sustained flight and were known to move widely in search of recently dead large trees (*2*–*5*). Individuals in the Big Woods could cover hundreds of square kilometers to accommodate their resource requirements. Such low densities would, in turn, explain the paucity of vocalizations and drumming signals we encountered.

The Big Woods (fig. S6) (at 220,000 ha, the second-largest contiguous area of bottomland forest in the Mississippi River basin) includes 20 distinct types of swamp and bottomland hardwood forests (*17*). About 40% of the forest is currently approaching maturity (with the oldest trees being over 60 years old). The remainder, although younger (20 to 60 years), is growing rapidly. An additional 40,000 ha of adjacent or nearby land has been reforested in the past decade and is in early successional stages. If a few breeding pairs do exist, most of the conditions believed to be required for successful breeding and population growth (*5*) are becoming more available to them. Strategic additions to the public refuge system and successful restoration efforts by both public and private landowners are reestablishing mature hardwood forest, the crucial foraging habitat for ivory-billed woodpeckers (*5*). Increasing the extent and diversity of genuinely mature bottomland forest with large, very old trees and substantial standing dead and dying timber may allow future generations to see the awe-inspiring woodpecker again gracing old-growth treetops.

References and Notes

1. The other species are the Labrador duck (*Camptorhynchus labradorius*), Eskimo curlew (*Numenius borealis*), Carolina parakeet (*Conuropsis carolinensis*), passenger pigeon (*Ectopistes migratorius*), Bachman's warbler (*Vermivora bachmanii*), and dusky seaside sparrow (*Ammodramus nigrescens*).
2. J. A. Jackson, *The Birds of North America*, no. 711, A. Poole, F. Gill, Eds. (Birds of North America, Philadelphia, 2002).
3. J. A. Jackson, *In Search of the Ivory-billed Woodpecker* (Smithsonian Institution Press, Washington, DC, 2004).
4. A. A. Allen, P. P. Kellogg, *Auk* **54**, 164 (1937).
5. J. T. Tanner, *The Ivory-billed Woodpecker, Research Report No. 1* (National Audubon Society, New York, 1942).
6. P. Hoose, *The Race to Save the Lord God Bird* (Farrar, Straus, and Giroux, New York, 2004).
7. D. Eckelberry, in *Discovery: Great Moments in the Lives of Outstanding Naturalists*, J. K. Terres, Ed. (Lippincott, Philadelphia, 1961), pp. 195–207.
8. G. R. Lamb, *The Ivory-billed Woodpecker in Cuba* (International Commission on Bird Preservation, Pan-American Section, Research Report No. 1, New York, 1957).
9. American Ornithologists' Union, *Checklist of North American Birds* (American Ornithologists' Union, Washington, DC, ed. 7, 1998).
10. M. Lammertink, A. R. Estrada, *Bird Conserv. Int.* **5**, 53 (1995).
11. Materials and methods are available as supporting material on *Science* Online.
12. E. L. Bull, J. A. Jackson, *The Birds of North America*, no. 148, A. Poole, F. Gill, Eds. (Academy of Natural Sciences and American Ornithologists' Union, Philadelphia, 1995).
13. N. F. R. Snyder and H. A. Snyder (*18*) observed a pileated woodpecker in Florida with cream-colored secondaries, except for two normally pigmented black ones on the left wing.
14. D. Blume, *Schwarzspecht, Grüspecht, Grauspecht* (Westarp Wissenshaften, Magdeburg, Germany, 1996).
15. M. Tjernberg, K. Johnsson, S. G. Nilsson, *Ornis Fenn.* **70**, 155 (1993).
16. H. Christensen, *Dan. Ornitol. Foren. Tidsskr.* **96**, 187 (2002).
17. *Conservation Planning in the Mississippi River Alluvial Plain* (The Nature Conservancy, Washington, DC, 2002).
18. *Birds of Prey: Natural History and Conservation of North American Raptors* (Voyageurs Press, Stillwater, MN, 1991), p. 111.

19. We gratefully acknowledge financial support from J. Barksdale, R. Berry, I. Cumming, M. and J. Field, K. Gooch, S. and I. Johnson, E. and L. Morgens, J. Norris, H. and W. Paulson, E. W. Rose III, J. Ruthven, C. and L. Sant, R. and V. Sant, T. Spahr, C. and B. Ward, and the membership of the Cornell Laboratory of Ornithology. Further acknowledgments are listed in the SOM. J.W.F. is a past member of the Board of Governors, a Trustee of the Florida Chapter, and a donor to the Nature Conservancy; M.L.'s wife is currently employed as a research technician at the Nature Conservancy. M.D.L., B.R.H., and G.M.S. hold contracts from the Nature Conservancy to perform inventories of the study area mentioned in this Report.

Supporting Online Material

www.sciencemag.org/cgi/content/full/1114103/DC1
Materials and Methods
SOM Text
Acknowledgments
Figs. S1 to S6
Movie S1
References and Notes

8 April 2005; accepted 27 April 2005
Published online 28 April 2005;
10.1126/science.1114103
Include this information when citing this paper.

Accelerated Intestinal Epithelial Cell Turnover: A New Mechanism of Parasite Expulsion

Laura J. Cliffe,[1] Neil E Humphreys,[1] Thomas E. Lane,[2] Chris S. Potten,[3] Cath Booth,[3] Richard K. Grencis[1]*

The functional integrity of the intestinal epithelial barrier forms a major defense against invading pathogens, including gastrointestinal-dwelling nematodes, which are ubiquitous in their distribution worldwide. Here, we show that an increase in the rate of epithelial cell turnover in the large intestine acts like an "epithelial escalator" to expel *Trichuris* and that the rate of epithelial cell movement is under immune control by the cytokine interleukin-13 and the chemokine CXCL10. This host protective mechanism against intestinal pathogens has implications for our wider understanding of the multifunctional role played by intestinal epithelium in mucosal defense.

Worm infections are among the most prevalent of all known diseases (*1*). *Trichuris trichuria*, a cecal-dwelling parasitic nematode, actively penetrates the intestinal epithelium, forming syncitial tunnels through which they move and feed. The intestinal epithelium is under continual renewal. Enterocytes migrate luminally, undergoing proliferation, differentiation, and maturation before undergoing programmed cell death and extrusion into the intestinal lumen (epithelial cell turnover) (*2*). The mechanisms through which turnover is controlled remain elusive.

After infection with *T. muris*, the murine model for human whipworm, mouse strains that generate a T helper 2 (TH2) immune response expel their parasites; conversely, mice that generate a TH1 immune response are highly susceptible and maintain infection to chronicity. Interleukin-13 (IL-13) plays a critical role in parasite expulsion (*3*, *4*), and interferon-γ (IFN-γ) is essential for progression to chronic infection (*5*). The actual effector mechanisms by which parasites are expelled from the intestine remain to be defined, however. Antibody, eosinophils, natural killer cells, γδ T cells, and mast cells are not essential (*6*–*8*).

We now ask if an elevation in the rate of intestinal epithelial cell turnover acts as an epithelial escalator to displace worms from their optimal niche within the intestine, causing their eventual expulsion by rapidly removing them together with their immediate habitat, the intestinal epithelium. In addition, we assessed whether the increase in rate of turnover was under immune control.

Initially, the levels of epithelial cell proliferation within the cecum were assessed in mice susceptible to infection (AKR) and mice resistant to infection (BALB/c). AKR mice maintained infection to patency, whereas in the BALB/c, expulsion was under way at day 14 and complete by day 21 after infection. In the BALB/c strain, we observed a transient increase in the percentage of cecal epithelial cells undergoing proliferation, with levels returning to baseline following expulsion. However, with the persistence of worms in AKR mice, an elevation in proliferation was evident (Fig. 1, A and B), coincident with the development of crypt-cell hyperplasia throughout the cecum (*9*) (fig. S1).

In a bromodeoxyuridine (BrdU) pulse-chase experiment (*10*), the rate of cell turnover was elevated in both strains of mouse after infection, although the increase was almost double in the resistant strain at day 14, the time of worm expulsion (Fig. 1, C and D), when compared with the susceptible AKR strain. Indeed, in the BALB/c mouse, a greater loss of cells from the proliferative compartment (Fig. 1F, positions 0 to 10) and a large net gain of labeled cells higher up the crypt axis clearly illustrated that cells

[1]Faculty of Life Sciences, University of Manchester, Manchester M13 9PT, UK. [2]Department of Molecular Biology and Biochemistry, University of California Irvine, 3205 McGaugh Hall, Irvine, CA 92697, USA. [3]Epistem Limited, Incubator Building, Grafton Street, Manchester, M13 9XX, UK.

*To whom correspondence should be addressed. E-mail: Richard.K.Grencis@manchester.ac.uk

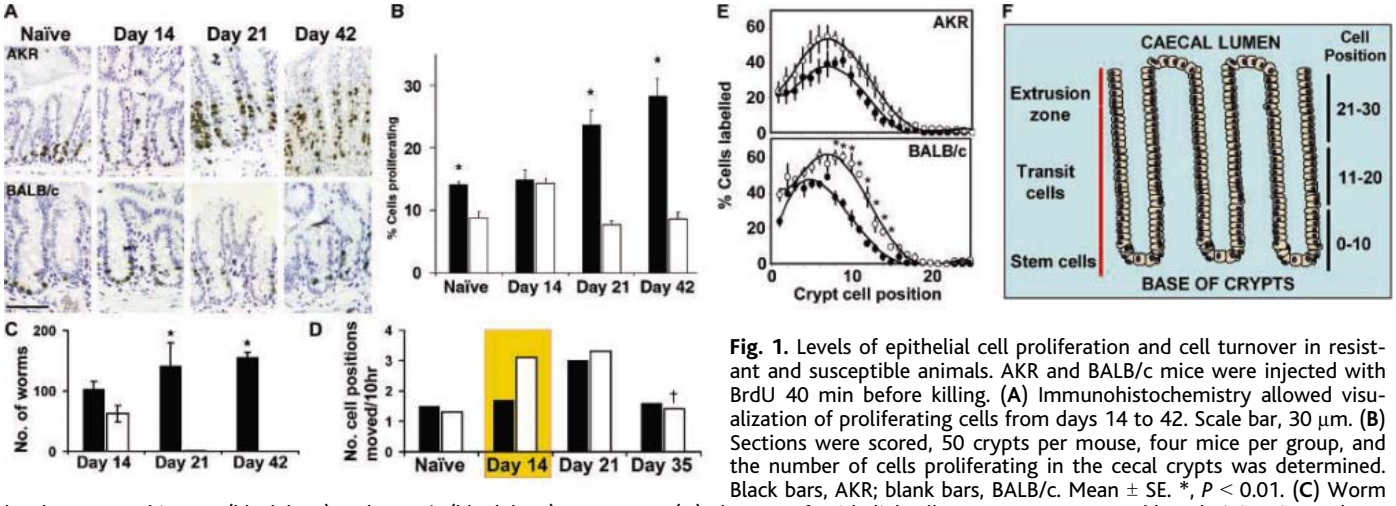

Fig. 1. Levels of epithelial cell proliferation and cell turnover in resistant and susceptible animals. AKR and BALB/c mice were injected with BrdU 40 min before killing. (**A**) Immunohistochemistry allowed visualization of proliferating cells from days 14 to 42. Scale bar, 30 μm. (**B**) Sections were scored, 50 crypts per mouse, four mice per group, and the number of cells proliferating in the cecal crypts was determined. Black bars, AKR; blank bars, BALB/c. Mean ± SE. *, $P < 0.01$. (**C**) Worm burden assessed in AKR (black bars) and BALB/c (blank bars). Mean ± SE. (**D**) The rate of epithelial cell turnover was assessed by administering BrdU to mice either 40 min or 12 hours before killing. With a position-based analysis, the rate of movement was expressed as number of cell positions moved per 10 hours. AKR, black bars; BALB/c, blank bars. Day 14 is a critical time for parasite expulsion. †, data point for day 28. (**E**) Positional distribution of labeled cells in AKR and BALB/c mice day 14, expressed as percentage of cells at each position (0 to 30) that were labeled. Black circles, 40 min; open circles, 12 hours. 50 crypts per animal were scored. *, $P < 0.01$. (**F**) Schematic diagram of epithelial crypts depicting cell positions and transit regions. Data in all panels are mean ± SE; four animals per group.

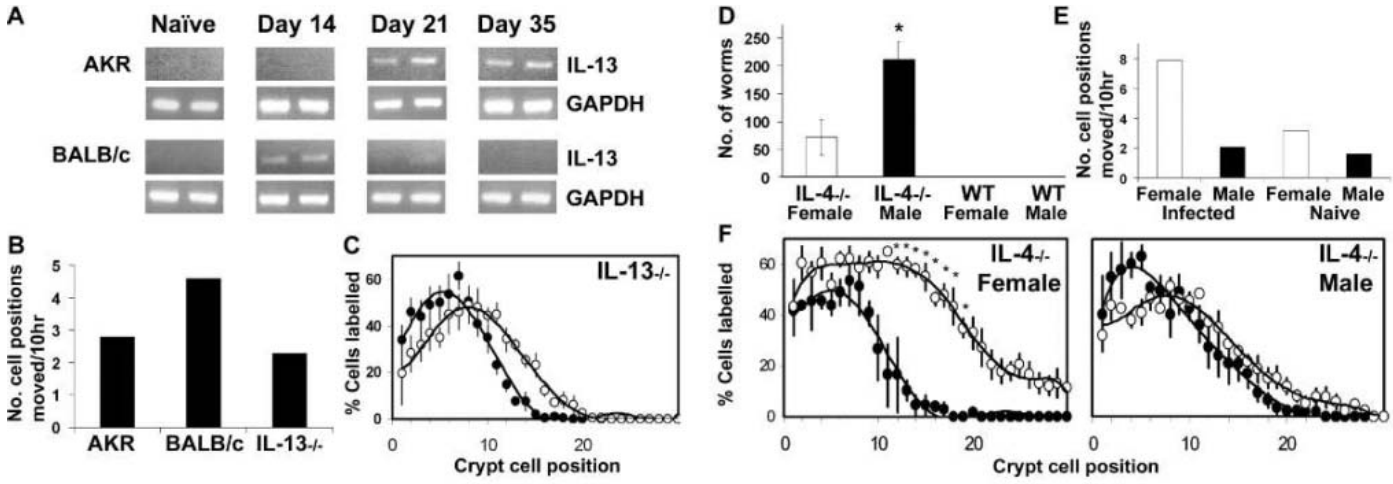

Fig. 2. Importance of IL-13 and GAPDH in epithelial cell turnover. (**A**) Expression of IL-13 in gut assessed by reverse transcription polymerase chain reaction (RT-PCR) in AKR and BALB/c mice. Each lane represents an individual mouse. (**B**) The rate of epithelial cell turnover in IL-13$^{-/-}$ mice, day 14. (**C**) Percentage of labeled cells recorded at each position (0 to 30), day 14 in IL-13$^{-/-}$ animals. Black circles, 40 min; open circles, 12 hours. (**D**) Worm burden in IL-4$^{-/-}$ female and male animals and wild-type counterparts, day 28. *, $P < 0.05$. (**E**) The rate of epithelial cell turnover assessed in male (black bars) and female (blank bars) IL-4$^{-/-}$ mice, both naïve and day 28. (**F**) Percentage of labeled cells recorded at each cell position (0 to 30) in IL-4$^{-/-}$ female and male mice, day 28. Black circles, 40 min; open circles, 12 hours. *, $P < 0.01$, IL-4$^{-/-}$ female versus male 12-hour BrdU pulse. Data in panels (B) to (F) are mean ± SE; four animals per group.

Table 1. Net change in percentage of labeled cells in each region over 12 hours. The movement of cells up the crypts was determined by calculating the percentage of cells labeled at each position 40 min and 12 hours after the BrdU pulse. By subtracting the values at 40 min from those at 12 hours, the net loss (–) or net gain (+) of cells from one region to the next was ascertained. Day column is days after infection.

Day	Mouse strain and treatment	Net loss (–) or net gain (+) of cells (%)		
		Crypt-cell position		
		0–10	11–20	21–30
14	AKR	+4	+1.50	+0.99
14	BALB/c	–25.80	+24.39	+5.52
14	IL-13$^{-/-}$	–4.16	+3.29	+0.87
28	IL-4$^{-/-}$ female	–40.18	+24.78	+15.40
28	IL-4$^{-/-}$ male	–14.78	+9.30	+5.48
21	AKR+ control Ig	–26.05	+21.55	+4.50
21	AKR+ mAb to CXCL10	–46.62	+23.95	+21.87
21	SCID+ control Ig	–25.25	+17.25	+8.00
21	SCID+ mAb to CXCL10	–0.48	+13.10	+27.38

were migrating at a much faster rate in resistant animals (Table 1 and Fig. 1E). Moreover, although there was significant crypt hyperplasia in the AKR as infection progressed, this was not seen in BALB/c mice. In fact, a small decrease in crypt size was repeatedly seen on day 14, consistent with an elevation in turnover (fig. S1). In the BALB/c mouse, the parasite is found in the lower/mid region of the crypt at the time the increase in turnover is occurring in this compartment. The elevated rate of turnover seen at day 21 in the AKR strain, to a level comparable to the BALB/c at day 14, suggested that at this later timepoint the level of turnover is not sufficient to displace the parasites, which by now are considerably larger. Between days 14 and 21, *T. muris* will have quadrupled in length and undergone a further molt. They reside much higher in the crypt and are not in the compartment where the fastest movement of cells is occurring (Table 1 and fig. S2). It is also interesting to note that in both AKR and BALB/c mice, the rate of turnover returned to naïve levels, despite the obvious difference in the presence (AKR) and absence (BALB/c) of worms in the two strains (Fig. 1, C and D). The slow rate of epithelial turnover and high level of proliferation explains the development of crypt-cell hyperplasia associated with chronicity.

IL-13 is a key mediator of gut nematode immunity (*3*, *4*) and is expressed in the intestine of BALB/c mice at the time of worm expulsion (Fig. 2A). IL-13$^{-/-}$ mice and wild-type (BALB/c) mice were infected with 200 *T. muris* eggs, and the rate of turnover was assessed at day 14 (Fig. 2, B and C, and Table 1). It was clear that the rate of turnover in these animals resembled that of a susceptible AKR and not the resistant wild-type BALB/c, demonstrating a clear role for IL-13.

To assess the relative roles of IL-4 and IL-13 in the response, we examined the capacity of IL-13 to regulate epithelial cell turnover, based on the fact that BALB/c female IL-4$^{-/-}$ mice expel parasites (through an IL-13–dependent mechanism), albeit more slowly than wild-type mice, whereas male IL-4$^{-/-}$ mice suffer chronic infection (*4*). Both male and female IL-4$^{-/-}$ animals and wild-type animals were infected with *T. muris*, and the rate of turnover was assessed. At day 28, male IL-4$^{-/-}$ animals harbored infection, whereas parasite expulsion was under way in female animals. All wild-type animals had expelled their worms (Fig. 2D). Comparison of the rate of turnover in IL-4$^{-/-}$ mice revealed that female animals had a much faster rate than male animals (Fig. 2E), and significantly greater numbers of labeled cells could be found higher up the crypt axis than in male animals (Fig. 2F and Table 1), again suggesting a prominent role for IL-13 but not IL-4. Interestingly, the rate of cell turnover in female IL-4$^{-/-}$ was twice that seen in BALB/c wild-type mice on day 14 during expulsion (Fig. 1D versus Fig. 2E), again indicating that a greater response is required to expel the larger stages of the parasite.

Chronic *T. muris* infection is dependent on IFN-γ (*5*), and recently the chemokine CXCL10 [IFN-γ–induced protein 10 (IP-10)] was shown to reduce the rate of epithelial cell turnover in a mouse model of colitis (*11*). After *T. muris* infection, the expression of CXCL10 was first detected in epithelial cells isolated from the large intestine of susceptible AKR mice at day 21, coincident with the

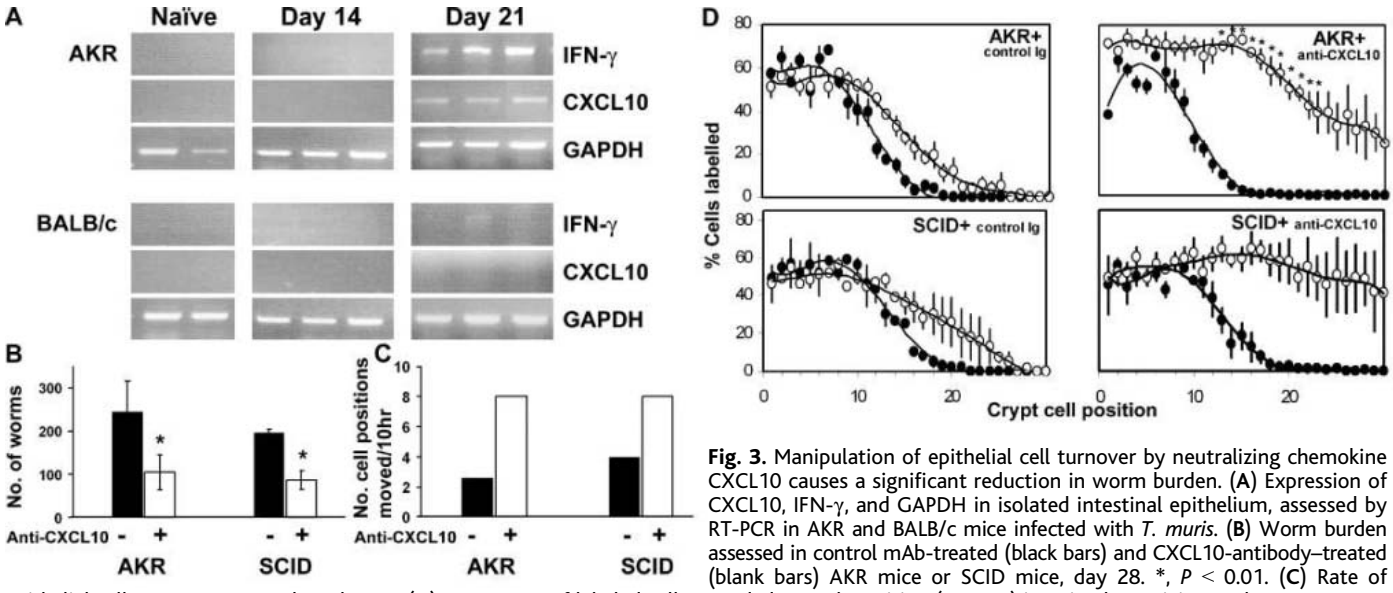

Fig. 3. Manipulation of epithelial cell turnover by neutralizing chemokine CXCL10 causes a significant reduction in worm burden. (**A**) Expression of CXCL10, IFN-γ, and GAPDH in isolated intestinal epithelium, assessed by RT-PCR in AKR and BALB/c mice infected with *T. muris*. (**B**) Worm burden assessed in control mAb-treated (black bars) and CXCL10-antibody–treated (blank bars) AKR mice or SCID mice, day 28. *, $P < 0.01$. (**C**) Rate of epithelial cell turnover assessed on day 21. (**D**) Percentage of labeled cells recorded at each position (0 to 30) in animals receiving mAb to CXCL10 or control mAb, day 21. Black circles, 40 min; open circles, 12-hour BrdU. *, $P < 0.01$, AKR mice treated versus untreated 12-hour BrdU pulse. Data in all panels are mean ± SE; four animals per group.

expression of IFN-γ (Fig. 3A and fig. S3A). Both were undetectable in resistant BALB/c mice. The receptor for CXCL10 (CXCR3) was also expressed in the intestine of infected AKR but not BALB/c at the time of CXCL10 induction (fig. S3B). Interestingly, IL-13 was also expressed in the gut of AKR on day 21 and day 35 (Fig. 2A). This would help explain the elevation in turnover seen in AKR on day 21 but also suggests that CXCL10 expression exerts a dominant effect even in the presence of IL-13. In vivo neutralization of CXCL10 in infected AKR mice caused a significant reduction in worm burden by day 28 (Fig. 3B). Furthermore, the treated group of animals showed a highly significant increase in the rate of epithelial cell turnover when compared with untreated animals (Fig. 3C). Also, a much higher proportion of labeled cells could be found higher up the crypt axis in treated animals (Fig. 3D and Table 1). The treatment of these animals with monoclonal antibody (mAb) to CXCL10 had no effect on the ongoing TH1 immune response (figs. S4 and S5) characteristic of a susceptible animal. This strongly suggests that epithelial cell turnover alone can mediate worm expulsion and reinforces the fact that it can remove later stages of the infection if the elevation in turnover is high enough.

Severe combined immunodeficient (SCID) mice lack B cells and T cells and therefore are incapable of generating an adaptive immune response, are highly susceptible to *T. muris* infection, and develop an IFN-γ–driven crypt-cell hyperplasia (*9*). This provides an ideal situation in which to modulate turnover in the absence of adaptive immunity. SCID mice in which CXCL10 was neutralized showed a significant reduction in worm burden compared with control-treated animals (Fig. 3B). Assessment of the rate of cell turnover clearly illustrated that the in vivo blockade of CXCL10 also significantly elevated the rate of cell turnover in these animals (Fig. 3, C and D, and Table 1). Therefore, elevating the rate of epithelial cell turnover was sufficient to displace parasites from the intestine.

Thus, epithelial cell turnover is an efficient and effective mechanism of gastrointestinal helminth expulsion from the large intestine. Furthermore, the parasite promotes its own survival in susceptible animals by inducing the production of IFN-γ, which acts to drive epithelial cell proliferation (*9*) and also locally induces CXCL10. This chemokine slows the epithelial escalator, resulting in crypt-cell hyperplasia and an increase in the epithelial niche. Resistant mice counter this in an IL-13–dependent manner, elevating the rate of epithelial cell turnover and displacing the parasite. Recently, a goblet cell–derived factor, RELMβ, has been described that is thought to affect the chemosensory apparatus of gastrointestinal-dwelling nematodes, thus impairing their survival (*12*). RELMβ expression is also regulated by IL-13, and the coordinated control of both turnover and RELMβ-mediated worm disorientation would be an extremely efficient method of removing the parasites from the gut. This finding identifies immune-mediated control of epithelial homeostasis as being an important mechanism in the control of infectious disease in the intestine. Indeed, many pathogens elicit intestinal hyperplasia under adaptive immune control, for example, *Citrobacter rodentium* (*13*). Investigation of epithelial turnover in response to such microbes would give new insights into the array of immune-mediated effector mechanisms that help control infection at mucosal surfaces.

References and Notes

1. A. Montresor, D. W. T. Crompton, T. W. Gyrkos, L. Salvioli, "Helminth control in school-age children: A guide for managers of control programmes" (World Health Organization, Geneva, 2002).
2. C. S. Potten, *Philos. Trans. R. Soc. Lond. B Biol. Sci.* **353**, 821 (1998).
3. A. J. Bancroft, A. N. McKenzie, R. K. Grencis, *J. Immunol.* **160**, 3453 (1998).
4. A. J. Bancroft, D. Artis, D. D. Donaldson, J. P. Sypek, R. K. Grencis, *Eur. J. Immunol.* **30**, 2083 (2000).
5. K. J. Else, F. D. Finkelman, C. R. Maliszewski, R. K. Grencis, *J. Exp. Med.* **179**, 347 (1994).
6. T. D. Lee, D. Wakelin, R. K. Grencis, *Int. J. Parasitol.* **13**, 349 (1983).
7. K. Koyama, *Parasite Immunol.* **24**, 527 (2002).
8. C. J. Betts, K. J. Else, *Parasite Immunol.* **21**, 45 (1999).
9. D. Artis, C. S. Potten, K. J. Else, F. D. Finkelman, R. K. Grencis, *Exp. Parasitol.* **92**, 144 (1999).
10. Materials and methods are available as supporting material on *Science* Online.
11. S. Sasaki *et al.*, *Eur. J. Immunol.* **32**, 3197 (2002).
12. D. Artis *et al.*, *Proc. Natl. Acad. Sci. U.S.A.* **101**, 13596 (2004).
13. T. T. MacDonald, G. Frankel, G. Dougan, N. S. Goncalves, C. Simmons, *Int. J. Microbiol.* **293**, 87 (2003).
14. We thank A. N. McKenzie for the IL-13$^{-/-}$ animals, J. Pennock and J. Hankinson for cDNA samples, E. J. Servier for technical assistance, and E. Bell, A. Bancroft, and K. Gull for useful comments and help with the manuscript. This study was supported by the Biotechnology and Biological Sciences Research Council, Epistem Ltd., The Wellcome Trust, and NIH.

Supporting Online Material

www.sciencemag.org/cgi/content/full/308/5727/1463/DC1
Materials and Methods
Figs. S1 to S5
References

14 December 2004; accepted 23 March 2005
10.1126/science.1108661

Epigenetic Transgenerational Actions of Endocrine Disruptors and Male Fertility

Matthew D. Anway, Andrea S. Cupp,* Mehmet Uzumcu,† Michael K. Skinner‡

Transgenerational effects of environmental toxins require either a chromosomal or epigenetic alteration in the germ line. Transient exposure of a gestating female rat during the period of gonadal sex determination to the endocrine disruptors vinclozolin (an antiandrogenic compound) or methoxychlor (an estrogenic compound) induced an adult phenotype in the F_1 generation of decreased spermatogenic capacity (cell number and viability) and increased incidence of male infertility. These effects were transferred through the male germ line to nearly all males of all subsequent generations examined (that is, F_1 to F_4). The effects on reproduction correlate with altered DNA methylation patterns in the germ line. The ability of an environmental factor (for example, endocrine disruptor) to reprogram the germ line and to promote a transgenerational disease state has significant implications for evolutionary biology and disease etiology.

Treatments, such as irradiation and chemotherapy, and compounds, such as environmental toxins, pose a threat to the integrity of the genome. Studies have shown that these agents can result in genetic or developmental defects in the offspring or F_1 generation from an exposed gestating mother. The ability of an external agent to induce a transgenerational effect requires stable chromosomal alterations or an epigenetic phenomenon such as DNA methylation (*1*). In the present study, transgenerational refers to a germline transmission to multiple generations, minimally to the F_2 generation. Transgenerational effects of irradiation were the first to be identified through transmission of DNA mutations in the germ line to multiple generations (*2*), often associated with tumor formation. Chemotherapeutic treatments (*3*) and environmental toxins such as endocrine disruptors (*4*) can cause effects in the F_1 generation, but they have not been shown to affect the F_2 generation. Although no effects have been shown to be transgenerational, the potential impact of such transgenerational effects of endocrine disruptors has been discussed (*5*).

Epigenetic alterations that could lead to transgenerational transmission of specific genetic traits have recently been identified (*1*, *6*). A transgenerational phenotype or genetic trait requires a permanent reprogramming of the germ line. During mammalian germ cell development the methylation state of the genome is reprogrammed. As primordial germ cells (PGCs) migrate down the genital ridge, a demethylation starts and is complete on colonization in the early gonad (*7*, *8*). Germ cells in the gonad then undergo remethylation in a sex-specific manner during gonadal sex determination (*9*). Although demethylation may not require the gonadal somatic cells, remethylation of the germ line appears to be dependent on association with the somatic cells in the gonads (*7*). Gonadal sex determination and testis development occur between embryonic days 12 and 15 (E12 to E15) in the rat (after midgestation in the human) and are initiated by the differentiation of precursor Sertoli cells in response to the testis-determining factor Sry. Aggregation of the precursor Sertoli cells, PGCs, and migrating mesonephros cells (precursor peritubular myoid cells) promotes testis morphogenesis and cord formation (*10*, *11*). During the period of gonadal sex determination, the fetal testis contains steroid receptors and is a target for endocrine agents. The androgen receptor (AR) and estrogen receptor–β (ERβ) are present in Sertoli cells, precursor peritubular myoid cells, and germ cells at the time of cord formation (E14) (*12*, *13*). Although steroids are not produced by the testis at this stage of development, estrogenic and androgenic substances have the ability to influence early testis cellular functions. Therefore, steroidal factors acting inappropriately at the time of gonadal sex determination potentially could reprogram the germ line through an epigenetic mechanism (altered DNA methylation) to cause the transgenerational transmission of an altered phenotype or genetic trait.

The estrogenic and antiandrogenic endocrine disruptors used in the current study are methoxychlor and vinclozolin, respectively. Vinclozolin is a commonly used fungicide in the wine industry that is metabolized into more active (i.e., higher affinity binding to androgen receptor) compounds (*14*). Methoxychlor is used as a pesticide to replace DDT and is metabolized into active compounds with the ERα agonist, the ERβ antagonist, and antiandrogenic activity (*15*–*17*). Vinclozolin or methoxychlor exposure in the late embryonic or early postnatal period influences sexual differentiation, gonad formation, and reproductive functions in the F_1 generation (*14*, *18*, *19*). Transient exposure (daily intraperitoneal injection of 100 or 200 mg/kg dose) of a gestating female rat to methoxychlor or vinclozolin between E8 and E15 promotes reduced spermatogenic capacity associated with increased spermatogenic cell apoptosis and decreased sperm number and motility in the adult F_1 generation (*20*, *21*). A similar exposure between E15 and E20 had no effect on the F_1 generation testis (*20*, *21*). These observations were extended in the present study by treating the gestating mother with vinclozolin. F_1 generation male rats were mated with F_1 generation females from different litters. Subsequent breeding continued for four generations with sufficient numbers of animals to avoid sibling inbreeding. Adult males from F_1, F_2, F_3, and F_4 generations between postnatal days PND60 and PND180 were killed. Testes were isolated for histological examination, and caudal epididymal sperm were collected for sperm counts and motility measurements. Only the original gestating mother (F_0) of the F_1 generation received a transient endocrine disruptor treatment. Control groups of animals were bred in a similar manner after vehicle treatment (dimethylsulfoxide buffer alone injected) of the F_0 gestating mother. Analysis of cellular apoptosis demonstrated a greater than twofold increase in spermatogenic cell apoptosis in the vinclozolin treatment animals for the F_1 to F_4 generations (Fig. 1A). Sperm numbers were reduced minimally, 20%, and sperm forward motility was reduced about 25 to 35% for vinclozolin generation animals (Fig. 1, B and C). More than 90% of all males analyzed from all generations had the germ cell defect of increased spermatogenic cell apoptosis. Therefore, the frequency of the phenotype was >90% and did not decline between the F_1 and F_4 generations. A similar experiment was performed with methoxychlor. After transient embryonic methoxychlor exposure (E8 to E15), a similar phenotype was observed in both the F_1 and F_2 animals (fig. S1). Therefore, both vinclozolin and methoxychlor induced transgenerational defects in spermatogenic capacity and sperm viability.

Center for Reproductive Biology, School of Molecular Biosciences, Washington State University, Pullman, WA 99164–4231, USA.

*Present address: Department of Animal Science, University of Nebraska, Lincoln, NE 68583–0908, USA.

†Present address: Department of Animal Science, Rutgers University, 84 Lipman Drive, New Brunswick, NJ 08901–8525, USA.

‡To whom correspondence should be addressed. E-mail: skinner@mail.wsu.edu

An outcross experiment was performed to determine whether the transgenerational phenotype was transmitted through the male germ line. Vinclozolin F_2 generation males (i.e., male progeny from an F_0 treated mother) were crossed with wild-type untreated control females, and the offspring were analyzed. The vinclozolin outcross (VOC) male progeny also had an increase in spermatogenic cell apoptosis and a decrease in sperm number and motility (Fig. 1). The reverse vinclozolin outcross (RVOC) with vinclozolin F_2 generation females and wild-type control males demonstrated no effect on the spermatogenic cells (Fig. 1). Therefore, the endocrine disruptor–induced transgenerational phenotype appears to be transmitted through the male germ line.

The morphology of the testes from control and treated rats was similar for all animals examined on PND60 in all F_1 to F_4 vinclozolin generations. Periodically, male rats older than 90 days of age developed complete infertility associated with small testis and severely reduced spermatogenesis, which was not seen in the PND60 animals. This occurred in 4 out of a total of 50 F_1, F_2, F_3, and F_4 generation animals. Therefore, 8% of the vinclozolin transgenerational males developed complete infertility. None of the 42 control F_1 to F_4 generation animals were infertile. The testis histology for a representative infertile vinclozolin F_3 generation animal is shown in Fig. 2 and demonstrates a loss of normal spermatogenesis (no germ cells present) and abnormal seminiferous tubule morphology. The control F_3 male showed normal morphology with normal spermatogenesis. Although most of the animals older than 90 days of age were fertile, ~20% developed a dramatic decrease in spermatogenic capacity (50% of the tubules having impaired germ cell development) in all the generations examined.The VOC males also had increased infertility in ~20% of the animals over 90 days of age. The treated males that were fertile showed no change in litter size, newborn pup weights, or testis weight per body weight when compared with the control animals of any of the F_1 to F_4 generations examined. Nearly all the treated male progeny had the minimal phenotype of twofold increase in spermatogenic cell apoptosis, and the majority had a decrease in epididymal sperm number (Fig. 1, A and B).

The transmission of this endocrine disruptor–induced testis phenotype in a transgenerational manner suggests an epigenetic alteration of the male germ line. The frequency observed for the phenotype (>90% of all males in all generations) cannot be explained through genetic DNA sequence mutational mechanisms. A high-frequency genetic (DNA sequence) mutation hotspot event would be an order of magnitude less than that observed (*2*, *22*, *23*). Subsequent segregation of this mutation would likely result in a reduction of the phenotype frequency with each generation. In addition, the random nature of genetic (DNA sequence) mutations is generally more variable in the phenotype observed (*2*, *22*, *23*). In contrast, an epigenetic mechanism involving reprogramming of the germ line could result in the high frequency observed. In addition, the developmental period used for the endocrine disruptor exposure was during the remethylation programming of the germ line. Although we cannot exclude the possibility of a novel genetic (DNA sequence) mutational

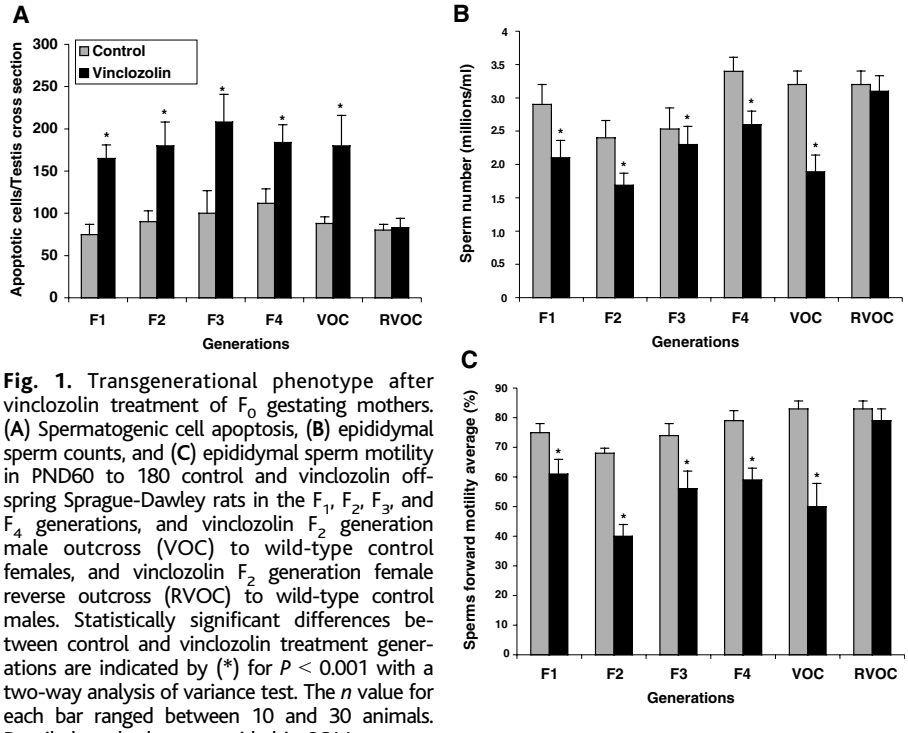

Fig. 1. Transgenerational phenotype after vinclozolin treatment of F_0 gestating mothers. (**A**) Spermatogenic cell apoptosis, (**B**) epididymal sperm counts, and (**C**) epididymal sperm motility in PND60 to 180 control and vinclozolin offspring Sprague-Dawley rats in the F_1, F_2, F_3, and F_4 generations, and vinclozolin F_2 generation male outcross (VOC) to wild-type control females, and vinclozolin F_2 generation female reverse outcross (RVOC) to wild-type control males. Statistically significant differences between control and vinclozolin treatment generations are indicated by (*) for $P < 0.001$ with a two-way analysis of variance test. The *n* value for each bar ranged between 10 and 30 animals. Detailed methods are provided in SOM.

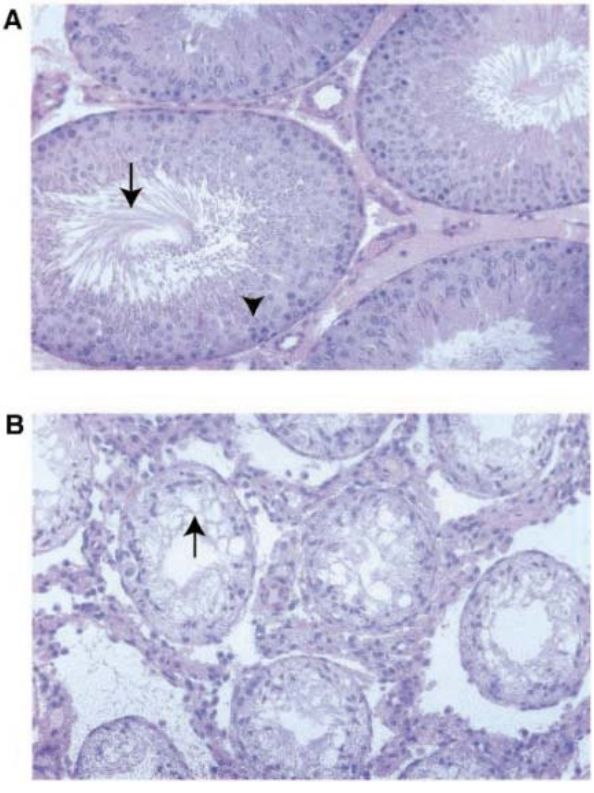

Fig. 2. Testis histology from control (**A**) and vinclozolin treatment (**B**) 100-day-old F_3 generation animals, ×200 magnification. The vinclozolin F_3 generation male is a representative infertile male. Arrow in (A) identifies the tails of elongate spermatozoa in the seminiferous tubule lumen; arrowhead labels spermatocytes in the tubule epithelial layer. Arrow in (B) identifies the lack of germ cells in the seminiferous tubule. Methods are provided in SOM.

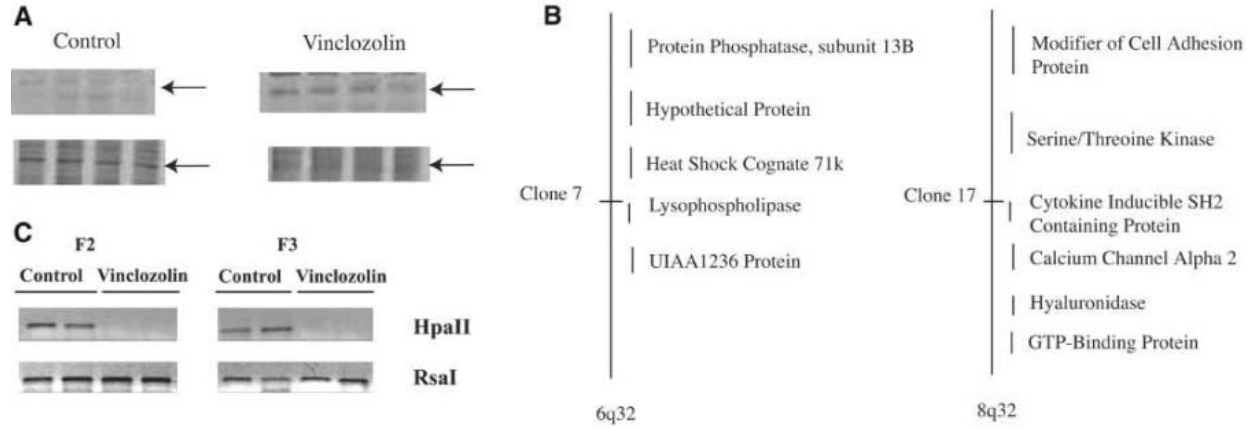

Fig. 3. DNA methylation analysis from control and vinclozolin offspring testis. (**A**) Representative gel images of the PCR-based methylation-sensitive Hpa II restriction enzyme digest analysis with representative band (arrow) affected in PND6 testis from control and vinclozolin treatment animals. Each lane represents a different individual animal (n = 4). (**B**) Location of selected sequences on specific chromosomes for two representative DNA sequences with altered DNA methylation patterns termed clone 7 and 17. (**C**) Methylation-sensitive restriction enzyme PCR analysis of the methylation state of clone 17 (i.e., cytokine-inducible SH2 protein) gene in epididymal sperm from F_2 and F_3 generations from control and vinclozolin-treated animals. The bands presented are representative of sperm DNA collected from different animals from different litters and are consistent in four out of eight F_2 animals and two out of five F_3 animals analyzed. Methods are provided in SOM.

event, available information suggests an epigenetic mechanism is involved.

The only epigenetic mechanism currently known to influence germline transmission involves the methylation pattern of imprinted genes. This study does not investigate specific known imprinted genes, but focuses on the effects of the endocrine disruptor on the total genome. Fisher rats were used because of reduced polymorphisms, which made methylation studies more consistent and reproducible. PND6 testes were collected from male F_1 progeny of vinclozolin-treated and control rats. A methylation-sensitive restriction enzyme digestion analysis involving a polymerase chain reaction (PCR)–based procedure was used to assess changes in DNA methylation patterns (Methods in SOM). Animals (n = 4) from different litters of control and treated animals were analyzed. The vinclozolin-induced methylation patterns were similar in the replicate animals. About 25 different PCR products were identified that had altered DNA methylation patterns after the endocrine disruptor treatment. A representative change in methylation pattern is shown in Fig. 3A and fig. S2. These methylation experiments were extended by isolating and cloning several of the DNA fragments with apparent altered methylation. Two of the DNA fragments were sequenced and mapped to CpG-rich regions on chromosomes 6q32 and 8q32 (Fig. 3B). Clone 7 mapped to 6q32 and was within the lysophospholipase (LPLase) gene (accession NM144750). LPLase is a critical enzyme in the synthesis of important bioactive lipids and associated signaling (*24*). Clone 17 mapped to 8q32 and is within 1 kb of the start site of an uncharacterized protein termed cytokine-inducible SH2 protein (accession AJ243907). Whether the genes identified are causal factors or simply markers (i.e., downstream) of the transgenerational epigenetic phenotype remains to be determined.

The epigenetic transgenerational transmission of the altered methylation pattern through the male germ line was investigated. PCR primers were designed for the flanking regions of the clone 17 gene, cytokine-inducible SH2 protein and were used to investigate altered methylation with the methylation-sensitive restriction enzyme digest procedure. Epididymal sperm were isolated from vinclozolin treatment F_2 and F_3 generation animals. As shown in Fig. 3C, the control animals had the PCR product, whereas the vinclozolin treatment F_2 and F_3 animals did not. The control Rsa I digest had a PCR product in all samples. Therefore, the vinclozolin treatment F_2 and F_3 generation sperm samples appeared to have altered DNA methylation in this clone 17 gene compared with control animal sperm. An alternate bisulfite DNA sequence analysis was used to confirm the methylation changes. Bisulfite analysis confirmed the altered methylations of the LPLase gene within the CpG island identified. This bisulfite altered sequence (fig. S3) was observed in ~25% of the vinclozolin treatment sperm DNA samples analyzed. A single-gene methylation event alone is not likely sufficient to promote the phenotype, but could cause alterations in a subset of genes. For example, 25 DNA sequences with altered methylation were identified, and if a random subset of genes with altered methylation promotes the phenotype, a 25% frequency for altered methylation of a single gene would be significant. Observations indicate that the endocrine disruptors can induce an epigenetic transgenerational change in the DNA methylation pattern of the male germ line. The epigenetic alterations observed involve both hypermethylation and hypomethylation events.

Two different endocrine disruptors, vinclozolin and methoxychlor, after a transient embryonic exposure at a critical time during gonadal sex determination (E8 to E15 in the rat), promoted an adult testis phenotype of decreased spermatogenic capacity and male infertility. No gross abnormality was observed in any other tissues examined, and serum testosterone levels were found to be normal in all the animals examined. This phenotype was found to be transgenerational and appears associated with altered DNA methylation of the male germ line. The phenotype was observed in nearly all males from all vinclozolin generations, such that a genetic mutation event (e.g., alteration in DNA sequence) is not likely to be a major factor. The frequency of a genetic mutation would be orders of magnitude less than the transmission frequency observed in the current study (*2*, *22*, *23*). Preliminary data demonstrate no major effect on the female, but a number of abnormal pregnancy outcomes were observed in pregnant females from offspring of vinclozolin-treated animals, but not controls. The abnormal phenotype has similarities to preeclampsia that include death, severe anemia, and blood cell defects. This study shows that environmental factors can induce an epigenetic transgenerational phenotype through an apparent reprogramming of the male germ line. It should be noted that the exposure levels used in these studies are higher than anticipated for environmental exposure; hence, future toxicology studies would be needed to ascertain the possible impact on animal populations.

References and Notes

1. V. Rakyan, E. Whitelaw, *Curr. Biol.* **13**, R6 (2003).
2. R. Barber, M. A. Plumb, E. Boulton, I. Roux, Y. E. Dubrova, *Proc. Natl. Acad. Sci. U.S.A.* **99**, 6877 (2002).
3. I. D. Morris, *Int. J. Androl.* **25**, 255 (2002).

4. C. M. Foran, B. N. Peterson, W. H. Benson, *Toxicol. Sci.* **68**, 389 (2002).
5. C. DeRosa, P. Richter, H. Pohl, D. E. Jones, *J. Toxicol. Environ. Health B Crit. Rev.* **1**, 3 (1998).
6. V. K. Rakyan *et al.*, *Proc. Natl. Acad. Sci. U.S.A.* **100**, 2538 (2003).
7. P. Hajkova *et al.*, *Mech. Dev.* **117**, 15 (2002).
8. G. Durcova-Hills, J. Ainscough, A. McLaren, *Differentiation* **68**, 220 (2001).
9. W. Reik, J. Walter, *Nat. Rev. Genet.* **2**, 21 (2001).
10. A. Jost, S. Magre, R. Agelopoulou, *Hum. Genet.* **58**, 59 (1981).
11. M. Buehr, S. Gu, A. McLaren, *Development* **117**, 273 (1993).
12. G. Majdic, M. R. Millar, P. T. Saunders, *J. Endocrinol.* **147**, 285 (1995).
13. H. O. Goyal *et al.*, *Anat. Rec.* **249**, 54 (1997).
14. W. R. Kelce, E. Monosson, M. P. Gamcsik, S. C. Laws, L. E. Gray Jr., *Toxicol. Appl. Pharmacol.* **126**, 276 (1994).
15. A. M. Cummings, *Crit. Rev. Toxicol.* **27**, 367 (1997).
16. K. W. Gaido *et al.*, *Endocrinology* **140**, 5746 (1999).
17. W. R. Kelce, C. R. Lambright, L. E. Gray Jr., K. P. Roberts, *Toxicol. Appl. Pharmacol.* **142**, 192 (1997).
18. J. S. Fisher, *Reproduction* **127**, 305 (2004).
19. R. E. Chapin *et al.*, *Fundam. Appl. Toxicol.* **40**, 138 (1997).
20. A. S. Cupp *et al.*, *J. Androl.* **24**, 736 (2003).
21. M. Uzumcu, H. Suzuki, M. K. Skinner, *Reprod. Toxicol.* **18**, 765 (2004).
22. B. S. Shi, Z. N. Cai, J. Yang, Y. N. Yu, *Mutat. Res.* **556**, 1 (2004).
23. H. Dong *et al.*, *Biochemistry* **43**, 15922 (2004).
24. A. Tokumura, *J. Cell. Biochem.* **92**, 869 (2004).

25. We acknowledge the technical contributions of I. Sadler-Riggleman, S. Rekow, and B. Johnston and the assistance of H. Suzuki with the methylation PCR procedure. This research was supported in part by a grant to M.K.S. from the U.S. Environmental Protection Agency's Science to Achieve Results (STAR) program involving endocrine disruptors.

Supporting Online Material
www.sciencemag.org/cgi/content/full/308/5727/1466/DC1
Materials and Methods
Figs. S1 to S3
References and Notes

2 December 2004; accepted 22 March 2005
10.1126/science.1108190

Kinesin and Dynein Move a Peroxisome in Vivo: A Tug-of-War or Coordinated Movement?

Comert Kural,[1] Hwajin Kim,[3] Sheyum Syed,[2] Gohta Goshima,[4] Vladimir I. Gelfand,[3]*† Paul R. Selvin[1,2]‡

We used fluorescence imaging with one nanometer accuracy (FIONA) to analyze organelle movement by conventional kinesin and cytoplasmic dynein in a cell. We located a green fluorescence protein (GFP)–tagged peroxisome in cultured *Drosophila* S2 cells to within 1.5 nanometers in 1.1 milliseconds, a 400-fold improvement in temporal resolution, sufficient to determine the average step size to be ~8 nanometers for both dynein and kinesin. Furthermore, we found that dynein and kinesin do not work against each other in vivo during peroxisome transport. Rather, multiple kinesins or multiple dyneins work together, producing up to 10 times the in vitro speed.

Conventional kinesin (kinesin-1) and cytoplasmic dynein are microtubule-dependent molecular motors responsible for organelle trafficking and cell division. The long-distance organelle transport within a cell occurs bidirectionally along the microtubule tracks. Plus (+) end directed kinesins carry the cargo to the cell periphery whereas minus (−) end directed dyneins bring the cargo back.

In vitro studies using optical traps (*1*) and single-molecule fluorescence imaging (*2*) have provided insight into how the microtubule motors work. Kinesin is a highly processive motor that can take hundreds of 8-nm steps, with a load of up to 6 pN, before detaching from the microtubule (*3*). Optical trap and in vitro motility studies have shown that a dynein-dynactin complex is also processive (*4*) and that dynein has an 8-nm step size under a load of up to 1.1 pN (*5*).

These studies, however, do not address how kinesin and dynein cooperate to achieve intracellular bidirectional transport. Do they move a cargo by engaging in a "tug-of-war," or is there a switch that turns off one or both of the motors? Do multiple motors of the same polarity act together or cooperatively (*6*–*8*)? Answering these questions requires observing the cargo molecules in vivo with high temporal and spatial resolution. In particular, the spatiotemporal resolution must be faster than the typical rate of moving at the physiological adenosine 5′-triphosphate (ATP) concentration.

We used fluorescence imaging with one nanometer accuracy (FIONA) (*2*, *9*) inside a live cell to track GFP-labeled peroxisomes being carried by microtubule motors with 1.5-nm accuracy and 1-ms time resolution, thereby allowing in vivo ATP concentrations. We used cultured *Drosophila* S2 cells that constitutively express enhanced green fluorescence protein (EGFP) with a peroxisome-targeting signal (*10*). Fluorescence images of peroxisomes, excited with total internal epifluorescence microscopy and labeled with numerous EGFP molecules, can be fit to a Gaussian function and then well-localized (Fig. 1). Figure 1 shows a cell in a bright-field image (treated as described below), a fluorescence image of the EGFP-peroxisomes, and a 1-ms point-spread-function of one peroxisome, which shows localization to 1.5 nm.

Most organelles use both microtubule motors and myosins for intracellular movement (*11*). To analyze the work of microtubule motors in the absence of myosin effects, we treated cells with 5 μM cytochalasin D, a drug that caps barbed ends of actin filaments, resulting in the disappearance of long filaments and therefore inhibition of actomyosin-dependent movement. Normal S2 cells plated on a substrate coated with concanavalin A have a discoid shape (*12*). Upon the loss of the actin filament network, S2 cells grow thin processes that are filled with microtubules (Fig. 1), but have no F-actin cables detectable by fluorescent phalloidin staining (*13*). We analyzed the polarity of microtubules in these processes using cells expressing EGFP-tagged EB1 (*12*). EB1 is a protein that specifically binds to (+) ends of growing microtubules (*14*). We found that in thin processes (diameter ≤ 1 μm), more than 90% of microtubules have (+) ends pointing away from the cell body (fig. S1). In contrast, in processes with a diameter >1 μm, only about 60% of microtubules have their (+) ends pointing away from the cell body, presumably due to a buckling of the microtubules inside the process. Consequently, only those peroxisomes moving in processes with a diameter <1 μm were analyzed (fig. S1).

Our measurements were performed at 10°C, and although low temperatures are known to favor microtubule depolymerization, immunofluorescent staining with antibody to tubulin demonstrated that the incubation at 10°C had no effect on the density or distribution of microtubules (fig. S2). We also determined the effect of microtubule lattice movements on peroxisome motion by performing fluorescence recovery after photo-

[1]Biophysics Center, [2]Physics Department, [3]Department of Cell and Structural Biology, University of Illinois, Urbana, IL 61801, USA. [4]Department of Cellular and Molecular Pharmacology, University of California, San Francisco, CA 94107, USA.

*Present address: Department of Cell and Molecular Biology, Feinberg School of Medicine, Northwestern University, Chicago, IL 60611, USA.
†To whom correspondence should be addressed. Department of Cell and Molecular Biology, Northwestern University School of Medicine, 303 East Chicago Avenue, Ward 11-080, Chicago, IL 60611–3008, USA. E-mail: vgelfand@northwestern.edu
‡To whom correspondence should be addressed. Loomis Lab of Physics, 1110 West Green Street, University of Illinois, Urbana, IL 61801, USA. E-mail: selvin@uiuc.edu

bleaching experiments on processes containing GFP-tubulin–based microtubules. The fluorescence recovery was longer than 1 s, indicating that microtubule lattice movements occur much more slowly than do kinesin- and dynein-driven organelle movements (fig. S4).

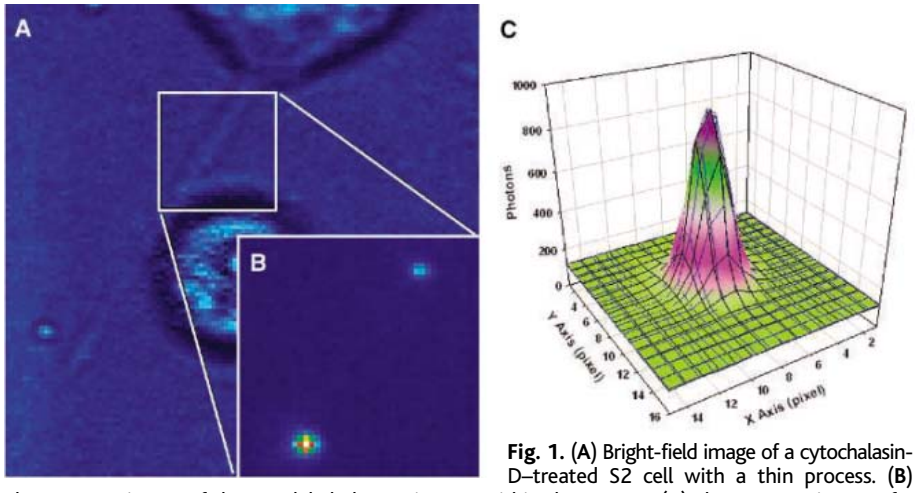

Fig. 1. (**A**) Bright-field image of a cytochalasin-D–treated S2 cell with a thin process. (**B**) Fluorescence image of the GFP-labeled peroxisomes within the process. (**C**) Fluorescence image of a peroxisome can be fit to a two-dimensional Gaussian (correlation coefficient $r^2 = 0.992$), enabling the center to be determined to 1.5 nm within 1.1 ms.

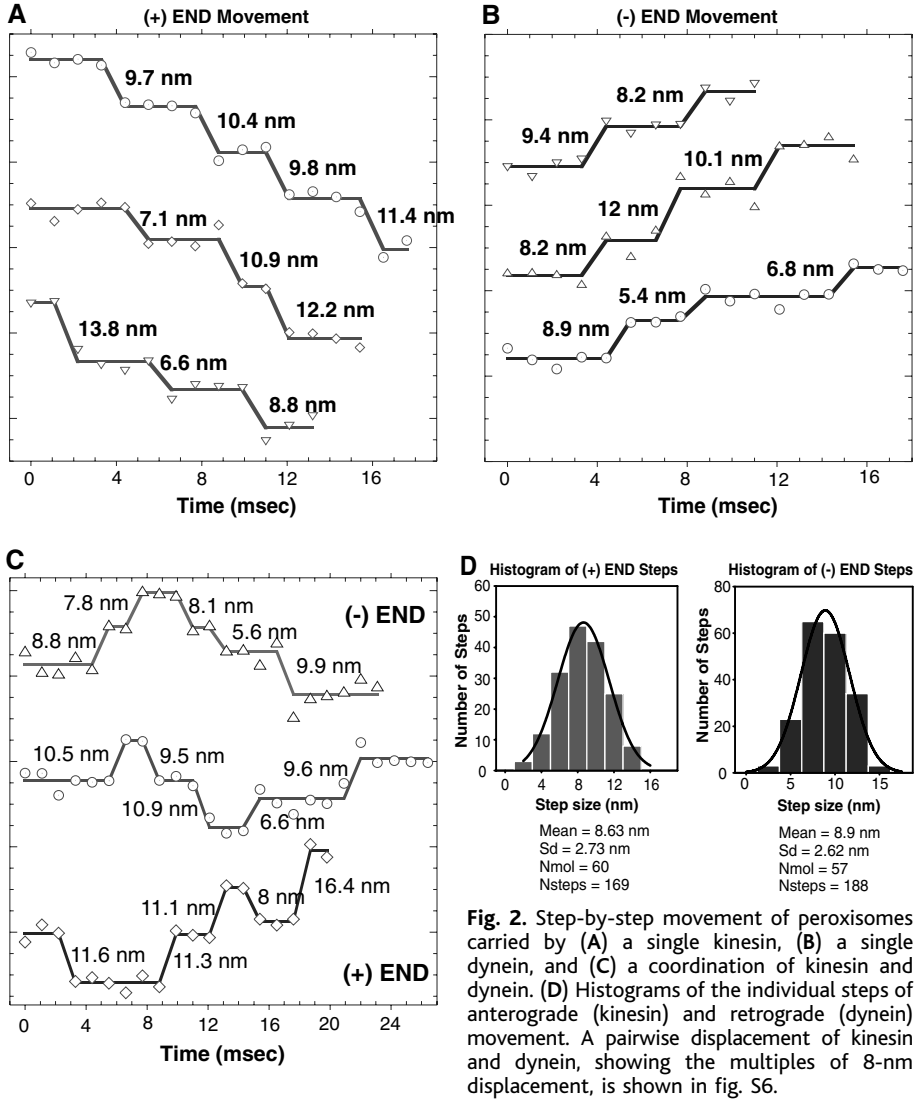

Fig. 2. Step-by-step movement of peroxisomes carried by (**A**) a single kinesin, (**B**) a single dynein, and (**C**) a coordination of kinesin and dynein. (**D**) Histograms of the individual steps of anterograde (kinesin) and retrograde (dynein) movement. A pairwise displacement of kinesin and dynein, showing the multiples of 8-nm displacement, is shown in fig. S6.

Drosophila S2 cells are highly sensitive to protein inhibition by RNA interference (RNAi) (*12*). We used RNAi to find which motors move peroxisomes along microtubules. We tested conventional kinesin (kinesin-1), three members of kinesin-2 family (Klp68D, Klp64D, and CG17461), three members of kinesin-3 family (Klp53D, Klp98A, and Klp38B), and ncd (a member of kinesin-14 or C-terminal kinesin family), as well as cytoplasmic dynein. We did not test depolymerizing kinesins, mitotic kinesins, and kinesins, which are not expressed above background level in S2 cells, as shown by microarray analysis (*15*). RNAi analysis showed that organelle transport was inhibited by RNAi only against kinesin-1 and dynein heavy chain, indicating that only these motors are responsible for movement (fig. S3).

FIONA localization showed that peroxisomes can move in a step-by-step manner in both anterograde (kinesin) and retrograde (dynein) directions (Fig. 2, A to C). With 169 motor steps, the average step size in the kinesin direction was 8.6 ± 2.7 nm (mean ± SD) (Fig. 3A), and the average speed was 1.5 ± 0.6 μm/s. In the dynein direction, 188 steps yielded an average step size of 8.9 ± 2.6 nm (Fig. 3B) and an average speed of 1.7 ± 0.9 μm/s. The step-size results are in agreement with in vitro kinesin and dynein assays (*3*, *5*), which yielded about 8 nm/step. The average speed for dynein (at a saturating ATP concentration) is within a factor of 2: 1.7 μm/s, as determined here, versus 0.7 μm/s (*4*) or 1.2 μm/s (*16*). It is within a factor of 2 of the calculated speed at the maximal rate of in vitro ATP hydrolysis by dynein [120 s^{-1} (*17*)], assuming one hydrolyzed ATP molecule per 8 nm/step (120 steps/s × 8 nm/step = 0.96 μm/s). Finally, the in vitro rate for kinesin is 1.0 μm/s (*4*), compared with 1.5 μm/s determined here.

Previous optical trap experiments on kinesin show that the bead-motor linkage behaves like an entropic spring (*3*). Consequently, if motors of opposite directions were operating simultaneously, then any compliance in the motor stalks would cause a degradation of step sizes, moving in either direction, as one motor took a step while its competitor was also bound to a microtubule (fig. S5). We found step sizes to be constant, implying that there is no "tug-of-war" between motors. It appears that motors are somehow regulated, being turned on or off in such a way that they are not simultaneously dragging the peroxisome. A distribution of the displacement driven by kinesins and dynein, showing 8-nm steps or multiples thereof, indicates no degenerated steps by opposite motors (fig. S6).

Figure 3, A and B, show a distribution of speeds for a peroxisome moving in the (+) or (−) directions. The graphs are highly spiked, at intervals corresponding to ≈1.2 μm/s, extending to ~12 μm/s. This implies that the spikes correspond to up to 11 kinesins

moving without appreciable hindrance from dynein (Fig. 3A), or up to 11 dyneins moving without much hindrance from kinesin (Fig. 3B). These distinct spikes in speed distribution occur when multiple kinesins and multiple dyneins hydrolyze ATP simultaneously in a stochastic manner, because reducing the cytoplasmic ATP concentration by an ATP-uncoupler FCCP (*p*-trifluoromethoxy carbonyl cyanide phenyl hydrazone) terminates the fast (>5 μm/sec) organelle transport (*13*).

In vitro kinesin assays do not show such high velocities; velocities of microtubules gliding on a kinesin-coated surface are independent of motor densities with 1 to 1000 kinesins/μm^2, yielding speeds just above 0.5 μm/s (*18*). In contrast, gliding assays done in more viscous media suggest that at higher loads, the velocity increases at higher motor densities (*19*), suggesting that kinesins can operate together. Other in vivo studies show similar fast organelle transport. Ashkin *et al*. have found that mitochondria carried on microtubules can move as fast as 15 μm/s (*20*). Endosomes in cells can be moved by dynein with speeds as fast as 4 μm/s, faster than the in vitro dynein speed (*21*). Maximum vesicle velocities in neurons are reported to be 3.5 to 5 μm/s, higher than can be achieved by a single microtubule-dependent motor (*22*–*25*).

Figure 4 shows traces of individual peroxisome movement, which demonstrate that the peroxisomes move at rates greater than the in vitro single-motor rate. Figure 4A shows one peroxisome moved by dynein at an average rate of 1.0 μm/s; kinesin then takes over for two steps, and then dynein takes over again, moving the peroxisome about two times as fast as the previous (−) end run (2.2 μm/s), still in a stepwise manner. Figure 4B shows a peroxisome moved by multiple (perhaps 11) kinesins, then by a few dyneins (perhaps two), then by kinesins (perhaps two), then by multiple dyneins. Figure 4C shows the movement of peroxisome to the (−) end at various speeds >150 ms. This clearly shows the ability of a peroxisome to be moved by several motors—up to 11 dyneins and 11 kinesins—without any apparent inhibition by the opposite motility partner.

The nature of the coordination between kinesin and dynein is unclear. One possibility is that a small molecule alternatively turns off kinesin and dynein, although it would have to react very quickly to account for a transition time of less than a millisecond between motors. Another possibility is that kinesin and dynein pull against one another until the stronger one "wins," which would cause the weaker one to uncouple quickly and therefore not creating any load. A third possibility is that the density and/or flexibility due to the lipid/membrane linkage of motor proteins on the peroxisomes are such that two motors of the opposite polarity cannot simultaneously bind to the microtubule. In either case, there must be a mechanism to allow the peroxisomes to move by multiple motors much faster than by independent, uncoupled, kinesins and dyneins.

Our results show that both kinesin and dynein move with 8-nm steps, transporting an organelle in vivo. Faster movements occur with the same step size but with greater rapidity. For the peroxisomes, in vivo, up to 11 kinesins or dyneins apparently can work in concert, driving the cargo much faster than seen in vitro.

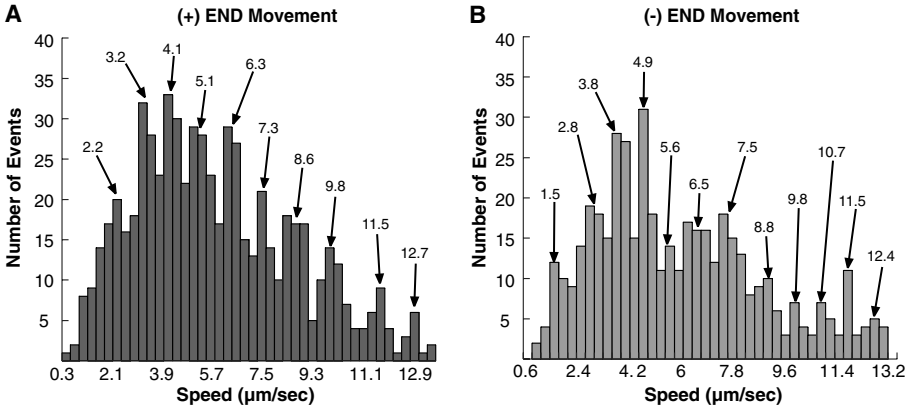

Fig. 3. (**A** and **B**) Stepping characteristics toward the (+) end (kinesin) and (−) end (dynein). Both graphs show multiple spikes, apparently corresponding to multiple kinesins [toward the (+) end] or dyneins [toward the (−) end] operating without load from the other motors. Both dynein and kinesin move rapidly (up to 12 μm/s), which is not seen in in vitro experiments. An event >20 nm was counted as a contiguous run (Fig. 4), independent of run length. The runs in the kinesin (+ end) and in the dynein (− end) directions were counted separately.

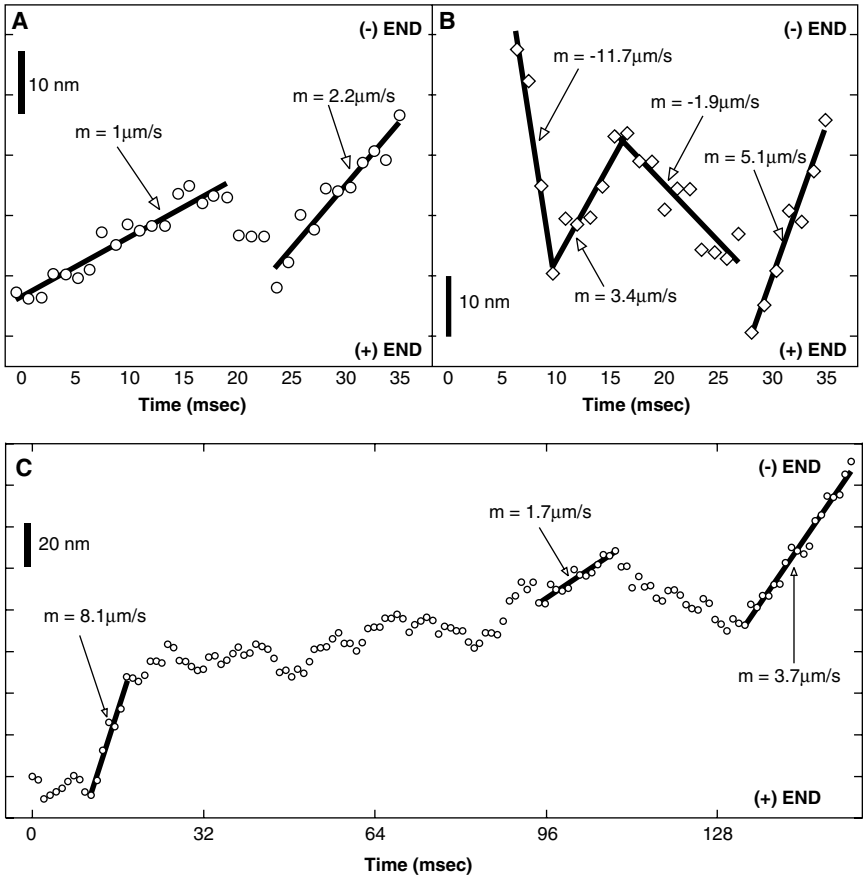

Fig. 4. Constant step size but variable speeds. (**A**) A peroxisome takes three steps driven by dynein, then two steps by kinesin, then about four steps by two dyneins, based on their average rate of stepping. (**B**) A peroxisome moved by about 11 kinesins, then two dyneins, then (one or) two kinesins, then three dyneins. (**C**) A peroxisome driven by dyneins at various speeds. (A), (B), and (C) are from different peroxisomes. "m" is the slope of the linear parts of the plot.

References and Notes

1. R. D. Vale, R. A. Milligan, *Science* **288**, 88 (2000).
2. A. Yildiz, M. Tomishige, R. D. Vale, P. R. Selvin, *Science* **303**, 676 (2004).
3. K. Svoboda, C. F. Schmidt, B. J. Schnapp, S. M. Block, *Nature* **365**, 721 (1993).
4. S. J. King, T. A. Schroer, *Nat. Cell Biol.* **2**, 20 (2000).
5. R. Mallik, B. C. Carter, S. A. Lex, S. J. King, S. P. Gross, *Nature* **427**, 649 (2004).
6. S. P. Gross, M. A. Welte, S. M. Block, E. F. Wieschaus, *J. Cell Biol.* **148**, 945 (2000).
7. R. Mallik, S. P. Gross, *Curr. Biol.* **14**, R971 (2004).
8. S. P. Gross *et al.*, *J. Cell Biol.* **156**, 855 (2002).
9. A. Yildiz *et al.*, *Science* **300**, 2061 (2003).
10. Materials and methods are available as supporting material on *Science* Online. For details of measurement, see (*9*). For microscopy, we used an Andor Model DV-860 BV, which is a back-illuminated camera that contains a 128 by 128 pixel sensor with 24 μm pixel size. A quarter chip is used to achieve 1 ms per frame. The incidence beam angle was tuned to get the best signal to noise. The cells were maintained at 10°C.
11. S. L. Rogers, V. I. Gelfand, *Curr. Opin. Cell Biol.* **12**, 57 (2000).
12. S. L. Rogers, G. C. Rogers, D. J. Sharp, R. D. Vale, *J. Cell Biol.* **158**, 873 (2002).
13. C. Kural *et al.*, data not shown.
14. Y. Ma, D. Shakiryanova, I. Vardya, S. V. Popov, *Curr. Biol.* **14**, 725 (2004).
15. G. Goshima, R. D. Vale, *J. Cell Biol.* **162**, 1003 (2003).
16. M. Nishiura *et al.*, *J. Biol. Chem.* **279**, 22799 (2004).
17. T. Kon, M. Nishiura, R. Ohkura, Y. Y. Toyoshima, K. Sutoh, *Biochemistry* **43**, 11266 (2004).
18. R. D. Vale, T. S. Reese, M. P. Sheetz, *Cell* **42**, 39 (1985).
19. A. J. Hunt, F. Gittes, J. Howard, *Biophys. J.* **67**, 766 (1994).
20. A. Ashkin, K. Schutze, J. M. Dziedzic, U. Euteneuer, M. Schliwa, *Nature* **348**, 346 (1990).
21. M. Lakadamyali, M. J. Rust, H. P. Babcock, X. Zhuang, *Proc. Natl. Acad. Sci. U.S.A.* **100**, 9280 (2003).
22. D. B. Hill, M. J. Plaza, K. Bonin, G. Holzwarth, *Eur. Biophys. J.* **33**, 623 (2004).
23. S. T. Brady, R. J. Lasek, R. D. Allen, *Science* **218**, 1129 (1982).
24. B. Grafstein, D. S. Forman, *Physiol. Rev.* **60**, 1167 (1980).
25. C. Kaether, P. Skehel, C. G. Dotti, *Mol. Biol. Cell* **11**, 1213 (2000).

26. We gratefully acknowledge R. Vale (University of California, San Francisco) and S. Rogers (University of North Carolina at Chapel Hill) for EGFP-EB1 and EGFP-tubulin cell lines. This work was supported by NIH grants AR44420 and GM 068625 (P.R.S.) and GM52111 (V.I.G.), an NSF grant (P.R.S.), and the U.S. Department of Energy, Division of Material Sciences (under award no. DEFG02-91ER45439), through the Frederick Seitz Materials Research Laboratory at the University of Illinois at Urbana-Champaign (P.R.S). P.R.S. also thanks J. Ackland, J. Stenehjem, and the other members of the Sharp Rehabilitation Center of San Diego for patient care, which made this science possible.

Supporting Online Material

www.sciencemag.org/cgi/content/full/1108408/DC1
Materials and Methods
Figs. S1 to S6
References

7 December 2004; accepted 30 March 2005
Published online 7 April 2005;
10.1126/science.1108408
Include this information when citing this paper.

Mechanism of Divergent Growth Factor Effects in Mesenchymal Stem Cell Differentiation

Irina Kratchmarova,[1]* Blagoy Blagoev,[1]* Mandana Haack-Sorensen,[2] Moustapha Kassem,[2] Matthias Mann[1]†

Closely related signals often lead to very different cellular outcomes. We found that the differentiation of human mesenchymal stem cells into bone-forming cells is stimulated by epidermal growth factor (EGF) but not platelet-derived growth factor (PDGF). We used mass spectrometry–based proteomics to comprehensively compare proteins that were tyrosine phosphorylated in response to EGF and PDGF and their associated partners. More than 90% of these signaling proteins were used by both ligands, whereas the phosphatidylinositol 3-kinase (PI3K) pathway was exclusively activated by PDGF, implicating it as a possible control point. Indeed, chemical inhibition of PI3K in PDGF-stimulated cells removed the differential effect of the two growth factors, bestowing full differentiation effect onto PDGF. Thus, quantitative proteomics can directly compare entire signaling networks and discover critical differences capable of changing cell fate.

Receptor tyrosine kinases (RTKs) regulate cellular processes ranging from cell growth and proliferation to survival and differentiation. After binding of their cognate ligands, these receptors undergo autophosphorylation on multiple tyrosine residues and become a platform for binding and consequent tyrosine phosphorylation of various signaling molecules, thus triggering multiple signaling cascades (*1*–*3*). To transmit the signal across the entire cell, various RTKs often activate universal signaling pathways. Nevertheless, distinct and even opposing biological effects of these receptors can arise.

Human mesenchymal stem cells (hMSC) are nonhematopoietic cells that reside within the bone marrow stroma. These cells are multipotent and serve as precursors for various mesoderm-type cells (*4*, *5*). Thus, hMSC have great clinical potential in tissue regeneration and engineering protocols (*6*). In cell culture, they can give rise to osteoblasts, adipocytes, and chondrocytes through processes largely controlled by various growth factors (*7*, *8*).

To study the effects of growth factors on hMSC, we first tested the effects of EGF, PDGF, fibroblast growth factor (FGF), and nerve growth factor (NGF) on cellular responses. Using immunoprecipitation and Western blotting with antibodies to phosphotyrosine, we observed that EGF and PDGF elicited the strongest responses (*9*) and that they induced phosphorylation of common and distinct subsets of proteins (Fig. 1A). Because one of the main characteristics of hMSC is their ability to differentiate to osteoblasts, we explored the possibility that these growth factors affect osteogenic conversion. The induction of the osteoblast differentiation pathway is indicated by increased alkaline phosphatase in the early stages (day 2 to 4), and in vitro mineralization is a marker for mature osteoblasts

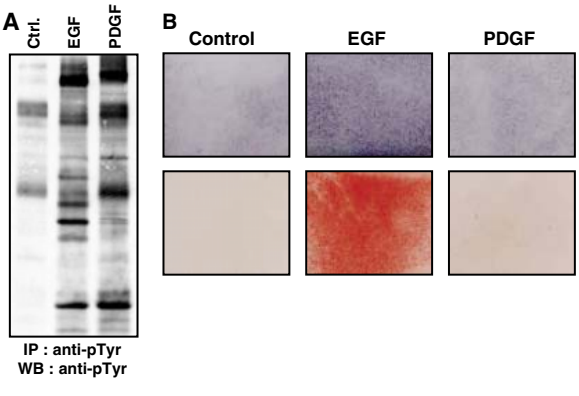

Fig. 1. Response of hMSC to EGF and PDGF stimulation. (**A**) Anti-phosphotyrosine (anti-pTyr) Western blotting (WB) of non-stimulated (Ctrl.) or EGF- or PDGF-stimulated hMSC, after immunoprecipitation (IP) with anti-pTyr. (**B**) Effects of EGF and PDGF on hMSC osteoblast differentiation. (Top) Alkaline phosphatase activity at day 3 of differentiation, visualized by in situ staining. (Bottom) Extracellular matrix in vitro mineralization after 9 days; staining with Alizarin Red S dye.

[1]Center for Experimental BioInformatics (CEBI), Department of Biochemistry and Molecular Biology, University of Southern Denmark, Campusvej 55, DK-5230 Odense M, Denmark. [2]Department of Endocrinology, Odense University Hospital, DK-5000 Odense C, Denmark.

*These authors contributed equally to this work.
†To whom correspondence should be addressed. E-mail: mann@bmb.sdu.dk

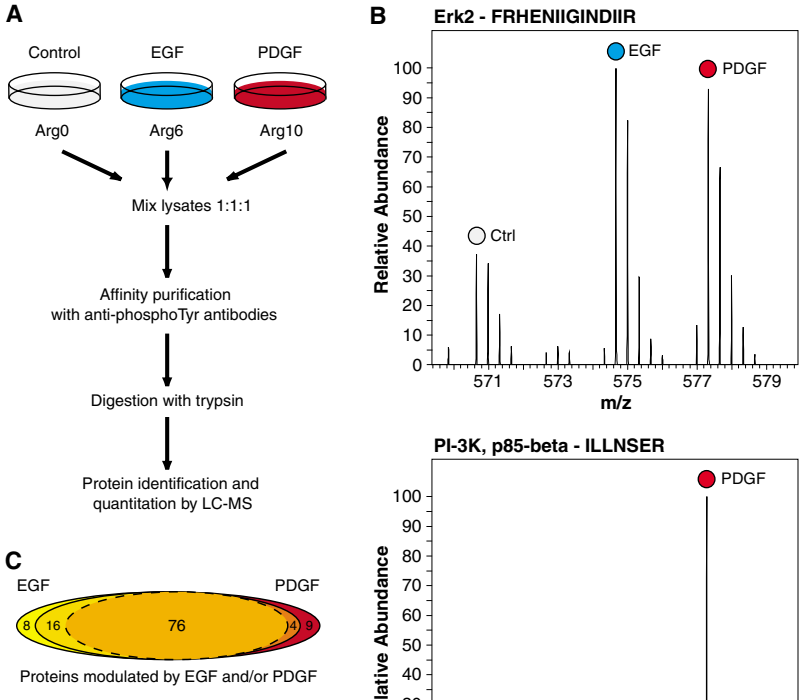

Fig. 2. Determination of EGF and PDGF phosphoprotein complexes in hMSC. (**A**) Strategy for identification and quantitative comparison of the global EGF and PDGF signaling networks. Three populations of hMSC are metabolically encoded with either normal arginine (Arg^0), or versions which are 6 daltons heavier (Arg^6) or 10 daltons heavier (Arg^{10}). After treatment with growth factors and immunoprecipitation with antibodies to pTyr, precipitated complexes are digested with trypsin and analyzed by mass spectrometry. (**B**) The degree of activation by EGF and PDGF is reflected in the ratio of the Arg^6 and Arg^{10}-containing peptides, respectively, over the Arg^0 peptides. The peptide FRHENIIGINDIIR of Erk2 (top) shows equal response of Erk2 to both growth factors, whereas the peptide ILLNSER of p85-β subunit (bottom) reveals PDGF-specific stimulation of PI3K. (**C**) Distribution of proteins involved in EGF and PDGF signaling networks. The two ellipses with solid lines contain all proteins involved in EGF (left) and PDGF (right) signaling. The overlapping area comprises the molecules common for the two signaling networks with the inner punctuated ellipse representing the proteins that were stimulated at comparable levels (within a factor of 3).

(day 9 to 12) (*10*, *11*). The addition of EGF during the course of differentiation resulted in increased activity of alkaline phosphatase (Fig. 1B, upper panel) and enhanced formation of mineralization nodules (Fig. 1B, lower panel), whereas PDGF had no effect, despite its ability to induce tyrosine phosphorylation.

To discover critical differences in the signaling mechanisms of EGF and PDGF that led to the differential effects on osteoblast differentiation of hMSC, we sought to identify and directly compare the signaling proteins regulated by tyrosine phosphorylation in response to these growth factors by mass spectrometry (MS)–based proteomics (*12*–*16*). We used stable isotope labeling by amino acids in cell culture (SILAC) (*17*), a quantitative proteomic strategy that metabolically labels the entire proteome, making it distinguishable by MS analysis. Three populations of hMSC were grown in medium containing distinct forms of arginine—either the normal $^{12}C_6$, $^{14}N_4$ version (Arg^0), or the isotopic variants $^{13}C_6$, $^{14}N_4$ (Arg^6) or $^{13}C_6$, $^{15}N_4$ (Arg^{10})—until full incorporation of the labeled amino acid was achieved. Arg^0 cells were left untreated and served as a control, Arg^6 cells were exposed to EGF, and Arg^{10} cells were exposed to PDGF (Fig. 2A). The combined cellular lysates from the three states were incubated with antibodies to phosphotyrosine. The precipitated complexes were resolved on one-dimensional SDS–polyacrylamide gel electrophoresis and proteolytically digested. The resulting peptide mixture was analyzed by liquid chromatography–tandem MS (LC-MS/MS). Tyrosine-phosphorylated proteins and proteins associated with them are efficiently isolated in this way. Arginine-containing peptides occur as triplets in the mass spectra and

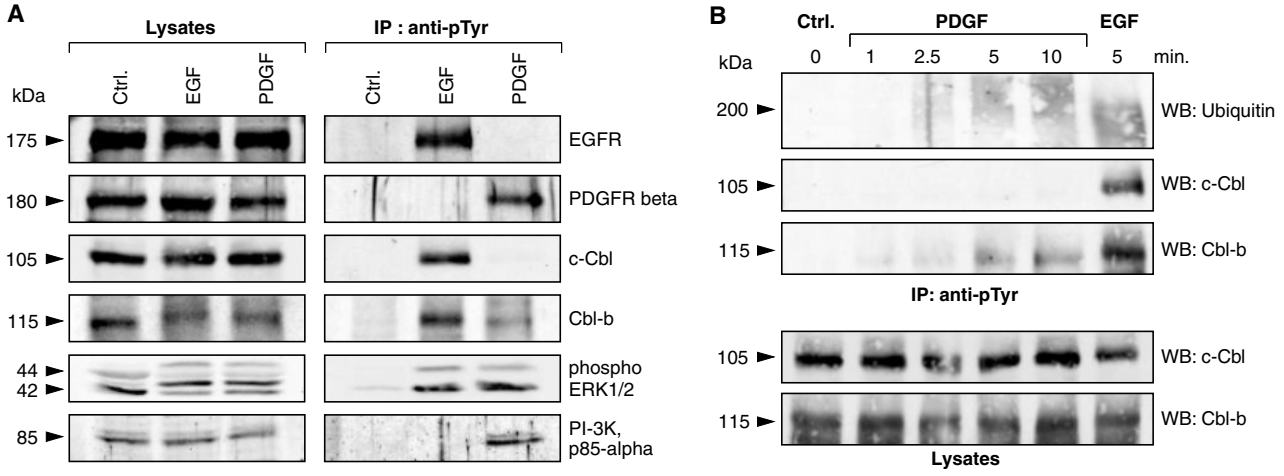

Fig. 3. Western blot (WB) analysis of selected proteins regulated by EGF and PDGF. (**A**) After 5 min stimulation with EGF or PDGF, hMSC were lysed and immunoprecipitated (IP) with antibodies to pTyr followed by Western blotting for indicated proteins. In the case of Erk1 and Erk2, lysates were directly probed with phospho-Erk1/2–specific antibody. Separate immunoblotting on the lysates is shown to serve as loading control. (**B**) Time course of PDGF receptor ubiquitination, c-Cbl and Cbl-b activation. hMSC were stimulated with PDGF for the indicated time points and 5 min stimulation with EGF was used for comparison. After anti-pTyr immunoprecipitation, Western blotting with the corresponding antibodies was used to visualize receptor ubiquitination and Cbl activation. In the lower panel, the cellular lysates were directly probed with antibodies against c-Cbl and Cbl-b to serve as loading control.

the intensity ratios of the Arg^6 and Arg^{10} to the control Arg^0 peptide directly reflect the degree of tyrosine phosphorylation of the corresponding protein or its association with other tyrosine-phosphorylated proteins as a result of the treatment with EGF and PDGF, respectively (Fig. 2B) (*15*, *16*).

We performed two independent experiments and in total identified 113 proteins with 1.5-fold or higher change in abundance in antiphosphotyrosine immunoprecipitates as a consequence of the treatment by at least one of the growth factors (Table 1). Each of these proteins was identified with at least two unique peptides, at high mass accuracy and with manual verification, ensuring no false-positive identifications in this data set. In the first experiment, we used 5×10^7 cells per condition and a quadrupole time-of-flight (QSTAR) mass spectrometer. From all 150 quantified proteins, we distinguished 79 proteins (table S1) whose abundance in the immunoprecipitates was altered after growth factor treatment. In the second experiment, we used 1.1×10^8 cells and a linear ion trap Fourier Transform (LTQ-FT) mass spectrometer and identified 106 modulated proteins from a total of 282 quantified proteins. The LTQ-FT analysis quantified all but seven of the proteins in the QSTAR data set and added another 34 because of its higher sensitivity, sequencing speed, and ability to handle larger sample amounts (table S1).

To verify the MS data set, we compared the proteomic results with a series of independent immunoblotting experiments with antibodies to 20 representative proteins regulated by EGF or PDGF. Although Western blotting is not quantitative per se, complete concordance was observed between immunoblotting and quantitative proteomic results (Table 1 and fig. S1).

After verifying the set of regulated proteins, we estimated the biological variability in the magnitude of the response of individual proteins within the measured sets. Quantitative proteomics indicated that about 90% of the proteins showed similar changes in abundance between the two large-scale experiments (within a factor of 1.3 of their average fold change; table S1 and fig. S2). For very high fold changes, agreement was also good; however, in some cases normalization to a low basal signal led to larger variation.

Many signaling molecules were found at similar amounts in the tyrosine-phosphorylated complexes of EGF- and PDGF-stimulated cells, whereas some proteins showed specific activation by one or the other of the growth factors. On the basis of the observed fold change in abundances, we categorized all 113 proteins (Table 1). Both EGF and PDGF activate a range of widely shared signaling pathways. Examples include the mitogen-activated protein kinase (MAPK) cascades and signal attenuation through receptor ubiquitination followed by endocytic removal from the cell surface (*1*, *18*). Therefore, it is not surprising that a large number of the molecules in Table 1 showed increased presence in phosphotyrosine-containing complexes from cells treated with either ligand. Less than 10% of the EGF- or PDGF-modulated proteins were unique to each growth factor (Fig. 2C).

Only five proteins showed decreased abundance in tyrosine-phosphorylated complexes of growth factor–treated cells, including a protein tyrosine kinase 9 (PTK9)–like kinase that had not previously been linked to regulation by EGF or PDGF receptors. This group contains breast cancer anti-estrogen resistance 1 protein (BCAR1), which is the human homolog of the focal adhesion docking protein p130Cas, and BCAR3, which is the human homolog of AND-34, a protein that binds to BCAR1 (*19*). The amounts of BCAR1 and BCAR3 in the immunoprecipitates were decreased in response to EGF but increased in response to PDGF (Table 1 and fig. S1), suggesting diverse roles downstream of these growth factors.

We further divided proteins based on the magnitude of their change in abundance in phosphotyrosine-containing complexes in cells treated with EGF or PDGF. We classified a protein as considerably more responsive to one ligand if its change in abundance was at least three times greater than that from cells treated with the other ligand. Several interesting observations became apparent through this categorization. For example, activated EGF and PDGF receptors appear to be preferentially attenuated by different mechanisms. Major proteins involved in the removal of the receptors from the cell membrane and its subsequent endocytosis were all much more abundant in immune complexes from EGF-treated cells, consistent with the well-known pathway involving Eps15 interacting protein (Epsin), Casitas B-lineage lymphoma proto-oncogene (Cbl), EGFR substrate 15 (Eps15), hepatocyte growth factor–regulated tyrosine kinase substrate (Hrs), signal-transducing adaptor molecule (STAM), and STAM2 (*18*, *20*) (Table 1 and fig. S1). Activated PDGF receptors, on the other hand, appear to undergo a different (or possibly delayed) endocytic pathway, mostly dependent on target of Myb1 (TOM1) and Toll-interacting protein (TOLLIP). These two proteins function in endosomal trafficking (*21*) but had not been associated with RTKs. The tyrosine phosphatase Shp-2 was also more responsive to PDGF, which could indicate faster dephosphorylation of members of the PDGF phosphoproteome (Table 1 and fig. S1).

Src homologous and collagen (Shc) and son of sevenless protein homolog 1 (Sos1)

Table 1. Proteins with altered amounts in phosphotyrosine-containing complexes after treatment of hMSC with EGF or PDGF. Proteins are categorized on the basis of their fold change (ratio) in abundances. Ratios are averages of two large-scale experiments (table S1) (*33*).

Protein name	Ratio in EGF	Ratio in PDGF
Specific proteins for EGF		
EGFR	33.7	1.09
ErbB2	12.3	1.06
c-Cbl	75	1.05
DOC-2	33.3	1.08
Acid phosphatase 1	1.62	0.87
Ribonuclease inhibitor	2.20	1.10
CYLD	21.7	1.00
KIAA2002	2.85	1.03
Specific proteins for PDGF		
PDGFR α	1.48	42
PDGFR β	0.90	56
PI-3K, p85-α	1.07	3.62
PI-3K, p85-β	0.96	6.2
PI-3K, p110-α	1.07	7.2
PI-3K, p110-β	0.91	2.20
PI-3K, p110-δ	0.86	5.9
Fyn	0.93	3.5
Protocadherin 43	1.07	14.1
Proteins with increased abundance in both EGF and PDGF		
Considerably higher in EGF		
Eps15	33.6	8.2
Cbl-b	9.5	2.01
Hrs	23.6	4.95
Epsin 2a	25.2	4.22
STAM	19.7	4.13
STAM2	27.4	5.8
Sts-1	10.9	1.93
Shc	5.7	1.49
Sos 1	7.93	1.73
SHIP2	9.0	1.73
p62Dok	17.7	2.35
p120 Catenin	7.50	1.78
CED12A	5.7	1.15
BICD2	5.69	1.12
NSAP1/hnRNP Q	4.07	1.23
EIF-2A	11.9	1.53
Considerably higher in PDGF		
Shp-2	3.74	18.0
RasGAP	2.48	16.5
TOM1	3.42	10.4
TOLLIP	2.57	7.0
Similar levels in EGF and PDGF		
Ubiquitin	11.8	17.3
TOM1L2	10.9	18.2
TSG101	4.98	8.7
Grb2	2.33	1.59
Sos 2	4.88	2.22
Erk1	2.76	2.05
Erk2	2.73	2.29
p38 Map kinase	2.77	1.92
ACK1	2.18	2.23
PLC-γ	10.7	15.7
Hypothetical- PLC-γ like	8.7	12.9
Gab1	3.11	2.91
Ras GAP-like, IQGAP 1	1.53	2.01
Vav-2	2.79	1.43
Rho GEF 6	1.48	2.40
Rho GEF 7	2.54	3.40
ARF GAP, GIT2	1.73	3.62

Table 1 continued.

Protein name	Ratio in EGF	Ratio in PDGF
Rab-6	1.61	1.46
NCK1	1.71	2.38
PDCD6-interacting protein	10.2	6.5
PDCD6IP	9.4	4.4
HECT domain LASU1	2.35	3.31
PP2A, subunit A	1.67	1.60
ApolipoproteinE receptor	2.16	2.48
AXL	1.94	1.79
Eck/EphA2	1.34	2.46
DDR2	2.57	2.23
Caveolin	1.70	1.49
PICALM	5.45	5.26
Vps28 homolog	2.83	2.26
Ymer	27.0	10.9
ANKRD13 protein	14.9	15.6
WWdomain binding protein2	4.26	5.79
FAK1	1.32	2.35
Vinculin	1.39	1.72
Paxillin	1.63	2.38
Ezrin	3.35	2.33
Catenin, β 1	2.36	1.17
Tight junction protein ZO-1	2.62	1.44
Tight junction protein ZO-2	2.54	1.48
Sorcin	4.96	2.27
Alpha-actinin 1	1.73	1.35
Alpha actinin 4	1.61	1.19
Tubulin α	2.02	1.11
ARP2	1.69	2.30
ARP3	1.53	2.06
ARP2/3, subunit 1A	1.37	1.84
ARP2/3, subunit 1B	1.77	2.21
ARP2/3, subunit 2	1.58	2.13
ARP2/3, subunit 3	1.56	2.05
ARP2/3, subunit 4	1.57	2.07
ARP2/3, subunit 5	1.60	2.10
Similar to ARP2/3, sub 5	1.71	2.05
Flightless I homolog	1.38	1.79
Gelsolin	1.37	1.87
hnRNP K	2.18	1.68
Major vault protein	1.42	1.81
PTRF	2.20	1.29
EIF-4H	1.76	1.28
NPAS 1	1.84	2.27
FAT gene product	3.24	1.48
TAK1-binding protein 1	5.70	2.22
TRK-fused gene	4.18	1.95
14-3-3 ζ/δ	1.50	1.45
14-3-3 τ	1.63	1.49
SNX3	2.45	2.94
SNX12	3.46	2.94
Annexin I	2.21	1.65
Annexin VI	1.33	1.60
Annexin VII	9.9	3.80
Annexin XI	10.9	4.0
Proteins with decreased abundance in both EGF and PDGF		
Cytochrome c	0.26	0.27
NDP kinase B	0.36	0.52
PTK9-like protein	0.61	0.59
Decreased in EGF but increased in PDGF		
BCAR1	0.44	1.64
BCAR3	0.42	1.78

had accumulated to greater extent in immunoprecipitates from EGF-stimulated cells, and growth factor receptor-bound protein 2 (Grb2) and Sos2 were also more abundant compared with immunoprecipitates from PDGF-stimulated cells. The critical role of the canonical Shc, Grb2, Sos pathway in MAPK activation is well established (*1*), yet we observed very similar amounts of phosphorylated extracellular signal–regulated kinase (Erk1) and Erk2 after exposure of cells to EGF or PDGF (Table 1 and Fig. 3A). This may imply existence of additional means of MAPK stimulation by PDGF in hMSC or of stronger negative-feedback regulation of the cascade in the case of EGF.

Surprisingly few signaling factors were uniquely affected only by one of the two ligands: only eight for EGF and nine for PDGF. This group includes the activated receptors: EGFR and ErbB2 for EGF and PDGFR α and PDGFR β for PDGF. We discovered a previously unrecognized kinase, KIAA clone 2002, specific to EGF but not PDGF signaling. A major difference in the activation profiles by the two growth factors is related to the ubiquitination of the EGF and PDGF receptors. c-Cbl is thought to be the main E3 ubiquitin ligase responsible for the ubiqitination of both types of receptors (*22*, *23*). We did find more than a 70-fold increase of c-Cbl in the phosphotyrosine immunoprecipitates from cells treated with EGF. In PDGF-stimulated cells, however, no increase in the amount of immunoprecipitated c-Cbl was detected (Table 1 and Fig. 3A), suggesting that c-Cbl does not associate with PDGF receptor. Although the abundance of Cbl-b, a related E3 ubiquitin ligase, in the immunoprecipitates was elevated as a result of the treatment with either of the growth factors, much higher fold increase was observed after EGF stimulation (Table 1 and Fig. 3A). However, the ubiquitination of the receptors after 5 min of stimulation (quantified from arginine-containing ubiquitin peptides derived from the same gel bands as the receptors) was similar or even slightly higher for the PDGF receptors (Table 1 and fig. S1). A possible explanation could be that within 5 min c-Cbl was already dephosphorylated and dissociated from PDGFR or that Cbl-b is the only E3 ubiquitin ligase downstream of PDGF receptors. We stimulated hMSC with PDGF for 1, 2.5, 5, or 10 min and monitored PDGFR ubiquitination and the levels of c-Cbl and Cbl-b activation. c-Cbl was not associated with PDGFR at any time up to 10 min, whereas receptor ubiquitination correlated with increasing presence of Cbl-b in phosphotyrosine-containing complexes (Fig. 3B). Similar results were observed in human embryonic kidney 293T cells by cotransfecting PDGFR along with c-Cbl or Cbl-b (fig. S3), supporting our finding that at least in some cell types Cbl-b is the Cbl ubiquitin ligase downstream of PDGF receptors.

A notable difference in the signaling pathways activated by the two growth factors in hMSC also stood out. Accumulation of components of the PI3K pathway was detected only after cells were treated with PDGF but not with EGF. However, both ligands caused accumulation of similar levels of Erk1, Erk2, and p38 (Table 1, Fig. 3A, and fig. S1). Moreover, we identified as specific for PDGF all of the regulatory (p85 α and β) and catalytic subunits (p110 α, β, and δ) of the PI3K; the amounts of these subunits increased on average fivefold. However, the highest ratio of any subunit upon EGF stimulation was 1.07, which is not a significant change. PI3K phosphorylates inositol lipids at the 3′ position of the inositol ring, leading to activation of Akt among other important signaling events. In osteoblasts, PI3K regulates migration and survival (*24*, *25*), but its role in the differentiation processes remains unclear and somewhat controversial (*26*, *27*).

As described above (Fig. 1B), treatment of hMSC with EGF resulted in stimulation of osteoblast differentiation, whereas PDGF did not have any effect. Because PI3K was the obvious difference between the signaling pathways induced by PDGF compared with those induced by EGF, we investigated whether the PI3K cascade could account for that divergence. We used a chemical biology strategy to block both common and specific branches of EGF- and PDGF-induced pathways. First, we applied a specific MAPK inhibitor, U0126 (*28*), to examine the role of MAPKs in osteoblast differentiation. U0126 (10 μM) completely eliminated phosphorylation, and thus activation, of Erk1 and Erk2 (fig. S4A). The addition of U0126, either to control cells or cells treated with the growth factors, also completely abolished the differentiation of hMSC to osteoblasts, verifying the critical importance of MAPK for the osteoblast conversion process (Fig. 4, A and B) (*10*, *29*). A similar effect on osteoblast differentiation was observed when hMSC were treated with p38 inhibitor (SB203580, 10 μM), suggesting that in these cells p38 activation is needed for osteoblast conversion (fig. S5).

Treatment of cells with the PI3K-specific inhibitor Wortmannin (75 nM) (*30*) inhibited PDGF-induced activation of the PI3K cascade, as measured by phosphorylation of a downstream effector Akt (fig. S4B) (*31*). Inhibition of PI3K by Wortmannin in PDGF-treated cells resulted in enhanced osteoblast differentiation compared with that of cells treated with PDGF alone. Alkaline phosphatase activity (Fig. 4A) and in vitro mineralization (Fig. 4B) in these cultures were substantially enhanced, completely mimicking the levels of stimulation observed after treatment with EGF. Furthermore, we implanted differentially treated hMSC into immunodeficient mice and determined new-

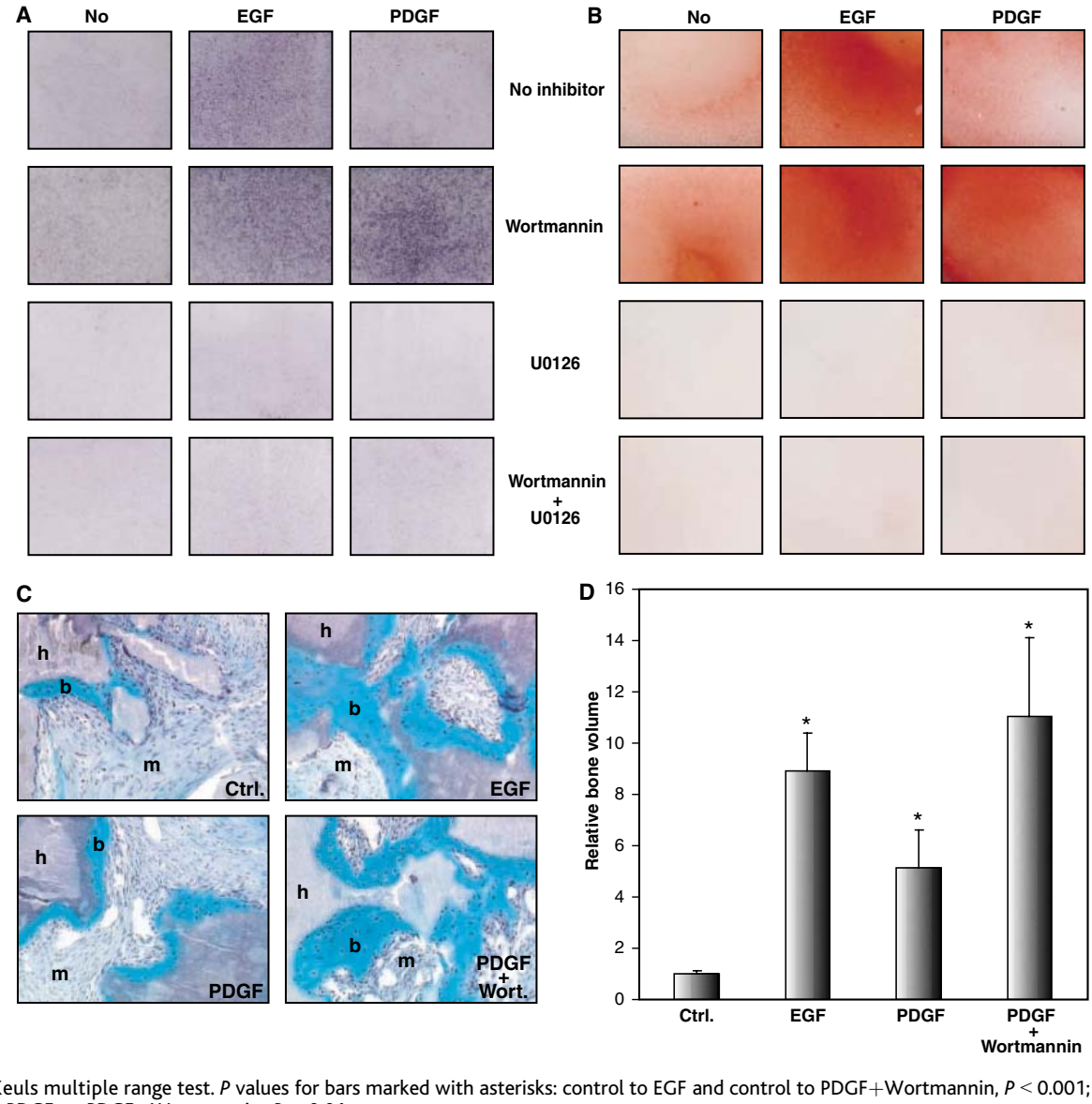

Fig. 4. Effects of PI3K and MAPK inhibitors on osteoblast differentiation and in vivo bone formation. Differentiation of hMSC to osteoblasts was carried out in the presence of EGF or PDGF. Where indicated, Wortmannin (75 nM) and U0126 (10 μM) were added in the media either alone or in combination. (**A**) Alkaline phosphatase in situ staining was performed 3 days after treatment. (**B**) Extracellular matrix mineralization at day 9 was visualized by Alizarin Red S staining. (**C**) In vivo bone formation of hMSC differentially treated for 4 days and recovered from mice after 5 weeks. Sections of implants (magnification 100×) were stained with Goldner's trichrome; bone (b), marrow (m), hydroxyapatite/tricalcium phosphate (h). Bone volume was quantified as percent of total implant volume and presented relative to control. (**D**) Three implants were used for each condition. Values are mean ± SEM. The bone volume was calculated from three distinct areas of each implant. Data were analyzed by one-way analysis of variance followed by Student-Newman-Keuls multiple range test. *P* values for bars marked with asterisks: control to EGF and control to PDGF+Wortmannin, $P < 0.001$; EGF to PDGF, $P < 0.03$; PDGF to PDGF+Wortmannin, $P < 0.01$.

ly formed bone in the transplants (Fig. 4, C and D) (*32*). In accordance with the results from cell culture differentiation, EGF-treated cells displayed enhanced bone formation in vivo. Although PDGF-treated cells also produced larger bone volume compared with that of the control, the combined treatment with PI3K inhibitor resulted in substantially increased bone formation to a level even higher than those induced by EGF (Fig. 4D). Thus, the PI3K pathway is indeed a critical control point that determines the differences of EGF and PDGF in stimulating hMSC differentiation.

We used global, quantitative phosphoproteomics to elucidate differences in closely related phosphoproteomes and to connect them with cell fate decisions. Mathematical models in systems biology have concentrated on MAPK signaling and it is hypothesized that strength and frequency of activation at this level influence cell fate. Our results demonstrated that, at least in some cases, decisions can be made by preferentially activating a small subset of the signaling network, beginning at the level of plasma membrane–associated signaling. Extensions of this work could be directed at following changes through the Ser-Thr phosphoproteome, especially related to transcription factors and transcriptional coregulators. This type of analysis provides a mechanistic "missing link" between different stimuli and resulting changes in transcription as measured by microarrays. It is possible, with a combination of proteomics and chemical biology, to discover pathways that influence cell fate. Such approaches could be beneficial for applications of stem cells to direct stem cell differentiation to clinical need more precisely.

References and Notes

1. J. Schlessinger, *Cell* **103**, 211 (2000).
2. T. Pawson, P. Nash, *Science* **300**, 445 (2003).
3. P. Blume-Jensen, T. Hunter, *Nature* **411**, 355 (2001).
4. M. F. Pittenger *et al.*, *Science* **284**, 143 (1999).
5. K. W. Liechty *et al.*, *Nat. Med.* **6**, 1282 (2000).
6. P. Bianco, P. G. Robey, *Nature* **414**, 118 (2001).
7. M. Reyes, C. M. Verfaillie, *Ann. N. Y. Acad. Sci.* **938**, 231 (2001).
8. J. L. Simonsen *et al.*, *Nat. Biotechnol.* **20**, 592 (2002).
9. I. Kratchmarova, B. Blagoev, M. Mann, data not shown.
10. R. K. Jaiswal *et al.*, *J. Biol. Chem.* **275**, 9645 (2000).
11. H. Qi *et al.*, *Proc. Natl. Acad. Sci. U.S.A.* **100**, 3305 (2003).
12. R. Aebersold, M. Mann, *Nature* **422**, 198 (2003).
13. W. X. Schulze, M. Mann, *J. Biol. Chem.* **279**, 10756 (2004).
14. J. A. Ranish *et al.*, *Nat. Genet.* **33**, 349 (2003).
15. B. Blagoev *et al.*, *Nat. Biotechnol.* **21**, 315 (2003).
16. B. Blagoev, S. E. Ong, I. Kratchmarova, M. Mann, *Nat. Biotechnol.* **22**, 1139 (2004).
17. S. E. Ong *et al.*, *Mol. Cell. Proteomics* **1**, 376 (2002).
18. I. Szymkiewicz, O. Shupliakov, I. Dikic, *Biochem. J.* **383**, 1 (2004).
19. R. B. Riggins, L. A. Quilliam, A. H. Bouton, *J. Biol. Chem.* **278**, 28264 (2003).

20. M. D. Marmor, Y. Yarden, *Oncogene* **23**, 2057 (2004).
21. Y. Katoh *et al.*, *J. Biol. Chem.* **279**, 24435 (2004).
22. C. B. Thien, W. Y. Langdon, *Nat. Rev. Mol. Cell Biol.* **2**, 294 (2001).
23. K. Haglund *et al.*, *Nat. Cell Biol.* **5**, 461 (2003).
24. F. Debiais *et al.*, *Exp. Cell Res.* **297**, 235 (2004).
25. R. Fukuyama *et al.*, *Biochem. Biophys. Res. Commun.* **315**, 636 (2004).
26. N. Ghosh-Choudhury *et al.*, *J. Biol. Chem.* **277**, 33361 (2002).
27. F. Vinals, T. Lopez-Rovira, J. L. Rosa, F. Ventura, *FEBS Lett.* **510**, 99 (2002).
28. M. F. Favata *et al.*, *J. Biol. Chem.* **273**, 18623 (1998).
29. C. F. Lai *et al.*, *J. Biol. Chem.* **276**, 14443 (2001).
30. T. Okada, L. Sakuma, Y. Fukui, O. Hazeki, M. Ui, *J. Biol. Chem.* **269**, 3563 (1994).
31. T. F. Franke *et al.*, *Cell* **81**, 727 (1995).
32. B. M. Abdallah *et al.*, *Biochem. Biophys. Res. Commun.* **326**, 527 (2005).
33. Materials and methods are available as supporting material on *Science* Online.
34. We thank all members of our laboratory for help and fruitful discussions, especially C. de Hoog for critical reading of the manuscript, J. V. Olsen for help with the LTQ-FT and statistical analysis and S.-E. Ong for help with data analysis. We thank I. Dikic for the kind gift of hemagglutinin-tagged constructs of c-Cbl and Cbl-b. Work in CEBI is supported by a grant by the Danish National Research foundation. This work was also supported by "Interaction Proteome," a 6th Framework program of the European Commission.

Supporting Online Material
www.sciencemag.org/cgi/content/full/308/5727/1472/DC1
Materials and Methods
Figs. S1 to S5
Table S1
References

17 November 2004; accepted 7 April 2005
10.1126/science.1107627

The Structure of Interleukin-2 Complexed with Its Alpha Receptor

Mathias Rickert,* Xinquan Wang,* Martin J. Boulanger, Natalia Goriatcheva, K. Christopher Garcia†

Interleukin-2 (IL-2) is an immunoregulatory cytokine that binds sequentially to the alpha (IL-2Rα), beta (IL-2Rβ), and common gamma chain (γ_c) receptor subunits. Here we present the 2.8 angstrom crystal structure of a complex between human IL-2 and IL-2Rα, which interact in a docking mode distinct from that of other cytokine receptor complexes. IL-2Rα is composed of strand-swapped "sushi-like" domains, unlike the classical cytokine receptor fold. As a result of this domain swap, IL-2Rα uses a composite surface to dock into a groove on IL-2 that also serves as a binding site for antagonist drugs. With this complex, we now have representative structures for each class of hematopoietic cytokine receptor–docking modules.

Interleukin-2 (IL-2), which is one of the first cytokines identified and a member of the four-helix bundle cytokine superfamily, acts at the heart of the immune response (*1*). IL-2 and its alpha receptor, IL-2Rα, are expressed by T cells after the activation of T cell receptors by peptide–major histocompatibility complexes. The subsequent autocrine interaction of IL-2 with its receptors leads to the stimulation of signal transduction pathways resulting in T cell, B cell, and natural killer (NK) cell proliferation and clonal expansion (*2*).

The pleiotropic biological activities of IL-2 are mediated by three cell surface receptors: the IL-2Rα chain; the IL-2Rβ chain; and the common gamma chain (γ_c), which is also a receptor for IL-4, IL-7, IL-9, IL-15, and IL-21 (*3*). These cell surface receptors form a complex that signals through the intracellular activation of the Janus tyrosine kinase 3 (Jak3) and the signal transducer and activator of transcription 5 (STAT5) (*4*). The IL-2Rα chain, originally identified as the Tac antigen (CD25) (*5*–*7*), is enigmatic in that it lacks signature features of the cytokine receptor superfamily (*8*). IL-2Rβ (p75) and the γ_c are both members of the hematopoietic growth factor receptor family, containing the signature cytokine-binding homology region (CHR), which is composed of two fibronectin type-III (FN-III) repeats (*2*, *8*).

Biochemical studies show that the assembly of the IL-2 receptor complex is initiated by the interaction of IL-2 with IL-2Rα, followed by sequential recruitment of IL-2Rβ and γ_c (*9*, *10*). IL-2Rα alone is the "low-affinity" receptor (dissociation constant $K_d \sim 10$ nM). When expressed together, IL-2Rα and IL-2Rβ form the pseudo–high-affinity receptor ($K_d \sim 30$ pM). Finally, the IL-2Rα$\beta\gamma_c$ complex forms the high-affinity receptor ($K_d \sim 10$ pM) that is the signaling complex found on activated T cells (*2*). The IL-2Rβ and γ_c binding sites on IL-2 have been mapped to locations analogous to the site I and site II cytokine-binding sites originally established in the human growth hormone (hGH) system (*11*). However, based on sequence analysis and mutagenesis studies, IL-2Rα is predicted to differ from other cytokine receptors in both its structure and its mode of interaction with IL-2 (*12*).

IL-2Rα is a target for therapeutic modulation because it is not expressed on resting T and B cells but is continuously expressed by the abnormal T cells of patients with forms of leukemia, autoimmunity, and organ transplant rejection (*13*, *14*). An antagonistic monoclonal antibody to IL-2Rα (anti-Tac) (Daclizumab) is effective in preventing the rejection of organ transplants (*15*). Small-molecule inhibitors of IL-2Rα have also been developed (*16*, *17*). IL-2 (Proleukin) itself is used to augment immune system function and has efficacy in treating metastatic renal carcinoma and melanoma (*18*). However, there is severe dose-limiting toxicity that is largely attributed to activation of the $\beta\gamma_c$ form of the receptor on NK cells (*18*). Currently, no structural information exists for any of the IL-2 receptors, and this information could assist in the design of improved therapeutics. Here we present a crystal structure at 2.8 Å resolution of human IL-2 in complex with the extracellular domain of IL-2Rα (*19*).

In the complex structure, the IL-2Rα ectodomain resembles an arm bent ~90° at the elbow between the N- and C-terminal domains (D1 and D2, respectively), engaging IL-2 along the length of the underside of D1 (Fig. 1, A and B). The IL-2 binding surface comprises helix A′, helix B′, and part of the AB loop. The long axes of the IL-2Rα β sheets are aligned parallel with the helical axes of the cytokine. This differs from the typical cytokine receptor interaction. For example, in the complex of hGH with its receptor (hGH-R), the CHR module of hGH-R, composed of two β-sandwich FN-III domains, forms a considerably larger, but similar, bent arm–like structure (Fig. 1B) (*20*). However, the protruding elbow region of hGH-R exposes loops that bind to the sides of the hGH four-helix bundle (*20*) (Fig. 1B). Although substantially different, the closest similarity can be found in the recently elucidated site III contact between gp130-class cytokines and the gp130 D1 domain (*21*). However, in that interaction, the cytokine forms contacts exclusively through loops at the tip of the cytokine, rather than with residues on the helical surfaces.

In the IL-2Rα structure, the core D1 and D2 domains are separated by a 42-residue interdomain linker peptide (Thr^{65} to His^{103}), and the second domain has an additional C-terminal 54-residue connecting peptide leading to the cell membrane (Gly^{165} to Glu^{217}). Neither of these linkers is visible in the electron density

Departments of Microbiology and Immunology, and Structural Biology, Stanford University School of Medicine, 299 Campus Drive, Fairchild D319, Stanford, CA 94305–5124, USA.

*These authors contributed equally to this work.
†To whom correspondence should be addressed. E-mail: kcgarcia@stanford.edu

map, and they are therefore not included in the IL-2Rα model (Fig. 1A). These linker segments do not contribute to ligand binding. Thus, 120 residues (D1 and D2 domains) of the 217–amino acid extracellular domain are structured. It is possible that this extensive amount of flexible polypeptide contributed to the difficulties in obtaining crystals suitable for a structure determination, as crystallization of the complex was originally reported in 1989 (*22*).

IL-2Rα deviates from the classical cytokine receptor fold, both in the structures of the individual domains and in the interdomain folding topology (Fig. 1A). Each of the two IL-2Rα domains exhibits ~30% amino acid homology to a group of β-sandwich protein domains variously called sushi domains, short consensus repeats (SCRs), or complement control protein (CCP) repeats (*23*) (Fig. 2B). Canonical sushi domains (~65 amino acids in a 2-on-3 sandwich) can be considered "mini" FN-III–type domains (~110 residues in a 3-on-4 sandwich). Like sushi domains, IL-2Rα D1 (residues 1 to 64) and D2 (residues 104 to 165) show an elliptical β-sandwich structure, containing several residues that are highly conserved in sushi domains of several complementary related proteins ($Cys^{3/30/46/61}$, Pro^{7}, Tyr^{20}, Gly^{33}, Phe^{34}, and Trp^{55}) (*24*). However, both IL-2Rα domains deviate substantially from canonical sushi topology; they are 1-on-4, instead of 2-on-3, β sandwiches. The folding topology of IL-2Rα also exhibits swapping of β strands across the N- and C-terminal sushi-like domains (Fig. 2A). Strands A and B exchange with strands F and G, respectively, to give the folding topology F-on-G-C-D-E for D1 and A-on-B-H-I-J for D2. Interdomain disulfide bonds between Cys^{3} and Cys^{46} of D1 and Cys^{147} and Cys^{104} of D2 enforce the strand exchange by pinning strand A of D1 to strand I of D2 and strand G of D2 to strand D in D1 (Figs. 1A and 2A). This strand exchange has not been seen among β−sandwich–type structures (Fig. 2B), or in classical FN-III–type cytokine receptors. The IL-15 α receptor is a single sushi domain, so there is not the possibility for a strand exchange in that case.

Despite the unstructured 42–amino acid linker peptide in IL-2Rα, the D1 and D2 domains are in intimate contact with one another through an extensive interdomain interface. A large hydrophobic core is formed between the swapped top strands in each domain, which likely imparts rigidity to the overall structure (Fig. 1A). These exposed aromatics on the surface of the top strands of the β sandwich would serve as the inner hydrophobic core between the top and bottom sheets of a canonical sushi domain, if the strands in IL-2Rα were not domain-swapped.

The IL-2 molecule has the common cytokine fold (*8*), with the typical up-up-down-down four-helix topology. The four-helix bundle structure of the IL-2 molecule in the IL-2/IL-2Rα complex closely superimposes with the free IL-2 molecule [0.74 Å root mean square deviation (RMSD) on 76 Cα positions], but with minor structural adapta-

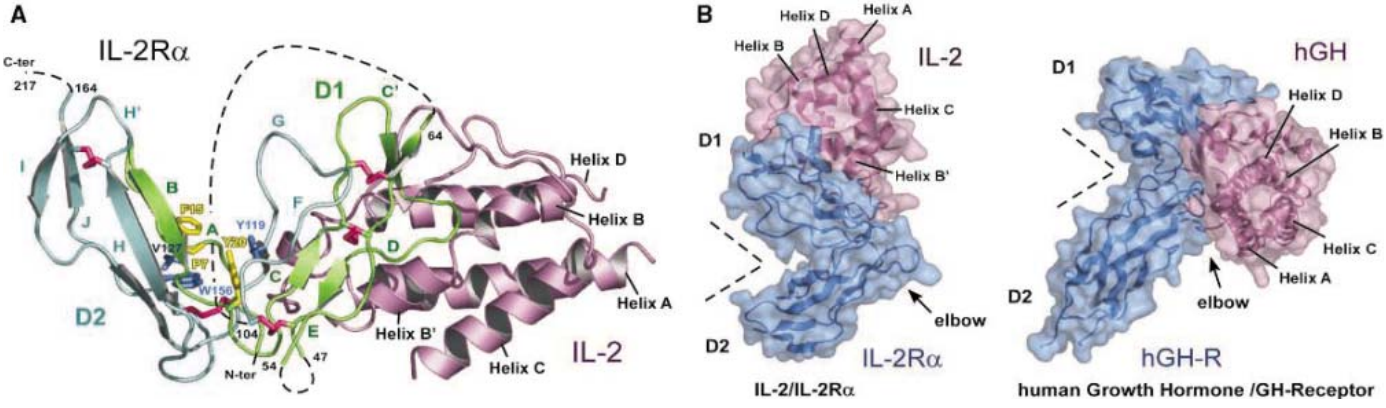

Fig. 1. Structure of the human IL-2/IL-2Rα complex. (**A**) Side view of the complex showing IL-2Rα covering the groove between the AB loop and helix B′. The IL-2Rα D1 domain is green, the D2 domain is cyan, and IL-2 is violet. Disulfide bonds of IL-2Rα are pink. Hydrophobic core residues between D1 and D2 are drawn as yellow and blue sticks, respectively. Disordered connecting regions, which are not part of the experimental model, are shown as black dotted lines. This coloring scheme is maintained in Figs. 1 to 4. (**B**) The binding mode between IL-2 and IL-2Rα versus the classical site I/II paradigm of hGH and its receptor, in which the elbow of the receptor binds to the sides of the cytokine four-helix bundle (*20*). A semitransparent surface representation with receptor chains in blue and ligands in violet is shown. Black dotted vees indicate the elbow regions of IL-2Rα and hGH-R.

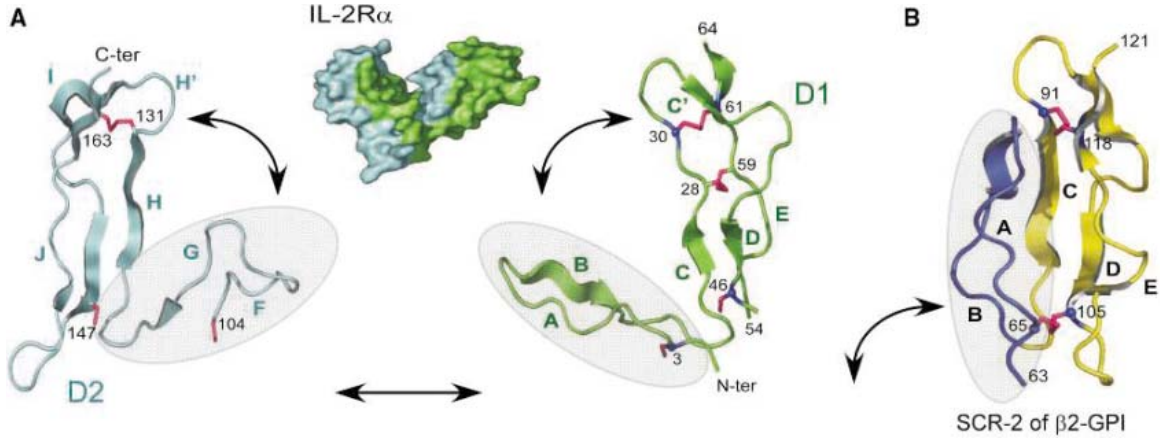

Fig. 2. Domain swapping in IL-2Rα. (**A**) The IL-2Rα model is separated into D1 and D2 domains revealing the swapped A and B, and F and G strand locations, respectively. Semitransparent ovals in two diagrams of the separated sushi domains highlight the corresponding strands, which are involved in the strand swap. A surface representation of IL-2Rα in the center shows the complete receptor molecule. (**B**) A representative structure of a sushi domain, or CCP module [second domain of β_2 glycoprotein-1 (Protein Data Bank entry 1QUB)] (*23*, *32*). The analogous strands to those involved in the strand swap between IL-2Rα D1 and D2 domain are blue and highlighted by a semitransparent oval.

tions in the receptor binding site (*25*, *26*). The IL-2 CD loop, which is usually disordered in uncomplexed IL-2 structures, is completely ordered in the receptor-bound IL-2 structure because residues Glu[106] to Asp[109] are involved in binding to IL-2Rα. The first and last turn of helix A′ as well as the last turn of helix B′ are partially unwound as compared with free IL-2 (fig. S1).

The interaction between IL-2 and IL-2Rα occurs between the four-stranded β sheet, strands G-C-D-E, and the IL-2 A′ and B′ helices (Fig. 3A). As a result of complex formation, 20 IL-2 residues and 21 IL-2Rα residues bury a total of 1868 Å (fig. S2 and table S2). Two prominent hydrophobic patches on IL-2 are consistent with thermodynamic measurements indicating that the desolvation of apolar surface is the primary energetic driving force of this interaction (red amino acids in Fig. 3B and red patches in Fig. 4A). The first patch is composed of Tyr[45] on the AB loop of IL-2, which packs into a pocket formed by the methylene groups of Arg[35] and Arg[36] of the IL-2Rα C′ strand. This hydrophobic cluster is surrounded by polar interactions. Mutations of IL-2Rα Arg[35] and Arg[36] disrupt interaction with IL-2 (*27*).

The most conspicuous and centrally located hydrophobic cluster is composed of Phe[42] and Leu[72] on the IL-2 AB loop and helix B′, respectively, inserting into a recessed pocket on IL-2Rα composed of Leu[42] to Tyr[43], and Met[25] (fig. S4 and Figs. 3B and 4A). Several salt bridges and hydrogen bonds surround this hydrophobic patch (Fig. 3A and table S2). Mutational studies identify this second hydrophobic region around IL-2 Phe[42] as the primary energetic determinant in the IL-2–binding epitope (*27*, *28*). T cells can express IL-2 splice variants, which are natural inhibitors of IL-2 signaling through the high-affinity $\alpha\beta\gamma_c$ receptor (*29*). The splice variants lack either exon 2 (IL-2δ2), which encodes Asn[30] to Lys[49], or exon 3 (IL-2δ3), which encodes Ala[50] to Lys[97]. Because these regions are involved in the interaction between IL-2Rα and full-length IL-2, the splice variants would almost certainly not bind IL-2Rα. Thus, the mechanism of inhibition appears to be the occupation of the IL-2Rβ and γ_c receptors, preventing recruitment of IL-2Rα by wild-type IL-2 and inhibiting signaling on activated T cells through the $\alpha\beta\gamma_c$ complex.

The disruption of protein-protein interactions with small molecules has proven to be an exceedingly difficult goal for the pharmaceutical industry in comparison to the inhibition of enzyme active sites. However, potent small-molecule inhibitors of the IL-2/IL-2Rα interaction have been developed (*17*). One of these small molecules, compound 1 (*16*), fits into a groove between the IL-2 AB loop and helix B′, wrapping around IL-2 Phe[42] as a hydrophobic anchor residue (Fig. 4B) (*17*). In binding to IL-2, the small molecule induces the rearrangement of residues Lys[35], Arg[38], Met[39], and Phe[42], compared with several unliganded IL-2 structures (*17*). In particular, a large change in conformation of the IL-2 Phe[42] aromatic ring creates the recessed channel used for binding the drug (Fig. 4B). This conformational adjustment does not occur upon receptor binding; in contrast, Phe[42] is a prominent knob fitting into a pocket on IL-2Rα. Superposition of the drug/IL-2 complex on the IL-2/

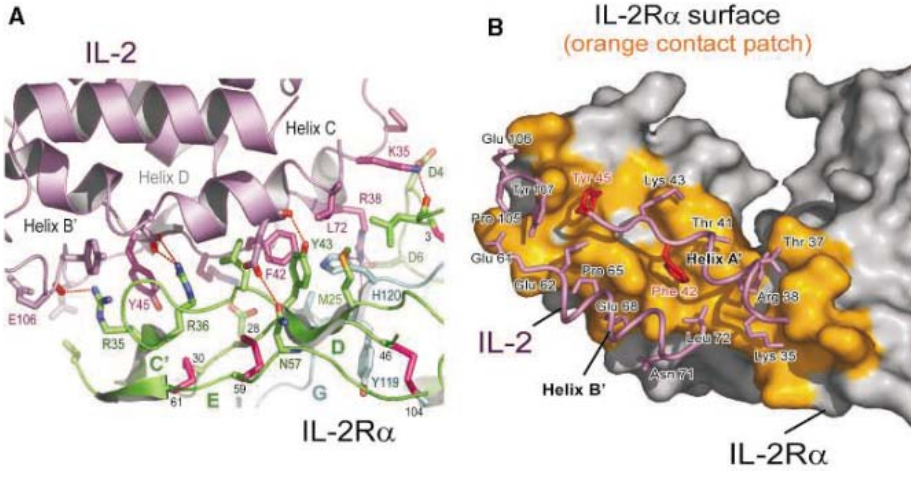

Fig. 3. Molecular anatomy of the IL-2/IL-2Rα interface. (**A**) Amino acid contact residues within the complex interface. IL-2 (violet) is at the top and the IL-2Rα D1 domain (green) and D2 domain (cyan) are at the bottom. Hydrogen bonds appear as red dotted lines; disulfide bonds are pink; corresponding cysteine residues are numbered; and β sheets and connecting loops of IL-2Rα are labeled as indicated. (**B**) "Footprint" surface representation of the IL-2Rα interface viewed through the IL-2 helices onto the IL-2Rα. Contact residues of IL-2 (violet sticks) are projected onto the buried surface (orange) of IL-2Rα. The hydrophobic anchor residues Phe[42] and Tyr[45] of IL-2 are colored red to orient the reader throughout the interface.

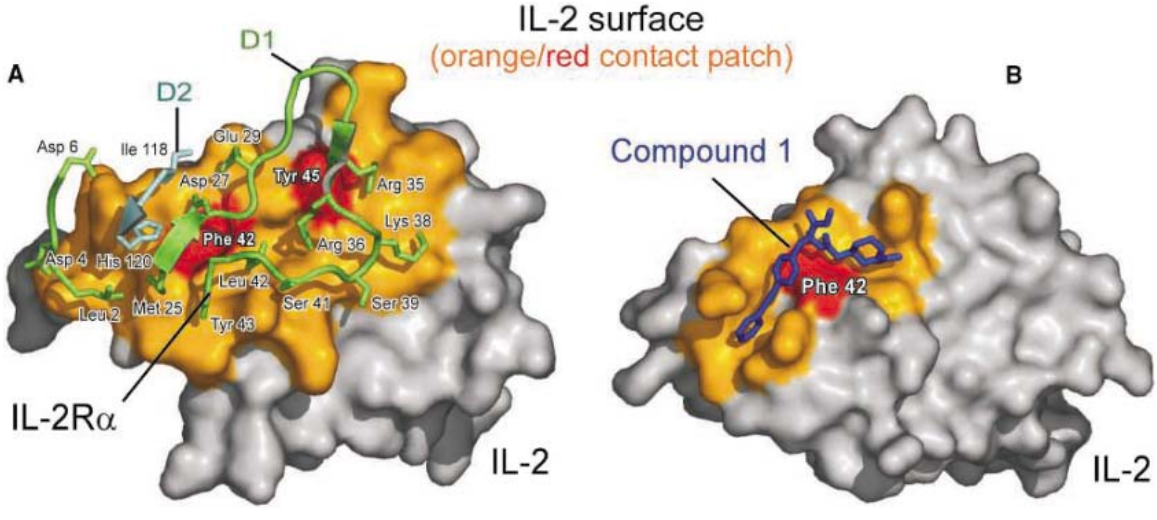

Fig. 4. Comparison of receptor versus drug binding to IL-2. (**A**) "Footprint" representation of IL-2 interface as viewed through the IL-2Rα β strands onto the IL-2 surface. Contact residues of IL-2Rα (green and cyan sticks) are projected onto the buried surface (orange) of IL-2. The hydrophobic anchor residues Phe[42] and Tyr[45] of IL-2 are red. (**B**) Analogous footprint view of the drug compound 1 bound to IL-2. Compound 1 is depicted with blue sticks [Protein Data Bank entry name 1M48 (*17*)] projected onto the buried surface (orange) of IL-2. Compound 1 uses IL-2 Phe[42] (red patch) as an anchor residue, thereby preventing IL-2Rα from binding to IL-2.

IL-2Rα complex reveals that although a substantial portion of the drug fits within open space in the interface, there are steric clashes with the IL-2 Phe[42] binding pocket. The drug apparently uses highly favorable enthalpic interactions to compensate for the entropic penalty of binding (*17*) and to overcome its small buried surface area. In contrast, binding of IL-2Rα to IL-2 is entropically favorable. Hence, even though the drug and receptor target a similar hydrophobic hot spot, they use opposite thermodynamic solutions for binding.

Previously determined binding modes between hematopoietic cytokines and their receptors involve combinations of the classical site I/II and the recently determined site III mode for gp130 cytokines (*21*). We suggest that the distinctive docking geometry of the IL-2/IL-2Rα interaction is a fourth binding mode and now gives us representative examples of all binary recognition modules used by hematopoietic receptors to recognize four-helix cytokines. These four modules can be used as building blocks, in different combinations, to construct topological models for complexes between all known cytokines and their receptors. As discussed, IL-2 also binds to two additional receptor subunits, the IL-2Rβ and γ_c chains, to form a quaternary signaling complex. Functional studies and molecular modeling placed the binding epitopes of IL-2Rβ and γ_c on the faces of adjacent helices A (IL-2 Asp[20]) and D (IL-2 Gln[126]), respectively (*11*, *14*, *30*) (figs. S1 and S5). It has been postulated that IL-2Rβ will bind in site I–type and γ_c will bind in site II–type geometries (Fig. 1B, hGH complex). The binding site of IL-2Rα is ideal for an initial engagement of cytokine, leaving sides of the helical faces open for engagement of the IL-2Rβ and γ_c components. By initially capturing IL-2 on the cell surface, the IL-2Rα would reduce the entropic cost for the subsequent recruitment of additional receptors (*31*).

References and Notes

1. K. A. Smith, *Science* **240**, 1169 (1988).
2. B. H. Nelson, D. M. Willerford, *Adv. Immunol.* **70**, 1 (1998).
3. P. E. Kovanen, W. J. Leonard, *Immunol. Rev.* **202**, 67 (2004).
4. Y. Minami, T. Kono, T. Miyazaki, T. Taniguchi, *Annu. Rev. Immunol.* **11**, 245 (1993).
5. T. Uchiyama *et al.*, *J. Clin. Invest.* **76**, 446 (1985).
6. W. J. Leonard *et al.*, *Nature* **300**, 267 (1982).
7. W. J. Leonard *et al.*, *Nature* **311**, 626 (1984).
8. J. F. Bazan, *Proc. Natl. Acad. Sci. U.S.A.* **87**, 6934 (1990).
9. S. F. Liparoto, T. L. Ciardelli, *J. Mol. Recognit.* **12**, 316 (1999).
10. M. Rickert, M. J. Boulanger, N. Goriatcheva, K. C. Garcia, *J. Mol. Biol.* **339**, 1115 (2004).
11. P. Bamborough, C. J. Hedgecock, W. G. Richards, *Structure* **2**, 839 (1994).
12. R. M. Stroud, J. A. Wells, *Sci. STKE* **2004**, re7 (2004).
13. A. C. Church, *Q. J. Med.* **96**, 91 (2003).
14. J. Theze, P. M. Alzari, J. Bertoglio, *Immunol. Today* **17**, 481 (1996).
15. T. A. Waldmann, J. O'Shea, *Curr. Opin. Immunol.* **10**, 507 (1998).
16. J. W. Tilley *et al.*, *J. Am. Chem. Soc.* **119**, 7589 (1997).
17. M. R. Arkin *et al.*, *Proc. Natl. Acad. Sci. U.S.A.* **100**, 1603 (2003).
18. J. W. Eklund, T. M. Kuzel, *Curr. Opin. Oncol.* **16**, 542 (2004).
19. Materials and methods are available as supporting material on *Science* Online.
20. A. M. de Vos, M. Ultsch, A. A. Kossiakoff, *Science* **255**, 306 (1992).
21. M. J. Boulanger, D. C. Chow, E. E. Brevnova, K. C. Garcia, *Science* **300**, 2101 (2003).
22. G. Lambert, E. A. Stura, I. A. Wilson, *J. Biol. Chem.* **264**, 12730 (1989).
23. M. Baron, D. G. Norman, I. D. Campbell, *Trends Biochem. Sci.* **16**, 13 (1991).
24. D. A. Shackelford, I. S. Trowbridge, *EMBO J.* **5**, 3275 (1986).
25. B. J. Brandhuber, T. Boone, W. C. Kenney, D. B. McKay, *Science* **238**, 1707 (1987).
26. J. F. Bazan, *Science* **257**, 410 (1992).
27. R. J. Robb, C. M. Rusk, M. P. Neeper, *Proc. Natl. Acad. Sci. U.S.A.* **85**, 5654 (1988).
28. K. Sauve *et al.*, *Proc. Natl. Acad. Sci. U.S.A.* **88**, 4636 (1991).
29. V. N. Tsytsikov, V. V. Yurovsky, S. P. Atamas, W. J. Alms, B. White, *J. Biol. Chem.* **271**, 23055 (1996).
30. S. M. Zurawski, J. L. Imler, G. Zurawski, *EMBO J.* **9**, 3899 (1990).
31. Z. Wu *et al.*, *J. Biol. Chem.* **270**, 16039 (1995).
32. R. Schwarzenbacher *et al.*, *EMBO J.* **18**, 6228 (1999).

33. We thank K. A. Smith, J. F. Bazan, P. Strop, D. McKay, B. Weis, and D. Bushnell for helpful discussions. This work was funded by grants from the Keck Foundation, Pew Trust, and NIH (AI51321). The coordinates and structural factors have been deposited in the Protein Data Bank with accession no. 1Z92.

Supporting Online Material

www.sciencemag.org/cgi/content/full/308/5727/1477/DC1
Materials and Methods
Figs. S1 to S5
Tables S1 and S2
References

13 January 2005; accepted 7 April 2005
10.1126/science.1109745

A Fluoroquinolone Resistance Protein from *Mycobacterium tuberculosis* That Mimics DNA

Subray S. Hegde,[1]* Matthew W. Vetting,[1]* Steven L. Roderick,[1] Lesley A. Mitchenall,[2] Anthony Maxwell,[2] Howard E. Takiff,[3] John S. Blanchard[1]†

Fluoroquinolones are gaining increasing importance in the treatment of tuberculosis. The expression of MfpA, a member of the pentapeptide repeat family of proteins from *Mycobacterium tuberculosis*, causes resistance to ciprofloxacin and sparfloxacin. This protein binds to DNA gyrase and inhibits its activity. Its three-dimensional structure reveals a fold, which we have named the right-handed quadrilateral β helix, that exhibits size, shape, and electrostatic similarity to B-form DNA. This represents a form of DNA mimicry and explains both its inhibitory effect on DNA gyrase and fluoroquinolone resistance resulting from the protein's expression in vivo.

Increasing resistance to two bactericidal compounds that act on rapidly growing *Mycobacterium tuberculosis*, isoniazid and rifampicin, is driving the search for new therapies. Fluoroquinolones exert their powerful antibacterial activity by interacting with DNA gyrase and DNA topoisomerase IV (*1*). They bind reversibly to the enzyme-DNA complex and stabilize the covalent enzyme tyrosyl-DNA phosphate ester, which is normally a transient intermediate in the topoisomerase reaction. Hydrolysis of this linkage leads to the accumulation of double-stranded DNA fragments and is the bactericidal consequence of fluoroquinolone treatment. Newer fluoroquinolones, including moxifloxacin and gatifloxacin, exhibit powerful in vitro activity against mycobacteria (*2*, *3*), and they can reduce multidrug treatment regimens from 6 to 4 months when substituted for isoniazid (*4*). Resistance to fluoroquinolones remains rare in clinical isolates of *M. tuberculosis* (*5*), but it has been increasing as their use in the treatment of multidrug-resistant *M. tuberculosis* infections increases (*6*). High-level resistance to fluoroquinolones in laboratory strains of *M. tuberculosis* and *M. smegmatis* (*7*, *8*) is known to result from amino acid substitutions in the putative fluoroquinolone binding region of the *M. tuberculosis gyrA*-encoded A subunit of DNA gyrase (*7*, *8*). This is the only type II topoisomerase encoded in the *M. tuberculosis* genome (*9*) and thus is the unique target for fluoroquinolones in this organism (*10*, *11*).

[1]Department of Biochemistry, Albert Einstein College of Medicine, 1300 Morris Park Avenue, Bronx, NY 10461, USA. [2]Department of Biological Chemistry, John Innes Centre, Colney Lane, Norwich NR4 7UH, UK. [3]Laboratorio de Genética Molecular, Centro de Microbiología y Biología Celular, Instituto Venezolano de Investigaciones Científicas, Caracas 1020A, Venezuela.

*These authors contributed equally to this work.
†To whom correspondence should be addressed. E-mail: blanchar@aecom.yu.edu

Genetic selection for fluoroquinolone resistance in *M. smegmatis* identified a new resistance mechanism (*12*). The *mfpA*-encoded protein, when expressed from a multicopy plasmid, resulted in low-level resistance (a 4- to 8-fold increase in the minimum inhibitory concentration) to ciprofloxacin and sparfloxacin. The sequence of MfpA revealed it to be a member of the "pentapeptide repeat" family of bacterial proteins (*13*), in which every fifth amino acid is either a leucine or phenylalanine. *M. tuberculosis* contains a 183–amino acid MfpA homolog (*Mt*MfpA), encoded by the *Rv3361c* gene, that is 67% identical to the 192-residue *M. smegmatis* MfpA protein. A second member of the pentapeptide repeat family is the McbG protein responsible for resistance to microcin B17 in *Escherichia coli* (*14*). Microcin B17 also inhibits DNA gyrase (*15*), although by a different mechanism of action than fluoroquinolones (*16*). A third member of the pentapeptide repeat family is the plasmid-encoded Qnr protein, originally identified in quinolone-resistant strains of *Klebsiella pneumoniae* (*17*). This plasmid-encoded protein protects DNA gyrase against fluoroquinolone inhibition (*18*), and similar proteins have been identified in fluoroquinolone-resistant clinical isolates of *Enterobacteriae* in Japan (*19*) and Europe (*20*).

The *M. tuberculosis* Rv3361c open reading frame was amplified by polymerase chain reaction from *M. tuberculosis* strain $H37R_v$ genomic DNA and ligated into a pET28a plasmid. Expression in *E. coli* strain BL21(DE3), induced by isopropyl-β-D-thiogalactopyranoside and transformed with the plasmid, yielded extracts from which the protein could be purified to homogeneity using nickel-nitriloacetate chromatography.

The expressed MfpA protein was tested for its effect on both adenosine triphosphate (ATP)–dependent DNA supercoiling and ATP-independent relaxation reactions catalyzed by *E. coli* DNA gyrase. *Mt*MfpA inhibited both reactions in a concentration-dependent manner (Fig. 1, A and B). The apparent median inhibitory concentration (IC_{50}) values were calculated to be ~1.2 μM (based on an active dimer, see below) for both reactions. To distinguish between indirect effects on catalysis or the direct interaction of MfpA with gyrase, we performed surface plasmon resonance experiments using standard amine coupling of MfpA to carboxymethyl sensor chips. The signal was saturable with increasing concentrations of gyrase and allowed us to calculate a dissociation constant (K_d) value of 460 nM from the ratio of k_{on} and k_{off} values of $\sim 10^3$ M^{-1} s^{-1} and $\sim 10^{-4}$ s^{-1}, respectively (Fig. 1C). These values are in approximate agreement with the IC_{50} values obtained for gyrase inhibition, indicating that MfpA interacts directly with DNA gyrase.

MfpA was crystallized by vapor diffusion under oil, and both native and selenomethionine-substituted proteins were crystallized in several space groups that diffracted to 2.0 to 2.7 Å. Diffraction data on selenomethionine-substituted protein crystals in space group $P3_221$ were collected at three wavelengths (table S1). Higher resolution data from the native protein in the $P2_1$ crystal form were added to extend the phases and improve the quality of the maps (fig. S1). The final structure was refined to 2.0 Å (Table 1 and table S2).

MfpA is a dimer in solution (*21*) and in the crystal, with the C-terminal α helices interacting to generate the dimer. The MfpA monomer is almost entirely composed of a right-handed β helix (Fig. 2A) (residues 2 to 165 out of 183 residues) that has eight complete coils, each with four nearly equivalent sides, giving the core of the structure a quadrilateral appearance (Fig. 2B). The coils are stacked upon each other with only a slight left-handed twist. Each of the sides is made up of one of the pentapeptide-repeating units, with the middle hydrophobic residue (i) and the first small polar or hydrophobic residue (i^{-2}) pointing inwards and the remaining residues (i^{-1}, i^{+1}, and i^{+2}) pointing outwards (Fig. 2C and fig. S2). There is extensive hydrogen bonding interaction between the peptide backbone atoms of neighboring coils,

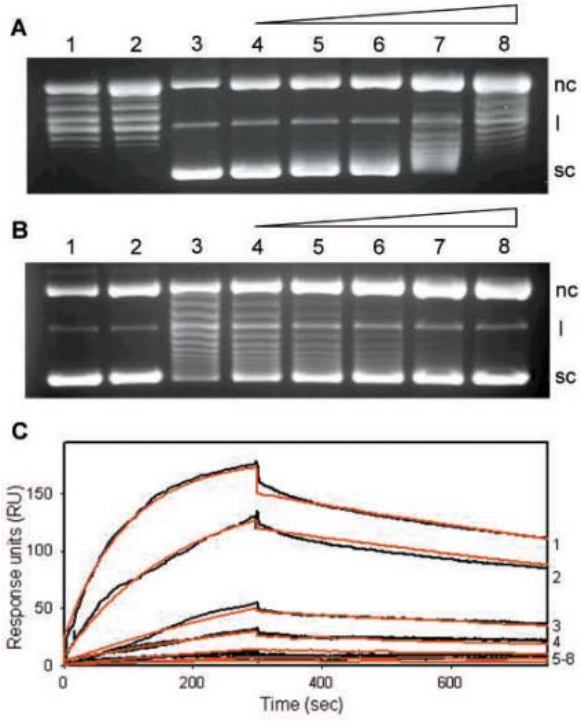

Fig. 1. (**A** and **B**) Inhibition of supercoiling and relaxing activity of *E. coli* DNA gyrase by MfpA. (A) Lane 1, relaxed plasmid pBR322 alone; lane 2, relaxed pBR322 containing 5 μM MfpA; lane 3, 3 units of gyrase; lanes 4 to 8, 3 units of gyrase and 1, 2, 3, 5, and 8 μM MfpA, respectively. (B) Lane 1, supercoiled pBR322; lane 2, supercoiled pBR322 containing 5 μM MfpA; lane 3, supercoiled pBR322 with 25 units of gyrase; lanes 4 to 8, 25 units of gyrase containing 1, 2, 3, 5, and 8 μM MfpA, respectively. nc, l, and sc represent nicked circular, linear, and supercoiled forms, respectively. Gyrase assays were performed as described elsewhere (SOM text). (**C**) BIAcore sensorgrams of DNA gyrase binding to MfpA. DNA gyrase, at 12 μM (line 1), 6 μM (line 2), 1.5 μM (line 3), 0.75 μM in duplicate (line 4), 0.375 μM in duplicate (line 5), 0.188 μM (line 6), and 0.094 μM (line 7), and the buffer alone (line 8) were injected to immobilized MfpA as described, and the sensograms were recorded. Black lines show experimentally recorded values; red lines are a fit of the data to a 1:1 Langmuir model.

Table 1. Data collection and refinement statistics for MfpA. Statistics for the highest bin are in parentheses. RMS, root mean square.

Data collection and refinement statistics	
Data statistics	
Space group	$P2_1$
Unit cell (Å/°)	a = 53.8, b = 31.0, c = 96.8, β = 93.2
Maximum resolution (Å)	2.0 (2.0 to 2.07)
Completeness (%)	98.8 (95.8)
R_{sym} (%)	3.2 (16.1)
Mean I/σ(I)	29.6 (7.4)
Redundancy	4.4 (3.5)
Refinement statistics	
Model	A1 to A183, B1 to B180, 205 H_2O, 1 SO_4
R_{work}/R_{free} (%)	17.7 (16.6)/21.8 (22.2)
RMS deviations from ideal Bond (Å)/angle (°)	0.021/1.89
Average B-factor (Å^2) Protein/nonbonded	18.7/28.9

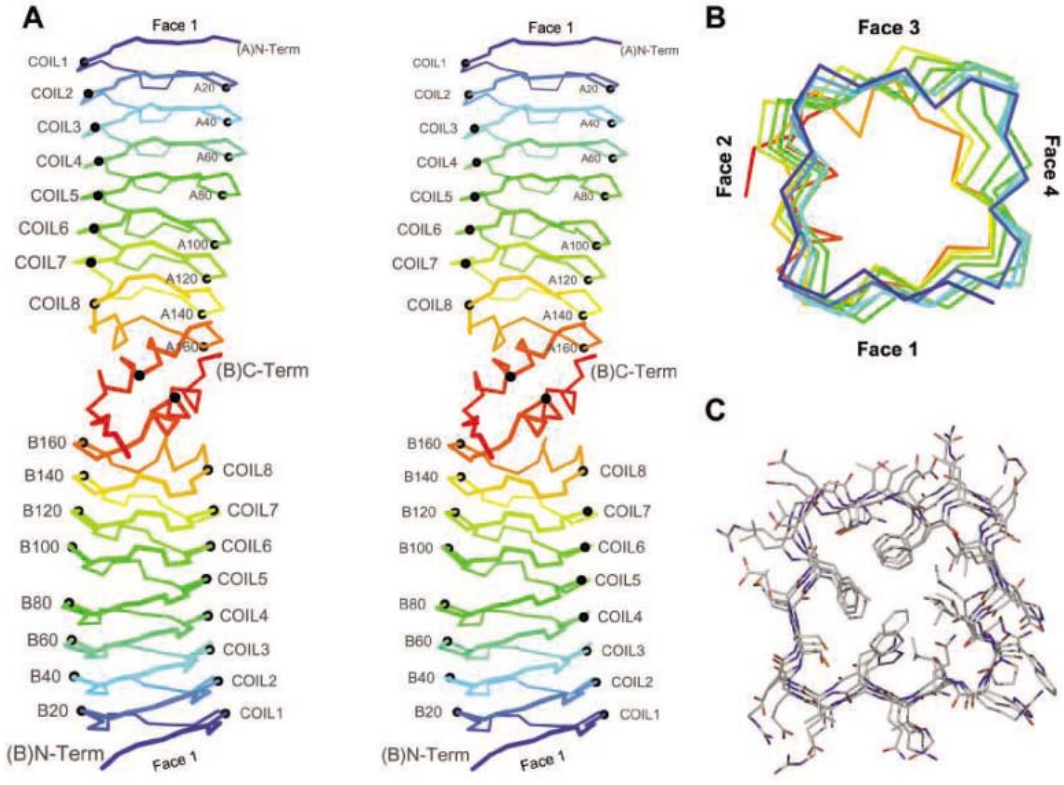

Fig. 2. MfpA structural fold illustrations. (**A**) Stereoview of the Cα trace of the MfpA dimer, shown with the monomers colored from blue (N terminus) to red (C terminus). Every tenth Cα is shown as a small sphere. Every 20th residue is labeled. (**B**) The Cα trace, from the N terminus (blue) to C terminus (red), viewed down the helical axis of an MfpA monomer. (**C**) Stick representation of residues 2 to 81 (coils 1 to 4), viewed down the helical axis, colored by atom type (carbon, gray; oxygen, red; nitrogen, blue; sulfur, orange).

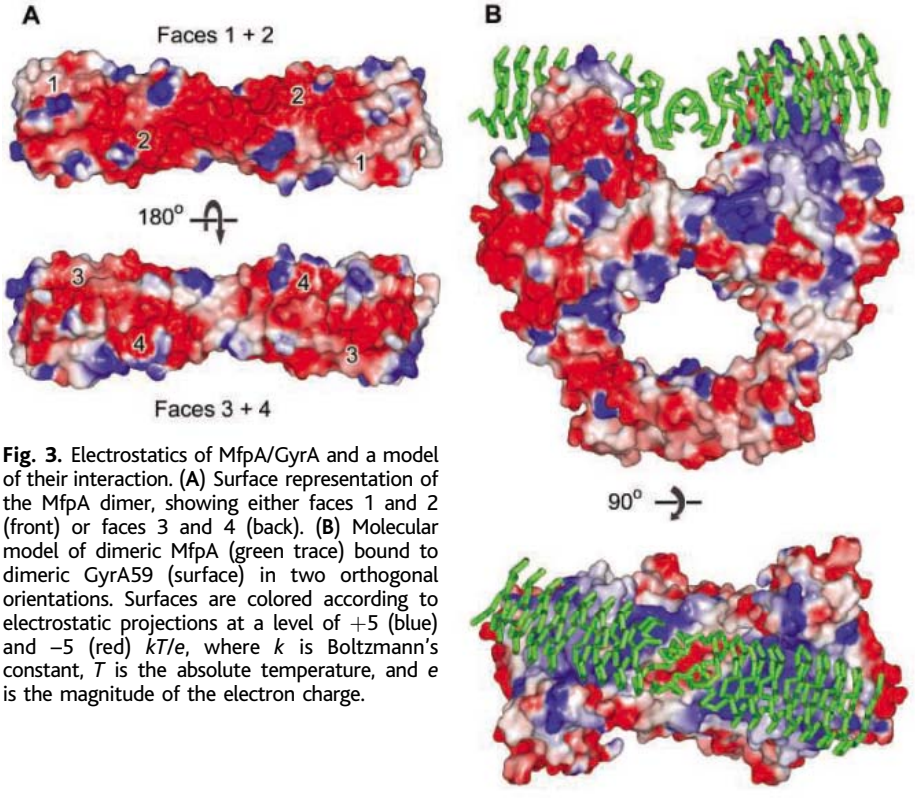

Fig. 3. Electrostatics of MfpA/GyrA and a model of their interaction. (**A**) Surface representation of the MfpA dimer, showing either faces 1 and 2 (front) or faces 3 and 4 (back). (**B**) Molecular model of dimeric MfpA (green trace) bound to dimeric GyrA59 (surface) in two orthogonal orientations. Surfaces are colored according to electrostatic projections at a level of +5 (blue) and −5 (red) kT/e, where k is Boltzmann's constant, T is the absolute temperature, and e is the magnitude of the electron charge.

including in the turns, although only the i^{-1} residue is consistently in a full parallel β strand interaction. Every 20 residues, the right-handed β helix completes a revolution and travels ~4.8 Å along the helical axis. The core of the β helix is devoid of water but is not entirely hydrophobic in nature. Where there are violations of the hydrophobic nature of the i residue, a compensatory polar residue is positioned nearby, to which it hydrogen bonds. For example, the side chains of Thr[24] and His[44] (i position residues in coils 2 and 3, respectively) are on consecutive coils on the same face and form a hydrogen bond. His[44] also forms a hydrogen bond with the side chain Ser[42] at the i^{-2} position. Where there is a small polar residue at position i^{-2}, its side chain typically points into the corner of the quadrilateral and forms hydrogen bond(s) with backbone amides or carbonyls of its own adjacent turn or with that of turns below its position. Where the small polar/hydrophobic residue at position i^{-2} rule is broken, this requires compensatory changes nearby to allow for a larger residue. For example, Asn[97] and Leu[102] are allowed at the i^{-2} position because the helical axis tilts here, creating a larger separation between coils 4 and 5. This tilt is caused by the presence of Pro[81] between faces 4 and 1, which leads to a disruption of the hydrogen bonding between coils 4 and 5 and a 12° change in the helical axis of coils 1 to 4 and 5 to 8. There are several tightly bound water molecules that accommodate the open hydrogen bonds thus created.

Both the N- and C termini of the β helix are capped by tryptophan residues in the i position (Trp[4] and Trp[154]). The 20 C-terminal residues appear as a two-turn (α1) and a three-turn (α2) helix, with the former occupying the place of the face 3 β strand of coil 8. The C-terminal α2 helices interact in an antiparallel manner to generate the molecular twofold axis and a hydrophobic dimer interface that is observed in all four crystal forms. The dimer is rod-shaped and highly asymmetric, with a length of ~100 Å and a diameter of 27 Å at

the N termini and 18 Å at the dimer interface. Although the main chain atoms form coils of nearly square quadrilaterals when viewed down the long axis, the outward-facing side chains of the i^{-1}, i^{+1}, and i^{+2} residues produce a protein surface with a more cylindrical shape when viewed in this direction. All of the charged residues (19 Arg, 1 Lys, 18 Asp, and 7 Glu residues) are located at these positions, generating a dimer with an overall charge of –10. However, the charge distribution is not uniform, and there is a distinct negative potential on faces 1 and 2 along the length of the molecule (Fig. 3A). The right-handed helical nature of the fold, the dimensions and shape of the dimer, and the negative electrostatic surface potential suggest that MfpA might be mimicking a 30–base pair segment of B-form duplex DNA and could be capable of interacting directly with DNA gyrase. No structures in the Protein Data Bank share significant similarity to MfpA.

The structures of the MfpA protein and the N-terminal domain of the *E. coli* gyrase A subunit (GyrA59) (*22*) could be readily docked, without steric clashes, to provide electrostatic complementarity between the highly cationic "saddle" at the gyrase A_2 dimer interface, thought to be the position where DNA binds and is cleaved, and the highly anionic surface of the MfpA dimer (Fig. 3B). The MfpA dimer extends across the entire GyrA dimer, providing an explanation for its powerful inhibition of gyrase activity and suggesting that MfpA will compete with B-form DNA for the gyrase surface. Because fluoroquinolones bind only to the DNA gyrase-DNA complex (*23*), MfpA binding to DNA gyrase prevents the formation of this complex and provides a molecular explanation for the resistance phenotype. Additional support for this mechanism comes from the recent report that Qnr from *K. pneumoniae* competes with DNA for DNA gyrase (*24*).

DNA mimicry by proteins has been reported for the interaction of $TAF_{II}230$ with the TATA box-binding protein (*25*) and in the structure of the highly acidic 107–amino acid residue HI1450 protein from *Haemophilus influenzae* (*26*). The HI1450 structure bears some overall structural similarity to the *gyrI*-encoded DNA gyrase inhibitor (*27*) that protects cells from microcin B17 (also referred to as SbmC), the structure of which has also been solved by crystallographic methods (*28*). The structure of the bacteriophage T7 Ocr protein (*29*) reveals a dimer with a surface anionic charge that has also been suggested to mimic the surface charge distribution of DNA. However, MfpA is folded into a structure that is itself a right-handed helix with a size, shape, and charge distribution markedly reminiscent of B-form DNA. It appears likely that the other members of this large bacterial family of pentapeptide repeat proteins (Protein family database: pf00805) (*30*) will adopt a similar overall fold.

The physiological role that might be played by the MfpA family of proteins in the various organisms in which they are found is not yet clear. The negative surface potentials and DNA-like proportions of other pentapeptide repeat proteins suggest that they may be a general class of inhibitors of DNA binding proteins, with properties analogous to MfpA inhibition of DNA gyrase. A single report has appeared in which the transcript level of *mfpA* (Rv3361c) has been altered by treatment of *M. tuberculosis* cultures (*31*), and its upstream and downstream neighbors (Rv3360 and Rv3362) have been reported as nonessential (*32*). In *M. tuberculosis*, expression of MfpA may be coordinated with cell replication to provide DNA topological assistance when needed, but maintain a condensed chromosome and prevent undesired topological changes during periods of replicative senescence. Viewed in this context, mechanisms that would either control expression of MfpA or modulate its activity would be likely. Finally, the core of the right-handed quadrilateral β-helix structure appears robust enough to allow for surface amino acid substitutions that could tailor specificity and could provide a platform for the rational design of proteins that specifically target DNA-binding proteins of known structure.

References and Notes

1. K. Drlica, M. Malik, *Curr. Top. Med. Chem.* **3**, 249 (2003).
2. J. Crofton *et al.*, "Guidelines for the management of drug-resistant tuberculosis" (World Health Organization, Geneva, 1997).
3. B. Ji, N. Lounis, C. Truffot-Pernot, P. Bonnafous, J. Grosset, *Antimicrob. Agents Chemother.* **42**, 2066 (1998).
4. E. L. Nuermberger *et al.*, *Am. J. Respir. Crit. Care Med.* **170**, 1131 (2004).
5. E. A. Sullivan *et al.*, *Lancet* **345**, 1148 (1995).
6. C. Xu, B. N. Kreiswith, S. Sreevatsan, J. M. Musser, K. Drlica, *J. Infect. Dis.* **174**, 1127 (1996).
7. H. E. Takiff *et al.*, *Antimicrob. Agents Chemother.* **38**, 773 (1994).
8. E. Cambau *et al.*, *J. Infect. Dis.* **170**, 479 (1994).
9. S. T. Cole *et al.*, *Nature* **393**, 537 (1998).
10. A. Aubry, X.-S. Pan, L. M. Fisher, V. Jarlier, E. Cambau, *Antimicrob. Agents Chemother.* **48**, 1281 (2004).
11. I. Guillemin, V. Jarlier, E. Cambau, *Antimicrob. Agents Chemother.* **42**, 2084 (1998).
12. C. Montero, G. Mateu, R. Rodriguez, H. E. Takiff, *Antimicrob. Agents Chemother.* **45**, 3387 (2001).
13. A. Bateman, A. G. Murzin, S. A. Teichman, *Protein Sci.* **7**, 1477 (1998).
14. M. C. Garrido, M. Herrero, R. Kolter, F. Moreno, *EMBO J.* **7**, 1853 (1988).
15. J. G. Heddle *et al.*, *J. Mol. Biol.* **307**, 1223 (2001).
16. O. A. Pierrat, A. Maxwell, *J. Biol. Chem.* **278**, 35016 (2003).
17. G. A. Jacoby, N. Chow, K. B. Waites, *Antimicrob. Agents Chemother.* **47**, 559 (2003).
18. J. H. Tran, G. A. Jacoby, *Proc. Natl. Acad. Sci. U.S.A.* **99**, 5638 (2002).
19. M. Hata *et al.*, *Antimicrob. Agents Chemother.* **49**, 801 (2005).
20. D. Jonas *et al.*, *Antimicrob. Agents Chemother.* **49**, 773 (2005).
21. S. Hegde *et al.*, unpublished data.
22. J. H. Morais Cabral *et al.*, *Nature* **388**, 903 (1997).
23. C. J. Willmot, A. Maxwell, *Antimicrob. Agents Chemother.* **37**, 126 (1993).
24. J. H. Tran, G. A. Jacoby, D. C. Hooper, *Antimicrob. Agents Chemother.* **49**, 118 (2005).
25. D. Liu *et al.*, *Cell* **94**, 573 (1998).
26. L. M. Parsons, D. C. Yeh, J. Orban, *Proteins Struct. Funct. Bioinform.* **54**, 375 (2004).
27. A. Nakanishi, S. Imajoh-Ohmi, F. Hanaoka, *J. Biol. Chem.* **277**, 8949 (2002).
28. M. J. Romanowski, S. A. Gibney, S. K. Burley, *Proteins Struct. Funct. Genet.* **47**, 403 (2002).
29. M. D. Walkinshaw *et al.*, *Mol. Cell* **9**, 187 (2002).
30. A. Bateman *et al.*, *Nucleic Acids Res.* **32**, D138 (2004).
31. M. A. Fisher, B. B. Plikaytis, T. M. Shinnick, *J. Bact.* **184**, 4025 (2002).
32. C. M. Sassetti, D. H. Boyd, E. J. Rubin, *Mol. Micro.* **48**, 77 (2003).

33. We thank U. Ramagopal at the National Synchrotron Light Source X9A beamline, H. Y. Cheng for assistance with the BIAcore experiments, and D. Dervincovsky, M. Auxiliadora Hinajosa, R. Garcia, E. Borges, and E. Baéz for sharing confirmatory results. The coordinates have been deposited in the Research Collaboratory for Structural Bioinformatics Protein Data Bank with accession codes 2BM4, 2BM5, 2BM6, and 2BM7. Supported by the National Institutes of Health (grant nos. AI33696 and AI60899 to J.S.B. and T32 AI07501 to M.W.V.), the U.K. Biotechnology and Biological Sciences Research Council (to A.M.), and European Commission grant no. ICA4-CT1999-10001 (to H.E.T.).

Supporting Online Materials

www.sciencemag.org/cgi/content/full/308/5727/1480/DC1
Materials and Methods
Figs. S1 and S2
Tables S1 and S2
References and Notes

4 February 2005; accepted 22 March 2005
10.1126/science.1110699

New Products

http://science.labvelocity.com

Transcription Factor Analysis

The BD TransFactor Universal Kits can be used to study any transcription factor–DNA interaction. The enzyme-linked immunosorbent assay-based method is compatible with nuclear, whole cell, and cytosolic extracts and can analyze several different transcription factors simultaneously.

BD Biosciences For information 800-662-2566 www.bdbiosciences.com/clontech

DNA Isolation

The PlasmidMAX DNA Isolation Kit provides all the reagents necessary to purify plasmids free of RNA and genomic DNA. The resulting high-quality DNA permits sequencing reads of at least 600 bases. The simple procedure requires only two 1.5-ml tubes and is scalable for larger volumes.

EPICENTRE Biotechnologies For information 800-284-8474 www.EpiBio.com

Laser Technology in Proteomics

Novel Smartbeam laser technology is now a feature of the Ultraflex II matrix-assisted laser desorption ionization–time-of-flight/time-of-flight (MALDI-TOF/TOF) mass spectrometer for cutting-edge proteomics applications. Conventional lasers used in TOF/TOF mass spectrometry can have significant limitations that make them less suitable for a number of important applications, including intact protein analysis, MALDI imaging, and typical MALDI sample protocols for proteomics such as thin-layer preparations or synthetic polymer analysis. These analytical limitations have been overcome with the innovative, proprietary Smartbeam technology used in a novel variable repetition-rate 1 to 200 Hz solid-state laser system on the Ultraflex II system. The new technology permits the use of all matrices and sample preparation methods typically used in MALDI-TOF analysis, from dried droplet to sandwich preparation techniques. It achieves highest sensitivity from robotic sample preparation methods like thin-layer preparation, which offers on-target sample purification and avoids time-consuming pre-purification steps.

Bruker Daltronics For information 978-663-3660 www.bdal.com

Gel Analysis Software

Dymension is software designed to increase productivity in proteomics research by accurately analyzing two-dimensional gels in seconds. In addition to its outstanding speed, Dymension has a new spot-finding algorithm for superb spot detection, resulting in minimal post-editing. Coupled with a completely automatic gel alignment process, Dymension eliminates the need to wait for the image to be analyzed. Instead, the whole imaging process to results and report generation takes just a few minutes.

Syngene For information +44 (0)1223 727123 www.2dymension.com

Transfection Technology

Magnetofection is a novel, simple, and efficient transfection method. This technology associates nucleic acids or viruses with cationic magnetic nanoparticles. The resulting molecular complexes are then transported into cells supported by an appropriated magnetic field. Magnetofection makes use of the magnetic force exerted upon gene vectors toward the target cells, allowing higher transfection efficiencies in primary and immortalized cells. Three types of reagents are available: PolyMag, for all nucleic acid and all cell types; SilenceMag, for small interfering-RNA delivery; and CombiMag, for all vectors.

OZ Biosciences For information +33 (0) 491-82-81-72 www.ozbiosciences.com

Vacuum Manifold

The MultiScreenHTS vacuum manifold for enhanced 96- and 384-well assay performance is suitable for both manual and automated laboratory environments. It can be configured easily for both flow-to-waste and analyte collection. For applications that require filtrate collection, the MultiScreenHTS vacuum manifold incorporates unique DirectStack technology to eliminate cross-talk. This feature enables the filter and collection plates to stack directly, thus removing any gaps between flow directors and receiver wells. In addition, DirectStack technology allows filtration cycles to be completed without manual intervention. The manifold's compact size makes it suitable for use with robotic systems.

Millipore For information 800-MILLIPORE www.millipore.com/HTSmanifold

PCR Optimization Kit

The FailSafe Probes Real-Time PCR Optimization Kit, for use with target-specific probes, enables fast and easy optimization of efficiency and specificity in just one round of polymerase chain reaction (PCR) experiments. The kit contains FailSafe Enzyme Blend and a set of eight PCR 2X premixes that represent a complete range of PCR conditions. The kit is compatible with all real-time PCR instrument platforms and types of fluorescently labeled probes.

Epicentre Biotechnologies For information 800-284-8474 www.EpiBio.com

Cryogenic Vials

New Bar-Coded Cryogenic Vials are for processing large numbers of cryogenic samples and for use with automated readers. The vials can be used for a wide range of applications, including research in pharmaceutical, biotechnology, and forensic laboratories, and commercial operations for cell, tissue, and sample storage. The pre-printed bar codes eliminate the need to individually print and attach labels, and allow for masking the identity of samples when needed. The codes are highly chemical resistant and guaranteed to have no duplicate numbers.

Nalgene For information 877-523-0635 www.nalgenelabware.com

For more information visit GetInfo, *Science*'s new online product index at *http://science.labvelocity.com*

From the pages of GetInfo, you can:

- Quickly find and request free information on products and services found in the pages of *Science*.
- Ask vendors to contact you with more information.
- Link directly to vendors' Web sites.

Newly offered instrumentation, apparatus, and laboratory materials of interest to researchers in all disciplines in academic, industrial, and government organizations are featured in this space. Emphasis is given to purpose, chief characteristics, and availability of products and materials. Endorsement by *Science* or AAAS of any products or materials mentioned is not implied. Additional information may be obtained from the manufacturer or supplier by visiting www.science.labvelocity.com on the Web, where you can request that the information be sent to you by e-mail, fax, mail, or telephone.

ScienceCareers.org

Classified Advertising

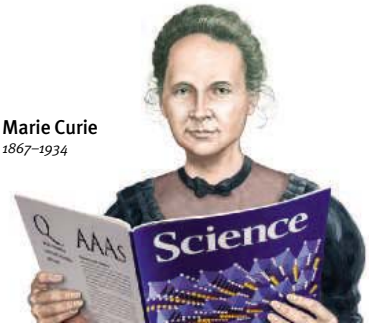

Marie Curie
1867–1934

For full advertising details, go to **www.sciencecareers.org** and click on **How to Advertise,** or call one of our representatives.

United States & Canada

E-mail: advertise@sciencecareers.org
Fax: 202-289-6742

JILL DOWNING
(CT, DE, DC, FL, GA, MD, ME, MA, NH, NJ, NY, NC, PA, RI, SC, VT, VA)
Phone: 631-580-2445

KRISTINE VON ZEDLITZ
(AK, AZ, CA, CO, HI, ID, IA, KS, MT, NE, NV, NM, ND, OR, SD, TX, UT, WA, WY)
Phone: 415-956-2531

KATHLEEN CLARK
Employment: AR, IL, LA, MN, MO, OK, WI, Canada; Graduate Programs; Meetings & Announcements (U.S., Canada, Caribbean, Central and South America)
Phone: 510-271-8349

EMNET TESFAYE
(Display Ads: AL, IN, KY, MI, MS, OH, TN, WV; Line Ads)
Phone: 202-326-6740

BETH DWYER
(Internet Sales Manager)
Phone: 202-326-6534

Europe & International

E-mail: ads@science-int.co.uk
Fax: +44 (0) 1223-326-532

TRACY HOLMES
Phone: +44 (0) 1223-326-525

HELEN MORONEY
Phone: +44 (0) 1223-326-528

CHRISTINA HARRISON
Phone: +44 (0) 1223-326-510

JASON HANNAFORD
Phone: +81 (0) 52-789-1860

To subscribe to *Science*:
In U.S./Canada call 202-326-6417 or 1-800-731-4939
In the rest of the world call +44 (0) 1223-326-515

Science makes every effort to screen its ads for offensive and/or discriminatory language in accordance with U.S. and non-U.S. law. Since we are an international journal, you may see ads from non-U.S. countries that request applications from specific demographic groups. Since U.S. law does not apply to other countries we try to accommodate recruiting practices of other countries. However, we encourage our readers to alert us to any ads that they feel are discriminatory or offensive.

POSITIONS OPEN

UNLV
UNIVERSITY OF NEVADA LAS VEGAS

UNIVERSITY OF NEVADA, LAS VEGAS

The University of Nevada Las Vegas (**website: http://www.unlv.edu**) invites applications for an **ASSISTANT PROFESSOR-IN-RESIDENCE** position in the Department of Biological Sciences, College of Sciences commencing fall 2005. This is a full-time, nine-month, nontenure-track, renewable, and promotable position. Applicants must hold a Doctorate in biology or related field and should have demonstrated competence in the field in teaching specified. Responsibilities include teaching 12 credit hours per semester (four courses per semester) of introductory biology and cell biology/physiology as required for majors and nonmajors, as well as upper-division courses in the candidate's area of expertise, and providing college, university, and professional service. The successful applicants will be expected to develop innovative teaching programs and secure funds to support such activities. Preference will be given to candidates with previous university teaching experience and a broad background in cellular biology and/or physiology. Review of applications will begin immediately. A detailed position description with application details may be obtained by visiting **website: http://hr.unlv.edu/Jobs.** *Affirmative Action/Equal Employment Opportunity Employer.*

CHAIR OF THE DEPARTMENT AND HOLDER OF THE ECCLES CHAIR IN PHARMACEUTICS
University of Utah, Salt Lake City

The Chair will lead the Department, building on a tradition of leadership in fundamental and applied pharmaceutical sciences. The Chair will complement existing strengths in targeted drug delivery, gene therapy, pharmaceutical chemistry, and biological and clinically based drug delivery science, extending those strengths into new interdisciplinary scientific programs across the Health Science Center and the greater University.

Candidates must have qualifications and experience appropriate for appointment to **FULL PROFESSOR** with tenure, including strong research and teaching, evidence of leadership ability, and an interest in building a multidisciplinary program within an interactive academic research environment.

Review of applications will begin June 15, 2005, and continue until the position is filled.

Please send complete curriculum vitae, a statement of research and related interests and plans, and the names and contact information of three references (as hard copy and via e-mail) to:

Pharmaceutics Chair Search Committee
College of Pharmacy, University of Utah
30 South 200 East, Room 201
Salt Lake City, UT 84112
E-mail: jane.sumner@pharm.utah.edu

The University of Utah is an Equal Opportunity/Affirmative Action Employer, encourages applications from women and minorities, and provides reasonable accommodation to the known disabilities of applicants and employees.

POSTDOCTORAL POSITION available immediately to study molecular mechanisms of novel cardiac growth and survival pathways. Projects involve the use of several genetically engineered mouse models. Candidates will be involved in all aspects of biochemical and physiological evaluation. Candidates should be highly motivated and have a strong background in molecular biology.

Please send curriculum vitae and names of three references to: **Dr. Robb MacLellan, Cardiovascular Research Laboratories, UCLA School of Medicine, MRL 3-645, 675 C.E. Young Drive, Los Angeles, CA 90095-1760** or **e-mail: rmaclellan@mednet.ucla.edu.**

UCLA is an Affirmative Action/Equal Opportunity Employer. Women and minorities are encouraged to apply.

POSITIONS OPEN

ASSISTANT OR ASSOCIATE PROFESSOR FACULTY POSITION FOR NEUROPHYSIOLOGIST
University of Alberta

The Department of Physiology at the University of Alberta invites applications for a faculty position at the level of Assistant or Associate Professor in the area of vertebrate systems neurophysiology. Salary for rank will be according to the collective agreement with the University of Alberta. Qualifications must include a Ph.D. or equivalent, at least two years of postdoctoral training, a demonstrated ability to conduct high quality research and the potential to establish an externally funded research program. The research program should be designed to elucidate neuronal mechanisms underlying sensory, motor, or cognitive behavior in vertebrates. The successful applicant will have the opportunity to collaborate with members of the Rehabilitation Motor Control and Perinatal Respiratory Research Groups that are affiliated with the Centre for Neuroscience and Perinatal Research Centre.

Deadline for receipt of applications is July 15, 2005. Commencement date is negotiable. Please submit curriculum vitae, brief statement of research interests and career goals, and the names of three references to: **Dr. C. I. Cheeseman, Chair, Search and Selection Committee, Department of Physiology, 7-55 MSB Building, University of Alberta, Edmonton, AB, T6G 2H7.**

All qualified candidates are encouraged to apply; however, Canadians and permanent residents will be given priority. If suitable Canadian citizens or permanent residents cannot be found, other individuals will be considered.

For further information, consult **websites: http://www.physiology.ualberta.ca, http://www.neuroscience.ualberta.ca, http://www.ualberta.ca/PERINATAL/.**

The University of Alberta hires on the basis of merit. We are committed to the principle of equity in employment. We welcome diversity and encourage applications from all qualified women and men, including persons with disabilities, members of visible minorities, and Aboriginal persons.

FACULTY POSITION ASSISTANT PROFESSOR
Department of Pharmacology

Applications are invited for a full-time, tenure-track Assistant Professor position in the Department of Pharmacology in the School of Pharmacy, University of Mississippi (Oxford campus). We seek an individual who will establish and maintain a research program in pharmacology, teach in the core curriculum of the professional and graduate program, and participate in service-related activities. Applicants must have a Ph.D. degree in pharmacology, toxicology, or a closely related field, with postdoctoral experience and a strong record of research accomplishments. High priority areas of research emphasis include molecular pharmacology, neuropharmacology, cardiovascular/autonomic pharmacology, endocrine pharmacology, and environmental toxicology. Exceptional candidates in other research areas will also be considered. Ample opportunities exist for collaborative research programs with members of the National Center for Natural Products Research and the Research Institute of Pharmaceutical Sciences. Visit our **website: http://www.olemiss.edu/depts/pharmacology** for additional information about the research and training programs of faculty in the Department of Pharmacology at the School of Pharmacy.

Applications must be submitted online at **website: https://jobs.olemiss.edu.** Applicants shall provide a letter outlining their research interests, teaching experience and qualifications, complete curriculum vitae, and names, addresses, telephone numbers, and e-mails of three references. Review of applicants will begin immediately and continue until the position is filled. The anticipated starting date is January 2006.

The University of Mississippi is an Equal Employment Opportunity/Affirmative Action/Title VI/Title IX/Section 504/ADA/ADEA Employer.

Positions @ NIH
THE NATIONAL INSTITUTES OF HEALTH

NATIONAL INSTITUTE OF DIABETES AND DIGESTIVE AND KIDNEY DISEASES (NIDDK) POSTDOCTORAL FELLOWSHIPS IN THE GENETICS & BIOCHEMISTRY BRANCH AND LABORATORY OF MOLECULAR BIOLOGY

We are a group of molecular and structural biologists who share state-of-the-art facilities on the main intramural campus of the NIH in Bethesda, Maryland. The intramural program of the NIH offers an outstanding research environment and many opportunities for collaborations. Applications are invited from individuals of the highest caliber with Ph.D., M.D., or M.D.-Ph.D degrees. Salary and benefits will be commensurate with the experience of the candidate. **Please send a letter and CV to the following email addresses or mail to the appropriate investigator(s) at: National Institutes of Health, Building 5, Room 201, 9000 Rockville Pike, Bethesda, MD 20892-0538**

- Mechanisms of protein transport across the ER and bacterial inner and outer membranes. (PNAS (2001) 98: 3471; EMBO J. (2001) 20: 6724; PNAS (2005) 102: 221). Harris Bernstein: harris_bernstein@nih.gov

- Structural biology of integral membrane proteins. (J. Mol. Biol. (2003) 332: 353; Mol. Microbiol. (2004) 51: 1027; FEBS Lett. (2004) 564: 294). Susan Buchanan: skbuchan@helix.nih.gov

- Mouse meiosis (Mol. Cell (2000) 6:975; Dev. Cell (2003) 4: 497; Nature Struct. Mol. Biol. (2005) 12: 449) and evolutionary genomics (Nature Genet (2004) 36: 642). Dan Camerini-Otero: camerini@ncifcrf.gov

- Molecular mechanism of retroviral integration. Biochemical and functional analysis of HIV integrase. http://orac.niddk.nih.gov/www/craigie/crahome.html.
Bob Craigie: bobc@helix.nih.gov

- Structural biology of the ectodomains of the Toll-like receptors of the innate immune system. (Trends in Immunology (2003) 24: 528). David Davies: david.davies@nih.gov

- Structural biology of DNA recombination. (Nature (2004) 432: 995; Mol. Cell (2002) 10: 327; (2004) 13: 403; Mol. Cell (2000) 5: 1025; EMBO J. (2004) 23:2972). Fred Dyda: Fred.Dyda@nih.gov

- Chromatin structure/function; histone modifications; boundary elements. (Science (2001) 293: 2453-2555; EMBO J. (2004) 23: 138-149; Mol. Cell (2004) 13: 291-298). Gary Felsenfeld: gary.felsenfeld@nih.gov

- Biochemistry and molecular biology of gene rearrangement in the immune system. (EMBO J. (2002) 21: 6625; PNAS (2003) 100: 15446). Marty Gellert: gellert@helix.nih.gov

- Molecular mechanisms of DNA mismatch repair. (Nature (2000) 407: 703; J. Mol. Biology (2003) 334: 949; PNAS (2003) 100: 14822). Peggy Hsieh: ph52x@nih.gov

-Transcriptional regulation of development. Molecular and genetic analysis of the transcriptional control of development in C. elegans (Development (2005) 132: 1795). Michael Krause: mwkrause@helix.nih.gov

- Single-molecule biochemical study of macromolecular complex assembly/disassembly dynamics involved in a variety of cellular processes. (Mol. Cell (2002) 10: 1367). Kiyoshi Mizuuchi: kmizu@helix.nih.gov

- Structural and functional studies of DNA repair (Mol. Cell (2001) 7: 1; EMBO (2000) 19: 5962), and replication. (Nature (2003) 424: 1083; Mol. Cell (2004) 13: 751). Wei Yang: wei.yang@nih.gov

- Role of the ubiquitin-proteasome system in ER quality control (Nature 2001, 414: 652-656; J. Cell Biology 2003, 162: 71-84; Nature 2004, 429: 841-847). Yihong Ye: yihongy@mail.nih.gov

NIH Women's Health Postdoctoral Fellowship

Qualified postdoctoral scientists are invited to apply for a newly established fellowship at the National Institutes of Health funded by Battelle through a grant to the Foundation for NIH. The fellowship is designed to facilitate collaborations, through co-mentored projects, between NIH intramural research laboratories in programs involving women's health. For more information, including a list of co-mentors and research projects, see **http://orwh.od.nih.gov/pdfellowships.**

Research opportunities include one or a combination of basic, translational, or epidemiological research, biomedical history, or biomedical bioinformatics research. Available to doctoral-level fellows within five years of receipt of the doctoral degree. Must be U. S. citizen or permanent resident.

Applications must be made on-line, by July 9, at http://www.training.nih.gov/transfer/WomensHealthAds.

The Women's Health Fellowship is co-sponsored by the NIH Intramural Program on Research on Women's Health and the Office of Research on Women's Health.

National Institute of Dental and Craniofacial Research (NIDCR)

The National Institute of Dental and Craniofacial Research (NIDCR), National Institutes of Health (NIH), Department of Health & Human Services (DHHS) is seeking applicants for a Health Scientist Administrator position in the Center for Biotechnology and Innovation (CBI).

The position is for a Director of the Applied and Translational Research Program. This program emphasizes salivary gland development, structure, physiology and function, salivary gland disease and disorders, development of novel saliva-based diagnostic technologies and high-throughput proteomics technologies. Relevant areas include studies regarding the molecular mechanisms involved in the development and function of salivary glands; synthesis, modification and secretion of salivary proteins and glycoproteins; etiology and pathogenesis of Sjögren's syndrome; restoration of salivary gland structure and function using tissue engineering and other approaches; development of microfuidic technologies for saliva-based diagnosis, identification of all protein components in human saliva, as well as their natural variants and complexes, development of a molecular "tool box" for the isolation and functional characterization of salivary proteins, establishment of a bioinformatics environment for the dissemination of salivary proteome data to the wider scientific community and genetic approaches for the development of novel therapeutic agents for craniofacial and oral diseases and disorders.

The incumbent will direct, administer and evaluate a portfolio of extramural grants, contracts and cooperative agreements and will stimulate interest in and provide advice to the extramural community regarding the respective portfolio. In addition, the incumbent will participate in funding decisions, policy development, as well as implementation and coordination with other programs both within and outside of the NIDCR.

The applicant is required to have a D.D.S./D.M.D., M.D., or Ph.D. or relevant experience equivalent to a Ph.D. degree. The salary range for this position is $88,369 to $114,882 per annum, commensurate with experience. Physicians may be eligible for a Physician's Comparability Allowance (PCA) up to $20,000 per year.

Applications will be accepted until June 30, 2005. Please submit materials to: **Judith Dulovich, Branch I, Office of Human Resources, NIH, 6707 Democracy Blvd., Suite 400, Bethesda, MD 20892-5482 or by email: Judith.Dulovich@nih.gov.** U.S. Citizenship is required.

WWW.NIH.GOV

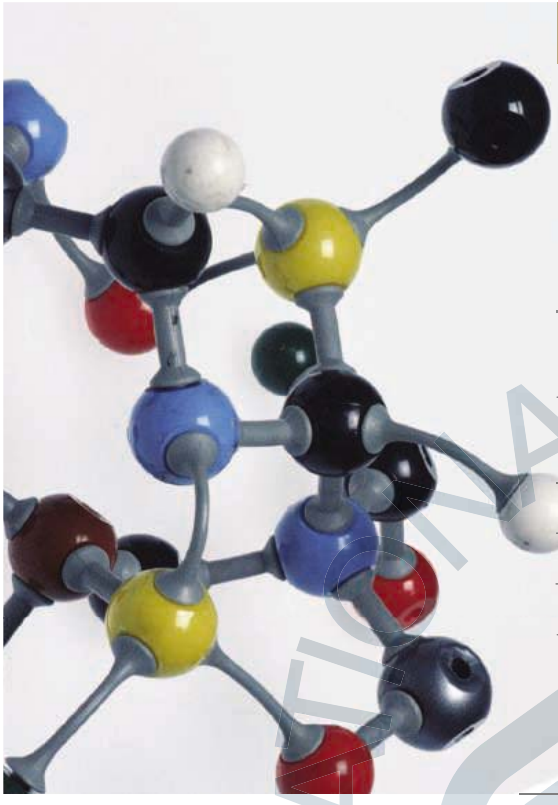

Postdoctoral Research Training at NIH

- Launch a career to improve human health
- Work in one of 1250 of the most innovative and well-equipped biomedical research laboratories in the world
- Explore new options in interdisciplinary and bench-to-bedside research
- Develop the professional skills essential for success
- Earn an excellent stipend and benefits
- Click on www.training.nih.gov

Office of Intramural Training and Education

Hire the World's Best Scientists

- Advertise your positions to the more than 3800 doctoral scientists and clinicians who are in training at the National Institutes of Health
- Reach scientists who are at the forefront of their fields
- Access a population large enough to guarantee interest in your position
- Post new positions with a click of your mouse
- Visit the NIH Virtual Job Fair @ www.training.nih.gov/careers

Office of Intramural Training and Education

THE ROYAL SOCIETY

Royal Society Research Professorships 2005

The Royal Society invites applications from internationally respected scientists or engineers for two Research Professorships. These prestigious posts are designed to enable individuals of proven ability to undertake independent, original research into any of the natural and applied sciences including medical and engineering science.

Research Professorships provide long-term support for world-class scientists of outstanding achievement and promise, allowing them to focus on research and collaboration. Applications are particularly welcomed from scientists currently resident outside the UK and who wish to return.

They are open to EU nationals and others who are either currently employed in the UK or have, at some time, been ordinarily resident in the UK other than for the purpose of full-time education for at least three years.

Previous holders of Royal Society Research Professorships include the current President of the Royal Society, Lord May and Sir Martin Rees, the President-Elect.

The prestige and duration of these awards means that vacancies arise infrequently. It is anticipated that two Professorships will be awarded in each of the next three years.

Subjects covered: any of the natural and applied sciences including medical and engineering science and interdisciplinary research.

Eligibility: must be a citizen of the European Economic Area (EEA), i.e. European Union, Iceland, Norway or Liechtenstein, or have a relevant connection to the EEA (a relevant connection can be established if an individual has a PhD from a university in the EEA, or has worked as a research scientist in a university or research institute in the EEA for at least the past three years, or has done so before taking up an appointment outside the EEA).

Length of tenure: 10–15 years, after which the Professor moves onto the established staff of the host university until retirement age.

Place of tenure: Professorships must be held at a UK university or not-for-profit research institute. The host university will be required to provide assurance that the award would be new and in addition to any existing posts, i.e. not used as substitution funding.

Value: Professorial minimum plus 60% (on UK university salary scales for non-clinical academics and related staff), with research expenses and start-up grants.

Closing date: 31 July 2005

Applications **can only be submitted online** through the Royal Society's electronic Grant Application and Processing (e-GAP) system (https://e-gap.royalsoc.ac.uk, or via the e-GAP logo on the front page of the Society's web site). Applications cannot be submitted on paper. If you would like any further information on this scheme, about the e-GAP process, or the submission of your application, please contact the **UK Grants Section, The Royal Society, 6–9 Carlton House Terrace, London, SW1Y 5AG** (email: ukgrants@royalsoc.ac.uk).

Registered Charity No 207043

excellence in science

Senior Faculty Position in Pharmacology at Texas Tech University Health Sciences Center El Paso School of Medicine

The Texas Tech University Health Sciences Center El Paso School of Medicine invites applications for a Full Professor who will serve as one of the founders of the basic science program(s) for the new 4 year medical school. As part of our growing vision, we are seeking individuals with outstanding credentials. Applicants should have senior academic experience with proven teaching skills in **Pharmacology**. We seek a candidate with outstanding scholarly achievements, a deep commitment to academic excellence, leadership skills, and a vision for basic science and translational research in an academic setting. The medical school is particularly committed to expanding its research programs in cancer (e.g., breast), diabetes, infectious diseases and environmental toxicology. The candidate needs to be committed to furthering interdisciplinary research, both within the department and in the larger institutional setting. He or she will also be expected to serve in a broader leadership role in the scientific enterprise within the new medical school. Candidates must possess a Ph.D. or M.D. degree with significant experience in obtaining extramural support as an established independent investigator. An attractive remuneration package will be negotiated with the successful candidate.

We encourage applicants who have experience teaching and interacting with an ethnically diverse population of students. The patient population at the Texas Tech El Paso School of Medicine consists primarily of Hispanic patients.

Interested candidates must apply on line at **http://jobs.texastech.edu**. Review of applicants will start **June 20, 2005** and continue until the position is filled. Four letters of reference, a curriculum vitae and a brief description of research interests should be attached to the on line application or can be sent to:

Frank Talamantes, Ph.D.
Assistant Dean for Research Development
Texas Tech University Health Science Center
4800 Alberta Ave
El Paso, Texas 79905

The Texas Tech University Health Sciences Center is an Equal Opportunity/Affirmative Action Employer.

CURATOR-FACULTY POSITION
BOTANY
UNIVERSITY OF ALASKA FAIRBANKS

World-class Outdoor Opportunities!

The University of Alaska Museum of the North and the Department of Biology & Wildlife at the University of Alaska Fairbanks seek qualified applicants for a **tenure-track, Assistant-Professor** position as **Curator of the Herbarium.**

Successful candidates are expected to: establish a vigorous, extramurally funded research program complementing the University's programs; curate the herbarium; teach one course per year (Systematic Botany or a specialized course); and advise undergraduate and graduate students. The position will also be associated with the Institute of Arctic Biology. A newly expanded museum and laboratory, greenhouse, core laboratory for nucleic acid research, and supercomputer facilities are available. Opportunities exist to use field areas such as the Bonanza Creek/Poker Creek and Toolik LTER sites.

Preferred applicants will have a strong background in developing, managing, and using museum collections and in a specialized research area (which is flexible). An earned Ph.D. is mandatory, and postdoctoral experience is preferred. Applicants who can successfully implement their vision for how traditional collections can be used on the leading edges of science are especially encouraged to apply. Laboratory space and startup funds are included.

Further information about the University and Museum is available at **www.uaf.edu/museum, mercury.bio.uaf.edu,** and **mercury.bio.uaf.edu/iab.** Applications should include: a completed applicant form (www.alaska.edu/hr/forms/hr_employmentforms); curriculum vitae; three letters of reference; and separate summaries of interests and experience in research, curation, and teaching.

Please send complete application package by 1 September 2005 to **Curator of the Herbarium Search, c/o UAF Human Resources, P.O. Box 757860, Fairbanks, Alaska 99775-7860.** Questions about this announcement can be addressed to Molly Lee (ffmcl@uaf.edu).

UAF FAIRBANKS — UNIVERSITY OF ALASKA MUSEUM OF THE NORTH

The University of Alaska is an Affirmative Action/Equal Opportunity Employer. Women and minorities are encouraged to apply.

ONE WORD TO DRIVE DISCOVERY

Rensselaer

why not change the world?sm

One university is advancing biotechnology in critical directions. Broadening its promise. Accelerating its potential. Where faculty and students discover at the intersection of the life sciences, engineering, and informatics. Where research can change the world. Rensselaer.

Learn more in the Rensselaer Research Quarterly

www.rpi.edu/research/magazine | www.rpi.edu

Senior Faculty Position in Microbiology and Immunology at Texas Tech University Health Sciences Center El Paso School of Medicine

El Paso

The Texas Tech University Health Sciences Center El Paso School of Medicine invites applications for a Full Professor who will serve as one of the founders of the basic science program(s) for the new 4 year medical school. As part of our growing vision, we are seeking individuals with outstanding credentials. Applicants should have senior academic experience with proven teaching skills in **Microbiology and Immunology**. We seek a candidate with outstanding scholarly achievements, a deep commitment to academic excellence, leadership skills, and a vision for basic science and translational research in an academic setting. The medical school is particularly committed to expanding its research programs in cancer (e.g., breast), diabetes, infectious diseases and environmental toxicology. The candidate needs to be committed to furthering interdisciplinary research, both within the department and in the larger institutional setting. He or she will also be expected to serve in a broader leadership role in the scientific enterprise within the new medical school. Candidates must possess a Ph.D. or M.D. degree with significant experience in obtaining extramural support as an established independent investigator. An attractive remuneration package will be negotiated with the successful candidate.

We encourage applicants who have experience teaching and interacting with an ethnically diverse population of students. The patient population at the Texas Tech El Paso School of Medicine consists primarily of Hispanic patients.

Interested candidates must apply on line at **http://jobs.texastech.edu**. Review of applicants will start **June 20, 2005** and continue until the position is filled. Four letters of reference, a curriculum vitae and a brief description of research interests should be attached to the on line application or can be sent to:

Frank Talamantes, Ph.D.
Assistant Dean for Research Development
Texas Tech University Health Science Center
4800 Alberta Ave
El Paso, Texas 79905

The Texas Tech University Health Sciences Center is an Equal Opportunity/ Affirmative Action Employer.

THE UNIVERSITY of York

DEPARTMENT OF CHEMISTRY

Chair in Physical Chemistry

Applications are invited for a Chair in Physical Chemistry, available from 1 October 2005, from individuals with an outstanding record of research achievement in any branch of experimental or theoretical physical chemistry or chemical physics.

The Department, rated 5 in RAE 2001, has strengths in laser spectroscopy, photochemistry and molecular dynamics, theoretical chemistry, crystallographic and modelling methods, analytical science and atmospheric chemistry and surface science and catalysis.

You will be expected to play a leadership role in advancing the international research standing of the Department, build your own research group and attract external funding.

General information about the University can be found on the University's website: http://www.york.ac.uk

Informal enquiries can be made to the Head of Department, Professor P H Walton, tel: +44 (0) 1904 432580, email: phw2@york.ac.uk

Salary will be within the Professorial range (current minimum £43,513 p.a.)

For further particulars and details of how to apply, please see our website: http://www.york.ac.uk/admin/persnl/jobs/ or write to the Personnel & Staff Development Office, University of York, Heslington, York YO10 5DD, quoting reference number BA05221.

Closing date: 23 June 2005.

The University of York is committed to diversity and has policies and developmental programmes in place to promote equality of opportunity. It particularly welcomes applications from ethnic minority candidates.

www.york.ac.uk

TEMASEK LIFESCIENCES LABORATORY

PRINCIPAL INVESTIGATORS

Temasek Life Sciences Laboratory (TLL), a recently established non-profit research organisation located within the campus of the National University of Singapore, is seeking applicants for **PRINCIPAL INVESTIGATOR** positions.

Current research interests in TLL include cell biology, developmental biology, neuroscience, pathogenesis and bioinformatics; further information is available at www.tll.org.sg. TLL is particularly interested in applicants whose work will complement, strengthen and extend the current developmental biology programs in both animal and plant models.

TLL provides a supportive environment for outstanding science, with generous funding, state-of-the-art facilities, and an intellectually stimulating and collegial atmosphere. Each appointment comes with full research support for supplies, equipment and three or four fully-funded positions.

Competitive salaries, medical, housing and other benefits are available for qualified candidates.

Applicants should send a curriculum vitae, three reference letters and a statement of research intent to:

CHAIRMAN
TLL Recruitment Committee

TEMASEK LIFE SCIENCES LABORATORY
1 Research Link, National University of Singapore, Singapore 117604
Email: recruit@tll.org.sg Fax: 65 6872 7089

FACULTY POSITIONS in Neuroscience of Human Nervous System Disease

nki

Applications are invited from highly qualified individuals with a Ph.D. and/or M.D. degree in a biomedical science for a tenure-track position at the level of **ASSISTANT PROFESSOR, ASSOCIATE PROFESSOR, OR PROFESSOR**, New York University School of Medicine (NYUSM) at the Nathan Kline Institute (website:**http://www.rfmh.org/nki**). NKI is located in the scenic Hudson River Valley region of New York, 15 miles north of Manhattan and is a New York University School of Medicine-affiliated institute. NKI faculty have active, funded program interests in Alzheimer's, Parkinson's and related dementias, schizophrenia and addictive disorders. Research areas include amyloid biology, vesicular trafficking, cytoskeleton dynamics, neuronal cell death, signal transduction, transgenic modeling and gene targeting, genomics, *in vivo* electrophysiology, animal and clinical neuroimaging, and clinical trials.

The successful applicant should have an active research program that is extramurally funded or fundable and will complement existing interests and/or expand into new areas of molecular, cellular, systems, or clinical neuroscience. Candidates with research interests in synapse electrophysiology, molecular or human genetics, and behavioral model analysis are especially encouraged to apply. Excellent opportunities exist for interdisciplinary collaborations on multiple campuses.

Applications, including curriculum vitae, statement of research interests, and three references should be sent to: Search Committee, Attn: Janet Rosdil, Nathan Kline Institute/NYUSM, 140 Old Orangeburg Road, Orangeburg, NY 10962.

EOE/AAE. Applications from women and underrepresented minorities are particularly encouraged.

Research Opportunities

VIRGINIA BIOINFORMATICS INSTITUTE AT VIRGINIA TECH VBI

Associate and full professorships in experimental, computational life science and biomedicine

The Virginia Bioinformatics Institute (VBI) invites applications for several faculty positions from established researchers in experimental and computational life sciences and biomedicine. Areas of strength among the 16 research groups at VBI include infectious diseases, ranging from the molecular to the population scale, systems biology approaches to study stress response in several organisms, modeling and simulation of biological networks, functional genomics, metabolomics, proteomics and bioinformatics/computational biology. Candidates are expected to have an established research program and a track record of extensive extramural research funding.

Established in 2000 by the Commonwealth of Virginia, the Institute is a part of Virginia Tech (VT) and has its own 130,000 sq ft research facility with state-of-the-art core laboratory and computational facilities. VBI strongly emphasizes synergistic interactions among faculty and is organized around the concept of team science. VBI places strong emphasis on systems biology and bioinformatics rather than organizing research according to academic disciplines. Instead, the research areas represented at VBI organize themselves around the specific needs of individual research projects. Extensive national and international collaborations complement the expertise of the faculty, including strong interactions with several biomedical research centers. Faculty entrepreneurial activities are strongly encouraged and the university provides support for the establishment of commercial ventures.

VBI is currently establishing a facility in the Washington, DC area, as part of Virginia Tech's expansion into that region. Faculty members whose programs will not require their own laboratory facilities will have the option of basing their primary research operation there. Faculty whose research programs require laboratory facilities will necessarily be primarily located at VBI's on-campus facility in Blacksburg, where state of the art laboratory facilities are available. The new faculty may also have the option of joint affiliations with other departments at Virginia Tech and prominent medical schools.

Along with a strong research environment, the Institute actively participates in "Genetics, Bioinformatics, and Computational Biology" an interdepartmental Ph.D. program, widely recognized for its strengths in computational and experimental sciences, which attracts outstanding students with an interdisciplinary research focus. posting 042478

Other professional research opportunities requiring advanced degrees:

- Biological Pathogen Curator, posting 041973
- Bioinformaticians, posting 041438
- Genomics Curator/Annotators, posting 041080
- Head Curator, posting 041595
- Proteomics Database Analyst, posting 042098
- Scientific Web Production Administrator, posting 041790
- Senior Metabolomics Specialist, posting 041981
- Senior Proteomics Specialist, posting 041525
- Software Developers, posting 041435
- Software Development and Quality Control Manager, posting 042039
- Software Evaluators, posting 041457

Postdoctoral appointments:

- Computational Biologist, posting 042479
- Metabolomics Specialist, posting 041979
- Microbiologist in Plant-Microbe Interactions, posting 030262
- Rickettsiae/Coxiella Bioinformatician, posting 041864

For more Information:

To Apply, visit www.jobs.vt.edu and search by posting number. To learn more about VBI and opportunities available, please visit us at www.vbi.vt.edu.

To learn more about the Interdisciplinary PhD program in Genetics, Bioinformatics, and Computational Biology, visit http://www.grads.vt.edu/gbcb/overview.htm.

Virginia Tech

Memorial
University of Newfoundland

Tier 2 Canada Research Chair
in
Marine Biotechnology

The Faculty of Science at Memorial University seeks candidates for a tenure-track Tier 2 Canada Research Chair in the area of Marine Biotechnology. Tier 2 chairs "are for exceptional emerging researchers, acknowledged by their peers as having the potential to lead in their field." Details of Canada Research Chairs can be found at **www.chairs.gc.ca**.

Further details of this position can be found at:
www.mun.ca/research/chair_ads.php

Consideration of applications will begin **20 June 2005** and continue until the position is filled. Inquiries are welcome. Interested persons should submit a curriculum vitae, a one page summary of proposed research, and arrange for the names, postal addresses, and email addresses of three referees to be sent to:

Dr. David Schneider, Associate Dean of Science
Memorial University of Newfoundland
St. John's, NL, A1B 3X9
Email: a84dcs@mun.ca
Telephone (709) 737-4752
FAX (709) 737-3316

All appointments are subject to budgetary approval. Memorial University of Newfoundland is committed to employment equity and encourages applications from qualified women and men, visible minorities, aboriginal people and persons with disabilities.

Senior Faculty Position in Biochemistry/ Molecular Biology
at
Texas Tech University Health Sciences Center
El Paso School of Medicine

El Paso

The Texas Tech University Health Sciences Center El Paso School of Medicine invites applications for a Full Professor who will serve as one of the founders of the basic science program(s) for the new 4 year medical school. As part of our growing vision, we are seeking individuals with outstanding credentials. Applicants should have senior academic experience with proven teaching skills in **Biochemistry and/or Molecular Biology**. We seek a candidate with outstanding scholarly achievements, a deep commitment to academic excellence, leadership skills, and a vision for basic science and translational research in an academic setting. The medical school is particularly committed to expanding its research programs in cancer (e.g., breast), diabetes, infectious diseases and environmental toxicology. The candidate needs to be committed to furthering interdisciplinary research, both within the department and in the larger institutional setting. He or she will also be expected to serve in a broader leadership role in the scientific enterprise within the new medical school. Candidates must possess a Ph.D. or M.D. degree with significant experience in obtaining extramural support as an established independent investigator. An attractive remuneration package will be negotiated with the successful candidate.

We encourage applicants who have experience teaching and interacting with an ethnically diverse population of students. The patient population at the Texas Tech El Paso School of Medicine consists primarily of Hispanic patients.

Interested candidates must apply on line at **http://jobs.texastech.edu**. Review of applicants will start **June 20, 2005** and continue until the position is filled. Four letters of reference, a curriculum vitae and a brief description of research interests should be attached to the on line application or can be sent to:

Frank Talamantes, Ph.D.
Assistant Dean for Research Development
Texas Tech University Health Science Center
4800 Alberta Ave
El Paso, Texas 79905

The Texas Tech University Health Sciences Center is an Equal Opportunity/ Affirmative Action Employer.

POSITIONS OPEN

FACULTY POSITIONS
University of Pennsylvania
School of Medicine

The Department of Psychiatry at the University of Pennsylvania School of Medicine is seeking highly qualified candidates for several faculty positions. The faculty appointments will be at either the **ASSISTANT, ASSOCIATE,** or **FULL PROFESSOR** rank and in the tenure track. Rank will be commensurate with experience. The successful applicants will have experience in the fields of neuroscience, neurobiology and behavior, addictions research, neuropharmacology, genetics, genetics of epilepsy, and mathematical genetics depending on the specific qualifications for each position. Applicants must have an M.D. or Ph.D., or M.D./Ph.D. degree. For a specific description of each faculty position, please see "Job Opportunities" at **website: http://www.med.upenn.edu/fapd/.** For information about the Psychiatry Department, please visit **website: http://www.med.upenn.edu/psychiatry.html.** Please submit curriculum vitae, a letter of interest, three reference letters, and indicate Job Reference Number to: **Dwight L. Evans, M.D., c/o Ava Plotnick, Department of Psychiatry, University of Pennsylvania School of Medicine, 305 Blockley Hall, 423 Guardian Drive, Philadelphia, PA 19104. E-mail: plotnick@mail.med.upenn.edu.**

The University of Pennsylvania is an Equal Opportunity/ Affirmative Action Employer. Women and minority candidates are strongly encouraged to apply.

RESEARCH FELLOW: excellent opportunity. Cedars-Sinai Medical Center is looking for full-time Research Fellow to conduct basic science research with stem cells and myocardial regeneration and angiogenesis. Ideal candidate is postdoctoral or M.D. with experience or inclination to pursue basic science laboratory techniques. Send curriculum vitae to **e-mail: raj.makkar@cshs.org.**

POSITIONS OPEN

ASU
Arizona State University

BACTERIAL PATHOGENESIS RESEARCHER

The School of Life Sciences and the Biodesign Institute at Arizona State University (ASU) invite applications for a tenure-track **ASSISTANT PROFESSORSHIP** to provide basic understanding of the means by which bacteria succeed as pathogens. Candidates must have a doctoral degree at the time of appointment and two years of relevant postdoctoral training. Preference will be given to those conducting research with gram-negative enteric pathogens, especially with *Salmonella*. The successful candidate will be involved in developing an innovative, extramurally funded, independent research program, participating in undergraduate and graduate education in the School of Life Sciences, mentoring undergraduate, graduate, and postdoctoral students, and interacting in the multidisciplinary consortium of faculty in the Center for Infectious Diseases and Vaccinology in the Biodesign Institute. A competitive startup package and a teaching load compatible with high research productivity will be provided. To apply, send a cover letter, your curriculum vitae, three representative publications, statements of future research plans, and teaching philosophy and interests, and arrange for three letters of reference to be sent to: **Roy Curtiss, Chair, Bacterial Pathogenesis Search Committee, School of Life Sciences, P.O. Box 874501, Tempe, AZ 85287-4501.** Letters of reference, but not application materials, may be sent to **e-mail: nicole.barr@asu.edu.** The closing date for receipt of applications is July 1, 2005; if not filled, applications will be evaluated weekly thereafter until the search is closed. Anticipated start date is August 16, 2005. *ASU is an Affirmative Action/Equal Opportunity Employer.*

POSITIONS OPEN

EXECUTIVE DIRECTOR
U.S. Arctic Research Commission
Arlington, Virginia

The U.S. Arctic Research Commission (USARC), an independent government agency (**website: http://www.arctic.gov**), invites applications from qualified applicants with comprehensive terrestrial, marine, or atmospheric research experience in the Arctic, including research management and participation in the field or at sea. A Ph.D. is desired. We encourage applications from individuals whose research expertise is complemented by knowledge and experience in the Federal planning and budgetary processes; in international Arctic research activities and their management; and in the ongoing research interests of the State of Alaska, local jurisdictions, and nongovernmental organizations.

Strong interpersonal, negotiating skills are important. The Executive Director is the senior government employee of the Commission, whose duties (among others) include development and recommendation of a national Arctic research policy, and facilitation of cooperation of Arctic research and logistics activities between Federal, State, local, indigenous, and international entities. The Commission is mandated under the Arctic Research and Policy Act of 1984 (as amended). Additional details of the Commission, its activities, and its publications may be viewed at our website.

This opportunity is a Senior Executive Service position. It may also be filled through the Intergovernmental Personnel Act authority. The successful applicant will succeed the retiring incumbent on or about 31 January 2006. *U.S. citizenship is required.* Details and complete application requirements must be obtained from the USAJOBS **website: http://www.usajobs.opm.gov** under Vacancy Announcement OS-05-78. Applications must be submitted by July 15, 2005. Questions may be addressed to: **Sandra Wheatley** in the **MMS Human Resources Office** at **telephone: 202-208-6702.** *The USARC is an Equal Opportunity Employer.*

USDA Agricultural Research Service
www.ars.usda.gov

POSTDOCTORAL RESEARCH ASSOCIATE, RESEARCH GENETICIST, U.S. Department of Agriculture (USDA), Agricultural Research Service (ARS), Corn Insects and Crop Genetics Research Unit, Ames, Iowa. The incumbent will assist in research involving the analysis of the soybean genomic with respect to regions affecting the response of soybean to Asian Soybean Rust or other emerging diseases. Candidates must have experience in plant genomics or molecular genetics. Experience with genome evolution or disease resistance is beneficial. Candidate must have a Ph.D. in a related field. Thirteen month appointment with benefits; which may be extended. Salary commensurate with experience ($50,541 - 78,745 per year). Position will be opened until filled. Preference will be given to U.S. citizens.

For information on the position contact **Dr. Randy Shoemaker, (515) 294-6233 (rcsshoe@iastate.edu)**. Applications in response to this advertisement should be sent along with three letters of reference to: **Dr. Randy Shoemaker, USDA/ARS, G401 Agronomy Hall, Iowa State University, Ames, IA 50010.**

The USDA is an Equal Opportunity Provider and Employer.

Sonderforschungsbereich Transregio 3

The Transregional Collaborative Research Center SFB/TR3 „Mesial Temporal Lobe Epilepsies" at the Universities of Bonn, Berlin, Freiburg and Magdeburg invites applications for an

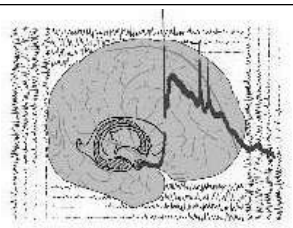

Independent Junior Research Group Leader Position

(salary scale BAT Ia)

at the University of Bonn (see see http://www.meb.uni-bonn.de/epileptologie/sfb-tr3/htm).

The candidate, a highly qualified junior scientist with a strong research interest in neuroscience shall hold a PhD, passed no longer than six years ago. We expect relevant postdoctoral research experience, an excellent scientific record, the ability to independently lead a research group, a strong commitment to interdisciplinary research, active collaboration and significant contributions to the research goals of the SFB/TR3.

The position is funded by Deutsche Forschungsgemeinschaft for up to five years. For further details on application criteria and funding conditions of this program, see: **http://www.dfg.de/forschungsfoerderung/formulare/download/60_5e.rtf.** Evaluation includes a personal presentation of the project and panel assessment.

Applications should include a research plan (max. 5 pages: previous work in the field, goals, methods and research program, time schedule, cost break down), CV, list of publications, copies of the most important publications and are to be submitted **by July 20, 2005** to:

Prof. Dr. Christian Steinhäuser, Exp. Neurobiology, Neurosurgery,
University of Bonn
Sigmund-Freud-Strasse 25 • D-53105 Bonn

For further information, please contact: Christian.Steinhaeuser@ukb.uni-bonn.de.

TENURE-TRACK POSITION

Department of Health and Human Services
National Institutes of Health
National Institute on Aging
Intramural Research Program

The **Laboratory of Neurosciences** (LNS) of the National Institute on Aging (NIA) is recruiting a scientist for a tenure-track position within its Intramural Research Program (IRP). This position is 100% research, includes an attractive set-up package and operating budget, and provides the unique and extensive resources of the NIH. Principal investigators in the LNS include Drs. Mark Mattson (Lab Chief), Nigel Greig, Mahendra Rao and Catherine Wolkow.

The successful individual will possess an M.D. or Ph.D. degree or equivalent degree in neuroscience, molecular biology or a related field and have an established record of scientific accomplishments within the neurobiology of aging or related fields, expertise in the area of synaptic signaling and a strong publication record. Preference will be given to those who apply modern electrophysiological, imaging and/or molecular biology technologies to key issues in the field. Salary is commensurate with research experience and accomplishments, and a full Civil Service package of benefits (including retirement, health, life and long term care insurance, Thrift Savings Plan participation, etc.) is available.

Additional information regarding the NIA IRP and the LNS are available at the following websites:

http://www.grc.nia.nih.gov/
http://www.grc.nia.nih.gov/branches/lns/index.html

To apply: Please send a cover letter, curriculum vitae, bibliography, statement of research interest and three letters of recommendation to: **Peggy Grothe, Intramural Program Specialist; Office of the Scientific Director (Box 09); Vacancy # IRP-05-02; National Institute on Aging, 5600 Nathan Shock Drive, Baltimore, MD 21224-6825**. Applications must be postmarked by **July 15, 2005**. If additional information is needed, please call **410-558-8012**.

DHHS and NIH are Equal Opportunity Employers.

PHYSICAL – BIOLOGICAL MODELER

The NOAA Great Lakes Environmental Research Laboratory (GLERL) seeks an enthusiastic research scientist to examine physical-biological coupling in Great Lakes and coastal ecosystems. Research will couple, spatially explicit models of Great Lakes ecological and physical dynamics, with particular emphasis on ecosystem forecasting. Experience with 3-d hydrodynamic (e.g., Princeton Ocean Model), hydrologic, and/or sediment dynamics models and with biological processes such as larval recruitment or/ phytoplankton transport models is required. The individual will present results in peer-reviewed publications and scientific presentations and grow the program by submitting research proposals.

This is a full-time, permanent federal position (GS-13) with a starting salary of $77,161. Closing date is **September 30, 2005**; however, the position may be filled before that date. Applications received by **June 30, 2005** will be given full consideration. Applications will be reviewed on a monthly thereafter until the closing date.

This position is posted on the U.S. Department of Commerce website: **www.jobs.doc.gov** under four vacancy numbers. For individuals with formal training in the biological sciences apply at **OAR-LABS-2005-0100** and **OAR-LABS-2005-0095** (current federal employees). For individuals with formal training in the physical sciences apply at **OAR-LABS-2005-0102** and **OAR-LABS-2005-0104** (current federal employees). Applicants must be U.S. Citizens and are required to submit applications on line. Further information can be obtained from **Peter.Landrum@noaa.gov**. In addition to making a formal application on line, please send a courtesy CV to **Dr. Landrum** either electronically or by mail to **Great Lakes Environmental Research Laboratory, 2205 Commonwealth Blvd. Ann Arbor, MI 48105**. Further information on NOAA's GLERL can be found at **www.glerl.noaa.gov**.

THE DEPARTMENT OF COMMERCE IS AN EQUAL OPPORTUNITY EMPLOYER.

POSITIONS OPEN

ASU
ARIZONA STATE UNIVERSITY

BIOIMAGING LABORATORY MANAGER

The Keck Bioimaging Laboratory in the School of Life Sciences at Arizona State University is seeking an **ASSISTANT RESEARCH PROFESSIONAL (NONTENURE TRACK**) responsible for user training, instrumentation upkeep, and preparation of equipment proposals. Candidates must have five years of experience in scientific management or research or a Master's degree with two years of experience or a Ph.D. degree. Preference will be given to candidates having experience in state-of-the-art bioimaging techniques such as confocal microscopy, cytochemistry, video microscopy, live cell imaging, fret, frap, or three-dimensional reconstruction analysis. Information on our bioimaging laboratories can be found at **websites: http://sols.asu.edu/klab** and **http://sols.asu.edu/lsem.**

To apply, submit a cover letter, curriculum vitae, and statement of research interests and experience in bioimaging. Candidates must request that two letters of recommendation be sent to: **Nancy Lesko, Bioimaging Manager Search, School of Life Sciences, P.O. Box 874501, Arizona State University, Tempe, AZ 85287-4501.** Letters of reference, but not application materials, may be submitted by **e-mail: sols@asu.edu.** *Application deadline is July 25, 2005; if not filled, applications will continue to be reviewed weekly thereafter until the search is closed.* See **website: http://sols.asu.edu/jobs/index.php** for complete qualification and application information. *Arizona State University is an Affirmative Action/Equal Opportunity Employer.*

CELL BIOLOGY (CHAIR)

The American University of the Caribbean (AUC), a 25-plus-year-old accredited medical school with over 3,000 graduate physicians is pleased to announce an opening for the Chair of cell biology, Ph.D., with postdoctoral training. Rank is commensurate with experience.

We seek an individual with experience and expertise, who both enjoys, and is dedicated to teaching. Primary focus would be directed towards individuals who can develop a solid, current course in molecular cell biology and tissue biology linked to ultrastructure and signal transduction. Administrative duties would be minimal, teaching would be team-taught, and research facilities are in planning.

Individuals familiar with U.S. medical education and evaluation systems are encouraged to apply. All lectures are in English, with PowerPoint formats preferred. The majority of the basic science AUC faculty are drawn from North America and the European Union; with clinical clerkships in the United States, United Kingdom, and Ireland.

AUC (**website: http://www.aucmed.edu**) is in a new up-to-date facility on the delightful island of St. Maarten in the Netherlands, Antilles, some three hours by air from Miami, Florida.

Interested parties should send their curriculum vitae, and the names of three references with coordinates to: **B. Salafsky, Ph.D., Dean, Basic Sciences** at **e-mail: buzs@aucmed.edu.** Responses to inquiries will be forthcoming after July 1, 2005.

RESEARCH ASSOCIATE or **INSTRUCTOR** position on orphan nuclear receptor-mediated gene regulation. We use molecular biology and "humanized" transgenic mice to study gene regulation by pregnane X receptor, constitutive androstane monophosphate, and liver X receptor, and its implications in liver diseases, lipid and hormonal homeostasis, drug development, and cancer (*Nature* **406:**435, 2000; *Proc. Natl. Acad. Sci.* **100:**4150, 2003; *Mol. Pharmacol.* **65:**292, 2004; and Epub May 4, 2005; *Hepatology* **41:**168, 2005; *Hepatology* **41:**497, 2005). Send curriculum vitae and names of three references to: **Dr. Wen Xie, Center for Pharmacogenetics, University of Pittsburgh, Pittsburgh, PA 15261. E-mail: wex6@pitt.edu.**

POSITIONS OPEN

Tufts-New England Medical Center

POSTDOCTORAL POSITION, MAP KINASES

A Postdoctoral position is available immediately to study MAPKs in neurofibromatosis. Applicants must have less than two years postdoctoral experience. *U.S. citizen or permanent resident preferred.* Address all correspondence to:

John M. Kyriakis, Ph.D.
Molecular Cardiology Research Institute
Tufts-New England Medical Center
750 Washington Street, Box 8486
Boston, MA 02111, U.S.A.
E-mail: jkyriakis@tufts-nemc.org

FACULTY POSITION
The Fred Hutchinson Cancer Research Center and The University of Washington

A position in the Clinical Research Division of the Fred Hutchinson Cancer Research Center and the Division of Medical Oncology at the University of Washington School of Medicine is available for a physician/scientist interested in developing a laboratory-based research program in gastrointestinal malignancies. Specifically, applicants should have experience in the conduct of laboratory-based experiments with potential for translation to the clinical setting of human gastrointestinal malignancy. Priority will be given to applicants who have a demonstrated track record in this area. The selected individual would be expected to become involved in selected aspects of patient care and participate in the instructional activities of the Division.

This would be a full-time faculty position based at the Fred Hutchinson Cancer Research Center at the **ASSISTANT MEMBER** level, with a joint appointment at the University of Washington at the **ASSISTANT PROFESSOR** level. Requirements include M.D. or M.D./Ph.D.

Candidates should send curriculum vitae, a concise statement of research plans and career goals, and the names of four references to: **Dan Meenach, Faculty Coordinator, Fred Hutchinson Cancer Research Center, 1100 Fairview Avenue North D5-310, P.O. Box 19024, Seattle, WA 98109-1024.** The closing date for application is July 3, 2005.

The Fred Hutchinson Cancer Research Center and the University of Washington are Affirmative Action/Equal Opportunity Employers. Both institutions are dedicated to building culturally diverse faculties and strongly encourage applications from women, minorities, individuals with disabilities, and covered veterans.

PROFESSOR – MICROBIAL GENOMICS
Department of Pathology and Laboratory Medicine
UC Irvine School of Medicine

Applications are sought for a position at the full Professor level to lead a new program focused on the genomic basis of microbial disease. The Department seeks a senior-level investigator (M.D., Ph.D., or M.D., Ph.D.) with expertise in the creation and application of novel high-throughput methods for the analysis of the genome and the transcriptome, and related analyses of gene regulation. Experience in the use of high-throughput sequencing is desirable. Applicants should have demonstrated expertise in statistical and bioinformatics methods to derive new clinical-pathological correlations. Candidates should have an established record of extramural support in the field, and will be expected to participate in the teaching and service missions of the Department. Applicants are invited to submit curriculum vitae and names of three academic references to: **Microbial Genomics Search Committee, c/o Michael E. Selsted, M.D., Ph.D., Professor and Chair, Department of Pathology and Laboratory Medicine, D440 Medical Science, UC Irvine School of Medicine, Irvine, CA 92697-4800.**

UC Irvine is an Equal Opportunity Employer committed to excellence through diversity.

POSITIONS OPEN

The Department of Medicine at the University of Chicago is seeking a Chief for the Section of Endocrinology, to be appointed at the rank of **ASSOCIATE** or **FULL PROFESSOR,** commensurate with years of experience and accomplishments. The Section Chief will be responsible for implementing new research programs and expanding current research strengths, further developing clinical opportunities, and enhancing education programs. The successful candidate must have demonstrated professional distinction in research, have an active ongoing research program which has attracted national funding, and have demonstrated effectiveness in mentorship, teaching, administration, and interpersonal skills. Applicants should submit curriculum vitae to: **Dr. Joe G. N. Garcia, Chairman, Department of Medicine, The University of Chicago, 5841 South Maryland Avenue, MC6092, Chicago, IL 60637.** *Affirmative Action/Equal Opportunity Employer.*

POSTDOCTORAL RESEARCH ASSOCIATE

Stony Brook University's Department of Psychiatry seeks a Postdoctoral with a recent doctoral degree in a neuroscience-related discipline. Required: demonstrated expertise in research using electrophysiological techniques including intracellular recordings. The incumbent shall investigate the mechanisms of action of antipsychotic drugs using the techniques of intracellular recording and voltage-clamp in brain slice preparations. Design, set up, and carry out all experimental procedures necessary for that research. Collect results, analyze them, and prepare them for public, verbal, and/or poster presentation and publication. If the incumbent is lacking particular expertise necessary for conducting such research, due diligent effort will be made to acquire that experience from inside or outside principal investigator's laboratory. If new tools or techniques are necessary for the research, the incumbent will assist with their identification, acquisition, and implementation. Send resume to: **Rex Wang, Ph.D., Stony Brook University, Department of Psychiatry, HSC, T10-020, Stony Brook, NY 11794-8101.** *Affirmative Action/Equal Opportunity Employer.*

RESEARCH POSITIONS

Research positions are available to study cell calcium, ion channels, signal transduction, and mitochondrial biology in cardiovascular and respiratory systems. Rank and salary will be commensurate with education and experience. Candidates who apply for molecular biologist positions should have basic training in molecular biology. Research background in transgenic mice, RNA interference, embryonic stem cells, development, and/or genetics is desirable. For electrophysiologist positions, applicants must have patch clamp and/or calcium imaging experience. If interested, please e-mail application letter and curriculum vitae to: **Dr. Yong-Xiao Wang** at **e-mail: wangy@mail.amc.edu; Center for Cardiovascular Sciences, Albany Medical College, Albany, NY 12208.**

CLINICAL CHEMIST
Temple University
School of Medicine

Department of Pathology and Laboratory Medicine–**ASSISTANT/ASSOCIATE PROFESSOR;** Ph.D./M.D. with fellowship training in clinical chemistry and an active research program. Responsibilities will include resident and medical student teaching as well as clinical/basic research. Send curriculum vitae to: **Henry Simpkins, Ph.D., M.D., Professor and Chairperson, Department of Pathology and Laboratory Medicine, Temple University School of Medicine, 3401 North Broad Street, Philadelphia, PA 19140.** *Temple University is an Affirmative Action/Equal Opportunity Employer and strongly encourages applications from women and minorities.*

Sandia National Laboratories

A Department of Energy National Laboratory

Theoretical Chemist

The Combustion Chemistry Department at Sandia National Laboratories in Livermore, California, seeks a theoretical chemist for a regular staff position. The successful candidate will be part of a team of experimental and theoretical scientists investigating fundamental chemistry relevant to combustion. Of particular interest are the calculation of chemical kinetic rates and the determination of reaction pathways. As a principal investigator, the successful candidate will be expected to develop and maintain an international scientific reputation in physical chemistry and combustion science and to form strong collaborative relationships with scientists inside and outside the facility, including both experimentalists and other theoreticians. Opportunities exist to broaden the scope of research to include fundamental aspects of light-matter interactions and the chemical physics of biologically relevant molecules.

A PhD in chemistry, physics, or a related discipline is required. Experience is required with gas phase reaction theory and modern ab initio electronic structure methods. The candidate must have demonstrated original research in relevant areas of theoretical chemistry and possess excellent written and oral communication skills. The ability to obtain a DOE clearance is required.

Experience is desired in molecular dynamics simulations, the utilization of high performance massively parallel computing, molecular dynamics, and molecular spectroscopy.

Please apply online at **www.sandia.gov**. Respond to requisition number **053237**.

Sandia is an equal opportunity employer

Johnson & Johnson

Ortho-Clinical Diagnostics, a Johnson & Johnson company, is a leading provider of high value diagnostic products and services for the global health care community. Ortho Clinical Diagnostics, Inc., provides in vitro diagnostic products to hospital, commercial and clinical laboratories, and blood donor centers. Its products include reagents and instrument systems used in blood typing and donor testing; clinical chemistry determinations and immunoassays for disease diagnosis and therapy management; as well as RhoGAM®, an injectable drug used to prevent hemolytic disease of the newborn. We are currently looking for a Senior Scientist.

Position Summary:
Responsible for the technical development of immunodiagnostic assays for the *Vitros* ECi analyzer and integration into the manufacturing areas against demanding project schedules.

Immunodiagnostic assay product development experience is essential. Technical Competencies include: Candidate must be highly technically competent and contribute to the process of innovation, typically within a group environment with a proven record of immunodiagnostic assay product development to internationally recognized quality and design control standards. The candidate should be able to demonstrate their ability to design, execute, analyze and interpret experimental work capable of establishing and validating the most suitable methods, reagents and design of immunodiagnostic products. Candidate should exhibit ingenuity, creativity and resourcefulness and be able to collaborate with and influence other functional groups in both written and verbal communications. Leadership Competencies include the ability to supervise and develop as required one or more R&D scientists as part of the R&D project team, a commitment to excellence and achievement, and the ability to participate in and lead interdisciplinary teams.

Preferred Education:

- BS with at least 5 years experience in immunodiagnostic assay product development or
- MS with at least 3 years experience in immunodiagnostic assay product development or
- Ph.D. with at least 1 year experience in immunodiagnostic assay product development

Qualified candidates should apply: (Set search controls to Requisition number 0502015) **https://www.jnj.com/careers/exp_search.html**. No phone calls please.

Ortho-Clinical Diagnostics is committed to providing Equal Opportunity to a diverse workforce.

ASSISTANT PROFESSOR

Anatomy and Cell Biology

The Department of Anatomy and Cell Biology invites applications for an Assistant Professor. Applicant should have a Ph.D. or M.D. degree with prior teaching experience or training in medical neuroanatomy and demonstrated ability to conduct independent research. The successful applicant will be expected to participate in graduate as well as medical education and to support his/her research program by extramural funding.

Curriculum vitae, a brief description of previous and anticipated research, and the names of three references should be sent to:

Dr. M.A.Q. Siddiqui
Professor and Chair
Department of
Anatomy and Cell Biology
State University of New York
Downstate Medical Center
450 Clarkson Avenue, Box 5
Brooklyn, NY 11203

Fax: 718-270-3732
E-mail: MAQ.Siddiqui@Downstate.edu

SUNY DOWNSTATE Medical Center

SUNY Downstate is an EOE

Children's National Medical Center

Director Stem Cell Research

Children's Research Institute
Children's National Medical Center (CNMC)
Washington,DC

Children's Research Institute (CRI) at CNMC is seeking applications for Director of its new Stem Cell Research Program. CRI has strong research programs in neurodevelopment, immunology, cancer biology, genetic medicine and neural/muscle degenerative diseases. CNMC is one of the leading research institutions in the Washington, DC area with over $50 million annually in research funding, and is undergoing a major expansion of research space.

The candidate must have: (1) established a nationally/internationally recognized research program in stem cell biology; (2) a successful track record in obtaining external funding, (3) the ability to coordinate with clinical programs that bring potential therapies to trial. The position includes a package of support and an endowed chair together with a Tenured Associate or Full Professor appointment at the George Washington University School of Medicine.

Applications should be sent by **August 1, 2005** and include a cv, a letter summarizing qualifications and three references to: **Vittorio Gallo, Ph. D., Children's Research Institute, 111 Michigan Ave. NW, Washington,DC 20010.**

ETH

Eidgenössische Technische Hochschule Zürich
Swiss Federal Institute of Technology Zurich

Postdoc and Group Leader Positions

The ETH Institute for Chemical- and Bio-Engineering has several vacancies for competitive postdocs and group leaders, who will foster novel research initiatives in gene therapy, drug discovery, host-pathogen crosstalk, tissue engineering and biopharmaceutical manufacturing. Successful candidates are highly skilled in standard molecular, cell biology and *in vivo* techniques, have a command of state-of-the-art transduction technologies and have advanced skills in cultivating primary cells. We expect an outstanding publication record and ambition to pursue an academic career or initiate technology transfer activities.

Please send two hard copies of your application including CV, publication list, a three-year research plan and three letters of recommendation to:

Prof. Dr. Martin Fussenegger
c/o Mrs. Marcia Schoenberg
ETH Institute for Chemical- and Bio-Engineering
ETH Hoenggerberg HCI F117
Wolfgang-Pauli-Strasse 10
CH-8093 Zurich
Switzerland

POSITIONS OPEN

ASSISTANT/ASSOCIATE/FULL PROFESSOR of psychiatry. The Department of Psychiatry and Behavioral Sciences and the Center for Neuroscience, University of California, Davis, invite applications for a Neuroscientist at the Assistant/Associate/Full Professor level, to begin July 1, 2006. Specialization within any area of cellular or molecular neuroscience consistent with the broad goals of the Department and Center is open but candidates with backgrounds in the neuropathology of schizophrenia are encouraged to apply, especially if their research can interact productively with existing and developing programs on the neuropathology of major mental illnesses in the School of Medicine. The successful candidate will be expected to demonstrate leadership in their research specialty, obtain extramural funds, and participate in teaching, and university and public service. Candidate will teach graduate students, medical students, and psychiatry residents. Candidates must possess a Ph.D. or M.D. degree. Some clinical responsibilities possible for qualified applicants but not essential.

Applicants should send a letter, in response to search #3824, describing their research and teaching interests, curriculum vitae, copies of representative publications, and the names of at least five persons from whom references can be obtained to: **Edward G. Jones, M.D., Ph.D., Director, Center for Neuroscience and Distinguished Professor of Psychiatry and Behavioral Sciences, 1544 Newton Court, University of California, Davis, CA 95616-8659.** All materials must be received by November 30, 2005, to be assured of consideration. The search will continue until the position is filled. **Website: http://www.ucdmc.ucdavis.edu/psychiatry/.**

The University of California is an Affirmative Action/Equal Opportunity Employer.

PROFESSOR – TRANSLATIONAL CANCER BIOLOGY
Department of Pathology and Laboratory Medicine
UC Irvine School of Medicine

Applications are sought for a position at the Full Professor level to lead a new program focused on molecular pathological basis of carcinogenesis and on the translation of these findings to new diagnostic, prognostic, and therapeutic applications. The successful candidate is expected to have a record of scholarship in translational carcinogenesis. Candidates should have expertise in developing methods for the analysis of tumor tissues and the derivation of diagnostic, prognostic, and therapeutic applications. Expertise in high-throughput analysis of gene regulation patterns would be particularly valued. Applicants should hold an M.D. degree, and certification in anatomic pathology by the American Board of Pathology is highly desirable. The successful candidate is expected to teach medical students and graduate students and to participate in other University service. Interested candidates are invited to submit curriculum vitae and names of three academic references to: **Translational Cancer Biology Search Committee, c/o Michael E. Selsted, M.D., Ph.D., Professor and Chair, Department of Pathology and Laboratory Medicine, D440 Medical Science, UC Irvine School of Medicine, Irvine, CA 92697-4800.**

UC Irvine is an Equal Opportunity Employer committed to excellence through diversity.

Additional job postings not featured in this issue can be viewed online at **website: http://www.sciencecareers.org.** New jobs are added daily!

Manage your job search more effectively by creating an account at **website: http://www.sciencecareers.org.** You can post your resume (open or confidentially) in our database and use it to apply to multiple jobs simultaneously. Track the jobs you have applied to in special tracking folders. Plus, you can create Job Alerts that will e-mail you notification of jobs that match your search criteria.

POSITIONS OPEN

POSTDOCTORAL POSITION available for three-dimensional nuclear magnetic resonance studies of enzyme mechanisms. Involves cloning, expression, isotopic labeling, and large-scale purification of mammalian and bacterial serine proteases. Candidates should submit resume and names of three references to:

Professor William W. Bachovchin
Department of Biochemistry
Tufts University
School of Medicine
136 Harrison Avenue
Boston, MA 02111

Tufts University is an Affirmative Action/Equal Opportunity Employer.

POSTDOCTORAL POSITIONS
Emerging Viral Pathogen Detection

Positions available as part of a Cornell University Medical Center–National Institute of Allergy and Infectious Diseases-funded Collaborative Project Grant for development of comprehensive DNA chip, capillary array, and single-molecule detection Quantum Dot based assays to distinguish Dengue, West Nile, and other emergent agents from common pathogens employing high throughput screening platforms using microbial signature profiles. Applicant should have M.D. with substantial research experience or Ph.D., preferably in infectious diseases, molecular biology, genomics, bioinformatics, protein-DNA interactions, DNA arrays, fluorescence detection, liquid-handling robotics, and/or automation in DNA and polymerase chain reaction technology. Competitive salary commensurate with experience. Send curriculum vitae and names of three references to either: **Dr. Linnie Golightly, Division of International Medicine and Infectious Diseases, Room A421, Cornell University Medical Center, 1300 York Avenue, New York, NY 10021. Fax: 212-746-8675; e-mail: lgolight@med.cornell.edu** or **Professor Francis Barany, Program Director, Department of Microbiology, Box 62, Cornell University Medical Center, 1300 York Avenue, New York, NY 10021. Fax: 212-746-7983; e-mail: barany@med.cornell.edu.** *Equal Opportunity Employer.*

POSTDOCTORAL POSITION
Harvard Medical School

Position available immediately in gene therapy/antibody engineering. The main focus of this research is to develop recombinant adeno-associated viral vectors (rAAV) for in vivo monoclonal antibody gene transfer. Recent Ph.D. and research experience in molecular biology, immunology, and biochemistry are required. Applicants with a publication record in antibody engineering/phage display, rAAV vectorology, and cancer immunotherapy are preferred. Visit **website: http://www.nfcr-ctae.org** for more information on the Marasco laboratory. Send curriculum vitae, brief description of research experience, and names of three references to: **Dr. Wayne Marasco, Dana-Farber Cancer Institute, JFB 824, 44 Binney Street, Boston, MA 02115. Fax: 617-632-3889.** *An Equal Opportunity Employer.*

NIH-funded **POSTDOCTORAL POSITION** is available at Tufts University Cummings School of Veterinary Medicine, Division of Infectious Diseases, to work on the molecular biology and genomics of *Cryptosporidium*. Candidates with strong background in molecular biology and experience with either DNA arrays, functional genomics, or bioinformatics are encouraged to apply. Curriculum vitae should be sent to: **Dr. Giovanni Widmer** at **e-mail: giovanni.widmer@tufts.edu.** *Tufts University is an Affirmative Action/Equal Opportunity Employer.*

POSITIONS OPEN

POSTDOCTORAL RESEARCHER
University of Kansas
Department of Medicinal Chemistry
Laboratory of Dr. Ernst Schonbrunn

Perform research in the molecular biology and chemistry of human testis-specific proteins. The successful applicant is experienced in modern methods of recombinant DNA technology and is familiar with bacterial, insect, and/or yeast overexpression systems. The applicant must have at least three publications in international peer-reviewed journals. For more information on our group visit **website: http://www.medchem.ku.edu/Faculty/schonbrunn.html.** Apply online at **website: https://jobs.ku.edu,** reference POOL: Postdoctoral Researcher and attach a cover letter and curriculum vitae. Arrange for three letters of reference to be sent to: **Lanaea Heine, 2099 Constant Avenue, Lawrence, KS 66047. E-mail: lheine@ku.edu.** *Equal Opportunity/Affirmative Action Employer.*

POSTDOCTORAL/TEACHING POSITION
Developmental Neurobiology
Hendrix College

A Postdoctoral/Teaching position is available immediately in the Biology Department at Hendrix College to study regulation of developing sensory neurons in the mammalian nervous system. The focus of the research project is to investigate the roles of growth factors and transcription factors in the regulation of sensory neuron development by generating and analyzing transgenic and knockout mice. In addition to training in modern genetic and molecular biological techniques, this position offers the opportunity to gain teaching experience at a premier undergraduate liberal arts college. Teaching responsibilities will include a one-semester, freshman-level course in cell biology per year.

Candidates must have a Ph.D. and experience in molecular biology is desirable. Salary is commensurate with experience and qualifications. Applicants should submit curriculum vitae, summary of research experience, copies of publications, statement of teaching philosophy, brief statement of their career goals, and contact information for three references to: **Dr. Richard Murray, Biology Department, Hendrix College, 1600 Washington Avenue, Conway, AR 72032. E-mail: murrayr@hendrix.edu.** Review of applications will begin on July 1, 2005, and will continue until the position is filled.

Hendrix is a distinguished liberal arts college with an endowment of $130 million, sheltering a chapter of Phi Beta Kappa, located in Conway, Arkansas, thirty miles from Little Rock at the foothills of the Ozark Mountains. The College, related to the United Methodist Church, has a strong commitment to excellence in teaching liberal arts. Information on Hendrix College and the Biology Department can be found at **website: http://www.hendrix.edu.**

Hendrix is an Equal Opportunity Employer. Women and members of minority groups are especially encouraged to apply.

SENIOR STAFF ASSOCIATE
Columbia University

Position entails research in patient safety and clinical outcomes studies. Primary responsibilities are analyses of regional and national datasets concerning epidemiology of vascular disease, developing grant applications for Phase II and Phase III clinical trials, and analyzing organizational, medical, and economic factors contributing to medical errors. Educational background (preferably advanced degree) and specific skills in biology, statistics, epidemiology, hospital management, and health policy analysis required.

Please fax curriculum vitae to: **Jeanne Scanlon, InCHOIR** at **fax: 212-305-4256.**

We are an Affirmative Action/Equal Opportunity Employer.

FACULTY POSITION

MASSACHUSETTS INSTITUTE OF TECHNOLOGY DIVISION OF HEALTH SCIENCES AND TECHNOLOGY AND DEPARTMENT OF ELECTRICAL ENGINEERING AND COMPUTER SCIENCE

The Massachusetts Institute of Technology (MIT) seeks candidates for a tenure-track faculty position (Assistant or Associate Professor level) offered jointly in the Harvard-MIT Division of Health Sciences and Technology (HST) and the MIT Department of Electrical Engineering and Computer Science (EECS).

We seek candidates with a doctorate in interdisciplinary fields of biomedical engineering and/or the biomedical sciences. We are especially interested in applicants working in areas related to speech and hearing biosciences and technologies. Faculty duties will include teaching at the undergraduate and graduate levels, research, and supervision of theses. We seek candidates who will interact productively with students and faculty in both HST and EECS, thereby fostering interdisciplinary research and teaching.

Candidates must register with the HST/EECS search website at **https://hst-eecs-faculty-search.csail.mit.edu.** All application materials should be submitted electronically to the website. (If this is not possible, the application may be sent to the address below.) Candidate applications should include a description of professional interests and goals in both teaching and research. Each application should include a curriculum vitae and the names and addresses of three or more individuals who will provide letters of recommendation. Candidates should ask recommenders to submit their letters directly to MIT on the website, or by mailing to the address below. Applications must be complete by September 30, 2005.

Send all materials not submitted on the website to: Martha L. Gray, PhD, Director, Harvard-MIT Division of Health Sciences & Technology (HST), Massachusetts Institute of Technology, 77 Massachusetts Avenue E25-519, Cambridge, MA 02139-4307

M.I.T. is an equal opportunity/affirmative action employer.

For more information about Speech and Hearing Bioscience and Technology at HST, please visit http://web.mit.edu/shbt. For more information about HST, please visit http://hst.mit.edu. For more information about EECS, please visit http://www-eecs.mit.edu.

Massachusetts Institute of Technology

web.mit.edu/hr

PRIZES

"GAGNA A. & CH. VAN HECK PRIZE - 2006"

Application field:
The "Gagna A. & Ch. Van Heck Prize" is awarded to a researcher or physician whose work has contributed to the treatment of a currently incurable disease, or has significantly contributed to research into such an outstanding progress.

Amount:
The Prize will amount to **75,000 Euros.**

Nominations:
This triennial and international Prize, awarded for the second time in 2006, is reserved for a work submitted by one or two researcher(s).

Nominations must be received by the Secretary general of the National Fund for Scientific Research , F.N.R.S., rue d'Egmont 5, BE - 1000 Brussels, Belgium, by **October 3, 2005**.

The personality proposing the nomination must provide a memorandum written in English on the candidate's merits.

Regulations:
The complete regulations can be obtained from the secretariat of the F.N.R.S., rue d'Egmont 5, BE - 1000 Brussels, Tel. : 32 (0) 2.504.92.11,
Tel. Prize : 32 (0) 2.504.92.40,
Fax : 32 (0) 2.504. 92.92,
E-mail : mairesse@fnrs.be, website : www.fnrs.be

COURSE

Believe it!

DNA Sequencing for $2.50 per reaction.

- Read length up to 900 bases.
- High quality electropherograms.
- Fast turnaround.
- Plasmid and PCR purification available.

POLYMORPHIC
Polymorphic DNA Technologies, Inc.℠

www.polymorphicdna.com
info@polymorphicdna.com

1125 Atlantic Ave., Ste. 102
Alameda, CA 94501

Polymorphic exclusively uses ABI 3730XL sequencers.
Data delivered via secure FTP, email or CD.
No charge for standard sequencing primers.
96 sample minimum order.
96 well plates only- no tubes.

888.362.0888

For more information please visit
www.polymorphicdna.com